

**Development of Single Cam Rig for Accurate Simulation of Valve  
Train Tribochemistry**

By

**MacDonald Azubuike. Ofune**

Submitted in accordance with the requirements for the degree of  
**Doctor of Philosophy**

The University of Leeds  
School of Mechanical Engineering,  
Institute of Functional Surfaces.  
Leeds, UK

September, 2016

The candidate confirms that the work submitted is his own, except where work which has formed part of jointly authored publications has been included. The contribution of the candidate and other co-authors in published work from this thesis has been clearly indicated. The candidate confirms that appropriate credit has been given within the thesis where reference has been made to the work of others.

In the papers contributing to this thesis, the candidate (first author) carried out all the experiments, analysis and preparation of the manuscripts. All other authors contributed by proof reading and providing insight on the discussions. Simulation results presented in Figure 8-2 (a) & (b) were done by information given to members of the consortium at TOTAL Raffinage Marketing Lyon, France.

This copy has been supplied on the understanding that it is copyright material and that no quotation from this thesis may be published without proper acknowledgement.

© 2016 The University of Leeds and MacDonald A. Ofune

## **Publications**

---

1. MacDonald Ofune, Paul Banks, Ardian Morina, Anne Neville. Development of Valve Train Rig for assessment of Cam/Follower Tribochemistry. 41<sup>ST</sup> Leeds Lyon Symposium on Integrated Tribology, 7-9<sup>th</sup>, Sept, 2014. Leeds, UK (Published)
2. Ali Ghanbarzadeh, MacDonald Ofune, Ardian Morina, Anne Neville. Effects of Tribofilm Composition, Structure and Durability on Insert Wear in a Single Cam Tribometer'. Wear of Materials (in preparation).
3. MacDonald Ofune, Vishal Khetan, Ardian Morina and Anne Neville. Effect of coatings on camlobe wear. A tribological investigation. Wear of Materials ( In preparation)

## **Conferences - Oral presentations**

---

1. MacDonald Ofune, Paul Banks, Ardian Morina, Anne Neville. Development of Valve Train Rig for assessment of Cam/Follower Tribochemistry. 41<sup>ST</sup> Leeds Lyon Symposium on Integrated Tribology, 7-9<sup>th</sup>, Sept, 2014. Leeds, UK.
2. MacDonald Ofune, Ardian Morina, Anne Neville. Tribochemical studies of two surfaces and the effect of oil type in the reduction of valve train wear. Swiss-Japanese Tribology Conference, Zurich, Switzerland, 5-6<sup>th</sup> Oct, 2014.
3. Ardian Morina, MacDonald Ofune Anne Neville,. Single Cam Rig – Mapping the Tribochemistry across a camlobe. International Tribology Conference (ITC), 16-20 September, 2015, Tokyo, Japan.
4. Ali Ghanbarzadeh, MacDonald Ofune, Ardian Morina, Anne Neville. Effects of Tribofilm Composition, Structure and Durability on Insert Wear in a Single Cam Tribometer'. TURKEYTRIB, Turkey, 7-9 October, 2015.

## ABSTRACT

The study of cam-tappet tribochemistry is on the rise due to the need for a better understanding of how nanoscopic tribofilms reduce friction (improved engine efficiency) and wear (durability) in internal combustion engine. Environmental legislation on exhaust gas emissions have further stimulated research on the use of less phosphorus and sulphur containing additives because phosphorus clogs the catalytic converters in an engine exhaust system.

Current tests evaluate the resultant surface films formed on the contact by the additive package which has made understanding of the test conditions crucial due to the increased complexity of tribochemistry. Diamond Like Carbon (DLC) surface coatings are also receiving significant attention even though their interaction with conventional lubricants additives is still unclear.

A vast majority of published studies look at these systems under steady-state conditions whereas, dynamic conditions are predominant. In this work, a newly modified '**SLICE**' single cam tribometer, which has incorporated a programmable dynamic speed and lubricant supply system, was designed and employed for the study of cam-follower tribochemistry. Information such as frictional torque and lubricant film thickness were obtained using a torque transducer and the Dowson mathematical model respectively.

XPS, RAMAN/FTIR, SEM/EDX surface analytical techniques are used to study the tribofilms. Properties of the tribofilms are evaluated with the aid of AFM, Nano-indenter and Surface Profilometry. Comparison of data with laboratory/conventional tribometers showed that the films had similar characteristics in the boundary lubrication regime and the friction data in a single cam rig closely mimics those in reciprocating pin-on-plate tribometers. The tribofilm was mapped in a unique spot wise manner on the cam and had similar trends with those of the plate in a PoP tribometer. A unique observation in this study was the effect of coating on cam wear. These values closely support those in the PoP reciprocating tribometer. This illustrates that reciprocating laboratory tribometers and bench test data can be used to establish how components in real engines may behave. The rig is capable of ranking candidate materials, surface coatings and fully formulated lubricants for valve train applications.



## **ACKNOWLEDGEMENTS**

I would like to express my sincere gratitude and special appreciation to my great supervisors Professor Ardian Morina and Professor Anne Neville for their help, guidance and also being supportive and encouraging through my PhD. They have been tremendous mentors and this work would not have been possible without their support. I would also like to say a big thank you to all members of the ENTICE consortium. I am honoured and humbled by your support and patience. It was a great opportunity to interact with experts in the field of tribology/tribochemistry.

I am also thankful to the members of iFS research group, especially to James, Earle, Doris, Ali, Vishal, Shahriar, Joe, Pourya, Siavash, John, Fiona, Lukman, Mohsen, Ogbemi, Jide, Zahra, Farnaz, and Elio. Special thanks to Mr Paul Banks for all his technical contributions throughout my PhD - your insights were invaluable. I equally appreciate the efforts of the technical staff at IFS - Mick Huggan, Bryan, Mark Batchelor and Ron Cellier. This will not have been possible without your support.

A special shout out goes to my parents (Sir MacDonald Ofune and Patricia Ofune) for their continuous encouragement and love. I would also like to thank my brothers (Charles and Kester) and Sisters (Lilian and Frances) for their emotional, mental and academic advice throughout my PhD programme.

Lastly, I would like to thank my wife and friend – Ides Mildred Ofune for her support and encouragement during the writing of my thesis. Your comforting words help stimulate me in writing the thesis. Her constant love, motivation, encouragement and patience during my PhD is invaluable.

## TABLE OF CONTENTS

<b>TITLE PAGE</b> .....	<b>i</b>
<b>ABSTRACT</b> .....	<b>iv</b>
<b>ACKNOWLEDGEMENTS</b> .....	<b>v</b>
<b>TABLE OF CONTENTS</b> .....	<b>vi</b>
<b>LIST OF FIGURES</b> .....	<b>xvi</b>
<b>LIST OF TABLES</b> .....	<b>xxiv</b>
<b>NOMENCLATURE</b> .....	<b>xxv</b>
<b>CHAPTER 1. INTRODUCTION</b> .....	<b>1</b>
1.1. Challenges Facing Internal Combustion Engines.....	1
1.2. Motivation for the Study of Engine Tribochemistry .....	2
1.3. Objectives.....	3
1.4. Thesis Structure.....	4
<b>CHAPTER 2. LITERATURE REVIEW ON VALVE TRAIN SYSTEMS</b> .....	<b>6</b>
2.1. Foreword of Valve Train System: Its Components and Operations .....	6
2.1.1. Types of Cam Follower Configurations and Their Associated Advantages /Disadvantages .....	7
2.2. Lubrication Regimes in Cam Follower Contacts.....	9
2.2.1. Boundary Lubrication .....	10
2.2.2. Mixed Lubrication.....	10
2.2.3. Elastohydrodynamic Lubrication (EHL) .....	10
2.3. Film Thickness Variation across Camlobe .....	11
2.4. Friction between Cam and Followers .....	13
2.5. Wear on Cam-Follower Systems.....	15
2.5.1. Volumetric Wear Measurements .....	15

2.5.2.	Surface Layer (Thin) Activation Technique for Real Time Wear Measurement ..	16
2.6.	Cam Follower Materials .....	17
2.6.1.	Cam Follower Surface Coatings: Special Attention to DLC Coatings .....	18
2.6.1.1.	Chromium Plating .....	19
2.6.2.	DLC Coatings for Cam Follower Applications.....	20
2.6.3.	Mechanisms of Failure for DLC Coatings.....	23
2.6.3.1.	Heat Induced Graphitisation of DLC Coatings.....	23
2.6.3.2.	Surface Temperature Phase Transformation of DLC Coatings .....	24
2.6.4.	Failure Mechanisms at Cam Follower Contacts and Mitigation Strategies .....	25
2.6.5.	Cam Follower Failure Mechanisms .....	25
2.7.	Cam Follower Kinematics (Direct Acting Cam and Flat Faced Follower) .....	26
2.8.	Operating Conditions for Cam Follower Contacts .....	27
2.9.	Tribometers Used to Simulate Cam Follower Contacts .....	28
2.9.1.	Miniature Traction Machine and Space Layer Interferometry .....	29
2.9.2.	Pin-on-Reciprocating Plate Tribometer .....	29
2.9.3.	Single and Multiple Cam Rigs .....	30
<b>CHAPTER 3. VALVE TRAIN TRIBOCHEMISTRY: LUBRICANTS, LUBRICATION AND THE ROLE OF ADDITIVES .....</b>		<b>33</b>
3.1.	Engine Tribochemistry at the Cam Follower Interface .....	33
3.2.	Lubrication, Lubricants the Role of Additives.....	33
3.3.	Lubricant Additives.....	34
3.4.	Antiwear Additives .....	34
3.4.1.	Zinc Dialkyl Dithiophosphate Phosphate (ZDDP) .....	34
3.4.1.1.	ZDDP – Thermal Degradation in (Hydrocarbon) Solutions.....	35
3.4.1.2.	ZDDP Adsorption on Metal Surfaces .....	36
3.4.1.3.	ZDDP Tribofilm Formation and Thickness.....	36

3.4.1.4.	ZDDP/Steel Tribofilm: Friction and Wear Properties .....	37
3.5.	Friction Modifier Additives .....	39
3.5.1.	Molybdenum Dithio Carbamate (MoDTC) Friction Modifier .....	39
3.5.1.1.	Factors Affecting MoDTC Tribofilm Performance .....	41
3.5.1.2.	MoDTC/Steel Interactions .....	41
3.5.1.3.	Ester-Containing Engine Oils .....	42
3.5.2.	Detergents .....	44
3.5.3.	Overbased Ca/Mg Sulphonates: Friction, Wear and Tribofilm Properties .....	44
3.5.3.1.	Overbased Phenates and Salicylates Type Detergents .....	46
3.5.4.	Dispersants .....	46
3.6.	Antioxidants .....	47
3.7.	Pour Point Depressant .....	47
3.8.	Engine Oil Additives – Additive/Additive Interactions .....	47
3.8.1.	ZDDP/MoDTC Interactions .....	47
3.8.2.	ZDDP/Detergent Interactions .....	48
3.8.3.	ZDDP/Dispersant Interaction .....	48
3.8.4.	GMO/Detergent Interactions .....	49
3.9.	Additive/DLC Interactions .....	49
3.9.1.	GMO/DLC Interactions .....	49
3.9.1.1.	MoDTC/DLC Interactions .....	50
3.9.1.2.	GMO/DLC Tribofilms .....	52
3.10.	Tribofilms Derived From FFO on Steel and DLC Surfaces .....	54
3.11.	Surface Analytical Tests .....	56
3.11.1.	Scanning Electron Microscope/Energy Dispersive X- Ray (SEM/EDX) .....	56
3.11.1.1.	Literature/Previous Works on SEM/EDX .....	58
3.11.2.	X-Ray Photoelectron Spectroscopy (XPS) .....	58

3.11.3.	Raman Spectroscopy .....	60
3.11.4.	Nano-indentation .....	61
3.11.4.1.	Nano Indentation Modulus Test Procedure .....	64
3.12.	Summary of Gaps in the Literature .....	64
<b>CHAPTER 4. PIN ON PLATE TRIBOMETER: INVESTIGATION OF THE FRICTION, WEAR AND TRIBOCHEMISTRY OF DIFFERENT DLC COATINGS/LUBRICANT COMBINATIONS .....</b>		
<b>66</b>		
4.1.	Motivation of DLC Studies.....	66
4.2.	Properties of DLC's Coatings Investigated .....	66
4.3.	Experimental Methodology.....	67
4.3.1.	Scratch Test .....	67
4.3.1.1.	Summary of Scratch Test .....	71
4.3.2.	Test Setup and Conditions.....	73
4.3.3.	Lubricants and Lubrication Regimes for Tests .....	73
4.3.4.	Wear Volume Measurement Procedure .....	74
4.3.5.	Materials/Coatings .....	75
4.4.	Results.....	76
4.4.1.	Friction Data with Fully Formulated Lubricant A (FFA) .....	76
4.4.2.	Friction Data with Fully Formulated Lubricant B .....	77
4.4.3.	Friction Data with Base Oils .....	78
4.5.	Optical Investigation of Surfaces.....	79
4.5.1.	Wear of Coatings with FFA, FFB and Base Oils.....	81
4.5.2.	Wear of Cast Iron Pins with FFA, FFB and Base Oils .....	83
4.6.	Surface Analytical Investigations.....	84
4.6.1.	SEM/EDX .....	84
4.6.1.1.	a:C-H/CI SEM/EDX Results .....	84
4.6.1.2.	ta:C-H/CI SEM/EDX Results .....	86

4.6.1.3.	Si1s/CI SEM/EDX Results .....	88
4.6.2.	XPS .....	89
4.6.2.1.	XPS Results on DLC Coatings with FFA and FFB (a:C-H, Si1s and ta:C-H) .....	90
4.6.2.2.	XPS Results on Steel Plates and Cast Iron Pins (Counter body) .....	91
4.6.3.	Raman Spectroscopy.....	94
4.7.	Summary of Findings .....	95
<b>CHAPTER 5. SINGLE CAM RIG DESIGN, DEVELOPMENT AND EXPERIMENTAL</b>		
<b>PLAN</b>	.....	<b>97</b>
5.1.	Foreword .....	97
5.2.	Development/Design of Single Cam Tribometer .....	98
5.2.1.	Modification of Engine Cylinder Head .....	98
5.2.2.	Camshaft Modifications.....	99
5.2.3.	Side Plates and Dummy Shaft .....	99
5.2.4.	Displacement Transducer and Cam Follower Dynamics .....	100
5.2.4.1.	Cam Lobe Profile and its Effects on Lubrication Films .....	101
5.2.4.2.	Cycloidal Motion of Cam Profiles .....	101
5.2.5.	Shaft Encoder .....	104
5.2.6.	Torque Transducer Operation, Mounting and Calibrations .....	105
5.2.7.	Electric Motor – ABB ACS 800.....	107
5.2.7.1.	Speed Controller Tuning and Its Effect on Noise.....	107
5.2.7.2.	Acceleration and Deceleration Ramps (Jogging) .....	108
5.3.	Lubricant Oil Bath and Temperature Monitoring.....	109
5.3.1.	Lubricant Oil Bath with Flow Loop.....	109
5.3.2.	Thermocouples .....	111
5.4.	Load Cell .....	111
5.5.	Hohner Alignment Couplings .....	112

5.6.	Newly Developed Single Cam Rig .....	112
5.7.	Data Acquisition.....	114
5.7.1.	Rig Operational Procedure: Routine Checks and System Setups .....	114
5.7.2.	Camshaft Positioning .....	116
5.8.	Noise and Vibration Filtering on Newly Developed Single Cam Rig .....	117
5.9.	Friction and Instantaneous Torque Measurements .....	119
5.9.1.	Valve Train Friction Torque.....	119
5.10.	Experimental Work .....	120
5.10.1.	Procedure I – Validation Testing Procedure .....	121
5.10.2.	Experimental Conditions Investigated on Single Cam Rig .....	121
5.10.2.1.	Temperature .....	121
5.10.2.2.	Test Duration .....	121
5.10.2.3.	Speed .....	121
5.10.2.4.	Oil Type .....	121
5.10.3.	Anticipated Outcome .....	122
5.10.4.	Experimental Conditions For Procedure I .....	123
5.11.	Procedure II.....	124
5.11.1.	Anticipated Goals .....	124
5.11.2.	Experimental Steps/Outline .....	124
5.11.3.	Tribofilm Characterization across Cam Profile .....	125
<b>CHAPTER 6. SINGLE CAM RIG VALIDATION AND COMMISSIONING TESTS.....</b>		<b>127</b>
6.1.	Background.....	127
6.2.	Introduction of Single Cam Rig Commissioning Tests and Validation .....	127
6.3.	Experimental Methodology.....	130
6.3.1.	Test Procedure .....	130
6.3.2.	Materials .....	132

6.3.3.	Lubricants .....	133
6.3.4.	Valve Train Friction Torque .....	134
6.4.	Results.....	135
6.4.1.	Friction Data .....	135
6.4.2.	Effect of Surface Finish on Average Friction Torque .....	137
6.4.3.	Effects of Engine Oil Formulation.....	139
6.4.4.	Insert Wear Measurement.....	140
6.4.5.	Effects of Oil Type on Wear .....	143
6.5.	Conclusions .....	143
<b>CHAPTER 7. TRIBOCHEMISTRY STUDIES OF FILMS DERIVED FROM NEWLY DEVELOPED SINGLE CAM RIG .....</b>		<b>144</b>
7.1.	Motivation for Tribocchemistry Studies .....	144
7.2.	Raman Surface Test Procedure.....	144
7.3.	FIB-SEM/TEM Imaging Procedure.....	146
7.4.	XPS Tests and Imaging Procedure .....	146
7.5.	Surface Analysis/Tribocchemistry Results and Discussion .....	147
7.5.1.	SEM/EDX Results.....	147
7.5.2.	Raman Spectroscopy – Investigation of Film Structure .....	151
7.5.3.	FIB-SEM Results .....	153
7.5.4.	TEM Results .....	155
7.5.5.	XPS Results .....	157
7.5.5.1.	Effects of ZDDP Type and Concentration on Wear .....	161
7.5.5.2.	Type of Detergent and Its Role on Film Dispersion/Morphology.....	164
7.5.6.	Effects of Tribofilm Thickness, Film Dispersion and Polyphosphate Chain Length on Insert Wear. ....	164
7.6.	Conclusions on Rig Development, Validation and Testing Protocol .....	166



<b>CHAPTER 8. THE ROLE OF DLCs IN CAM FOLLOWER APPLICATIONS – A FRICTION WEAR AND TRIBOCHEMISTRY STUDY .....</b>	<b>168</b>
8.1. Introduction to the Application of DLC For Cam Follower Systems .....	168
8.2. Experimental Methodology for DLC Coatings.....	171
8.2.1. Test Procedures .....	171
8.2.2. Breaking-in .....	172
8.2.3. Wear Methodology.....	173
8.3. Materials .....	175
8.4. Surface Analysis .....	177
8.4.1. XPS Analysis .....	177
8.5. Results.....	177
8.5.1. Friction Results .....	177
8.5.2. Friction Response from Coating both Cam and Tappet/Inserts .....	180
8.5.3. Torque Profiles .....	181
8.5.4. Wear Results .....	183
8.5.5. Wear Comparison with Standard Engine Tests.....	187
8.6. Surface Analytical Results .....	190
8.6.1. XPS Analysis (Tests were carried out only on the camlobe) .....	190
8.6.1.1. Si1s/Cl Combination .....	190
8.6.1.2. ta:C-H/Cl Combination.....	193
8.7. Consequences of DLC Coated Cam and Follower on Valve Train Friction and Cam Wear .....	194
8.8. Conclusions .....	195
<b>CHAPTER 9. DISCUSSION .....</b>	<b>196</b>
9.1. Outline of Discussion .....	196
9.2. Newly Designed Single Cam Rig - Novel Features .....	196

9.2.1.	Instrumentation: Data Capture, Torque Profiles & Dynamic Load Determination .....	196
9.2.2.	Noise Levels .....	197
9.3.	Coating Performance on SCR – Wear and Friction .....	198
9.4.	Coating Performance on PoP Tribometers – Friction and Wear .....	199
9.4.1.	Interaction of Additives with the DLC Surfaces.....	200
9.4.2.	Mechanism of Friction Reduction by DLC Coating .....	202
9.5.	Correlation between Tribometer and SCR Test.....	203
9.5.1.	Tribochemistry – Comparison of Tribofilms Structure and Composition on Ferrous surfaces .....	203
9.5.1.1.	Inserts.....	203
9.5.1.2.	Cast Iron Pins .....	204
9.5.1.3.	Camlobes .....	205
9.5.1.4.	Tribofilms Derived on DLC Coatings – Inserts, Plates and Camlobes ...	205
9.5.2.	Effect of Oil Type/Composition of Tribofilm and formation Mechanisms .....	206
9.5.3.	Friction and Wear Comparison .....	210
9.5.4.	Friction and Wear Mechanisms.....	212
9.5.4.1.	Oil B – Friction and Wear Mechanisms .....	212
9.5.4.2.	Oil A – Friction and Wear Mechanisms .....	212
9.5.4.3.	Base oil – Friction and Wear Mechanisms .....	213
9.6.	Level of Prediction & Economic Significance of Valve Train Tests .....	214
<b>CHAPTER 10.</b>	<b>CONCLUSIONS AND FUTURE WORK .....</b>	<b>216</b>
10.1.	Conclusions.....	216
10.1.1.	Single Cam Rig Development .....	216
10.1.2.	Single Cam Rig Tribochemistry .....	216
10.1.3.	Consequences of Insert Coating .....	217
10.1.4.	Consequences of Coating Both the Cam and the Insert .....	217

10.2.	Future Work .....	218
10.2.1.	On Single Cam Rig Development.....	218
10.2.2.	Effects of Tappet/Insert Rotation on Tribochemistry .....	219
10.2.3.	SLA Technique for Cam Wear Measurements. ....	219
10.2.4.	ECR for Indirect Determination of Film Thickness .....	220
10.2.5.	Lubricant Additive Investigation .....	221
10.2.6.	Single Cam Rig Modelling .....	221
10.2.6.1.	Friction and Wear Models .....	221
10.2.6.2.	Tribochemistry Models in Valve Train Systems.....	222
<b>APPENDIX A</b>	.....	<b>223</b>
<b>APPENDIX B</b>	.....	<b>224</b>
<b>APPENDIX C</b>	.....	<b>225</b>
<b>REFERENCES</b>	.....	<b>226</b>

## LIST OF FIGURES

Figure 1-1 Mechanical Losses in an Internal Combustion Engine .....	2
Figure 1-2 Structure of PhD Thesis .....	5
Figure 2-1 Schematic of a Direct Acting Mechanical Valve Train showing major components [6-8] .....	6
Figure 2-2 Cam Follower Configurations (a) Bucket type (b) Finger Follower (c) Rocker Arm (d) Short Push Rod Type (e) Long Push Rod Type [9] .....	7
Figure 2-3 Modified Stribeck Diagram Showing The Lubrication Regimes For Engine Components [9].....	9
Figure 2-4 Elastohydrodynamic Lubrication [15] .....	11
Figure 2-5 Electromechanical Circuit For Film Thickness Measurement .....	12
Figure 2-6 Voltage Drop Across Cam Follower Contact [12, 20] .....	12
Figure 2-7 Test Conditions and Variation of Friction Coefficient with Speed [32].....	15
Figure 2-8 (a) Abnormal Cam Wear and (b) Friction Measurement with a Single Cam Rig [18] .....	16
Figure 2-9 Oil storage capacities of thermally sprayed Coating/honed and Fax film picture of a hone surface [58] .....	19
Figure 2-10 Effect of Hydrogen on DLC Films [65] .....	22
Figure 2-11 Graphitisation of DLC Coating [73] .....	23
Figure 2-12 Cam Follower Mechanisms Showing (a) Pitting and (b) Scuffed Surface [10]. .....	25
Figure 2-13 Geometry of Direct Acting Cam and Follower [12, 13] .....	27
Figure 2-14 (a) Miniature Traction Machine [82] and (b) Space Layer Interferometry Mapping [14, 83].....	29
Figure 2-15 Pin on Disc Tribometer and Typical Operating Conditions [32] .....	30
Figure 2-16 Single Cam Test Rig [32] .....	31
Figure 3-1 Structure of Zinc Dithiophosphate [96] .....	34
Figure 3-2 Thermal Degradation of ZDDP[93].....	35
Figure 3-3 Structure of Antiwear Pads From ZDDP [109].....	38

Figure 3-4	Mechanism of MoS <sub>2</sub> Formation from MoDTC: Chemical Model [114] .....	40
Figure 3-5	Showing New Reaction Pathway of MoDTC Additives [116]. .....	41
Figure 3-6	Effects of Environment on Friction and Surface Roughness in Oils Containing MoDTC [118] .....	42
Figure 3-7	Chemical Structure of GMO [111] .....	43
Figure 3-8	Chemical Structure of Sorbitan Monooleate [120] .....	43
Figure 3-9	Structure of Overbased Calcium Sulphonate [129].....	44
Figure 3-10	Model structure of OBCaSu [134].....	45
Figure 3-11	Structure of an Overbased Calcium Phenate Type Detergent [137] .....	46
Figure 3-12	Synergistic Action of Esters and Detergent in Minimisation of Engine Deposits [151] .....	49
Figure 3-13	(a) DLC/Oil Additive low Friction (b) GMO/Base oil Friction Properties[44]	50
Figure 3-14	SEM Images of Sliding Surface in Base Oil and Oil containing MoDTC [153]. .....	51
Figure 3-15	Comparison of composite wear with BO and MoDTC in DLC/Steel tribopairs [155] .....	52
Figure 3-16	Hydroxylated Films Formed by Ester Containing Additives[111].....	53
Figure 3-17	XPS Spectra of ta-C Lubricated By Glycerol (a) Novel ta-C Surface (b) Inside Wear Track (c) Outside Wear Track [158].....	53
Figure 3-18	(a) AES Spectra for Fresh Oil (b) IR Spectra for Fresh Oil (Upper Spectra Inside Tribofilm and Lower Spectra 8mm Outside Tribofilm [88].....	55
Figure 3-19	(a) Phosphorus Map on DLC Coated Bucket (b) Calcium Map on DLC Coated Bucket [87] .....	56
Figure 3-20	Schematic of Scanning Electron Microscope [159].....	57
Figure 3-21	Energy Dispersive X-ray Spectroscopy Showing Key Components [160] ...	57
Figure 3-22	Principle of X-ray Photoelectron Spectroscopy.....	58
Figure 3-23	XPS Spectra of Oils Containing MoDTC and MoDTC+ZDDP [165] .....	59
Figure 3-24	Renishaw In-Via Raman Apparatus.....	60
Figure 3-25	Raman Spectra of Films Formed From Fresh Oil in Cylinder on Flat Experiment [168].....	61

Figure 3-26	Indentation Device and Indent on Test Surface [172] .....	62
Figure 3-27	Load Displacement Curve for Nano-indentation.....	63
Figure 4-1	Coating architecture for (a) taC-H and (b) a:C-H.....	67
Figure 4-2	Scratch Test On a:C-H Showing Critical Load at (a) 23 .70 N (b) 26.80 and (C) 30.1 N .....	68
Figure 4-3	Scratch Test on MnPO <sub>4</sub> Showing Critical Load (a) Onset Of Cracking At 0.65 N (b) Coating removal/delamination at 19.1 N (c) failure at 46 N .....	69
Figure 4-4	Scratch Test on Si1s Showing Critical Load (a) 17.0 N with cracks (b) 19.73 with coating delamination (c) 22.4 N with coating failure .....	70
Figure 4-5	Scratch Test on taC-H Showing Critical Load at (a) 15.16 N with minor cracks (b) 25. 5 N with delamination (c) coating failure at 29.0 N .....	71
Figure 4-6	Test Setup and Experimental Conditions .....	73
Figure 4-7	Wear Volume Measurement with Optical Interferometry Showing the Line Profile Along One Axis. ....	75
Figure 4-8	SEM Image of (a) taC-H (b) Si1s (c) a:C-H.....	76
Figure 4-9	Friction Plots of Different Coating against Cast Iron When Tested with Fully Formulated Oil A .....	76
Figure 4-10	Friction Plots of Different Coating against Cast Iron When Tested with Fully Formulated Oil B .....	77
Figure 4-11	Friction plots of different coatings against base oil.....	78
Figure 4-12	Diameter of the Wear Scar of Cast Iron Pins Rubbing Against (a) Polished plate (b) a:C-H (c) MnPO <sub>4</sub> (d) Si1s (e) ta:C-H in base oil.....	79
Figure 4-13	Diameter of the Wear Scar of Cast Iron Pins Rubbing against (a) Polished Plate (b) a:C-H (c) MnPO <sub>4</sub> (d) Si1s (e) taC-H in oil A .....	80
Figure 4-14	Diameter of the wear scar of Cast Iron pins rubbing against (a) Polished plate (b) a:C-H (c) MnPO <sub>4</sub> (d) Si1s (e) taC-H in oil B .....	81
Figure 4-15	Wear on Coated Plates as a Function of Different Oils .....	82
Figure 4-16	Wear on cast iron pins against different oils .....	83
Figure 4-17	SEM/EDX with Oil FFB on CI Pins Showing (a) Micrograph of Wear Track (b) Map on the Track with Key Additive Elements (c) Well Dispersed Tribofilm Composed of Ca, P and S (d) EDX Spectra of Track.....	85

Figure 4-18	SEM/EDX showing (a) Wear Track Morphology on a:C-H (b)EDX Spectra on Wear Track. ....	86
Figure 4-19	SEM /EDX with FFB Showing (a) Morphology, Map and Spectra of Wear Track for taC-H (b) Wear on CI pin (c) EDX Spectra of Wear Track (d) Morphology Wear Track with Hard Particle from Coating Surface .....	87
Figure 4-20	SEM /EDX with FFB showing (a) Morphology, Map and High Magnification of Wear Track on CI Pins with Traces of Coating Wear Particle (b) EDX Spectra of Wear Track on CI pin (c) Mapping of Wear Track on Si1s Plate (d) EDX Spectra of Wear Track on Si1s Pin .....	89
Figure 4-21	XPS Survey Spectra on a:C-H Plates with FFA and FFB. ....	91
Figure 4-22	XPS Analysis of Cast Iron Pins Inside and Outside Wear Track Showing (a) C1s Peaks (b) O1s Spectra (c) P2p Spectra showing Zn3s Peaks (d) Survey Spectra - inside wear track (e) Survey Spectra - Outside Wear Track and (f) Si2p Inside Wear Track.....	93
Figure 4-23	XPS Spectra of W4f on a CI pin indicating transfer film from a:C-H.....	94
Figure 4-24	Raman spectra of (a) coating surfaces and (b) Si1s with FFB .....	95
Figure 5-1	Modified Cylinder Head (SLICE) .....	98
Figure 5-2	SEM/EDX Spectra for Production Tappets of through Hardened 16MnCr5 Steel. ....	99
Figure 5-3	(a) Standard Ford Fiesta 1.25L Engine Camshaft (b) Modified Camshaft Assembly with Stud Shaft and M8 bolts .....	99
Figure 5-4	(a) Side Plate and (b) Dummy camshaft .....	100
Figure 5-5	Mounting of Displacement Transducer on Valve Train (Adapted from [32]) ..	100
Figure 5-6	(a) Effects of Camlobe Profile On Entrainment Velocity And (b) Film Thickness [12] .....	101
Figure 5-7	(a) Cam-Follower Lift Profile (b) Cam Follower Velocity Profile (c) Hertzian Contact Stress Profile .....	102
Figure 5-8	Mounting Instructions for Shaft Encoder .....	104
Figure 5-9	Shaft Encoder Pulse Readings .....	105
Figure 5-10	(a) SAW assembly for Sensor Rotary torque transducer (b) Fully assembled of Sensor Rotary torque transducer [181].....	105
Figure 5-11	Mounting arrangement of Torque transducer on single cam rig.....	106
Figure 5-12	Torque Transducer Calibration .....	106

Figure 5-13	(a) Image of ABB AC800 drive (b) Control Panel [183].....	107
Figure 5-14	Effect of Speed Tuning of Noise and Vibration of Motor/ Single Cam Rig Assembly [183] .....	108
Figure 5-15	Linear and S curve speed ramps of the motor .....	108
Figure 5-16	A typical ramping (jogging) procedure .....	109
Figure 5-17	Lubricant flow loop for single cam rig.....	110
Figure 5-18	HAAKE DC 200 Thermo Fischer Oil Bath.....	110
Figure 5-19	Mineral insulated thermocouples with miniature plugs.....	111
Figure 5-20	(a) Kistler load Cell (b) Instrumentation for Kistler load cell.....	112
Figure 5-21	(a) Specification of alignment couplings and (b) Pictorial view of coupling with M5 bolt assembly .....	112
Figure 5-22	Schematic of Single Cam Rig Assembly.....	113
Figure 5-23	Single cam rig test block.....	114
Figure 5-24	Data logging for Newly Developed Single Cam Rig .....	115
Figure 5-25	Flow chart showing operational procedure for Single Cam Rig.....	116
Figure 5-26	Frequency/Noise Response Due to Bearing /Valve Guide Contact .....	117
Figure 5-27	Characteristic torque wave forms at 750 and 2800 rpm with camlobe .....	118
Figure 5-28	Torque transducer output voltages at camshaft speed of (a) 300 rpm and (b) 2100 rpm .....	119
Figure 5-29	Camshaft test cycle .....	122
Figure 5-30	Regions on Cam Profile.....	126
Figure 6-1	SEM Image showing (a) Polished surface with $R_a$ of $0.025 \mu\text{m}$ (b) Polycrystalline structure of Mn-phosphate with $R_a$ of $0.35 \mu\text{m}$ (c) Chromium chilled cast Iron with $R_a$ of $0.055 \mu\text{m}$ (d) bucket and inserts.....	133
Figure 6-2	Friction torque data on newly developed single cam rig showing good repeatability with oil A against polished inserts at $105^\circ\text{C}$ .....	135
Figure 6-3	Friction torque data on newly developed single cam rig showing good repeatability with oil A against Mn-phosphate inserts at $75^\circ\text{C}$ .....	136
Figure 6-4	Effects of temperature on newly developed single cam test rig with Mn-phosphate coating.....	136



Figure 6-5	Effect of surface finish on friction torque with the newly developed single cam rig with (a) Oil A at 75 <sup>o</sup> C (b) Oil A at 105 <sup>o</sup> C.....	138
Figure 6-6	Effect of oil type on friction torque (a) Polished inserts at 105 <sup>o</sup> C (b) Instantaneous torque across cam profile at 300 rpm with polished Inserts at 105 <sup>o</sup> C.....	140
Figure 6-7	Wear scar measurement procedure from Inserts .....	141
Figure 6-8	Maximum Wear Depths with (a) Mid SAPS Oil A & (b) Normal SAPS Oil B..	142
Figure 7-1	Raman Image (a) Polished Insert Wear Scar – P1 (b) Polished Insert Wear scar - P2 (c) Polished Insert Wear Scar – P3.....	145
Figure 7-2	Procedure for (a) FIB-SEM Investigation (b) TEM Sample Preparation.....	146
Figure 7-3	Location P1 and P2 for XPS analysis.....	147
Figure 7-4	Scanning Electron Micrograph (a) Oil A with Polished inserts at 75 <sup>o</sup> C – Top left (b) Oil A with Polished inserts at 105 <sup>o</sup> C – Top Right (c) Oil A with Mn-phosphate at 75 <sup>o</sup> C – Mid left (d) Oil A Mn-phosphate at 105 <sup>o</sup> – Mid Right (e) Polished inserts against Oil B at 75 <sup>o</sup> C – Bottom left (f) Polished inserts against oil B at 105.....	150
Figure 7-5	Raman Image (a) Polished insert wear scar – P1 (b) Polished insert Wear scar - P2 (c) Polished insert wear scar – P3 .....	151
Figure 7-6	Raman spectra of films formed on polished inserts at P1, P2, and P3 at 105 <sup>o</sup> C by (a) Oil A – Mid SAPS and (b) Oil B – Normal SAPS .....	152
Figure 7-7	FIB-SEM showing tribofilm thickness with (a) Oil FFA at P1- top left (b) On track P2 – top right (c) Oil B at P1 –bottom left (d) Oil B at P2 – Bottom right .....	154
Figure 7-8	FIB –SEM Image showing dispersion of tribofilm with (a) oil FFA and (b) oil FFB at 105 <sup>o</sup> C .....	155
Figure 7-9	TEM Image showing tribofilm at centre with nano crystallites formed on interaction with Oil FFB at 105 <sup>o</sup> C .....	156
Figure 7-10	TEM Image showing two layered structure of tribofilm at 105 <sup>o</sup> C – P2 (6 mm from insert centre) with FFB.....	156
Figure 7-11	TEM Image showing the Diffraction pattern and large size of metallic wear particle in the tribofilm .....	157
Figure 7-12	XPS High resolution rescan on P2p, Zn3s and O1s with etching time showing the ratio of BO/NBO and binding energy difference of $\Delta$ Zn3s-P2p .....	158
Figure 7-13	XPS depth profiling at same location with Oil FFA and FFB at 105 <sup>o</sup> C .....	159
Figure 7-14	XPS Survey spectra showing key elements in the tribofilm with both oils FFA & FFB at 105 <sup>o</sup> C.....	160

Figure 7-15	XPS Survey spectra showing key elements in the tribofilm with both oils FFA & FFB at 75 °C .....	160
Figure 7-16	Polyphosphate chain length obtained on Insert with Fully Formulated Oil A & B .....	165
Figure 7-17	Interatomic layered arrangement for tribofilm .....	166
Figure 8-1	Single Cam Rig Test Cycle and Ramping Procedure .....	172
Figure 8-2	(a) Cam Nose profile before tribological test (b) Location for wear analysis (c) Lubricant entrainment velocity (d) Load per unit length (Adapted from [145]) .....	174
Figure 8-3	SEM Micrograph of (a) Si1s (b) ta:C-H (c) a:C-H as deposited .....	176
Figure 8-4	Scanning X-ray Images on Camlobes .....	177
Figure 8-5	Average Friction Torque Showing Repeatability of Data From the Single Cam Rig After 50 hrs Testing with ta:C-H .....	178
Figure 8-6	Effect of Surface Coating on the Friction Torque with Fully formulated oil B (FFB) after 50 hrs testing. ....	179
Figure 8-7	Effect of Coating Both Cam and Follower with taC-H on Single Cam Rig.....	180
Figure 8-8	Effects of Coating both the Cam and Tappets with a:C-H on Single Cam Rig....	181
Figure 8-9	Torque Profile of different surfaces at 300 rpm .....	182
Figure 8-10	Torque profiles at 300 rpm with ta:C-H coatings showing effects of coating both cam and follower .....	183
Figure 8-11	Cam Nose profile against Si1s coating .....	184
Figure 8-12	Cam Nose Profile against taC-H Coating .....	184
Figure 8-13	Optical Images of (a) Si1s coated inserts, (b) ta:C-H coated inserts, (c) a:C-H coated inserts .....	185
Figure 8-14	Camlobe position and corresponding wear area.....	186
Figure 8-15	Optical Images of Coated Camshaft after 50 hrs testing on a Single Cam Rig. ....	187
Figure 8-16	Sum of Wear Scar on Cast Iron Camlobes when interacting with several coated follower (red line denotes 90 $\mu$ m threshold value above which the oil will be deemed unsatisfactory in service).....	188

Figure 8-17	XPS Photoelectron spectra for (a) O1s 10° from can nose (b) at cam nose (c) 4° from the nose (d) P2p spectra 10° from the cam nose (e) P2p spectra 4° from the cam nose and (f) at the cam nose .....	192
Figure 8-18	XPS Photoelectron spectra for (a) S2p at Nose (b)S2p at 10° from nose (c) S2p at 4° from Nose (d) Si2p at 4° from the cam nose. ....	193
Figure 8-19	O1s spectra for CI/taC-H interaction.....	194
Figure 8-20	Showing (a) P2p spectra at 4° from cam nose (b) S2p spectra at 0° and 10°.. ..	194
Figure 9-1	Noise level with (a) Hwang et al [223] (b) Newly Developed Single Cam Rig	198
Figure 9-2	Friction Comparison for SCR and PoP Tribometer Showing The Effects of Different Coatings When Tested Against a CI Counter-body With Oil B .....	210
Figure 9-3	Wear Comparison for CI Camlobes and Pin against Different Coatings When Tested with Oil B.....	211
Figure 9-4	Mechanisms of Friction and Wear for Different Oils and Coating Combinations. ....	214
Figure 10-1	Film state measurement across cam profile using ECR [12].....	221

## LIST OF TABLES

Table 2-1	Comparison of Cam Follower Configurations .....	8
Table 2-2	Cam Follower Materials and Surface Coatings .....	21
Table 2-3	Showing The Operating Conditions In A Typical Cam Follower System [9, 11, 79] .....	28
Table 3-1	XPS Photopeaks of Molybdenum compounds .....	40
Table 3-2	Effect of Ester Friction Modifiers on Engine Fuel Economy [123] .....	43
Table 4-1	Details/Properties of Coatings Used .....	72
Table 5-1	Comparison of some cam profiles used in engineering systems[13, 179] ....	103
Table 5-2	Test Matrix for the Validation of Single Cam Rig Results .....	122
Table 5-3	Test Materials, and Conditions for Procedure A .....	123
Table 5-4	Test Materials, and Conditions for Procedure B .....	125
Table 6-1	Lubricant Composition .....	134
Table 7-1	EDX Spectra of All Regions On Polished Inserts at 75 <sup>0</sup> C and 105 <sup>0</sup> C With Oil A. ....	148
Table 7-2	Oil Type BO/NBO ratios, BE $\Delta$ (Zn3s-P2p), Intensity ratios P2p/Zn3s and their effects on wear at different points of an insert in a single cam tribometer .....	162
Table 7-3	Binding Energies of XPS spectras of S2p, O1s, and P2p spectra at two temperatures (75 °C and 105 °C) and the corresponding species formed on top surface.....	163
Table 8-1	Test Parameter for Tribological Test with DLC Coatings .....	171
Table 8-2	Contact Pressure across camlobe.....	174
Table 8-3	Properties of Lubricants/ DLC coatings .....	175
Table 9-1	Showing the comparison of tribofilms with a Pin on reciprocating plate tribometer and Single Cam Rig .....	207

## NOMENCLATURE

a-C	Amorphous Carbon DLC coating
AES	Auger Electron Spectroscopy
AFM	Atomic Force Microscopy
BDC	Bottom Dead Centre
BO	Bridging Oxygen
NBO	Non Bridging Oxygen
CI	Cast Iron
CVD	Chemical Vapour Deposition
DAMB	Direct Acting Mechanical Bucket
DOHC	Double Overhead Camshaft
DLC	Diamond Like Carbon
DPF	Diesel Particulate Filters
ECR	Electric Contact Resistance
EGR	Exhaust Gas Recirculation
EDX	Energy Dispersive X-ray
EELS	Electron Energy Loss Spectroscopy
FFO	Fully Formulated Oil
FM	Friction Modifier
GMO	Glycerol Monooleate
GDO	Glycerol Dioleate
HRTEM	High Resolution Transmission Electron Microscopy
ICE	Internal Combustion Engines
ILSAC	International Lubricant Standardization Approval Committee
IRRAS	Infrared Reflective Absorption Spectroscopy
ISO	International Standard Organisation
LEFET	Laboratory Engine Fuel Economy Test
MnPO <sub>4</sub>	Manganese Phosphate coating
MoDTC	Molybdenum Dithio Carbamate
MTM	Miniature Traction Machine
OBCaSU	Overbased Calcium Sulphonate Detergent
PAO	Polyalpha Olefins
PIBSA	Polyisobutylene Succinimide
PLD	Pulse Layer Deposition
PVD	Physical Vapor Deposition
PACVD	Plasma Assisted Chemical Vapor Deposition
SAE	Society of Automotive Engineers
SAPS	Sulphated Ash Phosphorus -Sulphur
SCR	Single Cam Rig
SEM	Scanning Electron Microscope
SLIM	Space Layer Interferometry
SMO	Sorbitan Monooleate
ta:C-H	Tetrahedral Amorphous carbon DLC with Hydrogen
TDC	Top Dead Centre
ToF-SIMS	Time of Flight Secondary Ion Mass Spectroscopy
XPS	X-ray Photoelectron Spectroscopy
XANES	X-ray Absorption Near Edge Spectroscopy
WD	Wear Depth
ZDDP	Zinc Diakyl Dithiophosphate

# CHAPTER 1. INTRODUCTION

## 1.1. Challenges Facing Internal Combustion Engines

Mechanical losses in internal combustion engines (ICE) account for about 15 % and this can be effectively divided among the engine components such as the piston assembly, valve train systems, bearings, pump losses and engine drive systems (pumps, flow systems & gears – (see Figure 1-1). By adequately reducing friction, significant savings can be achieved on the Earth's depleting hydrocarbons which are predominantly used to power these engines.

A major challenge already impacting ICE manufacturers is environmental legislation. This is following the European commission's action on the reduction of carbon dioxide (CO<sub>2</sub>) exhaust emission from commercial and passenger vehicles from 120 g/Km (2012 target) to 95 g/Km (2020 target) [1]. Linked with this issue is where the use of an effective zinc dialkyl dithiophosphate (ZDDP) antiwear additive poisons the catalytic converters in an engine exhaust system thereby propagating the emission of CO<sub>2</sub> and worsening the engine exhaust requirements.

Zinc DialkylDithioPhosphate (ZDDP) antiwear additives in automotive lubricants have experienced a steady decline due to their damaging effects on engine three way catalytic converters. This has led lubricant manufacturers to the formulation of low graded (Mid, Normal and ultra-low) or even zero Sulphated Ash Phosphorus-Sulphur (SAPS) engine lubricants.

Conversely, other additives (particularly dispersants and detergents) have had greater concentrations in lubricant blends. These have been influenced by certain engine designs and requirements such as direct injections, exhaust gas recirculation (EGR), extended drain intervals, and sludge/soot emission control [2]. Unfortunately, these additives suppress, and in some cases, entirely inhibit the film forming characteristics of the antiwear additive - ZDDP. Under these circumstances, asperity interactions on tribological components are more severe, thereby increasing the likelihood of surface damage on highly loaded engine valve train systems.

## 1.2. Motivation for the Study of Engine Tribochemistry

By adequately fine tuning engine designs, lubricant additive packages, and material surfaces, the friction and wear on mechanical components can be greatly reduced thereby leading to significant monetary savings [3].

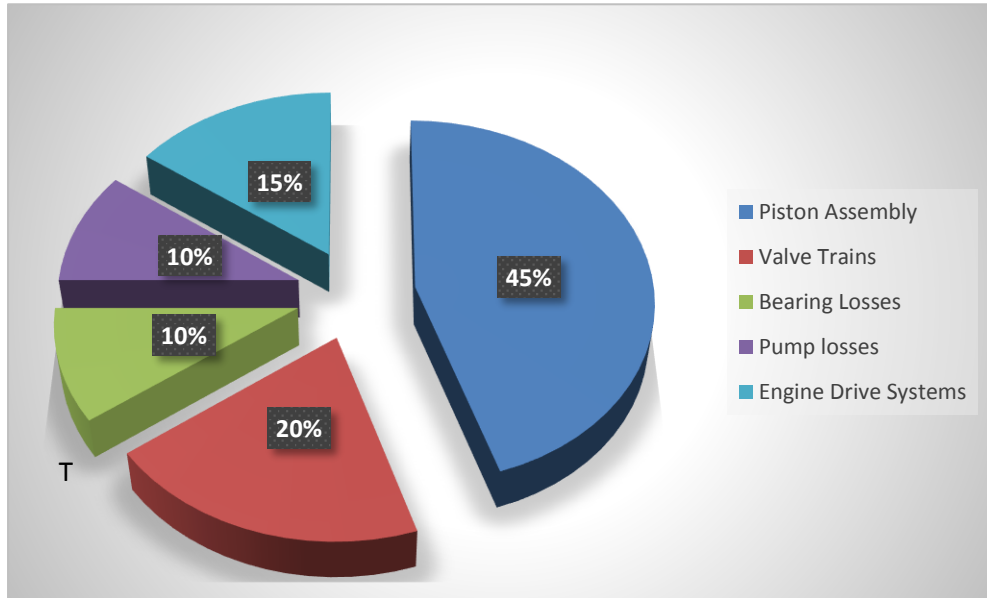


**Figure 1-1 Mechanical Losses in an Internal Combustion Engine**

This has stimulated integrated research on the improvement of engine valve train components by evaluation of lubricant additive chemistries, and surface coating techniques. These coatings, particularly Diamond Like Carbon (DLC) are widely used for engine valve trains [4] because they provide combined effects of lower friction, improved durability and excellent running-in properties on interacting surfaces. Engine oils on the other hand were designed for ferrous surfaces and their interaction with inert amorphous carbon surfaces are quite different.

By evaluating these coatings in a pin-on-plate reciprocating plate and a cam-follower component bench tests, which was developed during the course of this project, a better understanding of their performance in service can be obtained. This is because component bench tests better simulate the characteristics of the system in terms of slide-roll ratio, lubricant film thickness, temperature and contact pressures. A prime example by Mufti [5] showed that the friction behaviour in the inlet camlobes of bench tests mirrors those in a fired engine. This could lead to huge monetary saving by reducing the number of tests required and avoiding the complex or long engine fired tests carried out for evaluating materials.

In these assessments, the effects of the engine oils were also given adequate consideration. Two commercial 5W30 Mid and Normal SAPS oils were used for the study. The novel aspects of this study involve the mapping of the tribochemical films formed across the cam/inserts and correlating this to the wear profiles which were observed with optical interferometry and contacting Taylor Hobson talysurf. The change of form across the camlobe width was also investigated with white light interferometry to show how wear modifies the form on the camlobes which, ideally would result in lower engine efficiency. Coatings which showed better response to this phenomena were identified as potential candidates for valve train applications.

### **1.3. Objectives**

The aim of this work is to improve the knowledge on the tribochemistry associated with direct acting mechanical bucket (DAMB) engine valve train configurations under lubrication with Mid SAPs and normal SAPs engine oils. This is as a result of reduced concentration of Zinc dialkyldithiophosphate (ZDDP) antiwear additives in automotive lubricants following their damaging effects on engine three-way catalytic converters. This work establishes a mechanism for the interaction of engine oils with commercial DLC-coated surfaces and polished steel surfaces. The main objectives of this research work can be summarized as follows;

- To develop a single cam rig that is sensitive enough to differentiate lubricants with close chemistries and surface coatings of diverse chemical structures and mechanical strengths.
- To investigate the properties and composition of the tribological formed layers from Mid/Normal SAPS on interacting surfaces as well as their effect on friction and wear.
- To evaluate different coating performance for cam follower application using a pin on reciprocating plate and single cam rig.
- To map the tribochemical films across the cam profile and correlate this to the wear mechanisms based on lubricant entrainment velocity, load and contact pressure.
- To investigate the tribological formed layers on DLC coatings in both pin on plate tribometer and single cam rig.
- To evaluate the links between tribometer and component level systems like the Single Cam Rig (SCR) in tribochemistry studies.



## 1.4. Thesis Structure

In this thesis, Chapter 2 discusses the literature review on cam-follower tribology while Chapter 3 focuses on tribochemistry. Chapter 4 describes tests that were carried out on DLC coatings and steel as a preliminary evaluation. Chapter 5 discusses the development of a single cam tribometer and equally highlights the novel features of the apparatus. Chapter 6 shows the validation tests which was carried out on the rig with excellent repeatability characteristics. Chapter 7 evaluates the tribochemistry and characterisation of the tribofilms derived on the rig. The last results chapters (Chapter 8) show the methodologies which was used on ranking DLC coatings on the cam follower system. Mapping of the wear across the camlobes was carried out at 7 locations and correlated to the tribofilms, load per unit length, entrainment velocity and contact pressures.

In simple terms, the result chapters of the thesis can be split into two sections. **Section 1** relates to tests which were performed on the pin-on-reciprocating plate tribometer – Chapter 4. **Section 2A** relates to the development of the newly developed valve train rig. This is covered in Chapter 5 and has no experimental results but highlights the experimental conditions which were used for the validation of the rig.

**Section 2B** can be subdivided into Procedures I and II. Procedures I has to do with the validation, calibration and testing of the newly-developed single cam rig apparatus. It spans through Chapter 6 & 7. **Procedure II** evaluates different DLC coatings in the cam follower system and embarks on novel investigation of tribochemistry maps across the cam profile. Further investigations into the benefits of coating both the cam and the follower were also highlighted – this is covered in Chapter 8. Surface analytical techniques including FIB-SEM/EDX, HRTEM, XPS, RAMAN, Nano-indentation, AFM and Profilometry, will be performed before and after the test to determine the surface modification that have occurred. A schematic of the experimental procedure in this report is summarised in Figure 1-2.

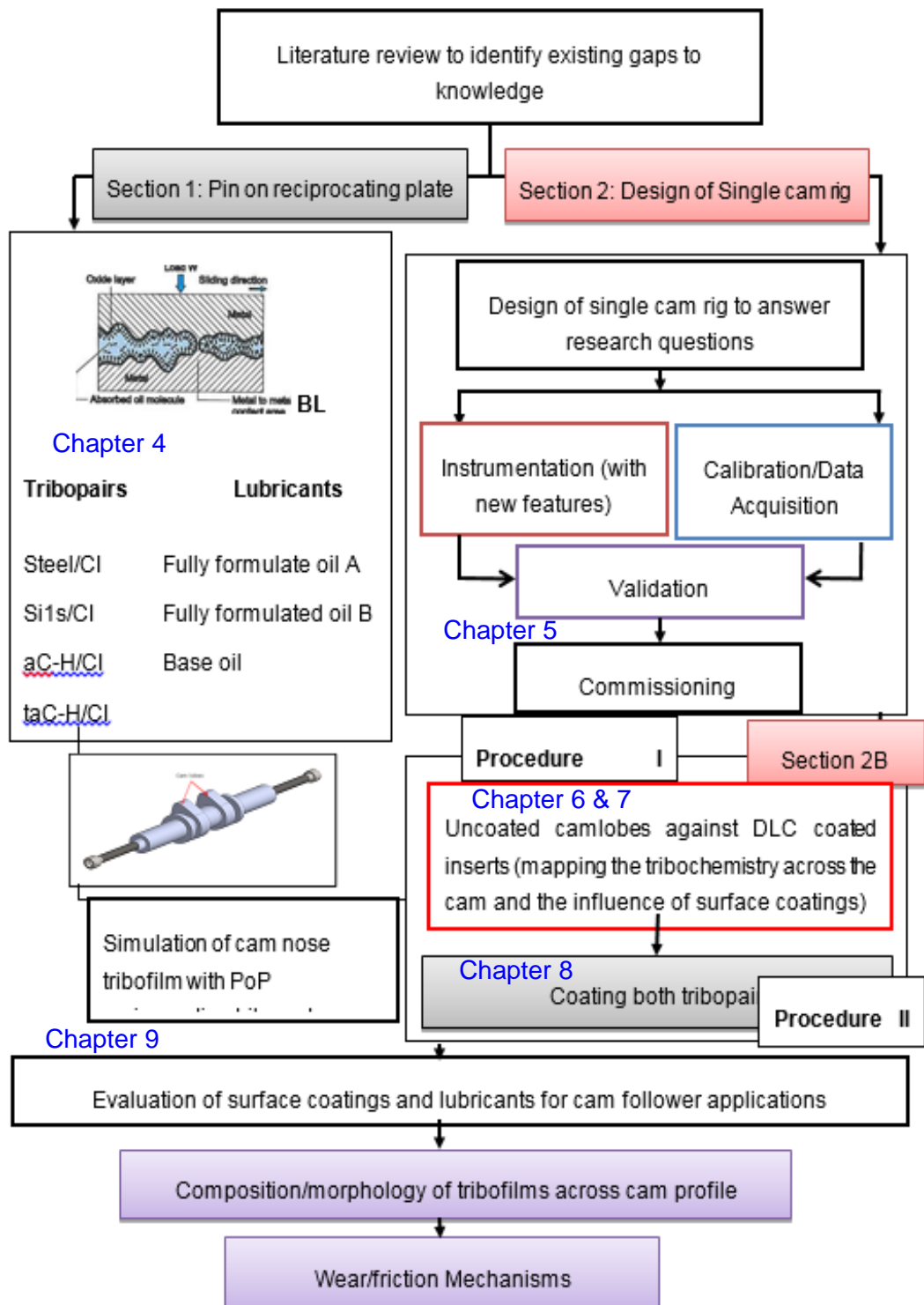
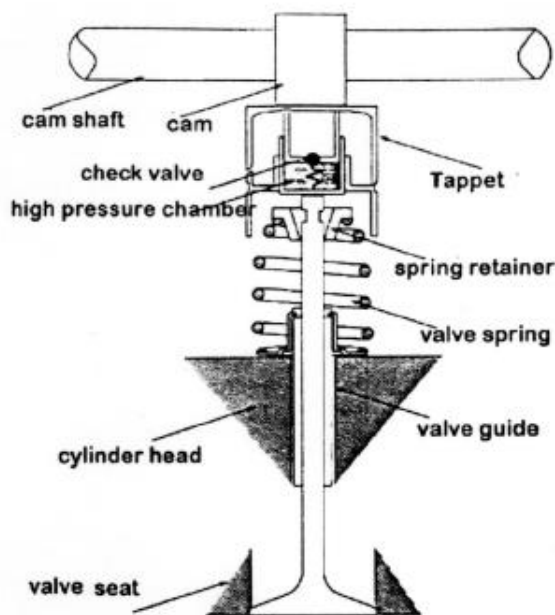


Figure 1-2 Structure of PhD Thesis

## CHAPTER 2. LITERATURE REVIEW ON VALVE TRAIN SYSTEMS

### 2.1. Foreword of Valve Train System: Its Components and Operations

The valve train controls the induction and exhaust processes of an internal combustion engine. Essentially, the more effectively an engine breathes, the more efficiently it will produce power. The valve train components vary based on engine design but typically, they consist of valves, camlobes, collets, valve seats, springs, retainers, shims/inserts, buckets/tappets, rocker arms, push rods and support bearings. The camshaft is usually rotated by the crankshaft assembly with toothed belt or gear drive assembly which serves as the frame for opening the valves. Two turns of the crankshaft correspond to a single revolution for the camshaft. Belts are usually cheaper, can be mounted externally, and can equally act as dampers to torsional vibrations generated in the system. Gear designs give significant power transfer although they are noisy, susceptible to wear and must be incorporated at design stage. A direct acting mechanical bucket (DAMB) type valve train configuration is shown in Figure 2-1.



**Figure 2-1 Schematic of a Direct Acting Mechanical Valve Train showing major components [6-8]**

As per lubrication, for most inline camshaft engines, an abundance of lubricant is made available from the crankcase. With most overhead camshaft systems, lubricant is pumped from the sump through the cylinder head, flowing through galleries/vents to the cam-follower contact. A prime example is in the DAMB. Each of these design

configurations has their tribological merits and demerits which are explained in **Table 2-1**

### 2.1.1. Types of Cam Follower Configurations and Their Associated Advantages /Disadvantages

There are varying configurations of overhead valve (ohv) and overhead camshaft (ohc) employed by engine manufacturers. Typically, they have certain advantages and disadvantages. For instance, certain high performance spark ignition engines use four valves per cylinder where the inlet and exhaust valve are not in line and driven by double ohc (dohc). This is typical for most V engine configurations. This second shaft has an associated cost element and increases engine weight. The British Leyland pent roof valve assembly is one method of minimising weight in this configuration. In this system, one camshaft controls the camlobes which opens the inlet valves directly while the exhaust valve is controlled indirectly with rockers arms. Common cam follower types found in IC engines are shown in **Figure 2-2**. These mechanisms have some unique features in terms of designs, friction, wear and lubrication (see **Table 2-1**).

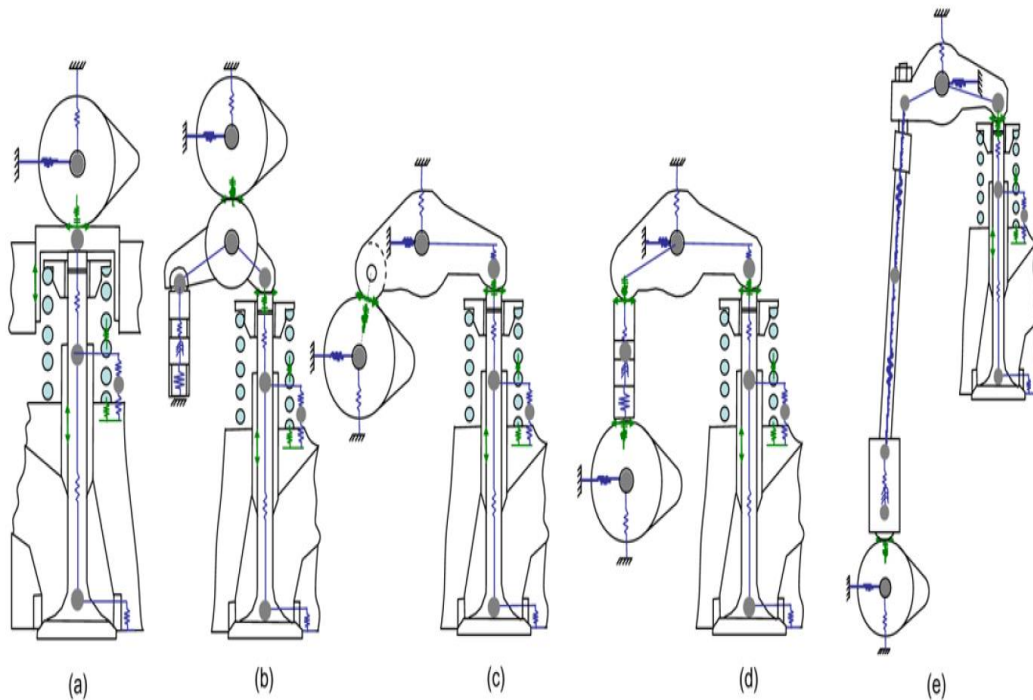


**Figure 2-2 Cam Follower Configurations (a) Bucket type (b) Finger Follower (c) Rocker Arm (d) Short Push Rod Type (e) Long Push Rod Type [9]**

**Table 2-1 Comparison of Cam Follower Configurations**

Cam Follower Designs System Property	Roller Finger Follower	Rocker arm Follower	Bucket Type Follower	Push Rod Types
Friction	Low Friction. Scuffing can be experienced in many cases	High friction experienced and sliding/scuffing can be experienced at high speed	Moderate friction	Friction can be high from interaction between multiple surfaces
Lubrication	Difficult to lubricate	Poor lubrication due to film breakage.	Good Lubrication Fluid film lubrication can be achieved	Good lubrication characteristics are experienced
Failure/Wear	Scuffing/polishing problems. High wear due to extreme Hertzian contact stresses. Wear is also concentrated at a point	Fatigue wear is likely on roller followers. Material selection can be used to overcome this.	Low wear	Minimal wear as system is exposed to glut of lubricant from the main engine bearings due to closeness to oil sump.
Dynamics/Vibration & Misalignment	Vibration occurs with successive wear and misalignment	Little but can be severe at higher engine speeds	Minimal.	Minimal if lubrication is maintained. However, due to high interacting members, it will always persist.
Noise	High	Minimum noise though jouncing can be experienced at high speed	May be excessive after progressive wear due to impact along cam profile.	Low
Design	Very Simple	Simple	Simple	Complex
Load carrying Capacity	Not suitable for high speeds/loads. Engine suffocation/overheating problems.	Greater noise /erratic motion due to increased sliding	High load bearing capacity. Good engine breathing are usually achieved	Low. It limits engine breathing. Overheating can be a problem
Maintenance Cost /Weight saving	High due to regular wear	-	May be difficult if valves are not inline. Increased weight due to large cam lobes and support bearings	Easy Adjustments can be made

Adapted from Various sources [10-13]

## 2.2. Lubrication Regimes in Cam Follower Contacts

The lubrication of the cam follower mechanism can best be described as mixed regime [14] which is an intermediate level from boundary to elastohydrodynamic lubrication. The relationship between the coefficient of friction and lubrication regime can best be explained with the reports of Richard Stribeck (1902).

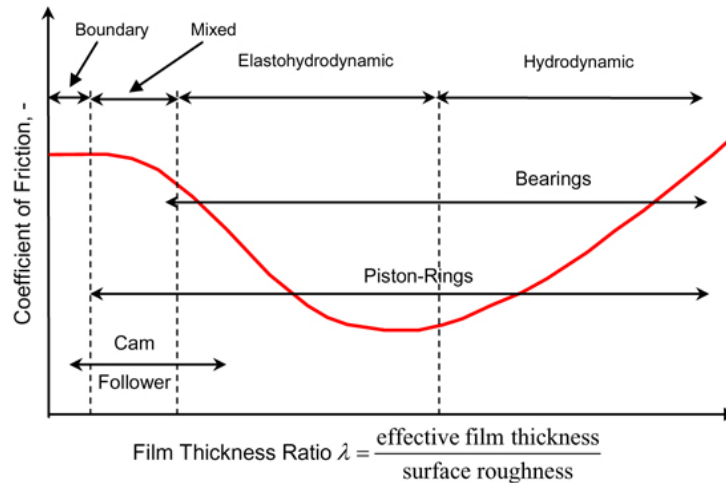


**Figure 2-3 Modified Stribeck Diagram Showing The Lubrication Regimes For Engine Components [9]**

The minimum film thickness can be calculated from the Dowson and Higginson equation for line contact.

Minimum film thickness formula 
$$\frac{h_{min}}{R_e} = \frac{2.65G^{0.54}U^{0.7}}{W^{0.13}} \quad \text{Equation 2-1}$$

Dimensionless material parameter 
$$G = \alpha E^1 \quad \text{Equation 2-2}$$

Dimensionless speed parameter 
$$U = \frac{\eta_o}{E^1} \times u \quad \text{Equation 2-3}$$

Dimensionless load parameter 
$$W = \frac{w}{E^1 \times R_e} \quad \text{Equation 2-4}$$

Where  $\alpha$  is the pressure viscosity coefficient,  $\eta_o$  is the dynamic viscosity,  $w$  is the load per unit length (N/m),  $E^1$  is the equivalent elastic modulus (N/m<sup>2</sup>),  $u$  is the entrainment velocity (m/s) and  $R_e$  is the equivalent radius (m).

### 2.2.1. Boundary Lubrication

This occurs when the ratio of minimum film thickness to the composite surface roughness is less than 1 ( $\lambda < 1$ ). Under this condition, direct contact between interacting asperities is inevitable. It is usually characterised by high friction forces in tribological contacts. For boundary lubrication;

$$\lambda = \frac{h_{min}}{\sum R_a} = \frac{h_{min}}{\sigma} \quad \text{Equation 2-5}$$

$$\lambda < 1 \quad \text{Equation 2-6}$$

$$0.005\mu m \leq h_{min} \leq 0.01\mu m \quad \text{Equation 2-7}$$

Where  $h_{min}$  is the minimum/effective film thickness,  $R_a$  is the centre line average roughness,  $\sigma$  is the root mean square roughness and  $\lambda$  is the specific film thickness which has no units. The frictional properties are controlled by physical and chemical properties of thin surface molecular boundary films formed by the lubricant additives. Lubricant properties, essentially viscosity have little or no role to play in boundary lubrication [15].

### 2.2.2. Mixed Lubrication

In this regime, both the bulk physical properties of the lubricant and molecular boundary lubricating films are important. The film thickness is several magnitudes greater than the composite roughness of the interacting surfaces but there are regions where contacts between interacting asperities occur. The governing equations for mixed lubrication are;

$$1 \leq \lambda \leq 5 \quad \text{Equation 2-8}$$

$$0.05\mu m \leq h_{min} \leq 1\mu m \quad \text{Equation 2-9}$$

### 2.2.3. Elastohydrodynamic Lubrication (EHL)

This region experiences the lowest friction but huge pressure variation coupled with viscosity increase which gives rise to deformation of solids. The fundamental laws of fluid dynamics, Hertzian contact stress, lubricant variation with pressure fail to explain

its phenomena but rather a bridging together of these laws gives the necessary information.

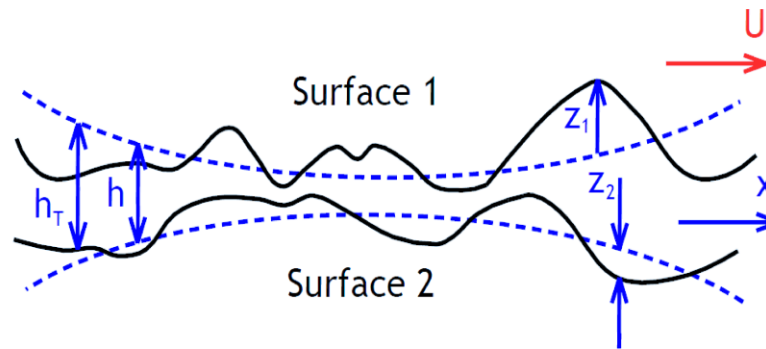


**Figure 2-4 Elastohydrodynamic Lubrication [15]**

The fundamental regime where this exists can be determined with Equation 2-10 and Equation 2-11;

$$4/5 \leq \lambda \leq 10 \quad \text{Equation 2-10}$$

$$0.1\mu m \leq h_{min} \leq 1\mu m \quad \text{Equation 2-11}$$

In summary, it can be observed that most engine components enjoy several lubrication regimes through each cycle of operation. The piston ring and liners exhibit boundary lubrication regimes at the top dead centre (TDC) and bottom dead centre (BDC) where the piston entrainment velocity is zero and squeeze film phenomena persist. Elasto-hydrodynamic lubrication is also experienced during highly loaded expansion stroke after firing but the most predominant is hydrodynamic lubrication. In cams-tappets, boundary lubrication is predominant at the nose and under this condition, additive packages provide the chemical and physical boundary molecular films for reduction of friction and wear. The flank, shoulder and ramp region transit from mixed to elasto-hydrodynamic regimes.

### **2.3. Film Thickness Variation across Camlobe**

Film thickness variation at the cam-follower interface has been itemised as one of the crucial parameters for improved component durability [16-18]. One of the most widely used techniques for the assessment of this condition is **electric contact resistance (ECR)**. Fundamentally, this technique involves applying a fixed electrical parameter to the contact (e.g. voltage) and measuring another variable which is controlled by



the contacting surface (resistance). Insofar, application of small potential (usually 15mV) provided by a voltmeter connected in parallel across the surfaces and measuring the current, thus obtaining the film resistance is by far the most common approach [19]

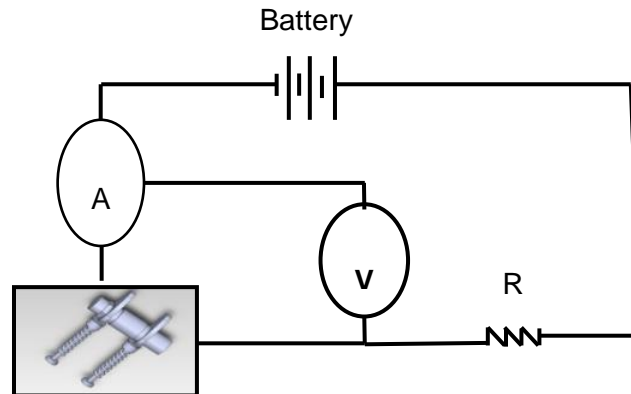


**Figure 2-5 Electromechanical Circuit for Film Thickness Measurement**

Williamson [20] used a capacitance technique to measure oil film thickness using different oils.

Figure 2-6a illustrates the variation of oil film thickness with cam angle.

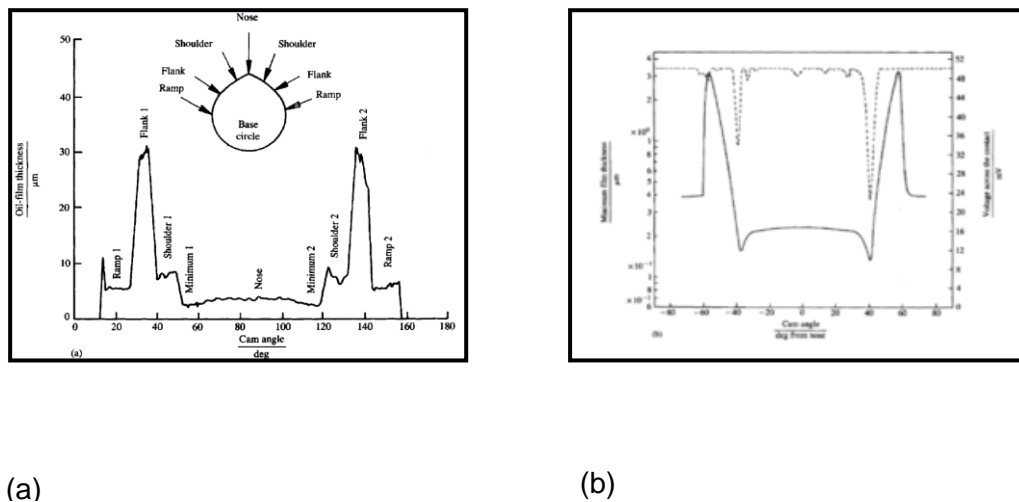


**Figure 2-6 Voltage Drop Across Cam Follower Contact [12, 20]**

The use of capacitance gauges for measurement of film thickness across the cam follower have been reported to pose some difficulties due to film breakdown [21]. Dowson in 1990 [12] employed an electric resistivity technique to study film state at

the cam follower interface. The voltage reading (dotted lines) was compared with the elastohydrodynamic equation for line contact as shown in

Figure 2-6b. it reveals a significant similarity in behaviour between voltage and film thickness[12]. Gao [22] observed using ECR that increased phosphorus concentration reduces the induction time for tribofilm formation. ECR voltage readings have also been reported to mirror frictional behaviours of certain ZnDTP additivated oils where highly resistive/insulating films gave rise to very low potentials across tribocouples [23, 24].

## 2.4. Friction between Cam and Followers

Friction characteristics at the cam follower interface are still a very arduous endeavour based on the combination of sliding/rolling motion, lubrication difficulties, film thickness variation, high loads/applied stresses experienced at the contact of interacting asperities. In spite of these challenges, significant improvements can be achieved with surface coatings, material selections and lubricant formulations. For instance, replacement of steel tappet and retainer with Al-Si with 11% Si achieved 40% reduction in friction and noise [6]. In a multiple cam rig of a FORD 3.5L V6 engine head, polished and DLC coated tappets reduced friction satisfactorily in-lubro conditions with GF4 SAE 5W20 [25]. Surface texturing such as parallel V circular/square grooves and shot peening on shims have also been studied as viable options [4]. The nature of the V parallel groove allows free flow of lubricants and wettability on the surface of the shims without retardation along the edges. Shot-peening on the other hand, increases the surface roughness [4] and the peening intensity creates surface and subsurface cracks on the material which causes deformations, thus leading to poor tribological properties. Lapping of surfaces to lower surface roughness ( $R_a = 0.07\mu\text{m}$ ) coupled with reduction of valve spring loads can help achieve huge cam follower friction reductions. In a report by Katoh [26], this approach yielded up to 40% reduction in friction torque. Effects of slide/roll ratio (**Equation 2-14**) were studied using a steel ball in contact with plane surface of a glass disc [27]. Both steel ball and glass plate were driven by different motors to enable easy variation of the slide roll ratio (*SRR*)

$$\text{Sliding speed} = V_c - V_f \quad \text{Equation 2-12}$$

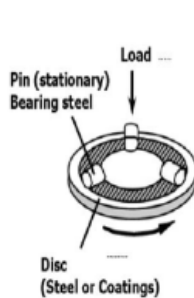
$$\text{Mean entraining speed} = \left( \frac{V_c + V_f}{2} \right) \quad \text{Equation 2-13}$$

$$\text{slide roll ratio} = \left( \frac{\text{sliding speed}}{\text{Mean entraining velocity}} \right) = \frac{2(V_c - V_f)}{V_c + V_f} \quad \text{Equation 2-14}$$

Where  $V_f$  is the velocity of follower and  $V_c$  is the velocity of the cam.

It was observed that the *SRR* had an effect on the EHL friction coefficient with a rapid decline of film thickness at high *SRR*. Gangopadhyay et al [22] observed an increase in friction torque with increase in slide roll ratio. One method of reducing valve train friction is to employ rolling element bearings at specific location in the cam-follower system. Significant load carrying capacity and fuel economy (approx. 2.9%) can be achieved and this is typically applied to racing engines like the FORMULA 1 cars [28]. TiN hard coatings deposited by arc ion plating with  $5\mu\text{m}$  thickness (max) were observed to reduce valve train friction by 40% with 1-2% savings in fuel economy [29]. Considerable weight savings in automobiles is also a feasible means of reducing friction, noise, inertia loads and wear. Hanula [30] utilized both modelling and experimental data to show how this can be achieved with SiN (ceramic pads). Up to 50% reduction in valve train friction was realized with lesser  $\text{NO}_x$  emissions. Super-carburizing of tappet shim to produce the optimum carbide morphology, (typically  $50\mu\text{m}$  diameter) also give rise to materials with improved surface roughness, and better pitting resistance. Tribological test of super carburised tappet shims gave rise to 40% reduction in valve train friction which translates to 5% reduction in overall engine and 1.4 – 3.6% fuel economy benefits [31].

Currently, most tappet surfaces in passenger cars are DLC-coated. In high performance engines like Formula 1, both the cam and follower are coated. Ultra-low friction values of 0.006 with ta:C surface under lubrication with PAO+GMO as shown in Figure 2-7 have been reported [32]. A 45% reduction in friction torque was achieved when compared with conventional phosphate coatings.



	Lubricated condition
Rotational speed (sliding velocity)	30 rpm – 1000rpm (0.03 m/s – 1m/s)
Load (contact pressure)	490 N (0.7 GPa)
Circumstance	Oil bath
Temperature	80 °C
Test duration	60 min.

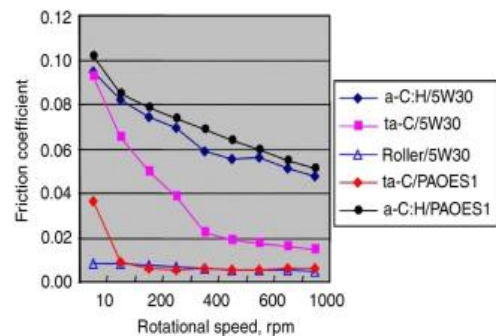


**Figure 2-7 Test Conditions and Variation of Friction Coefficient with Speed [32].**

Test with three different DLCs and varying oil compositions revealed that DLC reduced valve train friction by approximately 40% when compared to steel. The largest reduction achieved in one of the DLC's was attributed to the presence of a dopant element Si which improves the reactivity of DLC's [33]. Kodai [34] examined a:C-H deposited by RF Plasma CVD for valve train application. This coating optimised the tribological properties when compared with CrN, TiN and MoS<sub>2</sub> even though the author suggested that doping with Tungsten (i.e. W-DLC) was later studied as the most reliable option. Vengudusamy et al [35] studied twelve different DLCs using an MTM device with slide roll ratio (SRR) maintained at 0.5. It was observed that ta:C provided the lowest friction but a:C-H and Si-DLC performed better with no measurable wear.

Ashless lubricant based on ILSAC GF4 standards were developed by Okuda and coworkers [36]. A 0.5% in fuel economy was achieved when compared with GF3 Mo-FM. However, the International Lubricant Standardization and Approval Committee (ILSAC) GF 5 has further reduced the amount of phosphorus in 10W30 and introduced a phosphorus volatility condition of 79%. This is aimed at reducing emissions and increasing fuel economy by 0.5% when compared with its GF4 counterpart.

## **2.5. Wear on Cam-Follower Systems**

### **2.5.1. Volumetric Wear Measurements**

Experimentally, the most widely used method for measuring wear of machine components is the volume loss technique. This is obtained by using a stylus profilometry/optical interferometer to get linear dimensions of test samples before and after the test [37]. This gives rise to a change of shape which is used to evaluate the wear volume (in mm<sup>3</sup>). An alternative method uses with the Archard wear equation (shown below) to obtain the dimensional wear parameter K.

$$K = \frac{V_i}{F \times x}$$

**Equation 2-15**

Where  $V_i$  represents the volume loss of the tribocouples (cam and follower),  $F$  is the applied load and  $x$  is the sliding distance. The dimensional wear parameter  $K$  is widely used in tribology for design considerations [15]

In 1980, Dyson [16] examined the kinematics and wear pattern of three different finger followers. Significant wear damage was seen with a talysurf apparatus at two distinct regions of zero entrainment velocity where the lubricant film was lowest.

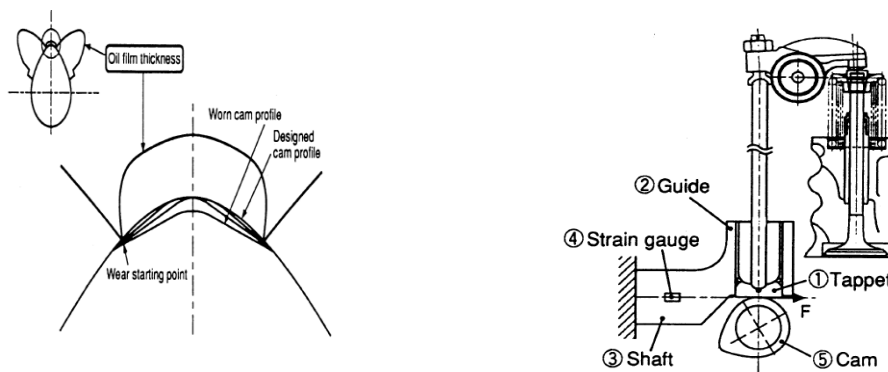


**Figure 2-8 (a) Abnormal Cam Wear and (b) Friction Measurement with a Single Cam Rig [18]**

This is in close agreement with the detailed paper from Taylor [17]. Valve train wear studies using a cam-tappet rig revealed that tappet wear is independent of camshaft speed while friction torque maintained a steady decline at high velocity [4] though certain models suggest that maximum wear depend on velocity at the point of contact without consideration of oil minimum film thickness, contact pressures and flash temperature effects [18, 38]. Similar tests of model oils composed of PAO, ZDDP and MoDTC improved the DLC shim wear characteristics with a lower wear area of  $0.007\text{mm}^2$  [39]. Booth and co-workers [40] used an electric charge detection technique to study cam follower wear of motorised TU3 engine with significant success.

### **2.5.2. Surface Layer (Thin) Activation Technique for Real Time Wear Measurement**

This technique allows the online *in-situ* wear measurement of engine components both effectively and in real time. It involves bombarding the test material with a small portion of a radionuclide source which forms a matrix with the substrate material. In

a tribosystem, the degree of activity of the nuclide is read from a Geiger counter as an indication of the wear.

An application of this technique with steel surface can be carried out by bombarding with  $^{56}\text{Co}$  isotope thereby covering the topmost layer of  $^{56}\text{Fe}$  [22, 41]. Certain reports activate the cam nose as this is the region of paramount wear but this might be misleading as wear still occurs along shoulder/flank due to edge effects [41]. Gauthier and Devigne [42] investigated real online monitoring of wear on cam lobes with the Thin Layer activation technique. Both fresh and used oil (15W40) were tested and no direct correlation between wear and soot levels were found. The authors suggested that threshold soot levels as well as the consumption of antiwear additives are responsible for the erratic cam wear behaviour. This technique has also been employed for the continuing evaluation of additives for motor oil based on the activation of overhead camlobes [43]. Stable isotopic tracers of  $^{13}\text{C}$  were employed for synthetic oil composed of GMO with both mineral and base oil. Significant reduction in friction was recorded and the  $^{13}\text{C}$  had no adverse effect on the friction or wear properties of the system [44]. Thin Layer activation is, however, an indirect technique which measures decrease in activation on low energy irradiated surface and increase in activation in a lubricant in lubricated wear test. A situation where this will be inapplicable will be in adhesive wear. In this case, wear particles are transferred to the other surface and the Geiger counter will record a zero reading when wear has actually taken place.

## 2.6. Cam Follower Materials

Conventional materials for cam are nodular cast iron (CI), grey CI and chilled hardened alloy **CI**, but trends for the use of forged steel, Aluminium, ceramics and sometimes titanium for valve train components are increasing [45-47]. Tappets are usually made of hardened/chromium steel, 16MnCr5 or typically harder than the camshaft. The selection criteria are based on factors such as cost, lubricant retention, material availability, durability in service (wear) and weight savings [48]. Cast Iron is very cheap and available though they are susceptible to pitting. An extensive study of Cam/follower tribopair was studied by Michalski et al [49] and it was observed that chromic grey CI camshaft with chilled surface finish and surface hardened steel follower pair optimized the tribological properties of the system in 1000hr engine test.

The use of **ceramics** roller followers ( $\text{Al}_2\text{O}_3 - \text{TiC}$ ,  $\text{SiC}$ , and  $\text{SiN}$ ) has also shown some promise even though reports from Becker [50] suggests otherwise. For

instance, in lubro test with SiN shows they exhibited better scuffing resistance than CI [51]. SiN with a surface finish of 0.2 $\mu$ m reduced valve train friction by 20-25% and this corresponds to about 2-3% reduction in engine fuel economy[52]. SiN and partially stabilized zirconia were used for tappet material in diesel and LPG engines in Japan around the late1980s [28, 53, 54]. SiN inserts are finding increasing application in automotive valve train components because of their low weight, high wear resistance and rigidity [4, 28] but careful consideration of the temperature, surface finish, lubricant supply, and cam-follower clearance are required when ceramic materials are used as valve train components [53]. Optimisation can aid in preventing failure modes such as grain pull out, micro-chipping and fatigue.

Aluminium materials for valve tappets have also been touted for their low density/weight savings. Reduction in friction torque as high as 40% have been achieved with the use of aluminium tappets and spring retainer with thinner walls when compared with steel [55]. Common valve sheets are made from aluminium with a ring by press fit on sintered alloy of Fe-Ni-Co-Mo-Pb [48]. It is worthwhile to mention that most aluminium alloys (except for AA390 which has high silicon content of approx.17-18%) have poor tribological properties; hence, galling, scoring and/or scuffing are difficult to manage. AA390 on the other hand has some manufacturing difficulties [50]. Titanium has excellent corrosion resistance, low density and good wear characteristics at high temperature. This is why it is suited as valve train material for motor racing. However, it is a very expensive material. In selection of the most appropriate material, a trade off must be reached based on the operating conditions and specific application.

### **2.6.1. Cam Follower Surface Coatings: Special Attention to DLC Coatings**

Alloying and/or coating of CI with small amounts of Cr, Mo, V, Cu, Al and Ti to give better tribo-mechanical properties are not uncommon and the merits/demerits of alloying elements are available in literature elsewhere [56, 57]. Surface coatings can be broadly divided into running-in and wear resistant coatings although some coating architectures exhibit both properties. Phosphating, Tufftriding and sulfonuz finishing provide surface topography that promotes the wettability and spreading of the lubricant on interacting asperities [45, 56]. This can be particularly significant when scuffing is a predominant issue [45]. Sulfonitriding on nodular CI has been reported to be detrimental due to small compressive stresses [49].

### 2.6.1.1. Chromium Plating

Chromium plating by electro-deposition techniques has improved tribological characteristics of CI/steel substrates, by some factors in cam follower systems[28, 56]. However, poor wettability of the surface by lubricant complicates the surface finishing procedures. Under this condition, a tribo-pair may be starved of lubricants needed for its optimum performance. One method of improving this condition is to reverse the plating current after the deposition of the main chromium. This produces a network of pores or cracks (ref Figure 2-9) on the surface for the retention of lubricant [56]. Care must be taken not to use an excessive reverse current or etching too deep as greater cracks may occur which may ultimately result in the premature failure of the tribo-coating.

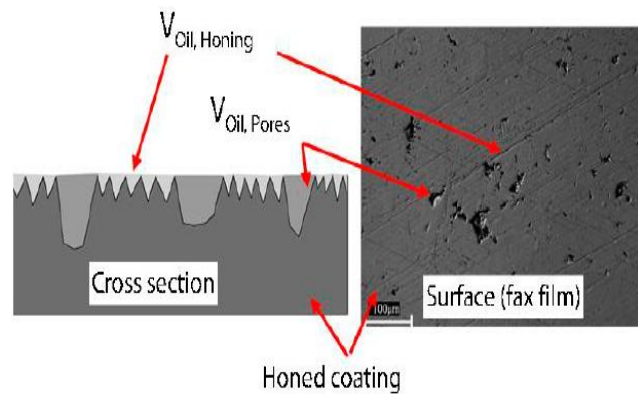


**Figure 2-9 Oil storage capacities of thermally sprayed coating/honed and fax film picture of a hone surface [58]**

Theoretical and experimental studies of CrN surfaces have shown that they exhibit better tribo-mechanical properties than only steel substrates or Cr plated materials [48, 56, 59-61]. CrN surface give lower friction (0.01-0.015) when compared to Cr plated surfaces with 90% and 15% reduction in ring wear and bore wear respectively. This was attributed to sizes of the pores for oil retention [48]. Similar techniques could be employed for valve train components. The use of DLC coatings for tappet materials has been widely studied because of its ultra-low friction in boundary lubrication regime even in un-lubricated conditions [34, 35, 62-64]. A brief summary of the surface engineering (SE) methods which have been employed in the valve train systems is shown in Table 2-2 along with some of their merits/demerits.



### 2.6.2. DLC Coatings for Cam Follower Applications

Diamond like carbon coatings are widely been used in engine valve train components to reduce friction, and increase machine durability. Typically, their friction coefficients range from 0.001 to 0.65 which is dependent on the ratio hydrogen,  $sp^2$  (graphitisation) and  $sp^3$  (diamond) bond [65, 66] Structurally, all DLC's are alike with an amorphous nature but there are many variants of DLC coatings with varying chemical, physical and mechanical characteristics. DLC films can be very hard ( $>90\text{GPa}$ ) and very soft ( $<13\text{GPa}$ ) depending on the deposition technique, and dopant element [67, 68] . They are “**chemically inert**” and are strongly affected by relative humidity, water vapour, dopant element and temperature [65, 69-71].

**Table 2-2 Cam Follower Materials and Surface Coatings**

Trend \ Component	Camshaft	Tappet/Shim	Running-in/Wear Resistant Coatings	Merits/Demerits
<b>Conventional Materials/Surface Coatings</b>	Grey CI	Nodular Iron, High Cr containing ferro-based powdered sintered alloy	Phosphating <sup>R</sup> /Oxidation <sup>R</sup>	Coating produces a thin crystalline surface layer which inhibits adhesive wear and scuffing. Effective lubrication can be achieved.
	<b>Nodular/ Chilled CI</b>	High Chromium cast Iron, Silicon Nitride Ceramics	Tufftriding <sup>R</sup> /Sulfinuz <sup>R</sup> (deposition of layers of Nitrogen, Sulphur and Carbon by diffusion)	Similar to phosphating <sup>R</sup> but with improved wear, fatigue and corrosion resistance
	Malleable CI	Induction <sup>R</sup> and Flame Hardened Steel/CI	Induction <sup>R</sup> and Flame Hardening <sup>R</sup>	Good Wear Characteristics and running-in properties due to increased bond strength
	Ceramics Composite Materials	Powered Sintered Alloy	Carburising <sup>R</sup> : Applied to steels with low carbon content (typically 0.1 – 0.2%C)	Improved wear resistance
			Carbo-Nitriding <sup>RW</sup> of nodular Iron	Improved wear, fatigue and corrosion resistance
<b>Recently Used Materials/Tribo-Coatings</b>	Forged steel	Low Chromium Steel		
	Chilled CI/ Titanium	<b>Hardened Steel (16MnCr5-SAE 5115)</b>	<b>DLC<sup>RW</sup> Coatings on steel tappets and DLC coated camshafts</b> <b>Si doped DLC, taC-H and non-doped aC:H</b>	Good running in properties. Ultra low friction can be achieved with most DLC's.
		Chromium plated steel	Chromising <sup>w</sup> /CrN	Difficult lubrication maybe experienced due to mirror-like smooth surface

RW – Running in and Wear Tribo-coating, R – Running-in Coatings, W – Wear Resistant Coatings [45, 49, 50]

Tests carried out with a:C-H DLC at temperatures ranging from 100 – 300°C exhibited severe wear at elevated temperature while the friction coefficient decreased from **0.12 – 0.03** [71]. Andersson and coworkers [66] recorded an increase in HDLC friction from 0.01 – 0.07 from vacuum to water vapour containing environment respectively. In Figure 2-10, it was demonstrated that HDLC had low friction coefficient of 0.003 in dry Nitrogen. In an identical test, Hydrogen free DLC had higher friction values from 0.7-0.25 in ambient air. Low friction was attributed to reduction of the hard covalent and  $\pi - \pi^*$  bonds on interacting asperities [65]. High hydrogen content on DLCs reduces the friction but the hardness of the coating is usually lost. In this scenario, spontaneous shear thinning and consequent delamination of the coating may occur and the tribological surface becomes stripped of the coating necessary for its optimal performance.

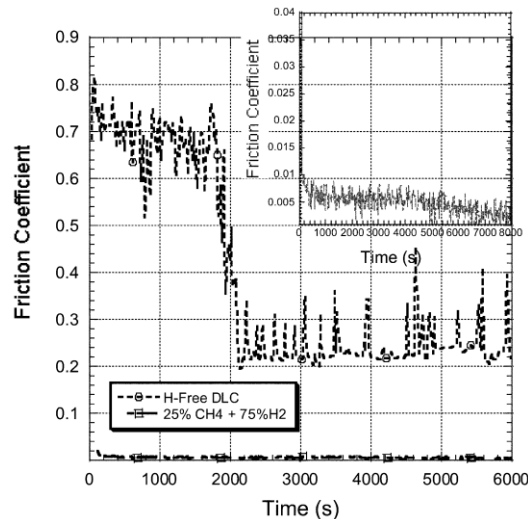


**Figure 2-10 Effect of Hydrogen on DLC Films [65]**

In addition, the presences of carbide-forming elements like Si, Ti, W and S, in DLCs ensure they maintain good tribological properties in RH of 5 – 95% while improving their high temperature application. DLC doped with 4 at.% **Si** have been reported to maintain coefficient of friction at 0.08 with RH ranging from 5-85% [72]. Investigations involving ta:C in base oil have shown that they exhibit low friction from **0.06-0.02** in boundary to mixed lubrication regimes respectively. Superlubricity values from 0.04 to 0.006 have also been reported in oils composed of PAO+GMO [32, 35]. In reality, it is not usually economical to coat both cam/follower with DLCs. Most car manufacturers usually coat the tappet/shim which is in agreement with the paper from Podgornik [69].

Despite their excellent tribological properties in unlubricated conditions, most DLC coatings still require some form of lubrication. The reasons are numerous. Lubricants reduce friction heating/serve as coolant and keep unwanted particles in suspension. Dispersant additives also inhibit the polymerisation of monomers to form varnishes and lacquers on engine surfaces which somewhat makes their application on interacting surfaces inevitable.

### 2.6.3. Mechanisms of Failure for DLC Coatings

#### 2.6.3.1. Heat Induced Graphitisation of DLC Coatings

Graphitisation on DLC coating is a process where  $sp^3$  –  $sp^2$  transformation takes place in the core matrix of the surface due to non-conservative heat load. This suggests a friction-induced annealing process which removes the internal stress of the coating. Sliding of asperities also has associated strain energy which can facilitate the transformation. These processes have been adequately reported in sliding contact of 0.8 – 1.1 GPa under controlled relative humidity [73, 74]. Hydrogen supports the  $sp^3$  matrix but at high temperature, diffusion from the core takes place and the surface is gradually stripped off with the coating. This is not only prevalent in HDLCs, graphitisation has also been recorded for a:C made from Pulse Layer Deposition (PLD) techniques. Raman spectra after  $10^5$  cycles reveal a D peak at  $1350\text{ cm}^{-1}$  which was not observed at 3000 cycles [73].

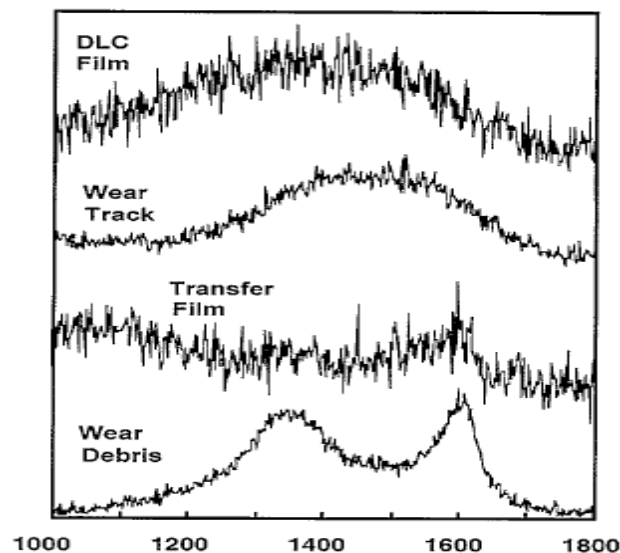


Figure 2-11 Graphitisation of DLC Coating [73]

According to literature studies [71, 73-77], at temperatures between 350 – 400 °C, graphitisation begins to occur. The asperity contact temperature rise due to friction can best be described with the model from Rabinowicz [78]

$$\Delta T = \frac{1}{4a} \left( \frac{\mu W_N \times v}{K_{ic} + K_{if}} \right) \quad \text{Equation 2-16}$$

$$a = \left( \frac{W_N}{\pi H} \right)^{\frac{1}{2}} \quad \text{Equation 2-17}$$

Where  $\Delta T$  is the temperature rise,  $\mu$ ; coefficient of friction,  $W_N$  applied load in Newtons,  $v$  is the sliding velocity,  $a$  is the contact radius,  $K_{ic}$  and  $K_{if}$  are the thermal conductivities of the cam and follower materials respectively.

### 2.6.3.2. Surface Temperature Phase Transformation of DLC Coatings

Based on DLC studies, temperature phase transformation can be divided into three stages by mirroring the friction characteristics [74]; these are in running-in stage with features of high friction values. Subsequently, an intermittent stage involving the build-up of transfer film is achieved and characterised by a decline in friction. Steady state ultra-low friction is reached when significant films have been generated on the interacting asperities. Coating delamination resulting from thermal and strain effects. *In-lubro* conditions, shear-thinning and coating strip off have been reported as reaction pathways for delamination [77]. The asperity temperature rise can best be described with a simple model;

$$T = T_c \exp \left[ \frac{\Delta \rho}{J_T} \times \Delta p \right] \quad \text{Equation 2-18}$$

Where  $T_c$  and  $J_T$  are the phase transformation temperature and Energy respectively,

$\Delta \rho$  is change in specific volume and  $\Delta p$  is the change in Hertzian contact pressure.

## 2.6.4. Failure Mechanisms at Cam Follower Contacts and Mitigation Strategies

### 2.6.5. Cam Follower Failure Mechanisms

The predominant failure modes of cam followers are polishing, scuffing and pitting. Conventionally, the tappet is more resistant to pitting and the camlobes are designed to be opposed to scuffing [10].

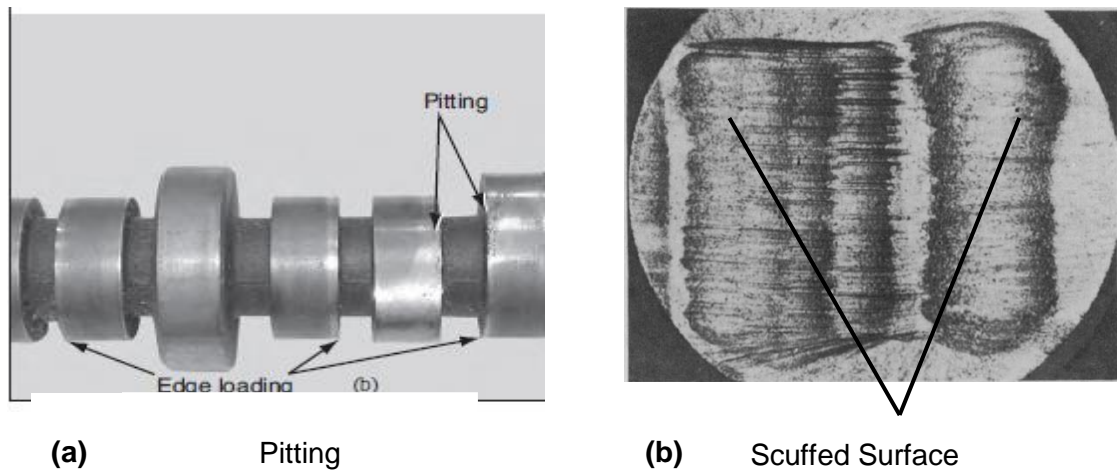
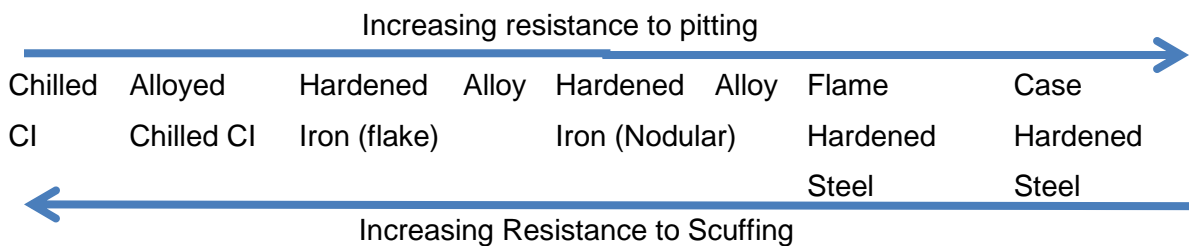


**Figure 2-12 Cam Follower Mechanisms Showing (a) Pitting and (b) Scuffed Surface [10]**

As a guide, the trend of pitting and scuffing for convention materials is illustrated below.



Durability of cam follower components can be improved considerably by the following methods;

- By selecting hard tribopair with comparable hardness
- Increasing the hardness of the cam with thermo-mechanical or heat treatment processes
- Use of coatings such as DLC coatings , phosphate running (in coatings), TiC and TiN hard coatings
- Selection of the appropriate engine oil for cam follower applications

Also, recent studies have shown that, friction losses can be reduced with selection of lighter materials, spring load design and DLC surface coatings for a specific engine oil formulation [25].

## 2.7. Cam Follower Kinematics (Direct Acting Cam and Flat Faced Follower)

The analysis of the cam motion is paramount for the understanding of valve train tribology. Considering the figure shown in Figure 2-13, the cam is designated as component 1 with velocity  $[U_c, V_c]$  along the  $[x, y]$  direction respectively while the follower/shim is designated as component 2 with velocity  $[U_f, V_f]$  along the  $[x, y]$  direction respectively. The cam rotates about its centre at O with its centre of curvature perpendicular to the instantaneous contact point at P. The linear velocity for the follower along the x axis is zero.

Thus

$$U_f = 0 \quad \text{Equation 2-19}$$

$$V_f = l\omega \quad \text{Equation 2-20}$$

The acceleration of the follower can be obtained from the derivative of the follower velocity as;

$$a_f = \frac{dV_f}{dt} = \dot{l}\omega \quad \text{Equation 2-21}$$

The x component of the cam velocity in contact with the follower is derived as;

$$U_c = (r_b + y)\omega \quad \text{Equation 2-22}$$

Giving due consideration to sign the velocity along the contact point on the cam surface can be calculated as;

$$\dot{s} = U_c + \dot{l} = [(r_b + l)\omega] + \dot{l} \quad \text{Equation 2-23}$$

Thus the instantaneous radius of curvature ( $R_c$ ) of corresponding contact points moving along the cam profile with velocity  $\dot{s}$  such that the angular velocity of the tangent to the point of contact at  $\dot{\varphi}$  is given by;

$$R_c = \frac{\dot{s}}{\dot{\varphi}} = \frac{ds}{dt} \times \frac{dt}{d\varphi} \quad \text{Equation 2-24}$$

However, for a flat faced follower, the mathematical expression is given by;

$$\frac{dt}{d\varphi} = \frac{1}{\omega} \quad \text{Equation 2-25}$$

$$R_c = \frac{\dot{s}}{\omega} \quad \text{Equation 2-26}$$

$$R_c = (r_b + y) + \frac{\dot{l}}{\omega} = (r_b + y) + \frac{a_f}{\omega^2} \quad \text{Equation 2-27}$$

Good approximation can be obtain from the velocity of the cam contact point on the follower and the velocity at the corresponding points on the instantaneous radius of curvature .

$$U_{c1} = U_c = (r_b + y)\omega = (R_c - \frac{a_f}{\omega^2}) \quad \text{Equation 2-28}$$

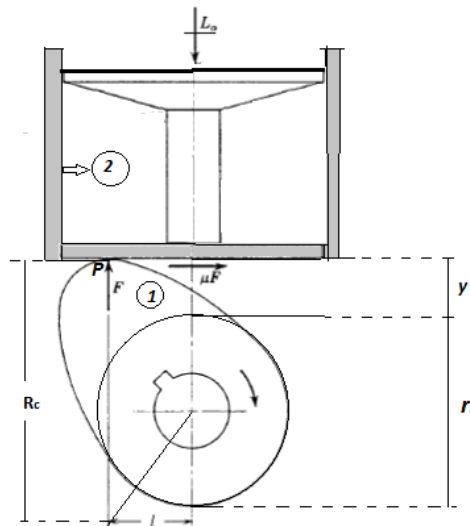


**Figure 2-13 Geometry of Direct Acting Cam and Follower [12, 13]**

## 2.8. Operating Conditions for Cam Follower Contacts

The cam follower component undergoes huge dynamic variation in load and applied stresses. Despite the appreciation of its importance from various research work [4],



its tribological/tribochemistry characteristics are not thoroughly understood; which is a direct reflection of its complexity. Based on engine designs, the operating conditions at the contact can also vary. A typical example is in high performance engine (Formula 1) where a pneumatic type finger follower is employed. This system experiences higher contact pressure than the DAMB counterparts.

**Table 2-3 Showing the Operating Conditions In A Typical Cam Follower System [9, 11, 79]**

Parameter	Cam follower – Normal passenger cars	High performance engines (Formula 1)
Temperature	80 – 120 °C	100 – 160 °C
Maximum Pressure/load	0.5 – 0.75 GPa	1.2 GPa max.
Speed	250 – 3000 rpm	7500 rpm
Minimum film thickness	0.1 -0.15µm	0.08-0.10µm
Power Rating (losses)	0.04-0.20 KW	-
Minimum Shear rate	10 <sup>7</sup> s <sup>-1</sup>	-
Composite Roughness	20 – 30 nm	10 – 15 nm

## 2.9. Tribometers Used to Simulate Cam Follower Contacts

Laboratory tribometers are used to conduct experiments to simulate engine components under controlled environments, often following prescribed international and instrumentation standards such as the ASTM, ISO, and Cummins M11 HST. Though the friction, wear and lubrication characteristics are obtained with a high degree of confidence, the fundamental question is how applicable these laboratory data are to the real engine system. According to reports from Czihos [80, 81], this section outlines some of the tribometers used for laboratory studies of tribology/tribochemistry as well as their operating conditions which typically falls below real fired engines.

### 2.9.1. Miniature Traction Machine and Space Layer Interferometry

Current developments in instrumentation have led to the design of more sophisticated rig for measurement of friction, wear and lubricant film thickness. The miniature traction machine (Figure 2-14a) is mostly employed with a Space Layer Interferometry Method (SLIM) as shown in Figure 2-14b, for lubricant film thickness on additivated ZDDP oils [82]. Different slide-roll-ratios can be set up on this device and optical interference image can be done **in-situ**. SLIM is an effective way of mapping out optical lubricant film thickness in mixed/elastohydrodynamic contacts which is usual converted to the real film thickness with refractive index of 1.60 for phosphate glass [83]. This is however an indirect method as the antiwear films are complex and, extremely thin made up of a composite structure of ZnS, Zn Phosphates, FeS<sub>2</sub>, oxides etc. The typical operation temperature with this device is 100 °C, and the applied load can vary up to 31N (corresponding to an applied stress of approximately 1.0GPa). It is worthwhile to mention that the tribological interacting system is similar to a ball on disc device where ball and disc can be driven by different small electric motors for the variation of slid roll ratio. It is limited from an actual cam follower rig by the **operating** speed, load carrying capacity and lubrication system

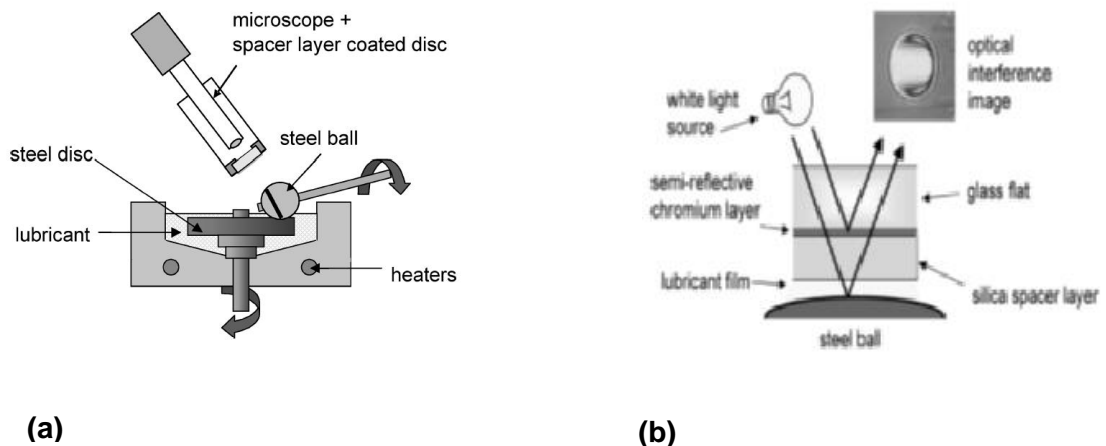


**Figure 2-14 (a) Miniature Traction Machine [82] and (b) Space Layer Interferometry Mapping [14, 83]**

### 2.9.2. Pin-on-Reciprocating Plate Tribometer

Pin on disc tribometers are widely used to simulate the piston cylinder component of an engine where the cylinder (pin) is stationary and the disk (Piston) is made to rotate. However, there have been situations where they were employed for simulating the cam follower system by using contact pressures which occur at the cam nose [77,

84]. Assessment of the linear force measurement of the stationary component is a direct indication of the frictional force of the system. However, pin misalignment, volume wear measurement and reduction of contact pressure with system operation are fundamental problems with this system. In reality, the piston is not only in reciprocating motion. Lateral deflections within the cylinder are also common. The above notwithstanding, Pin on Disc tribometers are widely used as laboratory screening tribotesters for cam follower and piston cylinder assembly. Kano [32] and Haque [85] employed pin on disc for evaluation of materials and lubricants in a cam follower system. Morina et al. [86] evaluated the effects of temperature on MoDTC and ZDDP tribofilm with a pin on disk. Temperature was observed to affect the ratio of friction reducing  $\text{MoS}_2$  to the high friction specie  $\text{MoO}_3$ . Details of a pin on disc tribometer and typical operating conditions are given in Figure 2-15

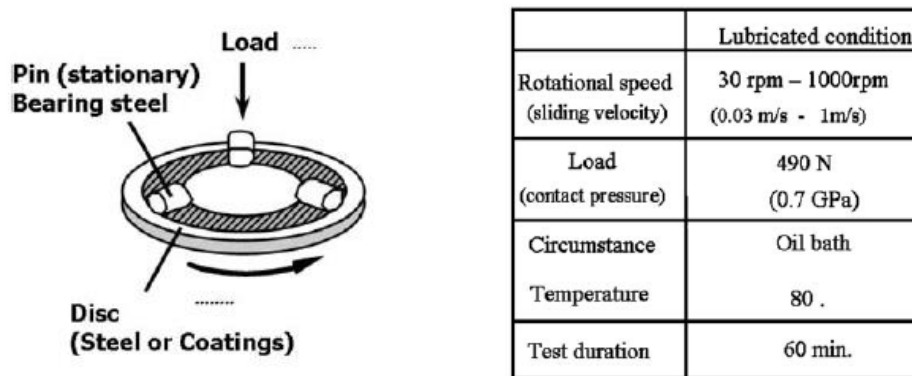


**Figure 2-15 Pin on Disc Tribometer and Typical Operating Conditions [32]**

### 2.9.3. Single and Multiple Cam Rigs

The single cam tribometer (SCT) is the most amenable test apparatus for the study of tribological behaviour of the engine valve train. In light of several designs of cam follower mechanisms discussed in **Table 2-1**, the direct acting tappet bucket type follower (**DAT**) will be the focus of this study. Several researchers [18, 21, 22, 27, 39, 87-89] have developed or used Single/multiple cam tribometers to solve different valve train engine applications problems because it closely mimics the operating condition of a real engine. In Figure 2-16, Kano used SCT for the study of ester containing oils. Kodai Gangopadhyay and co-workers [87, 90] have examined friction and wear of cam tappets with various surface architectures and lubricant additives. Uy et al [88] studies valve train tribochemistry with a valve train rig and compare data with cylinder on flat, ball on flat experiments. **AES, RAMAN** and **IRRAS** were used

for the characterisation of the tribofilms. There were close similarities with the films formed on the tappets in the valve train experiments. Fresh oil tests on tappets revealed calcium phosphates, sooty carbon, calcium carbonate, Mg, Zn, succinimide and hydrocarbon. Laboratory tribometers showed similar species with some  $\text{FeS}_2$ . Haque et al [77] have shown that the lubricant additives can affect HDLC durability for valve train application. Ito evaluated cam follower wear with a push rod assembly shown in section 2.5. Shaub and Wong [43] also studied overhead camshaft wear and lubricant formulation using radionuclide method. Camshaft was activated and the degree of increase in activity of the lubricant was indicative of the wear. Hamilton [21] also study valve lubrication with capacitance gauges. Significant difficulties were observed but the author suggested that the lubricant film thickness should be five times greater than surface roughness to improve tribopair interactions.

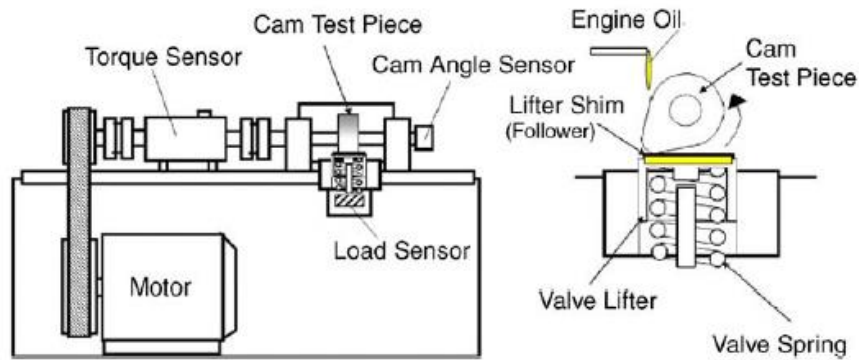


**Figure 2-16 Single Cam Test Rig [32]**

Booth [40] also employed electric charge for real online monitoring or scuffing detection on a multiple TU77 cam rig. The technique proved to be viable for the assessment of valve train wear. Willermet [91] derived ZDDP antiwear films on cam tappet which was studied with infra-red spectroscopy. This was to understand the nature of antiwear films and how they can be optimised in both valve train systems and lubricant formulation chemistry. Mistry [39] studied the friction and wear of DLC coated tappets in formulated oil of PAO, ZDDP and MoDTC with single cam tribometer. Friction and wear [22, 88] studies with single cam tribometers have also revealed that aged oil can improve the tribological characteristics. However this should not be extended to the overall improvement of an engine tribosystem. Cam followers operate in the mixed lubrication regime where considerable increase in viscosity due to soot in aged oil may not adversely affect the tribological system. For components like piston ring/liner and bearings where hydrodynamic lubrication

regimes persist, increase in viscosity increases the friction/wear mechanism of the tribopair. In a vast majority of the literature studied, most tribological tests are carried out in steady state which is hardly ever this case—**significant gap**. Development of single cam tribometers which can simulate some transient effects will shed more light on valve train tribochemistry.

## **CHAPTER 3. VALVE TRAIN TRIBOCHEMISTRY: LUBRICANTS, LUBRICATION AND THE ROLE OF ADDITIVES**

### **3.1. Engine Tribochemistry at the Cam Follower Interface**

Engine tribochemistry is a branch of tribology that deals with the chemical reactions that take place due to interfacial friction and/or wear on interacting surfaces in the presence of lubricants. These chemical reactions involve the formation of tribofilms at the surface of interacting asperities with significantly different characteristics from the fully formulated/model lubricant and the properties of these films governs the tribological behaviour or more precisely friction and wear responses of the system. The nature of the films formed depend on the nature of interacting surfaces, temperature, lubricant chemistry, materials, relative motion and contact pressure. The cam follower motion is a combination of sliding and rolling. The degree of sliding or rolling depends on the design of the cam profile. For automobile cams, sliding motion around the cam nose was estimated to be around 60% which was responsible for the high friction and/or wear in this region [92].

### **3.2. Lubrication, Lubricants the Role of Additives**

Lubrication is the interposition of a substance between interacting surfaces to reduce friction and/or wear while the lubricant is a solid, liquid or gaseous substance which is fundamentally used to minimise friction and wear on interacting surfaces. In a much broader sense, lubricants are used to achieve the following;

- maintain cleanliness,
- reduce friction/wear,
- minimise oxidation/corrosion,
- regulate soot and sludge handling, and
- prevents overheating or provides cooling on engine surfaces.
- increase the lubricants ability to flow at low temperature (pour point depressants)
- should help reduce CO<sub>x</sub>, NO<sub>x</sub> particulate and hydrocarbon emissions.

These versatile properties are conferred by substances referred to as lubricant additives. They include friction modifiers, antiwear additives, dispersant, detergent, viscosity index improvers, corrosion inhibitors, pour point depressant and host of other components. This section of the report discusses key lubricant

additives of antiwear (ZDDP), friction modifiers (MoDTC), organic friction modifiers (Esters -GMO), detergents and dispersants.

### 3.3. Lubricant Additives

An engine lubricant consists of about 10 – 25 % additives. By careful selection of the additive type and quantity employed in service, lubricant formulators provide products which lead to better performance and long life of mechanical components.

### 3.4. Antiwear Additives

These additives help reduce wear, adhesion (scuffing) and scoring on interacting surfaces, by forming nanoscopic tribofilms between 50 – 150 nm thick. ZDDPs are by far the most commonly used although components such as the organo-chlorides, organophosphorus compounds, borates, amines and organosulphur are also used as antiwear additives [3, 82, 83, 93, 94].

Due to environmental concerns, ZDDP concentrations are decreasing in engine oils. These have led lubricant formulators to put major resources on the development of new antiwear additives. Determination of synergistic interaction and also using the right concentration in a lubricant product are also crucial in improving the performance of engine components.

#### 3.4.1. Zinc Dialkyl Dithiophosphate Phosphate (ZDDP)

Zinc di-alkyl dithiophosphate (ZDDP/ZnDTP) is the most widely used antiwear additive (AW) in engine oil formulations. It has unique characteristics as an antioxidant, corrosion inhibitor, antiwear additive [93, 95, 96] and extreme pressure agent [15]. The chemical structure of this compound is shown in **Figure 3-1** but it should be mentioned that more complex structures are observed in solution

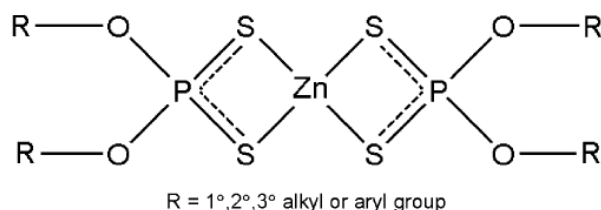


**Figure 3-1 Structure of Zinc Dithiophosphate [96]**

ZDDP exhibit their antiwear properties by the formation of tribofilms, however, how these films are formed is still unclear. These tribofilm affect the friction and wear

properties of the system. In a paper by Morina et al [3], the friction coefficient with ZDDP additivated oil changes with increase in temperature, which increases the rate of film formation on the surface even though a corresponding decrease in oil viscosity is observed. Several works have shown that the thermal instability and antiwear effectiveness is determined by the alkyl group (R) [93, 97].

Secondary Alkyl > Primary alkyl > aryl

Equation 3-1

### 3.4.1.1. ZDDP – Thermal Degradation in (Hydrocarbon) Solutions

At high temperature typically around 150-230°C, ZDDPs undergo an autocatalytic thermal decomposition reaction with mercaptides, alkyl sulphide, H<sub>2</sub>S and olefins as volatile products [93]. The main thermal films are made up of glassy insoluble phosphorus species, oxygen, Zn with some sulphur [93, 96, 97]. It is important to mention that the rate of degradation increases with increasing temperature (Ref Figure 3-2) [95] and activated by the presence of acids and not oxygen [93, 97]. Thus, as temperature increases, the concentration of the ZDDP in solution decreases in an asymptotic manner.

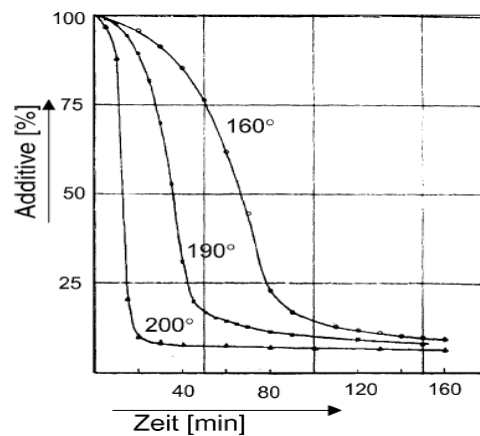
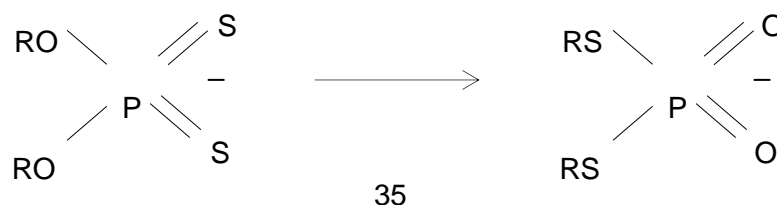


Figure 3-2 Thermal Degradation of ZDDP[93]

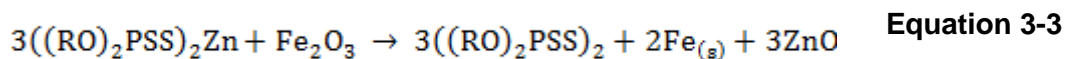
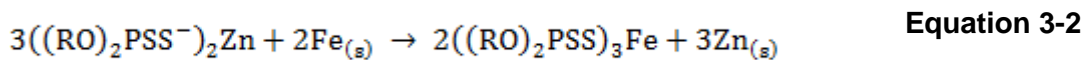
It has also been suggested that the thermal degradation process gives rise to the formation of an intermediate ligand isomer commonly referred to as O/S exchange isomer [97, 98].





### 3.4.1.2. ZDDP Adsorption on Metal Surfaces

Adsorption of ZDDP reaction films on interacting surface is essential for the prevention of wear on machine components. According to Wu and Dacre [99] the adsorption process is temperature dependent with significant physisorption at 1000C while chemisorption is dominant at >1000C. The adsorption process is also dependent on the interacting surface. Studies [100] have demonstrated that with iron, adsorption occurs at temperatures (in the range of 35-88<sup>0</sup>C) with some release of Zinc, while no zinc loss occurs with steel. This is in agreement with the works of Homann et al. Aktary et al [101] studied the growth of ZDDP films on gold at 150<sup>0</sup>C using SFM and IRRAS The authors observed thermal films with thickness of 420nm after 6hrs of testing. Piazza found that adsorption of ZDDP on iron increases with ZDDP concentration. Experimental studies reveal that this reaction take place through sulphur atoms in the P=S bond which suggests formation of iron dithiophosphate (Ligand/cation exchange) or hydrolysis by surface water or hydroxides [93].



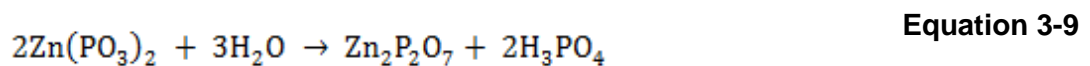
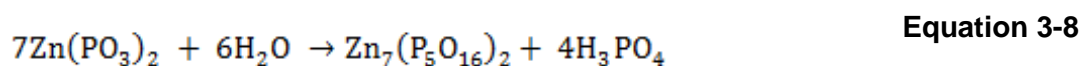
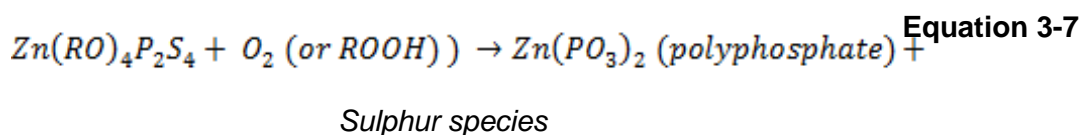
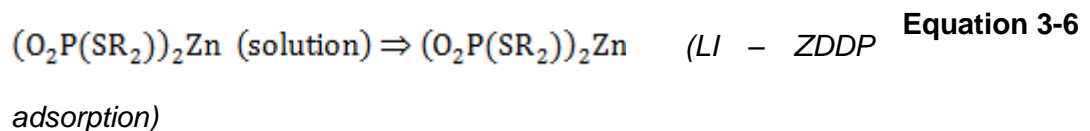
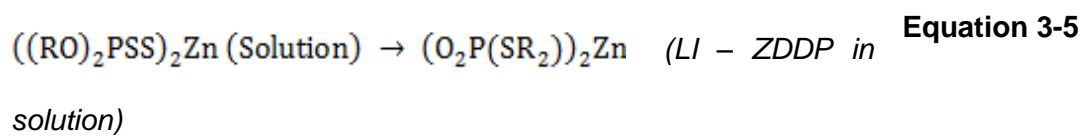
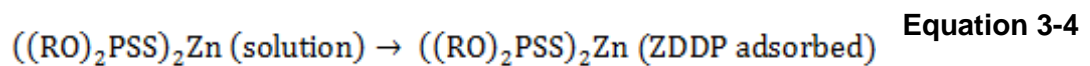
### 3.4.1.3. ZDDP Tribofilm Formation and Thickness

Even more puzzling is the film formation mechanism of ZDDP antiwear additives. Despite extensive research, mechanism of formation is still not well understood. In the literature, studies have focused on both the thermo-oxidative and tribochemical films derived from ZDDPs, yet, slight difference has been observed with tribofilm; revealing high concentration of ionic species on the surface. The forerunning decomposition mechanism which led to the formation of antiwear films was proposed by Willermet et al [102].

- ◇ Adsorption of ZDDP on metal surfaces
- ◇ Reaction of ZDDP with metallic surfaces to form phosphates species and phosphothionic parts which adhere to the metal surfaces
- ◇ ZDDP anti-oxidation reactions give rise to the formation of phosphate film precursors

- ◇ Condensation of phosphate/phosphothionates and their ester with the phosphate chains being terminated by the cations from ZDDP itself ( $Zn^{2+}$ ), metal substrates ( $Fe^{2+}$ ,  $Fe^{3+}$ ) or other cations (e.g.  $Ca^{2+}$ ,  $Mg^{2+}$ ) present in the dispersant/detergent

Other authors [98, 103, 104] have proposed slightly different formation mechanism. Yin et al [103] studied ZDDP films using X-ray adsorption near edge spectroscopy (XANES) and proposed three step mechanism with the formation of iron pyrophosphate ( $FeZnP_2O_7$ ) or iron orthophosphate ( $Fe_2Zn(PO_4)_2$ ) as possible final reaction pathways. Fuller et al [98] postulated a mechanism applicable to both thermal and tribofilm using XANES with the formation of an intermediate compound referred to as a Ligand Isomer. The process is expressed with the equations shown below;



#### 3.4.1.4. ZDDP/Steel Tribofilm: Friction and Wear Properties

Investigations into different ZDDP tribofilms using SEM/EDX and a reciprocating wear tester, showed that ZDDP types significantly react differently but the films typically consisted of Zn, P, S, and O [105]. IR spectroscopy studies of ZDDP derived tribofilm from fully formulated oils using a carbon steel cam and tappet rig, revealed they are composed of amorphous orthophosphates and pyrophosphate [91]. This is in contrast

with a vast majority of the literature [93, 98, 104, 106, 107]. However, it should be pointed out that IR is a bulk sensitive technique. Pereira [108] examined ZDDP films on AISI 52100 steel using XANES. The thick pads consisted primarily of medium chain polyphosphates with sulphur present primarily as ZnS. Yin's [103] report suggested a layered structure of ZDDP tribofilms composed of Iron oxide interwoven with short polyphosphate covered by thin long chain metal phosphate.

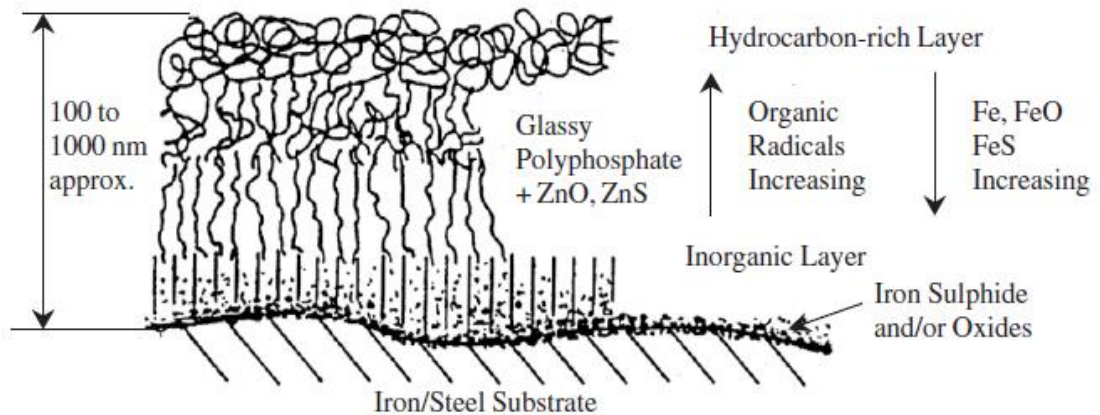


**Figure 3-3 Structure of Antiwear Pads From ZDDP [109]**

Beneath the hydrocarbon rich layer, there exists a thin form of padlike Zn and or Fe polyphosphates. Close to the metal surface, films are predominantly composed of iron and its oxides. The pad like polymer structural film has a rough texture and has been reported to increase friction on interacting surfaces [83]. This is in contrast with the report of Crobu [110]. This additive has been found to change its properties based on the operating conditions. This feature is responsible for the success of the material as an antiwear additive and also accounts for the variation observed in both its reaction kinetics and film formation components. Its action on wear reduction has been dependent on the type of ZDDP and concentration (typically between 0.01 to 1.0% by mass) though vast majority of reports indicate that its performance as an antiwear additive is exceptional.

Despite its unique characteristics, attempts are been made to minimise its use in gasoline and diesel engines. The reason is because, it poisons the action of three way catalyst in gasoline engine by reaction with phosphorus and sulphur, thus leading to deactivation. In diesel engines, during high temperature combustion the metallic Zn form ash which clogs the diesel particulate filter (DPF), eventually inhibiting fluid

flow and retarding engine performance. This study intend to assess the effects of mid SAP and normal SAP containing oils for valve train application with the aim of understanding how lower concentrations of sulphur and phosphorus in oils affect engine friction and wear.

### **3.5. Friction Modifier Additives**

Just as their names suggests, they reduce the friction between interaction surfaces in boundary/mixed lubrication regimes by forming thin tribofilm which maybe physisorbed or chemisorbed on the surface. Esters, amides and some metal soaps have been employed to reduce friction on the valve train with up to 40 % reductions [111]. The most widely chemisorbed friction modifier is MoDTC which forms MoS<sub>2</sub> sheets [112, 113]

#### **3.5.1. Molybdenum Dithio Carbamate (MoDTC) Friction Modifier**

MoDTC is an effective friction modifier used in engine oil formulations. It has been demonstrated that this additive gives rise to the formation of MoS<sub>2</sub> during tribochemical reactions [64, 84, 114, 115]. Grossiord et al [114] proposed a two-step process to the formation of MoS<sub>2</sub>. First step involve electron transfer from Mo-S to form three free radicals corresponding to the core and chain end radicals. Steps are shown in **Figure 3-4**. Studies with MoS<sub>2</sub> coatings in vacuum conditions have demonstrated that they exhibit super lubricity with friction coefficient as low as 10<sup>-3</sup> [114] which clearly supports MoS<sub>2</sub> as the fundamental compound responsible for low friction. MoS<sub>2</sub> have strong covalent bond between atoms but the lamellar layered lattice enjoys weak Van der Waal interactions which give rise to low friction. The use of current surface analytical techniques such as XPS, TEM, EELS, and SEM/EDX to elucidate the structure and promote understanding of MoDTC films are imperative. XPS surface analytical tests have revealed that the higher MoS<sub>2</sub>/MoO<sub>3</sub> ratio, the lower the friction coefficient [64, 86].

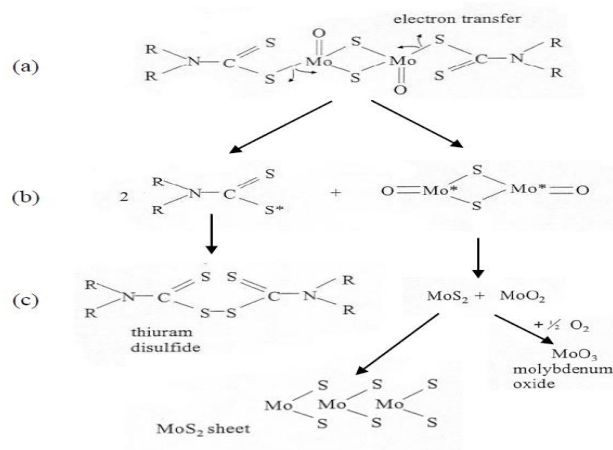


**Figure 3-4 Mechanism of MoS<sub>2</sub> Formation from MoDTC: Chemical Model [114]**

Using XPS, evaluation of the tribofilms on a:C-H/Steel tribopair indicate that they produce films with MoS<sub>2</sub>/MoO<sub>3</sub> ratio greater than five times those observed in a:C/Steel tribopair [64]. This can be attributed to the high reactivity of hydrogenated DLC's. The corresponding XPS photopeaks are shown in **Table 3-1**

**Table 3-1 XPS Photopeaks of Molybdenum compounds**

Element(Oxidation Number)	Compound	XPS Binding Energy
Mo3d (IV)	MoS <sub>2</sub>	229.7 eV
Mo3d(V)	MoDTC	231.0 eV
Mo3d(VI)	MoO <sub>3</sub>	232.7 eV

A more recent MoDTC reaction pathway has been proposed by Khaemba et al [116] with Raman spectroscopy, where FeMoO<sub>4</sub> was identified as the reaction species which is probably responsible for the high friction as opposed to MoO<sub>3</sub>. This was characterised by the observation of distinct Raman peaks at 335 cm<sup>-1</sup>, 453 cm<sup>-1</sup> and 925 cm<sup>-1</sup> corresponding to amorphous sulphur rich compounds - MoS<sub>x</sub> (x>2) and FeMoO<sub>4</sub>. The schematic of the reaction pathway is shown in Figure 3-5.



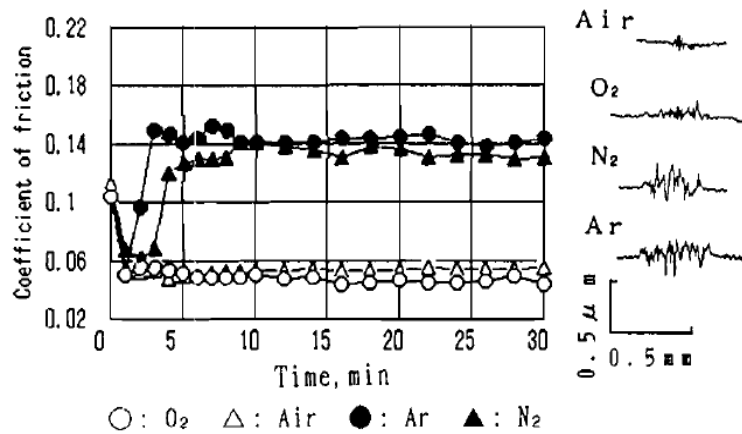


**Figure 3-6 Effects of Environment on Friction and Surface Roughness in Oils Containing MoDTC [118]**

In terms of wear reduction, during the induction stage of tribofilm formation, Mo-FM form nitrogenous compounds with significant wear reduction properties [119].

### 3.5.1.3. Ester-Containing Engine Oils

Unlike mineral oils, they do not decompose at high temperature but significantly improve engine cold starting. In the 1970's they were used to confer anti-corrosion and non-emulsion properties in turbine oils and diesel engine fuels [120]. During this period, their application was more widespread than conventional Mo-FM but followed a decline until the 20<sup>th</sup> century. However, due to current environmental legislation and their biodegradability characteristics, they are finding increasing application in lubricant formulation. Their volatility characteristic can be improved by the esterification process with the selection of the optimum carboxylic acid and di(poly) alcohol. Details can be found elsewhere [121, 122]. One significant advantage with esters is that they are compatible with mineral oils and synthetic oils (e.g. PAO). Engine lubricants composed of mineral and synthetic ester additives are referred to as semi synthetic oil and less commonly as hybrid oils.

Small proportions between 0.05 to 0.2wt % of glycerol fatty acid esters (GMO or GMO/GDO) have improved engine fuel economy by 1 – 3 % (see Table 3-2 for LEFET result). This GMO was blended into reference oil with 2.10% dispersant, 1.10% antioxidant, 1.00% basic metal detergent, 1.95% antiwear additive of ZDDP, 0.21% of pour point depressant and 0.001% antifoam [123]. Using a Low velocity friction tribometer (LVFM) with Mobil 1 as reference oil, mineral oil composed of Mobil 1 with

additions of 4 wt% GDO performed better than GMO and sorbitan monooleate (SMO) at low speed. 21% reduction in sliding friction was attained [120].

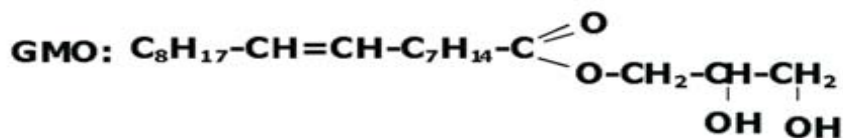


**Figure 3-7 Chemical Structure of GMO [111]**

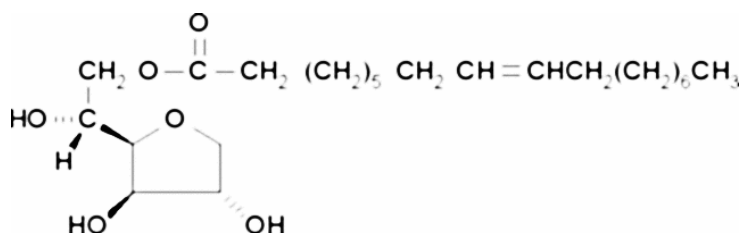


**Figure 3-8 Chemical Structure of Sorbitan Monooleate [120]**

The chain length of the ester appears to have effects on the friction and wear characteristics of the system. Test with long/branched chain GDO and SMO gave lower friction values at low speed. This suggests that they are capable of withstanding high contact pressures inherent in boundary lubrication regimes. Some ester additives possess both antiwear and friction reduction properties. A typical example is a diester (DIOD) of dodecanedioic acid where 10wt% additions into 10W40 improved friction in a four ball tribometer by 27% with astonishing wear benefits of 45%. Sequence engine test of this oil with part synthetic SAE0W30 performed remarkably with 3.7% fuel economy [124].

**Table 3-2 Effect of Ester Friction Modifiers on Engine Fuel Economy [123]**

Laboratory Engine Fuel Economy Test (LEFET)		
Engine Condition	Fuel Economy Credits in Percentage (%)	
	GMO	GMO/GDO
1 (Idle)	4.0	2.6
2 (30mph)	2.5	3.0
3 (30mph)	1.5	1.8
4 (150mph)	0.9	0.6

Adipates synthetic ester (e.g. TMPA, DTDA) have also been used as base oil but their additive solubility, compatibility with elastomers, and antiwear properties with ZDDP



are not very promising [124, 125]. This can be mitigated with Boron containing compounds which reduce their aggressiveness toward elastomers [126]. Certain organic amides (with C, H, O, N) provide good friction reduction with excellent high temperature decomposition characteristics, thus leading to engine cleanliness [127]. It is important to mention that these studies [120, 122, 123] were carried out on Fe-based surfaces. Currently, ester containing oils have proved to provide even better engine efficiency when used in combination with certain DLC coatings.

### 3.5.2. Detergents

These additives play a significant role in the neutralisation of acidic products which have been formed during the combustion processes in an engine. They equally prevent formation of lacquers and the deposition of unwanted material at high temperature on metal surfaces [128, 129]. Detergents keep the surfaces clean thereby preventing wear particles or decomposition products from being trapped on interacting surfaces. This can help reduce third body abrasive wear on pistons, valve train and bearing components

### 3.5.3. Overbased Ca/Mg Sulphonates: Friction, Wear and Tribofilm Properties

In the selection of an appropriate detergent, factors such as metal to sulphonate ratio, particle size and alkali metal, are of great importance for application on tribological systems [130]. Over based Ca/Mg sulphonate are the most widely used detergent additives with varied characteristics as antiwear, rust inhibitors and friction modifiers. They can provide adequate wear protection in mild condition [131] but in highly stressed systems such as four ball tests and valve train systems, their films begin to fail and the wear protection is lost. Typical structure of sulphonate type detergent is shown below.

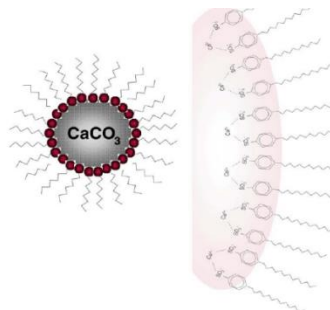


**Figure 3-9 Structure of Overbased Calcium Sulphonate [129]**

Depending on the type of detergent (neutral, basic or overbased), the friction can be reduced or increased [129, 130, 132-134]. This variation has been attributed to the structure of the alkyl chain in the sulphonate detergent molecule [129] as well as the metal cation [130]. On the other hand, OBCaSU have been observed to reduce the wear in comparison to base oil with concentrations from 1 -3% [132]

Based on the purity of the calcium carbonate core, the tribofilm can be composed of  $\text{CaCO}_3$  (in the form of Calcite),  $\text{CaO}$ ,  $\text{Ca(OH)}_2$ , and some residual calcium sulphonates [1, 128, 129, 132-135]. According to Kubo [135],  $\text{CaO}$  was obtained from the decomposition of  $\text{CaCO}_3$  during friction testing on steel surfaces. Continuous testing increases the thickness of the  $\text{CaO}$  film. These reports are in agreement with report of Costello [1] where XPS depth profile showed a thin layer of  $\text{CaCO}_3$  at the top of the surface and a thick  $\text{CaO}$  layer underneath after prolonged testing. EELS investigation of the tribofilm also reveals oxidation reaction from  $\text{C}=\text{C} \Rightarrow \text{C}=\text{O}$  with the wear scar region having lower concentration of Carbon and Fe [131] However, current investigation on DLC surfaces have revealed that the  $\text{CaO}$  layer formed are considerably very thin and can be transferred to the counterbody with high friction characteristics [135]. This should equally affect the wear properties of the system. Typical model structure of overbased detergent tribofilm is shown in Figure 3-10

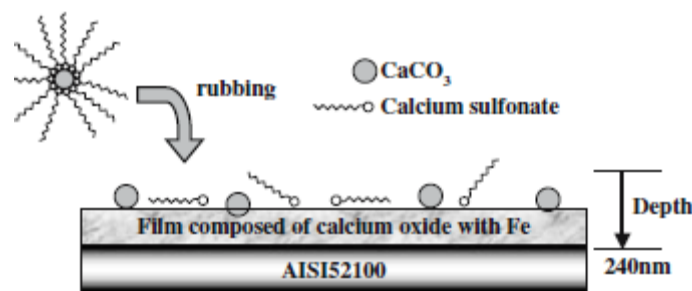


**Figure 3-10 Model structure of OBCaSu [134]**

Using various surface analytical techniques, these additives typically form films with 95- 200 nm thickness when observed with MTM-SLIM. Using PM-IRRAS and ellipsometry, Palermo and coworkers [136] obtained the film thickness of OBCaSU to be 80 nm while Kubo et al [134] showed the detergent tribofilm to have a thickness of 240 nm with TOF-SIMS. The varying thicknesses can be attributed to different operating conditions of applied load, temperature and rubbing time. The films are heterogeneously compact and have hardness between 0.001-0.1 GPa

### 3.5.3.1. Overbased Phenates and Salicylates Type Detergents

In phenate overbased detergents, the excess metal cations do not form the core neither do they form micelles. The calcium carbonate is incorporated into a long chain with aromatic ends bridged by a sulphur atom as shown in Figure 3-11 [137, 138]. According to reports from O'Connor et al [138], phenate type additives usually possess better friction and wear [139] characteristics than overbased sulphonates, and salicylate type detergents. Under high pressure conditions, their friction coefficient typically lies between 0.09-0.14 which is very similar to ZDDPs at 0.12-0.14.

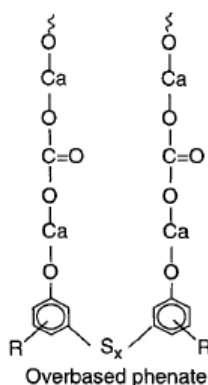


**Figure 3-11 Structure of an Overbased Calcium Phenate Type Detergent [137]**

The advantage of phenate over their sulphonate counterparts is their ability to give lesser deposits during combustion [139]. In three component systems with ZDDP and Sulphonate detergents, some benefits have been achieved [139]

### 3.5.4. Dispersants

These additives prevents the agglomeration on insoluble substances formed at low temperature. They achieve this action by ensuring that unwanted substances remain suspended and finely dispersed on the surface of the oil. The most widely used dispersants in engine oils are the poly isobutylene succinimide (PIBSA) [2] and they are reactive on carbonaceous surfaces [140]. This additive essentially gives rise to greater wear than OBSaCu and ZDDP additives [2, 139-142].

In the selection of dispersant, significant care should be taken on the concentration and structure/amount of the nitrogen in the molecule. In a high pressure four ball test, it has been demonstrated that a high concentration of PIBSA increase the wear scar until a steady state is reached [139]. The mechanism for this increase in wear was

investigated by Inoue and Watanabe [142], by using adsorption isotherms. It was proposed that PIBSA cover nascent iron surfaces necessary for the decomposition of the ZDDP. In terms of structure, Ramakumar and coworkers [139] showed that PIBSA molecules with high N concentration form more stable complexes in oil solutions containing ZDDP. This strongly inhibits or eliminates the film forming properties of the ZDDP additives. This effects of N concentration can be mitigated by treatment with ethylene carbonation or boration as report by Zhang et al. [2] and Shirahama [141].

### **3.6. Antioxidants**

They inhibit or delay the oxidation of additives in the oil thereby preventing the breakdown of additives in the oil. Oxidation in oil gives rise to the formation of acids, vanishes and lacquers which are detrimental for optimum tribological performance of engine components. ZDDPs are widely recognised as antioxidants. This is carried out by the decomposition of hydro-peroxides and peroxy radicals. The latter is a crucial step in the degradation of hydrocarbon in the oils. By inhibiting this step, huge benefits can be conferred to the engine oils.

### **3.7. Pour Point Depressant**

These additives enhance the lubricants ability to flow under extreme low temperatures. This will help reduce the pump power required to transport the lubricants through the cylinder head, bearings and other components of the engine.

### **3.8. Engine Oil Additives – Additive/Additive Interactions**

#### **3.8.1. ZDDP/MoDTC Interactions**

This is one of the most widely reported interaction of lubricant additives. It provides improved friction and better wear performance than any of the singular additives. While the ZDDP provide more sulphur atoms involved in the formation of MoS<sub>2</sub> Sheets – which reduce friction, the MoDTC also provide nitrogen which improve the wear properties of the tribofilm [84, 143].

Using XANES analysis [144], it was demonstrated that the uppermost layer of the film consists of ZnS while a dense matrix of metal phosphate and MoS<sub>2</sub> sheets was observed in the bulk. At concentrations <500 ppm, the films are composed of short chain phosphates [144] which have a detrimental effect on the wear of highly loaded valve train systems [145]

MoDTC was not the interest of this study but it is noteworthy to mention its friction modifying properties since it is the most widely used in its class.

### **3.8.2. ZDDP/Detergent Interactions**

Detergents are generally accepted to have an antagonistic effect on the film formation properties of ZDDP [141, 142, 146-149]. Some interaction takes place in the oil but no formation of complexes has been reported. According to Rounds [146], ZDDP peaks were slightly distorted following infrared spectras in two component systems of ZDDP/OBCaSu. This gives some evidence of a slight interaction in the liquid phase. While it has been widely reported that OBCaSu are surface active, they retard the decomposition rate of the ZDDP by raising its decomposition temperature. Following this action, they (detergent) tend to firstly adsorb on the surface and subsequently block or modify the sites necessary for ZDDP to form its padlike films. A prime example was shown using adsorption isotherm plots. Inoue [142] and Plaza [147] demonstrated that Ba/Ca sulphonates effectively reduce the adsorption of ZDDP on metallic powders. The bifilm has been reported to have a paste-like structure forming basal island that prevent the agglomeration of the antiwear films [146, 148].

Essentially, the film consists of short Ca phosphate films with increased wear than ZDDP alone [148, 149]. When used in combination with succinimide dispersant and detergents, the decomposition temperature is increased thereby leading to scuffing on valve train systems [141]. Therefore, the right combination of concentration, additive and material type can be used to overcome such challenges to ensure that the lubricant material pair is optimum in service.

### **3.8.3. ZDDP/Dispersant Interaction**

However, interactions between additives in the oil or during rubbing on metallic surfaces can inhibit or even eliminate the film forming characteristics of the ZDDP. Gallopoulos [150] and Ramakumar [139] observed additional infrared peaks when different dispersants were blended into oil containing ZDDP, indicating chemical and association reactions. The amino group or Nitrogen from the dispersant could coordinate with the ZDDP thereby forming complexes (N=P, C=N) and affecting the P=S bonds [2, 139, 140, 150]. These inhibit the film forming properties of the ZDDP during rubbing on metal surfaces. Zhang et al [2] also investigated the tribofilms formed on metallic surfaces with several dispersant/ZDDP interaction on an MTM. In some cases, no interlayered tribofilms were observed thereby leading to an increased wear on interacting surfaces.

### 3.8.4. GMO/Detergent Interactions

Organic Friction modifiers (esters) have proved to be compatible with sulphonate detergents. They both consist of a long/short hydrocarbon tail or oleophilic group and a polar end where that of the detergent is a metal ion of  $\text{Ca}^{2+}$ ,  $\text{Mg}^{2+}$  or  $\text{Na}^+$ . Detergents are used to minimise high temperature deposits of lacquers and varnishes in engine systems but it has been reported that small amount of GMO can help reduce the size/agglomeration of these monomers even further. This is illustrated in Figure 3-12

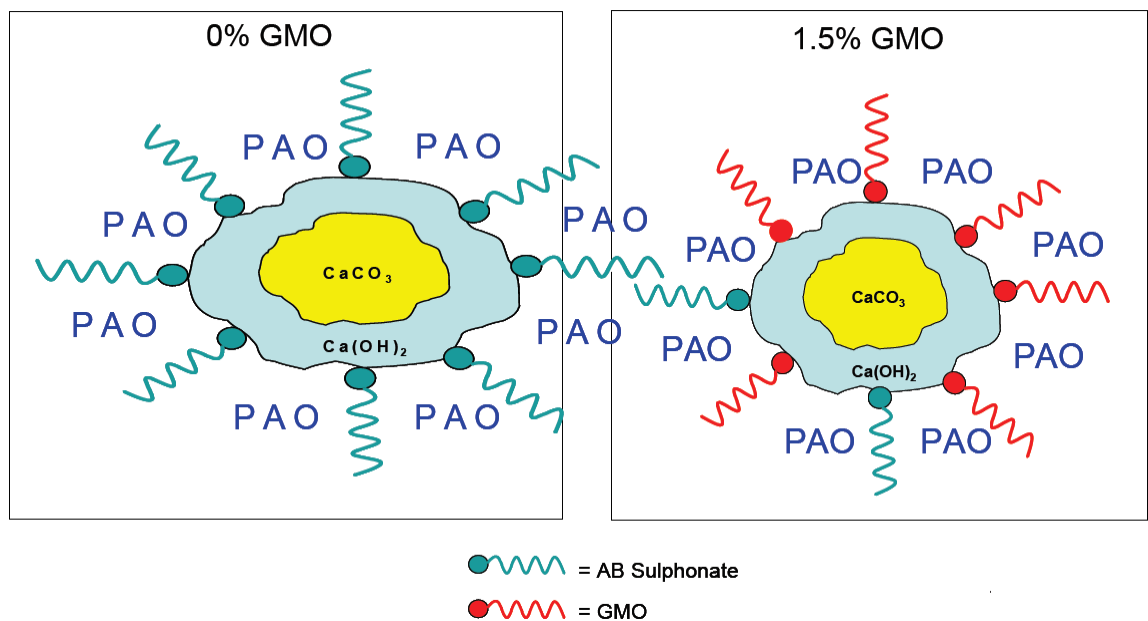


**Figure 3-12 Synergistic Action of Esters and Detergent in Minimisation of Engine Deposits [151]**

## 3.9. Additive/DLC Interactions

### 3.9.1. GMO/DLC Interactions

Different DLC surface architectures have revealed varying friction characteristics with esters. Non-hydrogenated DLC (ta:C) with 1% mass concentration of GMO had friction coefficient of 0.006 in a pin on plate tribometer but same cannot be said for a:C-H under identical operating conditions (see **Figure 3-1** for details of test) [111, 152]. Miklozic et al [152] reported that model oils composed of BO+GMO did not significantly improve boundary lubrication on Cr doped and HDLC coating. This was attributed to the inability of the tribofilm to withstand high loads and asperity contacts in low speed conditions where boundary lubrication persists. Minami and coworkers [44] observed that the steady state friction coefficients of GMO additivated oils are

lower than conventional MoDTC additives. Figure 3-13 reveals almost 50% reduction with mineral oils while lower values are achieved with polyalphaolefins (PAO)

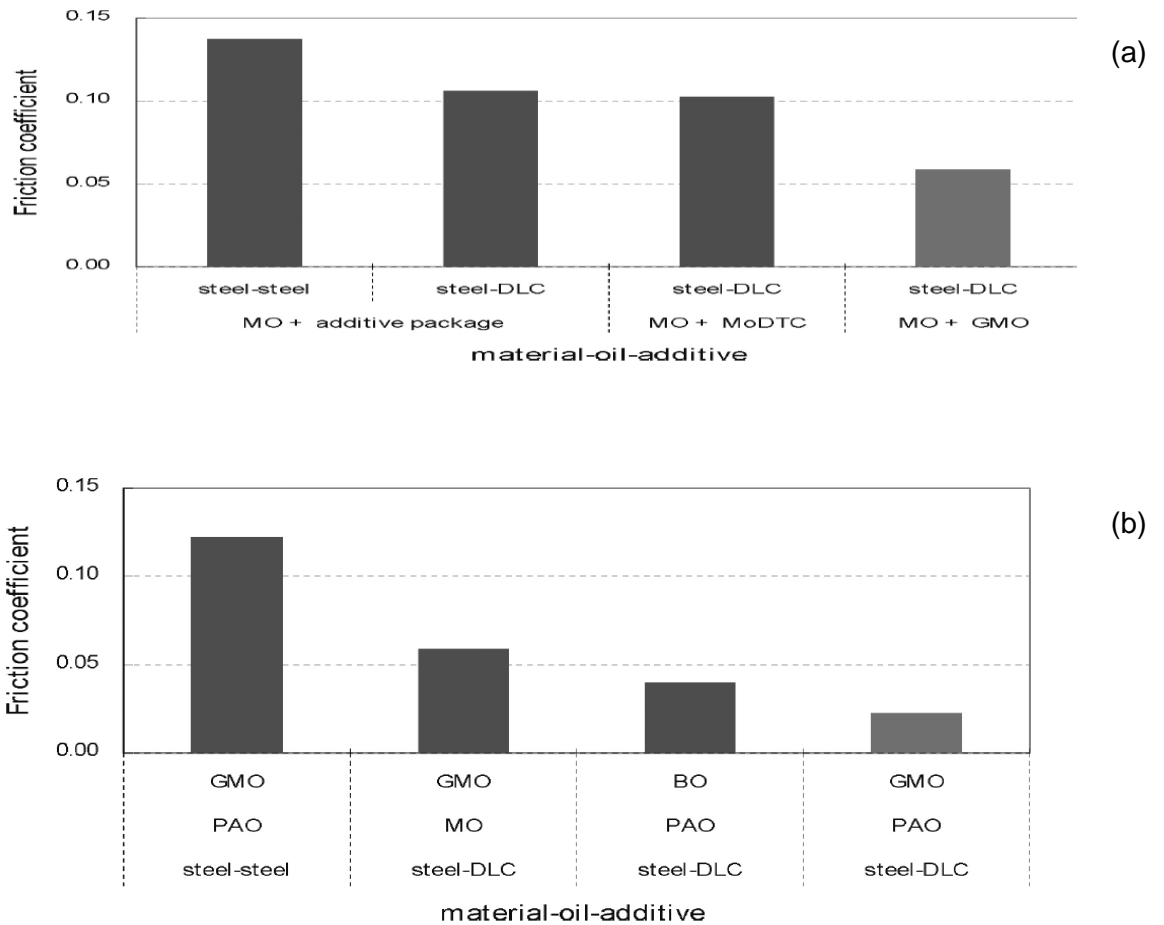


**Figure 3-13 (a) DLC/Oil Additive low Friction (b) GMO/Base oil Friction Properties[44]**

The variability of the operating conditions in each test and material production route such as dopant concentration/techniques are possible reasons for difference in laboratory results.

### 3.9.1.1. MoDTC/DLC Interactions

Not all DLCs react in the same manner. In fact, similar DLCs may not behave in an identical way. For a comparative assessment, attention must be given to the type of oil, the material and coating architectures in the submicron layer of the surface [33]. Even though a vast majority of the literature itemise the friction benefits of MoDTC/DLC interactions, for a full implementation of DLC's for valve train application, attention should also be focused on antagonistic interactions. A detailed report by

Shinyoshi [153] displays some of the inherent mechanisms of how MoDTC additives deteriorate the wear characteristics of DLC's. The decomposition pathway leads to  $\text{MoO}_3$  formations which significantly interact with C-H and dangling bonds thereby reducing the hardness of the coating. Ratio of I(D)/I(G) peaks shows huge increase and this corresponds to softer materials. Abrasive or scoring marks are clear indications of a softer materials interacting with a hard one. This is illustrated in Figure 3-14. Recently, tribotests with pin on plate device indicate that concentration of Mo-FM in fully formulated oils without ZDDP aggravate the wear characteristics of a:C-H. The mechanism was attributed to modification of mechanical properties of the coating by Mo [154]. In support of this findings, model oils containing 120ppm of MoDTC have also been reported to degrade the wear resistance of several DLCs with steel tribopairs [155]. This is illustrated in Figure 3-15 where BO is shown to have a competitive advantage in wear over Mo-FM additivated oils.

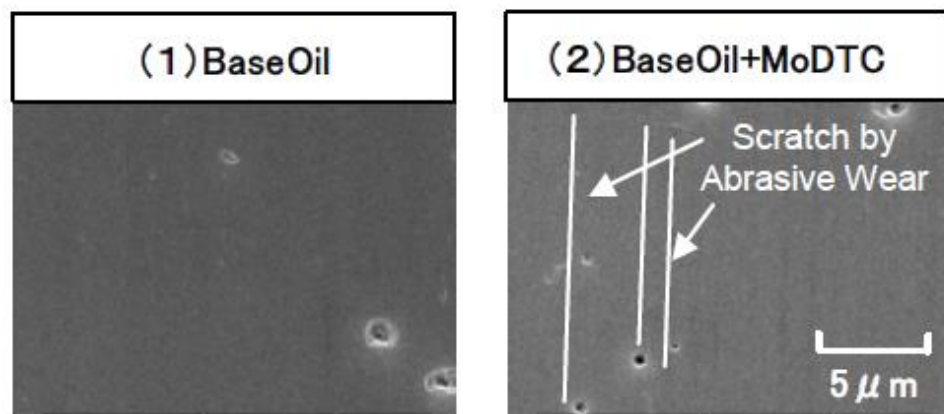


**Figure 3-14 SEM Images of Sliding Surface in Base Oil and Oil containing MoDTC [153]**

High concentration of Mo-FM (500ppm) in a pin on plate tribometer at  $100^{\circ}\text{C}$  also caused the delamination of HDLC coatings [77]. A mechanism of shear film thinning, followed by delamination has been proposed. Looking at the micrographs (see Figure 3-14) from the study of Haque et al [77] it appears a fundamental step of adhesive weakening of the coating occurs before the shear thinning process. Ashless 5W-30 GF 5 oils have also been introduced as better lubricants than Mo-FM containing oils in-lubro conditions with DLC and CrN. Mo-FM was reported to have a debilitating effect on the wear characteristics of DLC [36]. The mechanism of coating strip off due to MoDTC has not been thoroughly investigated and further studies will be required for a fundamental understanding of these processes.



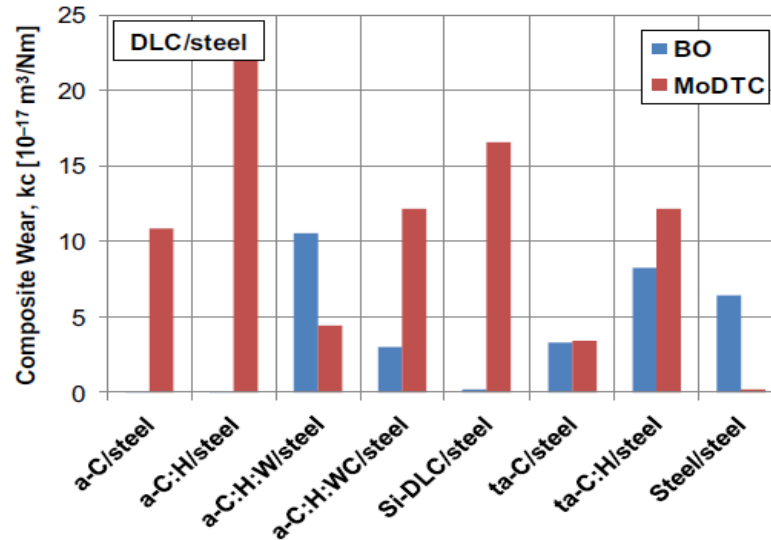


**Figure 3-15 Comparison of composite wear with BO and MoDTC in DLC/Steel tribopairs [155]**

### 3.9.1.2. GMO/DLC Tribofilms

Assessment of the super-low friction characteristics of DLC when lubricated with GMO requires very surface sensitive techniques. Time of Flight Secondary Ion Mass Spectroscopy (ToF-SIMS) is a widely used technique for the assessment of films formed by oil additives composed of Carbon, Hydrogen and Oxygen (CHO) [44, 111, 156]. Another important characteristic of this technique is that it can give the relative abundance of different atomic species/fragment ions in the mixture. In tribofilm characterization, comparison of the higher fragmentation ion of GMO ( $C_{21}H_{39}O_3$ ) with other lower fragmentation ion such as  $C_{17}H_{33}O_3$ ,  $C_{18}H_{35}O_3$ ,  $C_{16}H_{29}O_3$ , relative abundance in the ratio 2:1 was observed. Static mass spectrometer was also used to identify ions of specific masses. Significant increase in  $OH^-$  was observed on the tribosurface. This clearly indicates a friction induced rapid decomposition of GMO to yield  $OH^-$  (see Figure 3-16) [111]. As means of investigating ester containing additives, representation of GMO molecule into measureable products that are indicative of the original molecule can aid in post experimental test. One common candidate is glycerol. In a report by Habchi [157], glycerol was observed to dissociate at the tribocontact to produce water and other species. Matta [158] examined the boundary lubrication of ta-C with glycerol and  $H_2O_2$ . Ultra-low friction ( $\sim 0.025$ ) was observed with glycerol while  $H_2O_2$  exhibited corrosive properties with steel because it is a weak acid.

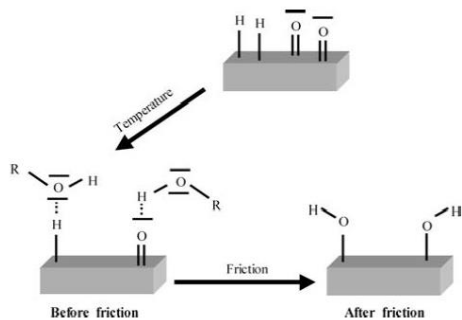


**Figure 3-16 Hydroxylated Films Formed by Ester Containing Additives[111]**

XPS spectra (see Figure 3-17) of regions inside tribofilm reveal significant contributions of 286.7eV and 289.2eV respectively. This corresponds to C-C-OH and C=O. The absence of these peaks on novel ta-C (and outside tribofilm) clearly illustrates that tribochemical reactions have occurred. The super low friction can be attributed to low energy interaction between the Hydroxylated carbon surfaces[111, 158]. This significantly reduced the traction force on the tribopair. Investigations with deuterate ( $^2\text{H}$ ) and  $^{13}\text{C}$  glycerol as marker techniques on ToF-SIMS have been used to validate this findings[156]. The mechanism of this process suggest breakdown of  $\text{sp}^2$  bonds of the glycerol molecule which promotes the deposition of carbon films on ta-C. Following this action is the ( $\text{OH}^-$ ) Hydroxylation of ta-C whereby the weak van der Waal interaction between sliding carbon surfaces and  $\text{OH}^-$  leads to ultra-low friction behaviours.

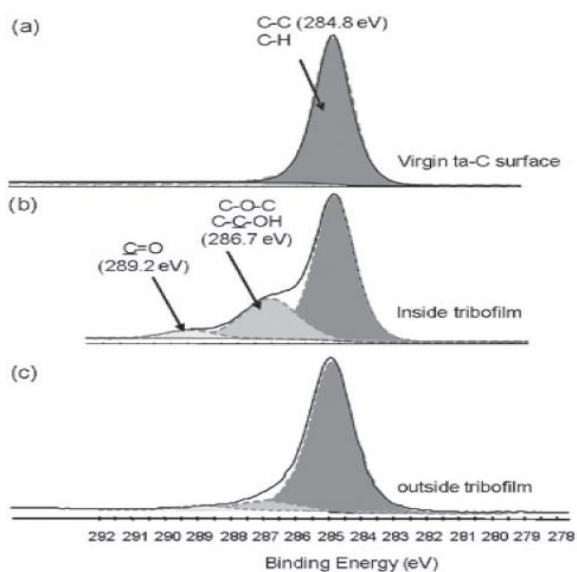


**Figure 3-17 XPS Spectra of ta-C Lubricated By Glycerol (a) Novel ta-C Surface (b) Inside Wear Track (c) Outside Wear Track [158]**

Esters or more precisely, GMO used in conjunction with tetrahedral amorphous carbon has stimulated research due to its super low friction, thus energy savings. This is coming at a very important time where both economic and environmental requirements are becoming stiffer. The mechanism of its friction reduction on the other hand suggests that certain other ester additives such as GDO, DGMO, SMO and SML should be able to provide a similar fit, if not better results.

Unfortunately, this is still a grey area. It is the objective of this study to assess other Organo-FM (esters) for valve train application. Compatibility with other oil additives will be examined to find potential environmentally friendly synthetic engine lubricant which will increase engine efficiency.

### **3.10. Tribofilms Derived From FFO on Steel and DLC Surfaces**

FFO are usually made up of the base stock and lubricant additives. Additives are used to confer beneficial properties; such as minimisation of destructive processes of oxidation, friction, wear, rust/corrosion inhibition, shear and dispersion of monomers which may be deposited in the oil. It is noteworthy to mention that these analyses are tedious but with an array of surface analytical techniques, the characterisation and morphology of tribofilms, can be obtained.

Although additivated oil have been studied in valve train rigs. For instance, Willermet et al [91] observed orthophosphate films in oil composed of ZDDP. Shirahama and Hirata [141] also investigated dispersants, detergent and ZDDP components on valve train wear. It was shown that the certain succinimide containing boron help improve the wear when in combination with ZDDP. Studies by Zhang [2] itemised some of the mechanisms responsible for their wear reducing action by forming boron species which are capable of reducing wear on their own.

It is important to mention that, a complete research endeavour should incorporate assessment of fully formulated oils. Using IRRAS, RAMAN and AES, fully formulated oil spectras were generated on tappet surfaces with both aged oil and fresh oil of GF SAE 5W30

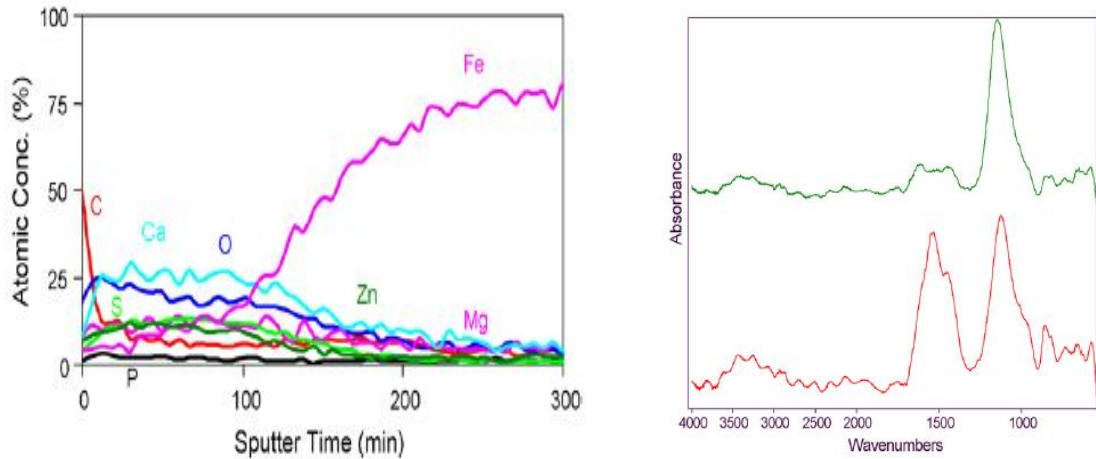
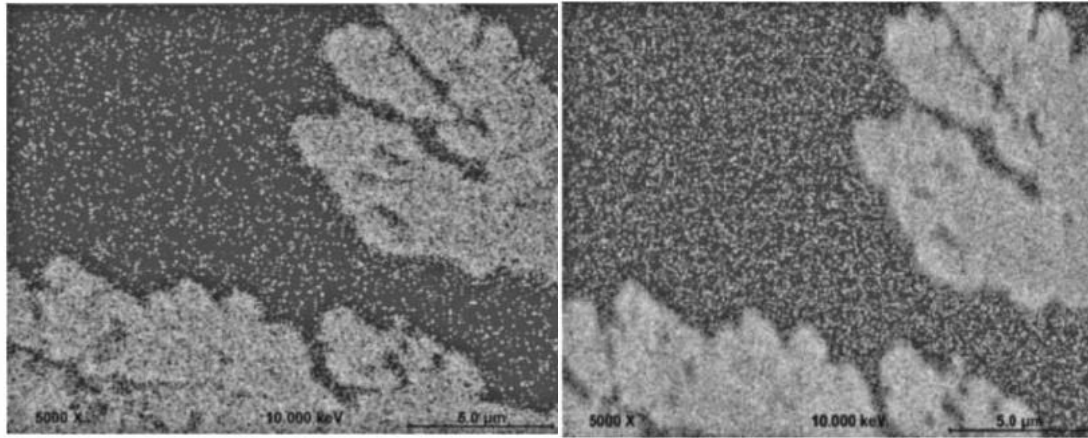


**Figure 3-18 (a) AES Spectra for Fresh Oil (b) IR Spectra for Fresh Oil  
(Upper Spectra Inside Tribofilm and Lower Spectra 8mm Outside Tribofilm  
[88]**

AES analysis reveals the presence of Mg and Ca which are from detergents used in the additives. This is supported by the IR spectra with wavenumber of  $855\text{cm}^{-1}$  and  $1450\text{cm}^{-1}$ , which corresponds to functional group  $\text{CO}_3^{2-}$ . Carbonates were detected on the surface. O-H intensity stretching around  $3400\text{cm}^{-1}$  on the IR spectra can be ascribed to products of phenols or carboxylic acids which are used as antioxidants in engine oils. Peaks of  $1608\text{cm}^{-1}$  are indicative of carbonyl mono or bis succinimides dispersants [88]. The presence of organic phosphates can be attributed to the secondary antiwear additives with narrow shoulders around  $950 - 980\text{cm}^{-1}$ . Aged oil spectras from RAMAN (not shown) contain  $\text{Fe}_3\text{O}_4$ , lower sulphur and calcium ions. The  $\text{Fe}_3\text{O}_4$  are due to wear particles which have been oxidised while lower concentrations of  $\text{Ca}^{2+}$  and  $\text{S}^{2-}$  are as a result of the consumption of the additives in the oil. Fresh oil tribofilms on tappets are composed of calcium phosphates, sulphides and carbonates.

In a similar work [87], SEM maps of 5W20 oils on a DLC polished bucket reveal phosphorus and Ca maps. Raman spectra give features of a strong G peak at  $1571\text{cm}^{-1}$  due to stretching vibrations at  $\text{sp}^2$  with phosphate peaks for a primary ZDDP around  $990\text{cm}^{-1}$



(a) Phosphorus Map

(b) Calcium Map

**Figure 3-19 (a) Phosphorus Map on DLC Coated Bucket (b) Calcium Map on DLC Coated Bucket [87]**

Friction torque data with FFO GF4 SAE 5W20 under a cam and follower rig reveals, that friction values are affected by temperature and functional coating surfaces [25]. The tribofilms consist of a complex matrix of Ca/Zn polyphosphates.

One important aspect of assessing tribofilms derived from fully formulated oil is the possibility to produce very low spectra of certain additives. Careful characterisation of Mo-FM in FFO were too small to fit XPS curves [76] but  $\text{Ca}^{2+}$  from detergents did not pose any detection problems.

In a recent study , Liu and Kouame [145], used XPS to map the tribochemical films on a steel cam profile at  $\pm 14^\circ$ ,  $\pm 10^\circ$ ,  $\pm 4^\circ$ , and  $0^\circ$  (Cam Nose). It was observed that long chain polyphosphate help to reduce the wear on specific locations on the cam profile and high temperature ( $>135^\circ\text{C}$ ) was observed to disrupt the stability of the tribofilm.

### 3.11. Surface Analytical Tests

#### 3.11.1. Scanning Electron Microscope/Energy Dispersive X- Ray (SEM/EDX)

Beam of electrons are generated from a tungsten coil or electron gun and excited by a high voltage (typically 20KV). This device obtains surface information from a sample through a raster pattern by tracing with an electron beam which has been focused in an imaging probe. When the electrons strike/penetrate the surface several

interactions between the electrons and the surface emit photons or electrons which are collected with a suitable detector to give information of the surface. It provides details about the morphology of the surface and the resolution can be determined by beam diameter.

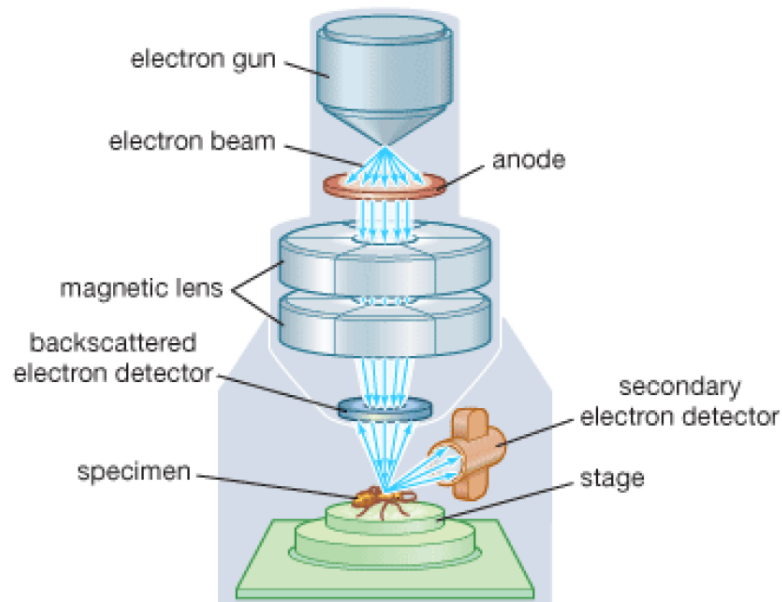


**Figure 3-20 Schematic of Scanning Electron Microscope [159]**

In combination with EDX/XEDS, elemental analysis or chemical characterisation of the surface can be achieved. This is due to the fact that each atom has its characteristic atomic structure allowing unique set of peaks on its X-ray structure. The EDX is made of three main components which are shown in Figure 3-21

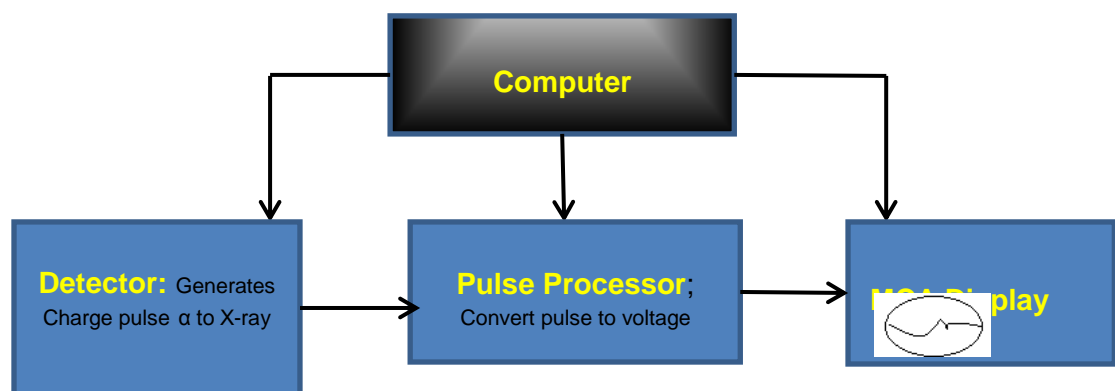


**Figure 3-21 Energy Dispersive X-ray Spectroscopy Showing Key Components [160]**

### 3.11.1.1. Literature/Previous Works on SEM/EDX

This surface analytical technique was used to study the morphology of tribofilms [71, 87, 88, 157] as well as the assessment of wear scars [77, 154, 161, 162]. It has also been used for the determination of hydrogen content in DLC's [35]. In surface characterisation involving oils containing glycerol, tribofilm reveals the presence of water, and other corrosive substances like aldehydes [157].

Indeed, it has been used to shed more light on the fundamental processes that affect the durability of coatings. In MoDTC/DLC interactions, the wear scar reveal scoring marks [161] and subsequent delamination [77] which clearly indicates material weakening and hardness reduction mechanisms. Scoring marks usually occurs when a hard material slides against a softer one where the asperity contacts ploughs out groves on the softer material. In tribofilm studies, SEM showed that the morphology of the tribofilm on DLC's are different from those of Fe based material. EDX characterisation identified the presence of Zn, phosphorus, and sulphur. It should be mentioned that SEM/EDX is not a very surface sensitive technique and only probes to the nearest  $\mu\text{m}$  on the surface [162]. It is thus possible to have information of the substrate overshadowing the characterisation of tribofilms.

### 3.11.2. X-Ray Photoelectron Spectroscopy (XPS)

This is a vacuum based technique where XPS spectras are obtained by irradiating a surface with an X-ray source while simultaneously measuring the Kinetic energy of electrons that escape from the surface in a range of **1 to 10nm**. The kinetic energy of the photoelectron is proportional to the binding energy and also indicative of the material surface investigated as every compound has a unique atomic structure allowing distinct set of peaks for the determination of the chemical nature of the atom. The underlining Figure 3-22 is used in the device

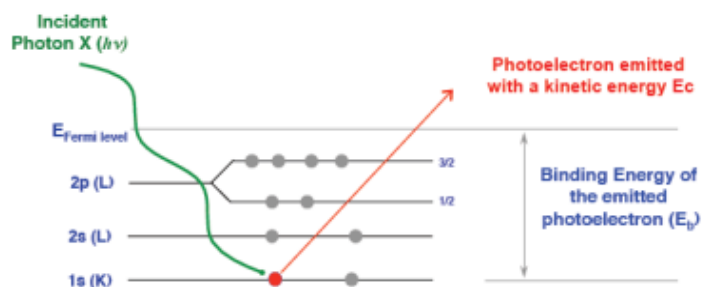


Figure 3-22 Principle of X-ray Photoelectron Spectroscopy

$$E_b = h\nu - E_c - \phi_A \quad \text{Equation 3-10}$$

where  $E_b$  is the bonding energy,  $E_c$  is the kinetic energy,  $h$  is the planch constant,  $\nu$  is the velocity of photoelectron and  $\phi_A$  is the work function of the spectrometer.

In XPS analysis, the inelastic mean free path (**IMFP**) is a parameter used to evaluate the surface sensitivity. For low energy electrons, this corresponds to only few atomic layers making the device one of the most sensitive. Mathematically, it is expressed in **Equation 3-11**

$$\lambda(\text{\AA}) = (E_K)^{0.5} \quad \text{Equation 3-11}$$

They are very surface sensitive and one of the most widely used technique for characterisation of tribofilms in boundary lubrication conditions [84, 110, 154, 163-166]. XPS have been employed for the study of cation rearrangement and degree of Bridging oxygen and non-bridging oxygen in phosphate glasses [166]. Quantification of tribofilms can also be carried out with this technique. In MoDTC/ZDDP additivated oils, significant carbon (from the oil), sulphur, phosphorus, Zn, Mo and oxygen were observed in XPS data after 5 mins etching. The S2p, O1s, and Mo 3d peaks reveal the presence of sulphide, oxides and MoS<sub>2</sub> sheets [84]. With carbon coatings, XPS analysis have shown that Mo-DTC/ZDDP react with a:C-H than Ti-DLC. Significant reactivity was attributed to Hydrogen in DLC but in general MoS<sub>2</sub> sheets, phosphate craters of zinc and oxygen were observed [64]. Typical XPS spectra for oils containing MoDTC+ZDDP are shown in Figure 3-23

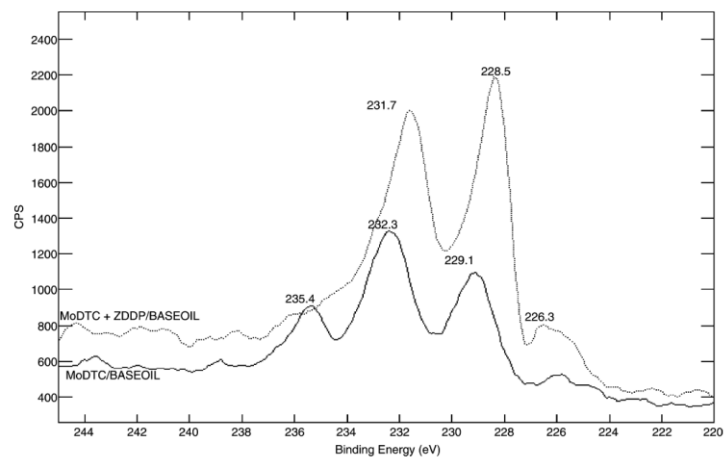


**Figure 3-23 XPS Spectra of Oils Containing MoDTC and MoDTC+ZDDP [165]**



### 3.11.3. Raman Spectroscopy

Raman is based on the inelastic monochromatic scattering of light source which gives rise to rotational, vibrational and other low frequency modes in a system. Light scattering is achieved by placing molecule in an electromagnetic field which disturbs charge distribution thus inducing a dipole moment which acts as a source of radiation. The oscillating dipole moment is usually expressed as the polarizability which is proportional to the inducing field [167].

$$\bar{P} = \alpha \bar{E} \quad \text{Equation 3-12}$$

Visible RAMAN spectroscopy will be performed with a **Renishaw in – Via RAMAN** spectroscopy having a Laser physics of Ar. 488nm and 785 nm wavelengths. Calibration will be performed with a standardized sample (**e.g. Silicon**) [39] to ensure the device is working correctly. Exposure to the laser source will be restricted between 8-12secs and the laser power will be manually controlled between 75-80% to prevent graphitisation on DLC coated surfaces. A Typical Renishaw in-Via RAMAN is shown below.



**Figure 3-24 Renishaw In-Via Raman Apparatus**

Notable authors [87, 88, 168] have used this technique for characterisation of tribofilm, determination of fractions of  $sp^3$  and  $sp^2$  bond on DLC coated surfaces [169] and evaluation of hardness on wear scars. The ratio of  $I_G/I_D$  was used as an indication

of hardness reduction [161]. Typical Raman spectra of films formed from fresh oils at different experimental timings is shown below.

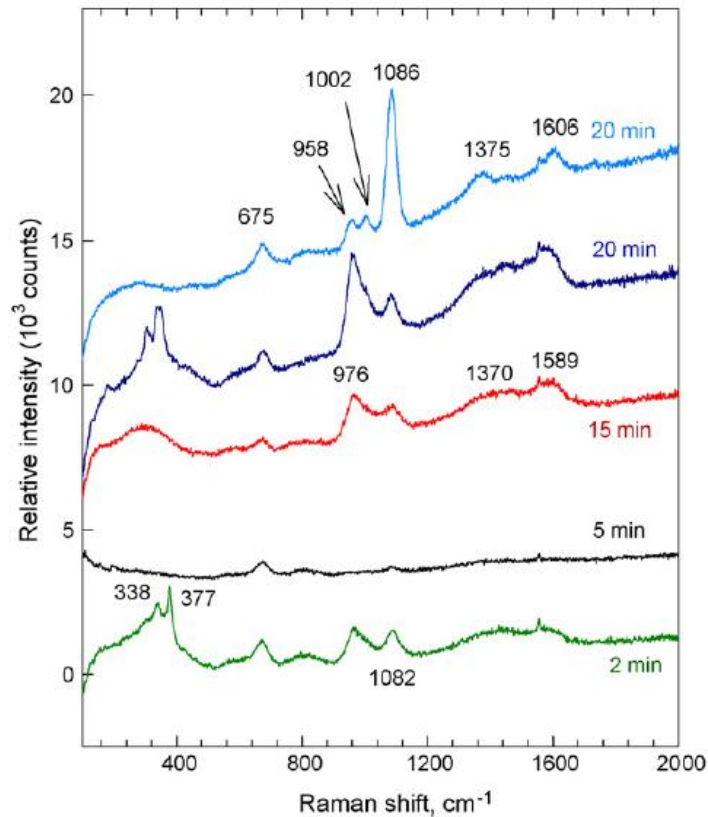


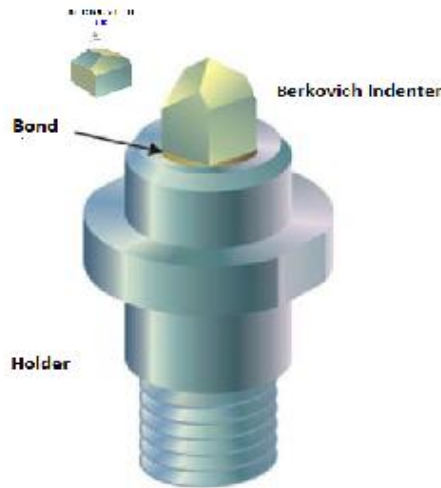
**Figure 3-25 Raman Spectra of Films Formed From Fresh Oil in Cylinder on Flat Experiment [168]**

Carbon peaks are observed around  $1350\text{-}1600\text{cm}^{-1}$ , with significant phosphate films at  $960\text{-}980\text{cm}^{-1}$ . Calcium carbonate peaks are also observed at  $1050\text{-}1090\text{cm}^{-1}$  which are derived from the detergents/dispersants used in the oil. It should be mentioned that the timings of each spectra does not reflect the kinetic of film formation. This is because of the spot to spot heterogeneity of tribofilms. This will be a suitable technique for the assessment of tribofilm as it can be used for liquids. Determination of the spectras for different esters should be carried out before the test to observe various molecular bonding.

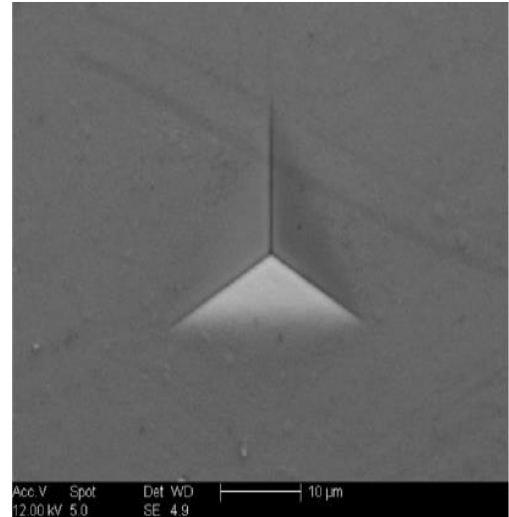
#### 3.11.4. Nano-indentation

This is an important technique for the mechanical characterisation of tribofilms and or coatings. It involves applying a small load with tip sizes to produce nano metre indentation on the substrate as shown in Figure 3-26. Based on the size of indent,

determination of the area is usually difficult and hence quantitative evaluations of hardness are cumbersome. One procedure of avoiding this is using a Berkovich (three sided pyramid) indenter with known geometry, and hardness. Traceable AFM can also be employed for the determination of indentation area [170, 171]



Nano-indenter Example



Nano-indentation of WC/C a: C-H (Force: 2.5N)

**Figure 3-26 Indentation Device and Indent on Test Surface [172]**

Following the above, area of the indent and corresponding hardness value can be easily evaluated from the equation

$$H = \frac{F_{max}}{A_{max}} \quad \text{Equation 3-13}$$

Where  $F_{max}$  is the maximum force which produces a penetration depth  $x_{max}$  with a corresponding area of  $A_{max}$ . **Figure 3-27** shows the typical load displacement curve for a standard test. The surface area of the nano-indenter at distance  $x$  can be obtained from Equation 3-14. According to ISO/IEC 14577 and 17025, the valid indentation depth should be  $x \leq 200nm$ .

$$A_s = \frac{3 \times \sqrt{3} \times \tan \phi}{\cos \phi} \quad \text{Equation 3-14}$$

$$MH = \frac{F_{max}}{A_S \times x^2}$$

**Equation 3-15**

Where  $A_S$  is the indented surface with value of 26.43 for a Berkovich indenter.

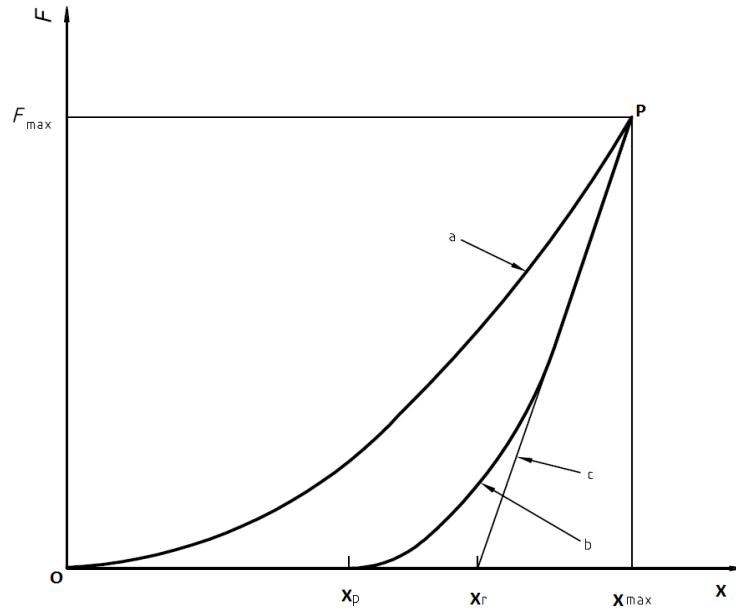


**Figure 3-27 Load Displacement Curve for Nano-indentation**

Evaluation of the indentation modulus is also a significant property of the tribofilm which affects wear. The hardness of tribofilm can be reduced by lubricant additives particularly MoDTC [161]. The corresponding equation for reduce modulus and indentation modulus are shown below.

$$E_r = \frac{1}{C_p} \sqrt{\frac{\pi}{A_S}}$$

**Equation 3-16**

$$E_{IT} = \frac{(1 - v_s^2)}{\frac{1}{E_r} - \left(\frac{1 - v_i^2}{E_i}\right)}$$

**Equation 3-17**

Where  $E_r$ ,  $E_i$  and  $E_{IT}$  are the reduced, indenter and indentation modulus respectively,  $v_s$  and  $v_i$  are the poison ratio of the test surface and indenter respectively,  $C_p$  is the compliance contact  $\left(\frac{dx}{dF}\right)$ .

#### 3.11.4.1. Nano Indentation Modulus Test Procedure

The mechanical properties of esters (**GMO, GDO and SMO**) will be studied. The aim of this test is to determine the **hardness** and **indentation Modulus** of tribofilms derived from ester containing lubricants. The nano-indentation test will include the use of a Berkovich trigonal indenter performed at room temperature (18-23°C) in a force displacement mode. Under this condition, the sensor device of the nano-indenter simultaneously measures the force and displacement to produce a curve during the loading and unloading cycles. Calibration will be performed with a standard Silica material with known hardness and modulus (Mohs = 7). Setup included the continuous quasi static measurement of the load against the normal displacement ( $X_d$ ). The thermal drift will be set at 60s and should not exceed 0.5°C/hr. to minimise the strain on the material due to the indentation process. The AFM device will be used as a complementary technique for the determination of wear profiles.

#### 3.12. Summary of Gaps in the Literature

Significant attention has been focused on the tribochemistry of the tappet with little consideration of the cam. This does not give a clear picture of the tribochemical reactions taking place with the tribopair. In this study, friction torque, lubricant film thickness and load (contact pressure), across the cam profile were evaluated with the aid of torque/load sensors, and a digital dial indicator. This involves mapping the tribochemical films at  $\pm 14^\circ$ ,  $\pm 10^\circ$ ,  $\pm 4^\circ$ , and  $0^\circ$  (Cam nose). These were then correlated to the tribochemical films across the cam ex-situ. This will add more knowledge to the nature of tribofilms formed across the cam profile which typically, has varying pressure, film thickness, slide roll ratio and lubricant entrainment velocities.

Optimisation of the cam follower component involves the use of various surface coatings, materials and lubricant chemistries. Current trends of improving this component use DLC coatings which are 'inert' and have a different interaction mechanism with lubricants designed for iron based surfaces. Recently, it has been observed that coating the tappets with DLCs have some antagonistic effects on the wear resistance of the cam [173]. A fundamental reason will be the difference in hardness by surface treatment. This study also aims to evaluate Si doped, Non Doped and taC-H DLC coated tappets against a CI camlobe. On a concluding aspect of coating study, this work also looks at the effects of coating the cam and the tappets to determine any performance improvement can be obtained on the friction and wear properties.

Another missing link in the literature is the comparison of tribofilm in conventional tribometers (e.g. pin on plate), cam follower test rigs and engine components. One point to note is that cam followers exhibit valve bounce, huge pressure variations, sliding and rolling motion which cannot entirely be simulated on ball on disc or reciprocating tribometers. In an attempt to mimic certain engine components with tribometers, consideration can be given to a limited amount of parameters such as contact pressure, sliding velocity, operating temperature, and applied load. These conditions will be used to compare the tribofilms formed on Cam followers and pin on plate tribometers. This is to evaluate the level of representation of tribometer data with component bench tests.

Due to the reduction of ZDDPs in engine oils, and research into low/Mid SAPS engine oils for improved automotive performance, two commercial 5W30 engine oils were studied. The friction, wear and tribochemical information obtained was correlated to the composition of the oil.

## CHAPTER 4. PIN ON PLATE TRIBOMETER: INVESTIGATION OF THE FRICTION, WEAR AND TRIBOCHEMISTRY OF DIFFERENT DLC COATINGS/LUBRICANT COMBINATIONS

### 4.1. Motivation of DLC Studies

This chapter characterises three different DLC coatings for their ability to interact with the oil and produce boundary/mixed nanoscopic tribofilms necessary to reduce friction and wear. All coatings had similar centre line average roughness values ( $R_a = 0.02 \mu\text{m}$ ) to ensure that the friction/wear and tribochemical responses were due to the coating properties and not the roughness. Rough surfaces have been reported to increase friction [174] and wear [175] of DLC coatings. The cast iron camlobes were also polished down to an  $R_a$  value of  $0.02 \mu\text{m}$ . These very smooth surfaces are useful for high performance engines such as Formula 1 cars. Tests were performed using a pin-on-reciprocating plate tribometer to establish a fundamental understanding of the coating properties before further investigations were carried out in a bench test single cam tribometer.

### 4.2. Properties of DLC's Coatings Investigated

Prior to deposition of the DLC coatings, each of the surfaces were cleaned and a thermochemical process was used for the removal of the soft running  $\text{MnPO}_4$  coating. A re-polishing was then carried out to a surface roughness ( $R_a$ ) of 20 – 30 nm. The A-Carbon coating were deposited with a PVD/PACVD process at high frequency with a coating temperature  $\leq 200 \text{ }^\circ\text{C}$ . It is made up of a Cr adhesion layer and WC support layer with a functional layer of a:C-H. The total thickness is 2.0 – 2.5  $\mu\text{m}$ .

Si1s can be deposited at a slightly higher temperature of  $240^\circ\text{C}$  by using a silicon/hydrogen/oxygen precursor. The thickness of the coating can be as high as 10  $\mu\text{m}$  but those employed for this study typically range from 2.0 – 2.5  $\mu\text{m}$ . The silicon has dual functionality in the coating where it acts as a stress relieving agent and improves coating stability at high temperature [72, 176, 177].

Cavidur taC-H coating architectures are deposited at high temperature of 300 – 350  $^\circ\text{C}$ . It is deposited at high frequency by a PVD/PACVD process like a:C-H. It has SiC, CrC and TiC interlayers with a functional layer made up of predominantly  $\text{sp}^3$  C-C bonds with hydrogen concentration between 5-10 %. The coating surface and substructure for taC-H and a:C-H are illustrated in Figure 4-1.

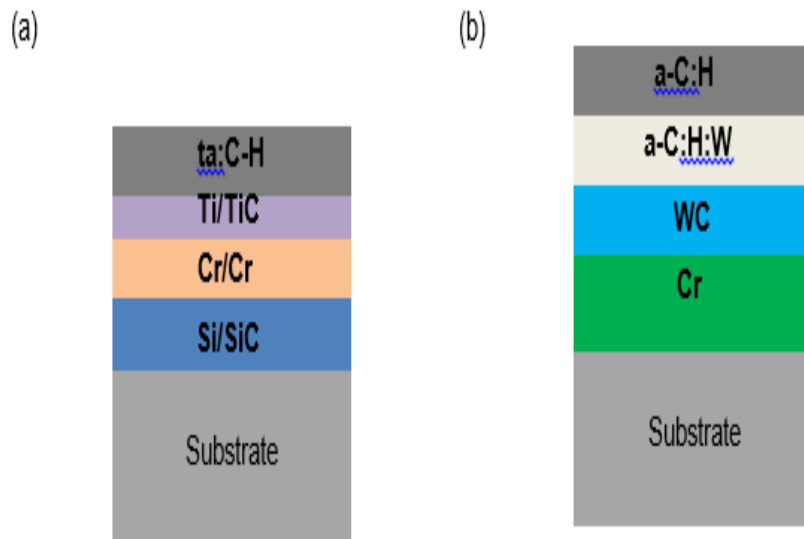


**Figure 4-1 Coating architecture for (a) taC-H and (b) a:C-H**

### 4.3. Experimental Methodology

#### 4.3.1. Scratch Test

The objective of the scratch test was to determine the adhesive strength and load bearing capacity of the coating used. Tests were carried out with a tribotechnic scratch tester with a diamond tip of 200  $\mu\text{m}$  in accordance with ROCKWELL C. Progressive load condition was set with 0.0 N as the starting load and 50 N as the final load. Loading speed rate was set at 10 N/min with sample speed of 10 mm/min and scratch length of 10 mm. The step load corresponds to 1N/mm for the DLC coatings. The acoustic emission sensitivity used for all the tests was 5.0 AE and a total of 80 – 85 scratches was used on each sample. Images were taken when unique characteristics from the Acoustic emissions were observed. Figure 4-2, Figure 4-3, Figure 4-4 and Figure 4-5 show the scratch test results. The images reveal the onset of crack initiation, delamination and coating failure.

**a:C-H (A Carbon)**

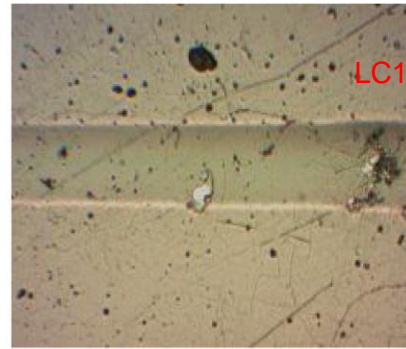


### Critical Load: 1

Load: 23.78 [N] Position: 2.749 [mm]  
Magnification : 200 x

#### Comments:

Crack

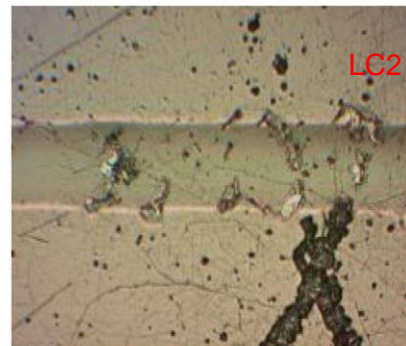


### Critical Load: 2

Load: 26.83 [N] Position: 3.050 [mm]  
Magnification : 200 x

#### Comments:

Delamination



### Critical Load: 3

Load: 30.13 [N] Position: 3.351 [mm]  
Magnification : 200 x

#### Comments:

Failure

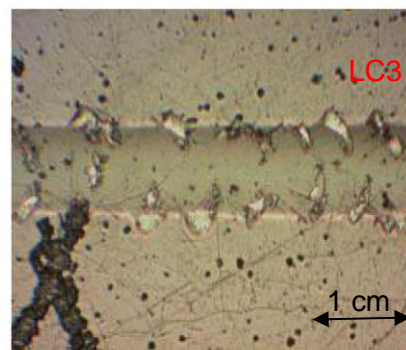


**Figure 4-2 Scratch Test On a:C-H Showing Critical Load at (a) 23 .70 N (b) 26.80 and (C) 30.1 N**

Since the load applied is increased continuously, forces induced by deformation and shear stress of the coating due to its contact with the stylus are placed on the hard thin coatings. Onset of coating failure occurs when the shear stress becomes greater than the shear adhesive strength between the coating and the substrate or when the coating cannot follow the elastic plastic deformation which arises from the continual increase of the load due to the pressing stylus. The onset of failure is monitored with an optical microscope and from the acoustic emission of the device. **Figure 4-2** shows the optical results from a scratch test. The onset of coating failure can be observed at 23.8 N while complete failure was seen at 31.1 N. The intermediate value at 26.8 N shows how the coating is going through an elastic-plastic deformation process prior

a catastrophic failure. This is evident by the presence of minor flasks at the edge of the coating which becomes more pronounced at the failure load of 31.1 N.

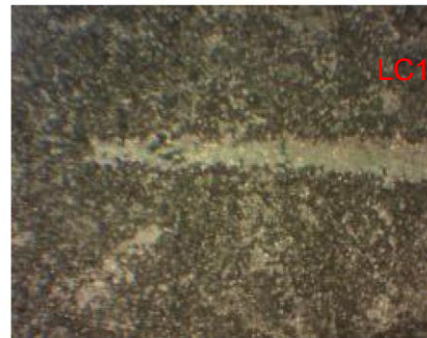
MnPO<sub>4</sub>

### Critical Load: 1

Load: 0.65 [N] Position: 0.051 [mm]  
Magnification : 200 x

### Comments:

Beginning of the scatch

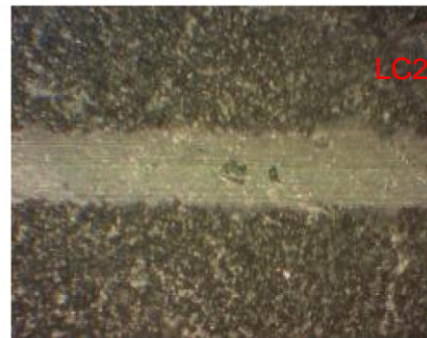


### Critical Load: 2

Load: 19.09 [N] Position: 2.225 [mm]  
Magnification : 200 x

### Comments:

Middle of scratch



### Critical Load: 3

Load: 45.91 [N] Position: 5.128 [mm]  
Magnification : 200 x

### Comments:

End of scratch

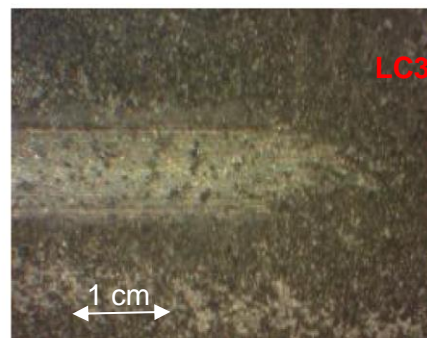


**Figure 4-3 Scratch Test on MnPO<sub>4</sub> Showing Critical Load (a) Onset Of Cracking At 0.65 N (b) Coating removal/delamination at 19.1 N (c) failure at 46N**

For the MnPO<sub>4</sub> coating, the onset of coating failure is not very clear. This is due to the polycrystalline nature of the coating and the colour closely mimics those from the substrate material. Notwithstanding, on continuous increase of the load,

the failure of the coating becomes more evident and can be observed at 19.09 N. This low adhesive strength is due to the thin soft running-in properties of the coatings.

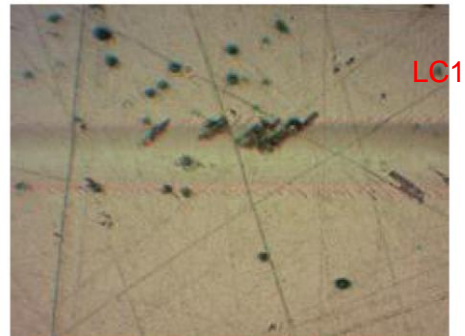
Si1s

### Critical Load: 1

Load: 17.05 [N]    Position: 1.951 [mm]  
Magnification : 200 x

### Comments:

Crack



### Critical Load: 2

Load: 19.72 [N]    Position: 2.332 [mm]  
Magnification : 200 x

### Comments:

Delamination



### Critical Load: 3

Load: 22.39 [N]    Position: 2.531 [mm]  
Magnification : 200 x

### Comments:

Failure

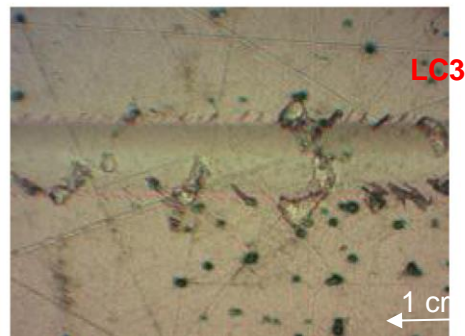


Figure 4-4 Scratch Test on Si1s Showing Critical Load (a) 17.0 N with cracks (b) 19.73 with coating delamination (c) 22.4 N with coating failure

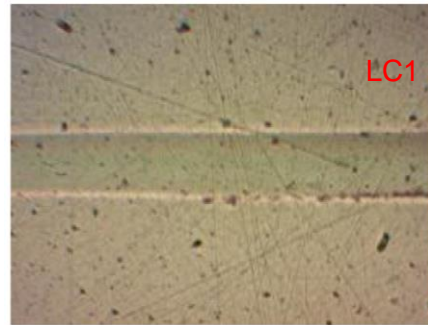
taC-H (Cavidur)

### Critical Load: 1

Load: 15.16 [N]    Position: 1.683 [mm]  
Magnification : 200 x

### Comments:

First crack

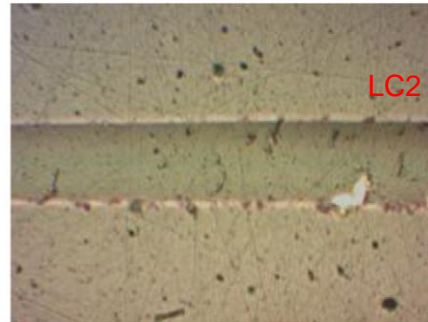


### Critical Load: 2

Load: 25.46 [N]    Position: 2.787 [mm]  
Magnification : 200 x

### Comments:

Delamination



### Critical Load: 3

Load: 29.02 [N]    Position: 3.126 [mm]  
Magnification : 200 x

### Comments:

Failure

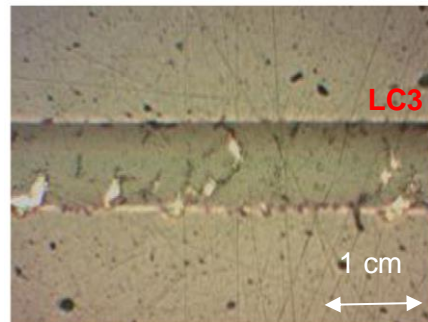


**Figure 4-5 Scratch Test on taC-H Showing Critical Load at (a) 15.16 N with minor cracks (b) 25.5 N with delamination (c) coating failure at 29.0 N**

#### 4.3.1.1. Summary of Scratch Test

From these images (see Figure 4-2, Figure 4-3, Figure 4-4 & Figure 4-5) it can be stated that a:C-H and ta:C-H DLC coatings possessed better adhesion than the Si1s coating. The adhesive strength for these coatings is about 30 N while those of the Si1s or silicon doped coating is 22.4 N with delamination of the coating occurring at around 19.0 N. As observed in the later aspect of this chapter, the low adhesive strength of the Si1s coating reduces its durability in tribological systems. Pictorial images from the Manganese Phosphate coating did not show any distinct delamination and the onset of coating failure was not clearly identified as the coating is very thin and the colour closely match those from the steel substrate.

**Table 4-1 Details/Properties of Coatings Used**

	Cavidur taCH	A-Carbon	Si1s	MnPO <sub>4</sub>
<b>Designation</b>	taCH	a-C:H	Si1s	MnPO <sub>4</sub>
<b>DLC thickness (μm)</b>	1.5	2.0 – 2.5	2.0 – 2.5	2.0 – 4.0
<b>Adhesion Lc (N)</b>	35	20 – 30	20	15 - 20
<b>Coating Temperature (°C)</b>	250 – 350	≤ 200	240	-
<b>Max temperature of use (°C)</b>	400	300	400	500
<b>Predominant C-C bond types</b>	sp <sup>3</sup>	sp <sup>2</sup> – sp <sup>3</sup>	sp <sup>2</sup>	Poly crystalline
<b>Colour</b>	Black	Black	Black	brown

**Table 4-1** shows the characteristics of each of these coatings as received from the manufacturer. The adhesion Lc are in agreement with the scratch test results evaluated in our labs. The structures of the DLC coatings were also investigated and found to be in close agreement with those reported in [169]. The taC-H and a:C-H both have a narrow shoulder around 1350 cm<sup>-1</sup> (D peak) and a pronounced G peak around 1550 cm<sup>-1</sup>. While the spectrum of taC-H and a:C-H are very similar, it must be stressed that taC-H is predominantly sp<sup>3</sup>. The reason being that the Raman spectra was taken under visible laser of 488nm and under this wavelength, the sp<sup>2</sup> sites have a much broader cross section thereby overshadowing the sp<sup>3</sup> contributions even though they (sp<sup>3</sup> sites) have a greater volume in the DLC structure [178].



### 4.3.2. Test Setup and Conditions

Tribological tests were conducted using a pin-on-reciprocating plate tribometer under boundary lubrication regime with an applied load of 390 N. Prior to testing, samples were cleaned and dried with acetone. The stroke length of the apparatus was 10 mm, running under frequency of 1 Hz. 3-10 mL of lubricant was injected into the contact region, which was then heated to 100°C. The curvature radius was 40 mm and the Hertzian contact pressure was calculated to be 0.69 GPa, which is in the same range of pressure as a cam follower component. The effective film thickness was between 0.20-0.30. Test duration was 12hrs. These test conditions closely meet those in the cam follower systems in terms of lubricant film thickness and time for running and steady state friction values. Friction data are recorded every minute from an average of 60 values per data point. The test conditions are illustrated in Figure 4-6. In order to account for steady state friction and eliminate the erratic nature of friction during running-in of the coating, friction values for the last hour are plotted as bar charts but the entire friction curves are discussed for further insight on tribological/tribochemistry processes.

Experimental Condition	
Sliding Speed	20mm/s
Temperature	100 <sup>o</sup> C
Load	390N
Lube Volume	3 -10mL
Test Duration	12 hrs
Effective Oil film thickness	0.24-0.31µm
Hertzian Stress	0.69GPa
Contact Type	Point Contact

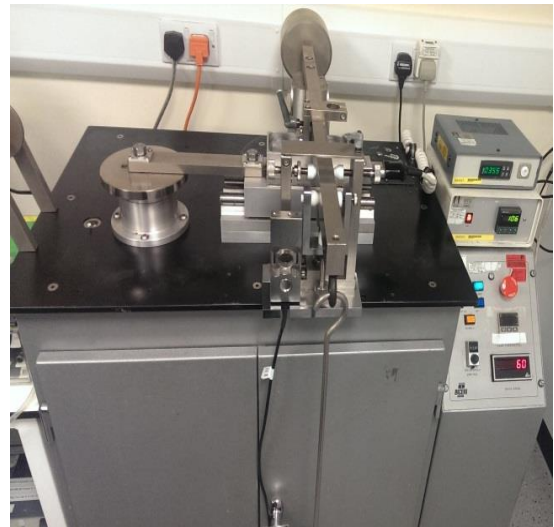


**Figure 4-6 Test Setup and Experimental Conditions**

### 4.3.3. Lubricants and Lubrication Regimes for Tests

Two fully formulated lubricants (Normal and Mid SAPS oils) and a group III base oil were used in the test. Fully Formulated lubricant A hereafter referred to as FFA or Oil A was a friction modified oil while fully formulated Lubricant B (hereafter referred to as FFA or Oil B) is a non-friction modified oil. For the base oil, its sulphur content is  $\leq$

0.03% and has a viscosity index  $\geq 120$ . The kinematic viscosity of the FFA, FFB and base oil at 100 °C are 9.84, 10.63 and 7.87 m<sup>2</sup>/s respectively. The film thickness and lambda ratio were calculated using the Dowson and Hamrock equation for point contact as shown in Equation 4-1 and Equation 4-2

$$h_{min} = 3.63 \times R [U^{0.68} G^{0.49} W^{-0.073} (1 - e^{-0.68k_e})] \quad \text{Equation 4-1}$$

$$\lambda = \frac{h_{min}}{\sqrt{R_{a1}^2 + R_{a2}^2}} \quad \text{Equation 4-2}$$

Where  $U = (\eta_o \times u_s)/(E^1 \times R)$ ;  $G = \alpha_p \times E^1$ ;  $W = \frac{P}{E^1 \times R^2}$ ;  $\eta_o$  is the dynamic viscosity at 100 °C,  $u_s$  is the entrainment speed (0.01m/s),  $\alpha_p$  - the pressure viscosity coefficient at 100 °C is  $1.57 \times 10^{-8} Pa^{-1}$ , R is the reduced curvature radius of the pin (20 mm), P is the normal load (390 N),  $E^1$  is the effective modulus of elasticity.  $k_e$  is the elliptical parameter which is equal to 1.0339 for a sphere on a flat type contact.  $R_{a1}$  and  $R_{a2}$  are the roughness of the coating and pin respectively. This gave specific film thickness ( $\lambda$ ) or lambda ratio of 0.29, 0.31 and 0.24 for Normal, Mid SAPS and base oils respectively. This confirms that all tests were carried out in the boundary lubrication regime thereby simulating the contact conditions in the nose of a cam lobe.

#### 4.3.4. Wear Volume Measurement Procedure

Before evaluation of the wear, the tribofilm was taken off by cleaning in acetone. The wear methodology used to evaluate the durability of the coating is in accordance with ASTM G99 -95a (standard test method with a pin on disk apparatus). The wear volumes of each of the coatings are measured with optical interferometry. Those of the pin were obtained with the diameter of the wear scar on the pin by using both optical interferometry and micrometer images (see Figure 4-7). Wear losses on the pin were calculated using Equation 4-3

$$Vol_{pin} = \left(\frac{\pi h}{6}\right) \left[\frac{3d^2}{4} + h^2\right] \quad \text{Equation 4-3}$$

Where  $h = r - [r^2 - d^2]^{\frac{1}{2}}$ , d = wear scar diameter and r = 40 mm,  $Vol_{pin}$  = pin volume, h is the height of the wear of pin worn after the wear test.

The wear volume on the plate was determined by using the geometrical information obtained from the optical interferometry. The wear depths were taken at five locations and an average value was used to evaluate the plate wear volume based on the width/(stroke) length. The information obtained from the optical information can also be used to determine whether the DLC coatings investigated have been completely removed during the tribological test.

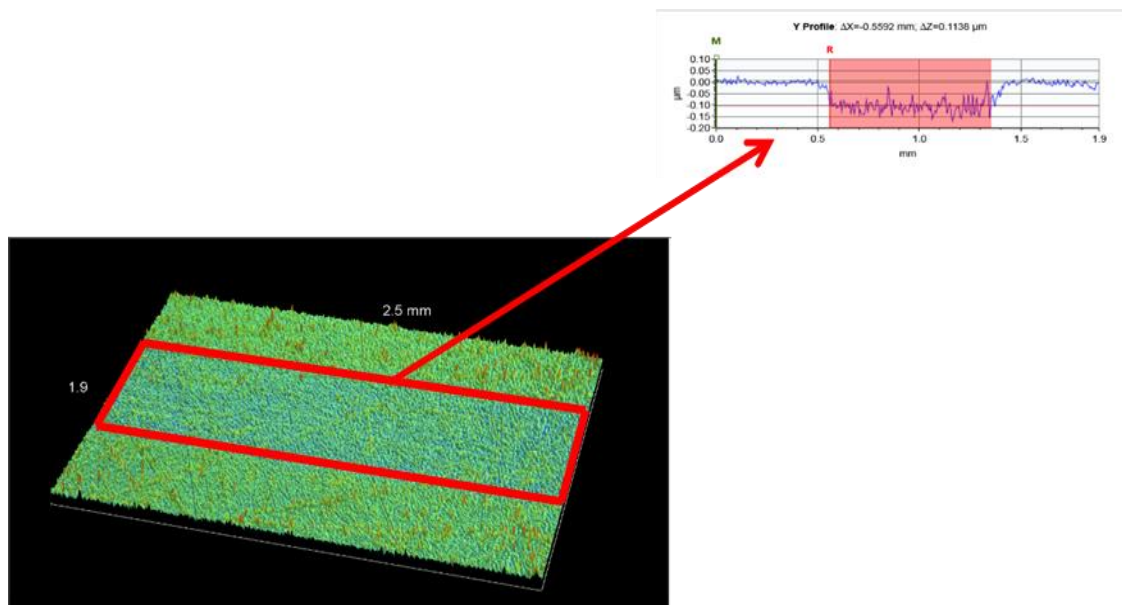


**Figure 4-7 Wear Volume Measurement with Optical Interferometry Showing the Line Profile Along One Axis.**

#### **4.3.5. Materials/Coatings**

The cast iron materials used as the pin is of grade BS 250 with hardness of 140 HB. In addition to the  $\text{MnPO}_4$  and polished steel surface, three different DLCs of SI1s, a:C-H (A-Carbon) and taC-H were tested with three different oils. All surfaces used in this test had centreline average roughness of 20 – 30 nm except for the  $\text{MnPO}_4$  coating with  $R_a$  of 0.25  $\mu\text{m}$ , which is a commercial standard production surface coating for inserts. This was to minimise effects of roughness on the friction and tribochemistry and the commercial specimen/polished surfaces were used as a reference. SEM images showing the microstructural details of the coatings are shown in Figure 4-8.



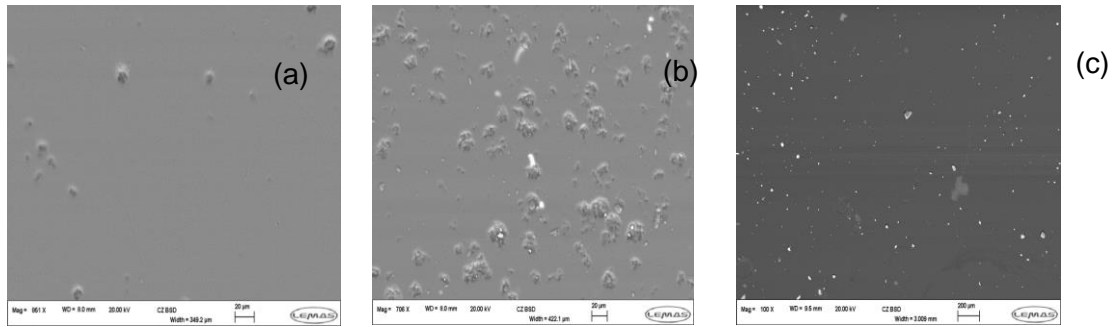


**Figure 4-8 SEM Image of (a) taC-H (b) Si1s (c) a:C-H**

#### 4.4. Results

##### 4.4.1. Friction Data with Fully Formulated Lubricant A (FFA)

The friction results of five different plate surfaces as a function of time are shown in **Figure 4-9** with a:C-H (A-Carbon) showing distinctively, lower friction. Steady state friction was obtained with the steel and a:C-H surface early and this was maintained for a larger portion of the test. Si1s, MnPO4 and taC-H surfaces were slower in attaining the steady state friction. This may be due to the interaction of the coating with the oil additives which delays the running-in phase of the coating.

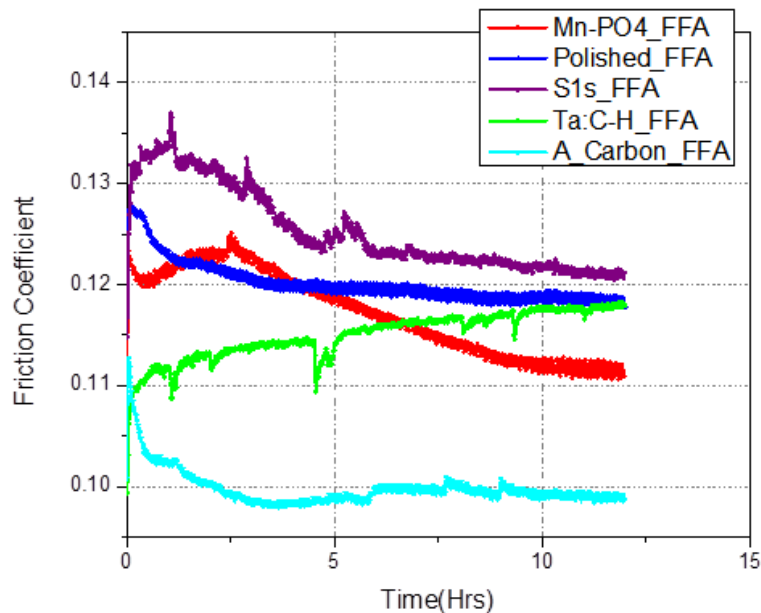


**Figure 4-9 Friction Plots of Different Coating against Cast Iron When Tested with Fully Formulated Oil A**

While most of the surfaces showed a decline in friction coefficient with time, taC-H exhibited low friction at the start with a steady rise in friction value throughout the duration of the test. The mechanism of this is still unclear but it appears to be either an unfavourable reaction between the oil additives and the coating or a gradual spalling of the coating which increases the friction continuously to a value similar to the rubbing action of steel/steel. It can, however, be a synergy of both reactions taking place on the surface.

The highest friction was obtained with the Si1s coating and this correlates well with the delamination images revealed by SEM. Si-O-X was removed and hard wear particles were trapped in the contact.

#### 4.4.2. Friction Data with Fully Formulated Lubricant B

Figure 4-10 shows the friction curve of five different surfaces against normal SAPS oil. Again, a:C-H shows exceptionally low friction when compared with other surfaces. The last 1hr shows steady state friction values of 0.095. taC-H also achieves steady state at an early stage of the test and considerably lower friction than oil A. This can be attributed to the additives in the oil which interact with the surfaces. Delamination of Si1s coating was experienced but this was more prolonged with oil B than those shown with oil A. In the final hours of the test, both polished and Si1s have identical friction coefficients while those of the MnPO<sub>4</sub> levelled off at a slightly higher value. In-lubro conditions with fully formulated oils, a:C-H /CI and ta:C-H/CI tribopair only reduced the friction from 0.12 for (steel/CI) to approximately 0.10.

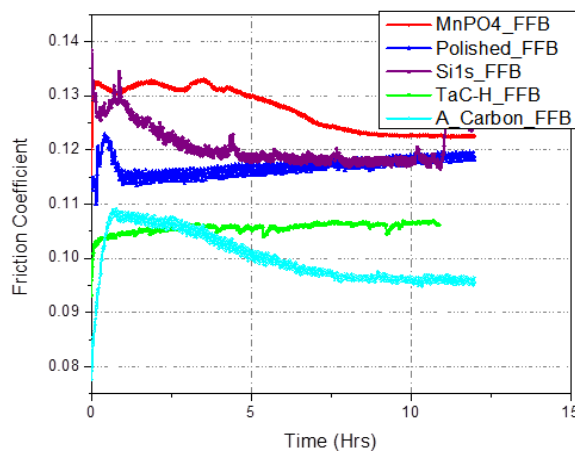


**Figure 4-10 Friction Plots of Different Coating against Cast Iron When Tested with Fully Formulated Oil B**

By comparing Figure 4-9 and Figure 4-10, FM oil A was not observed to reduce the friction for a:C:H and ta:C-H. This can be attributed to the effectiveness of the ester based friction modifier used in the oil.

#### 4.4.3. Friction Data with Base Oils

In tests with base oil, the friction coefficients are sufficiently lower for most of the surfaces (see Figure 4-11). The steady state friction was observed after a relatively short period of 2.5 hrs for Si1s and polished surfaces. The a:C-H and taC-H coatings showed very low friction. For the taC-H, there was a sharp decline in the friction curve after 5 hrs of testing. This phenomena was identical for the three rounds of test. Optical images of the cast iron pin shows that the wear scar surface is covered with a significant dark circle due to transfer layer build-up from the coating. Going through the friction curve, it suggests that these transfer layer take time to build up after which the tribological surface begins to behave like a taC-H sliding across taC-H surface.

With the a:C-H, this transfer process occurs faster and the friction values quickly drop to a low value of 0.06. These rubbing surfaces are similar to amorphous carbon sliding against amorphous carbon and the friction values are close to those of graphite/graphite interaction with friction value of 0.05 [15]. The surfaces of the pin with the coatings are tested with base oil is shown in Figure 4-11.

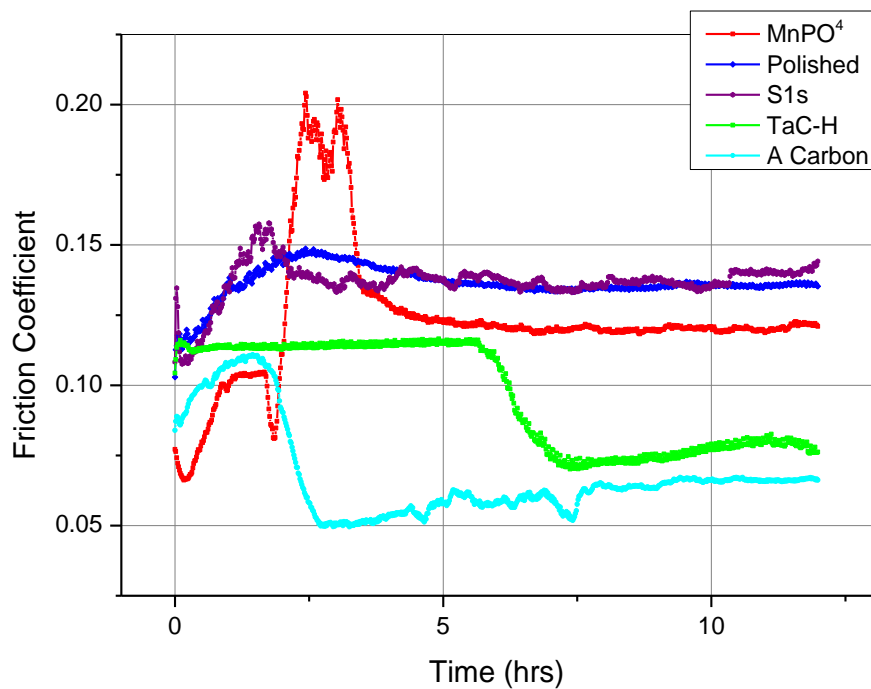
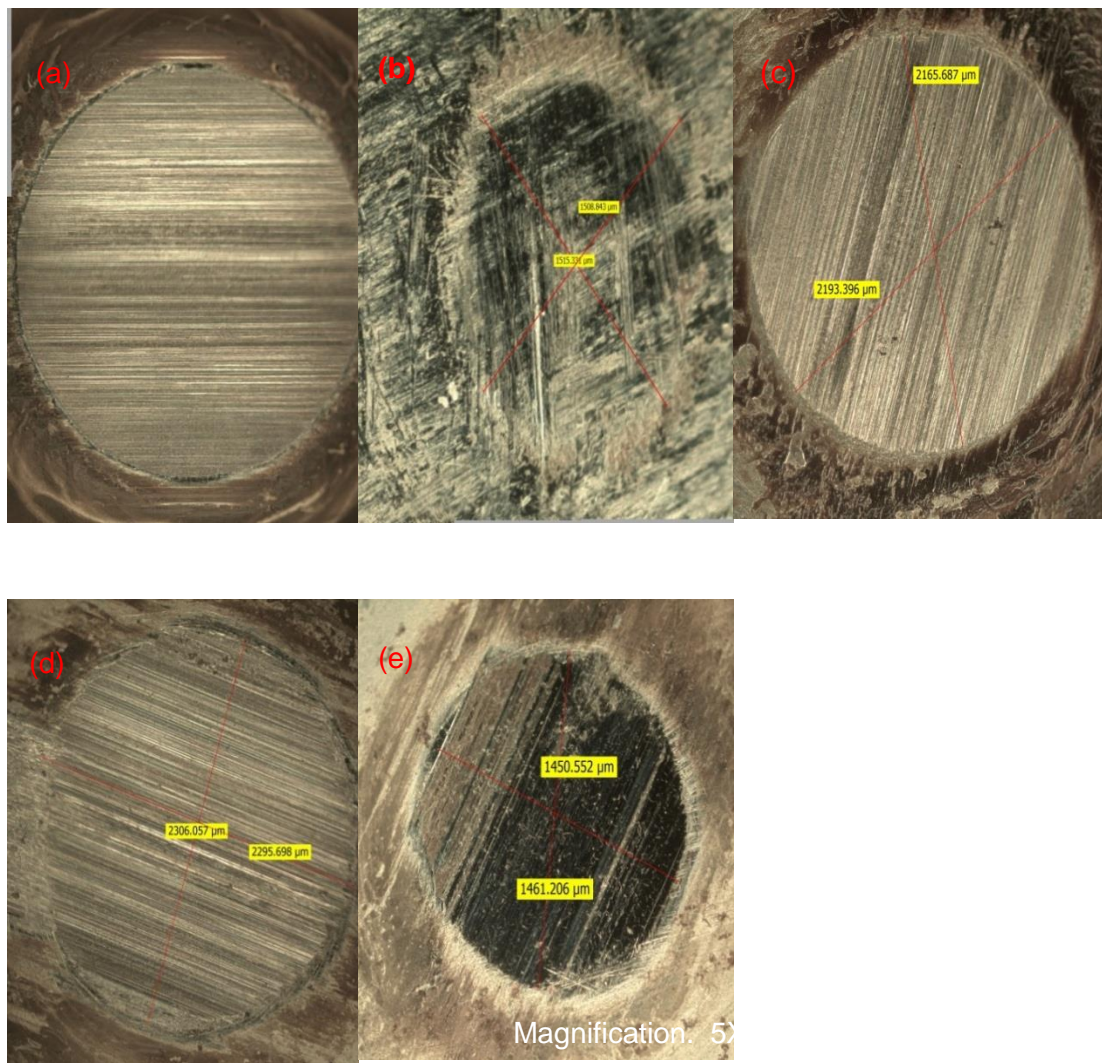


Figure 4-11 Friction plots of different coatings against base oil

The erratic friction curve from the MnPO<sub>4</sub> is unclear and this odd nature was seen for most tests carried out. However, there appears to be some interaction between the oil as well as the removal of this soft running-in coating. At the end of the test, the friction value approaches a steady state value similar to that of a steel/steel contact.

#### 4.5. Optical Investigation of Surfaces

The optical investigation was carried out with a Leica DM 600M Optical microscope in the bright field with objective lenses of 5X/0.15. Illumination was set in the range 7-2-148 to 10-5 – 135 which correspond to aperture, field and fine intensity respectively. A total magnification for active ports was set at 2.75X with the focus drive of 28.5 – 30.0 mm. These conditions were used to obtain the images of the wear scar diameter on the pins as shown in Figure 4-12, Figure 4-13 & Figure 4-14.



**Figure 4-12 Diameter of the Wear Scar of Cast Iron Pins Rubbing Against (a) Polished plate (b) a:C-H (c) MnPO<sub>4</sub> (d) Si1s (e) ta:C-H in base oil**



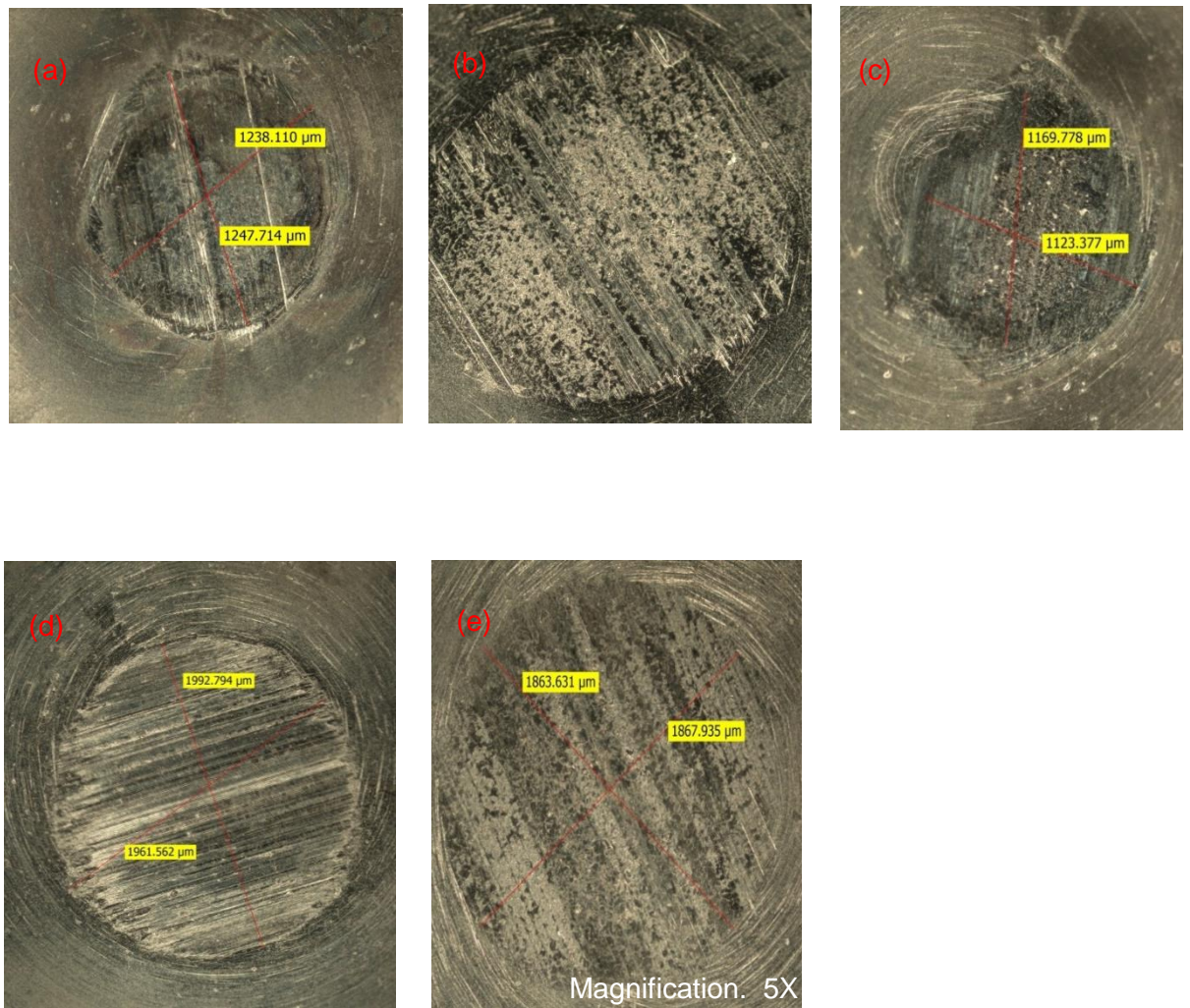


**Figure 4-13 Diameter of the Wear Scar of Cast Iron Pins Rubbing against (a) Polished Plate (b) a:C-H (c) MnPO<sub>4</sub> (d) Si1s (e) taC-H in oil A**

Optical images in base oil show the presence of thick and dense transfer layers with ta:C-H and a:C-H (see Figure 4-12). These transfer layers are responsible for the low friction observed with ta:C-H and a:C-H in the pin on plate tests with base oil [74]. Under these conditions, the systems are similar to ta:C-H/ta:C-H and a:C-H/a:C-H sliding over each other. The values are well in line for those tests with 5W30 oil in [32] and base oils in [35, 155, 179].

These coatings also had lower wear scar diameter than Si1s, Mn-phosphate and Steel in lubrication with base oil. For ta:C-H, the wear scar diameter was 1.45 mm and for a:C-H, it is 1.51 mm. These values are well below Si1s, Mn-phosphate and Steel which are 2.3, 2.37 and 2.55 mm respectively.

The wear scar values are considerably lower in Mn phosphate and steel when tested with FFA and FFB due to the ability of the oil to form a protective film on the CI surface (see section 4.6) but same cannot be said for Si1s, ta:C-H and a:C-H. The mechanism is two folds; firstly, the hardness of the coating affects the wear on the pin and the oil appear to provide some form protective film on the plates.

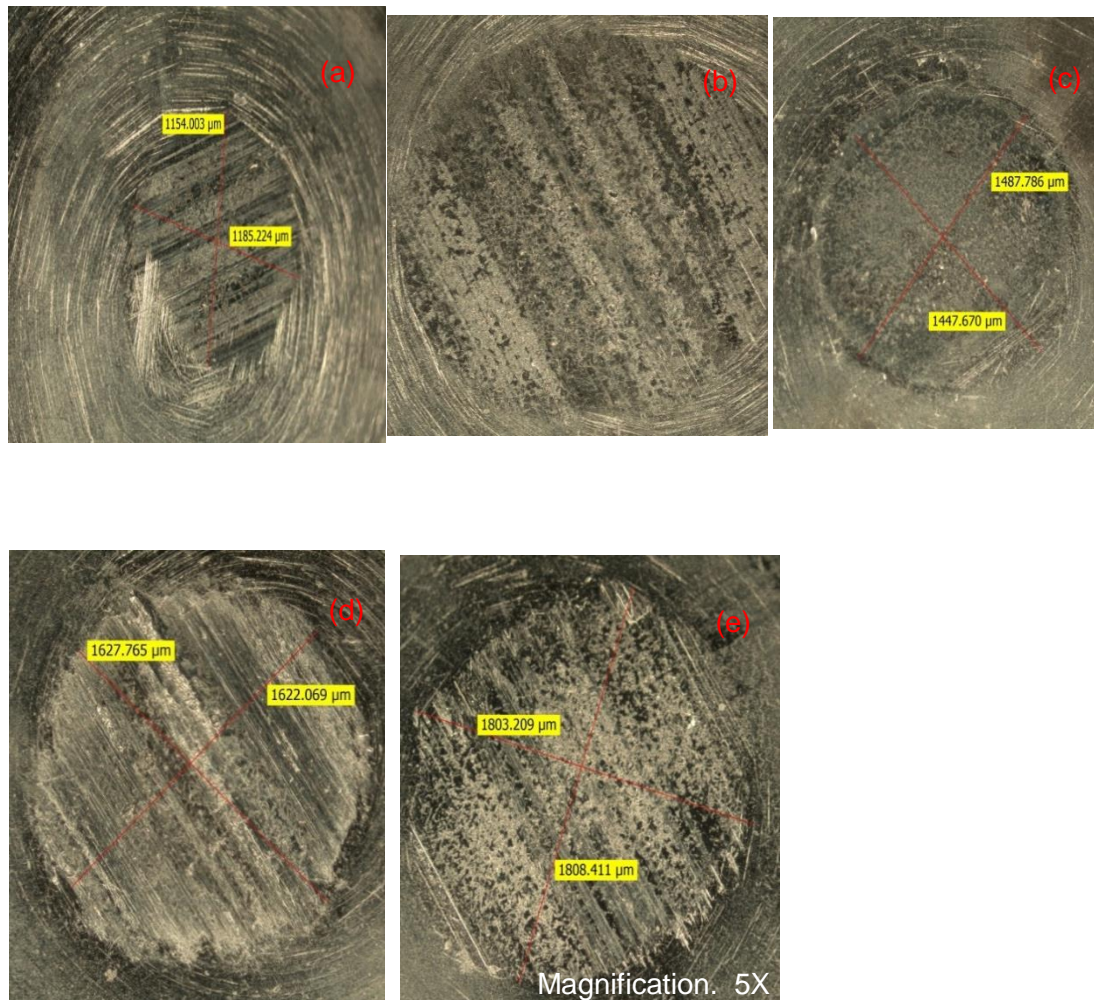


**Figure 4-14 Diameter of the wear scar of Cast Iron pins rubbing against (a) Polished plate (b) a:C-H (c) MnPO<sub>4</sub> (d) Si1s (e) taC-H in oil B**

#### 4.5.1. Wear of Coatings with FFA, FFB and Base Oils

Figure 4-15 shows the coating wear result of the plate surfaces against different oils. Non doped a:C-H and taC-H showed exceptional wear. It was observed that Si1s produced the highest wear. SEM micrographs reveal that the coating has been

delaminated during the rubbing action of the pin. EDX spectra show significant concentration of iron, thereby confirming that the entire coatings were stripped off during the tribological test. The trend also shows that base oil produced the maximum wear for Si1s, MnPO<sub>4</sub> and taC-H while FFB was observed to provide some wear protection due to its superior wear prevention properties. However, this cannot be said for a:C-H and steel.

One parameter responsible for this could be the hardness. It is widely accepted that hardness has a significant role on wear of interacting surfaces[15]. From the base oil section of the graph, ta:C-H was observed to produce higher wear. The hardness of this coating is about four to five times that of the cast iron pin which accounts for the wear observed. The reduced or negligible wear with fully formulated oil is due to the wear prevention properties of the oils as well as its ability to form boundary nanoscopic films which has the tenacity to inhibit asperity contacts. a:C-H on the other hand produces less wear than most coatings. This is due to lower hardness and the short time required for a transfer layer to cover the interacting surfaces, minimizing friction and thereby reducing the stresses necessary for deformation of solids. It is surprising though, that tests with a:C-H against base oil produce less wear than FFA. This suggests that oil FFA has low wear prevention properties.

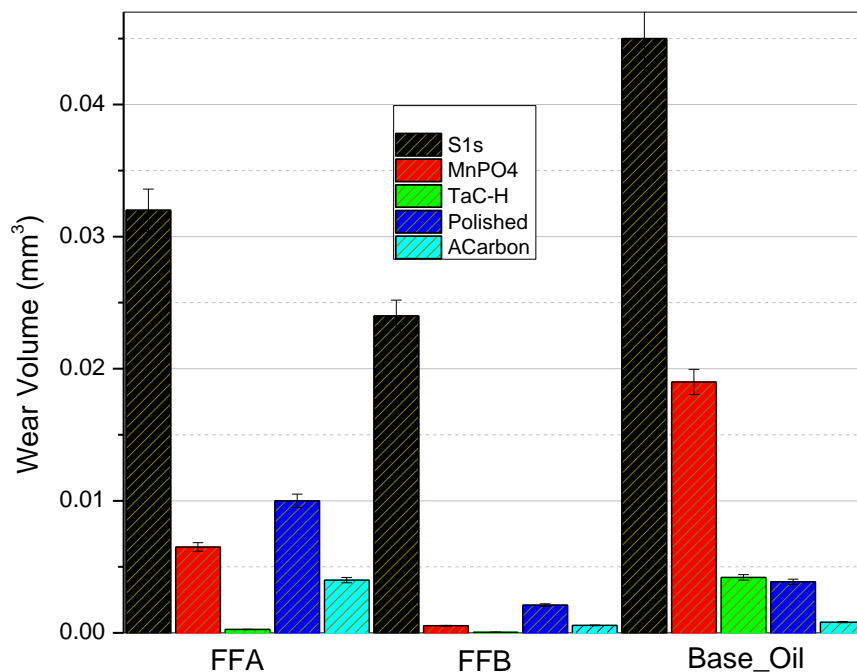


**Figure 4-15 Wear on Coated Plates as a Function of Different Oils**



This is similar for steel surfaces. The closeness in hardness and properties or interaction of the oil with the surface appears to be responsible for this phenomenon.

#### 4.5.2. Wear of Cast Iron Pins with FFA, FFB and Base Oils

The wear of the cast iron pin does not follow any particular order but it is important to note that significant advantages were gained by using the right coating on one surface in the presence of base oil. In the case of a:C-H/CI and taC-H/CI combinations in base oils, minimal wear was observed on the CI pin when compared with other combinations.

Although FFB produces lower wear in these combinations (a:C-H/CI and taC-H/CI), these values are considerably higher than those in base oil suggesting that the coating does not interact with the oil to form any protective layer. Even though nanoscopic tribofilms may be formed on the CI ferrous surfaces, they are easily removed by the hard asperity contact of the a:C-H and taC-H coatings. Steel/CI and MnPO<sub>4</sub>/CI combination gave better wear characteristic in FFA and FFB due to their reactivity with the oil and their ability to form boundary nanoscopic tribofilms.

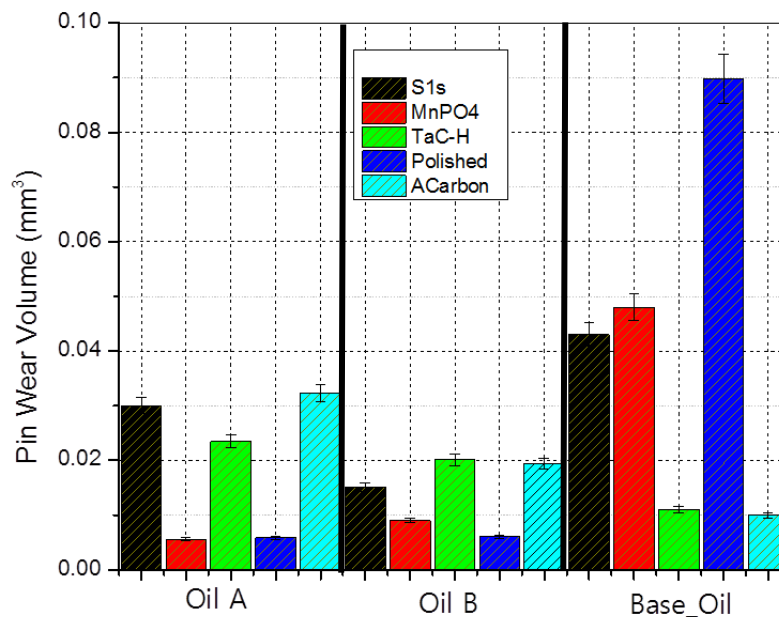


**Figure 4-16 Wear on cast iron pins against different oils**

As per the Si1s coating, despite having high reactivity with the oils, ploughing of the coating during tribological test occurred. In spite of the wear protection provided by oil FFB, complete coating strip off occurred after  $1\frac{1}{2}$  hrs of testing. This suggests that the properties of the coating are not suited for tribological applications.



## **4.6. Surface Analytical Investigations**

A series of complementary surface analytical techniques were used to investigate the composition, structure and morphology of the tribological films derived on the interacting surfaces. SEM/EDX was used to observe the morphology and composition of the film to depths of about 1  $\mu\text{m}$ . XPS was used to determine the film states and structure at depths of 10 nm. It is a very sensitive technique. Raman spectroscopy was also used to investigate film structure to support the results from XPS. The results from all these techniques are discussed.

### **4.6.1. SEM/EDX**

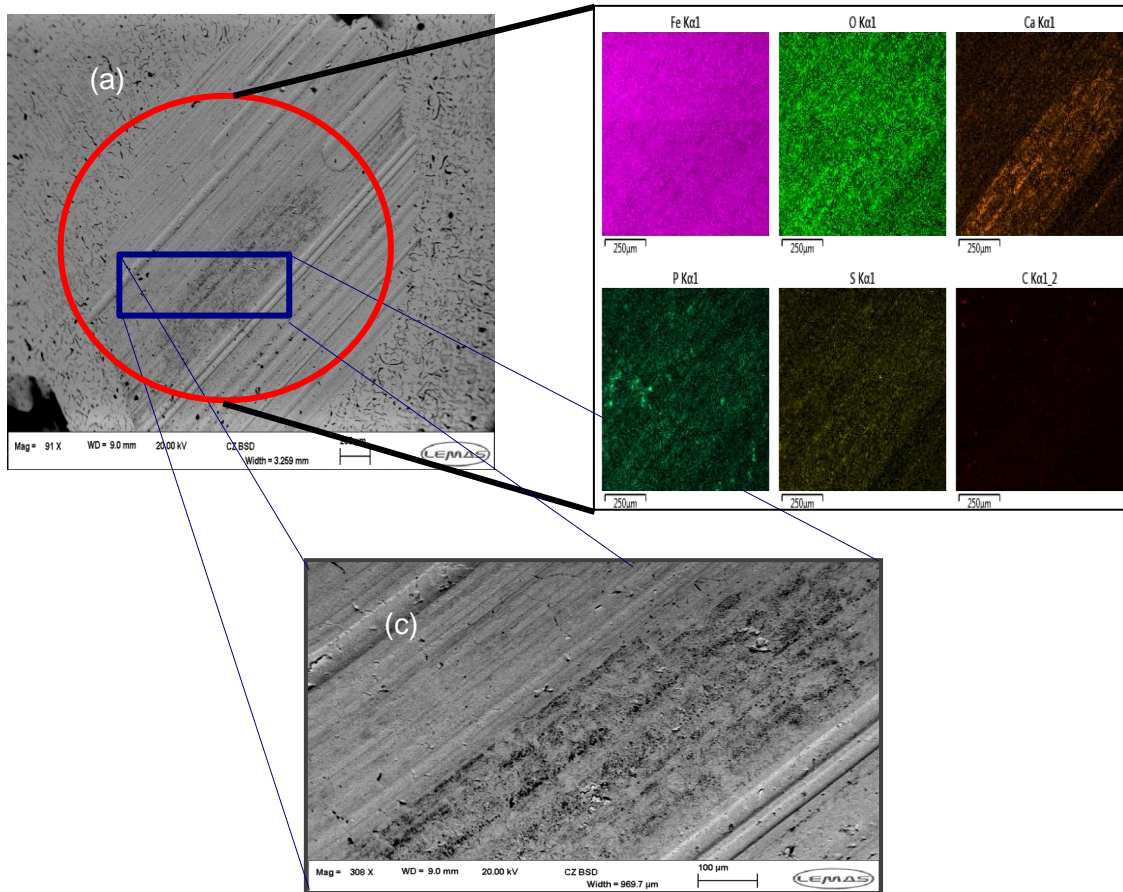
A Carl Zeiss Evo MA15 variable pressure SEM was used to study the tribofilm and microstructural properties of the coating. An Oxford instrumented EDX with scan size of 80mm<sup>2</sup> was incorporated into the device to give elemental composition of the different regions on the coating. Maps were taken at different regions to observe the level of coating failure which may have taken place on the surface during the tribological tests. Greater concentrations of the substrate or steel on the surface are indications of complete coating failure as was demonstrated by Si1s coatings.

#### **4.6.1.1. a:C-H/CI SEM/EDX Results**

The SEM/EDX micrograph and mapping of the pin surface (See Figure 4-17) shows that an interaction between the oil additive and the CI surfaces takes place. A thick layer of Ca and S is formed in the rubbing track of the pin. These are from the detergent used in the oils. The phosphorus film is evenly dispersed on the surface. The wear track also appears very smooth and no element from the coating interlayer was observed on the pin. This suggests that no severe wear took place on the coating.

The only element from the uppermost layer (0.2-0.4  $\mu\text{m}$ ) consisting mainly of amorphous carbon could have interfered during the tribological interaction. These are supported by the optical micrographs which shows dark patches of amorphous carbon transfer layers. The combination of the smooth wear surface, the presence of boundary nanoscopic films and absence of wear particles in the track give credence to the lower wear observed on the pin when compared with oil A. Another supporting factor is by a closer observation of the micrographs. With a:C-H, none of the pin surfaces showed remarkable abrasion and the wear mechanism was considered to be predominantly adhesion. Thus, the a:C-H does not cause any significant abrasion on the CI pins. This phenomena has been reported in [69]. Smoothing of the steel

surface on interaction with harder DLC coating has been one mechanisms required for lower friction. When compared with other coatings (taC-H and Si1s) it is surprising to note that the coating still aggravates the wear of the counter body. Further surface analytical techniques were used to achieve analysis of the ultra-thin reaction layer. XPS was used to probe the chemical states/structure of the species formed on the surface. These are discussed in section 4.6.2



(b)

(d)

**Figure 4-17 SEM/EDX with Oil FFB on CI Pins Showing (a) Micrograph of Wear Track (b) Map on the Track with Key Additive Elements (c) Well Dispersed Tribofilm Composed of Ca, P and S (d) EDX Spectra of Track.**

In **Figure 4-18**, the EDX spectra reveal that only phosphorus and calcium is adsorbed on the surface of a:C-H coating. The coating microstructure equally appears unchanged after 12 hrs of testing. The tungsten interlayer observed is due to the technique which probes a few microns into the substrate. XPS analysis was used to confirm that the interlayers were not stripped off during the tests.

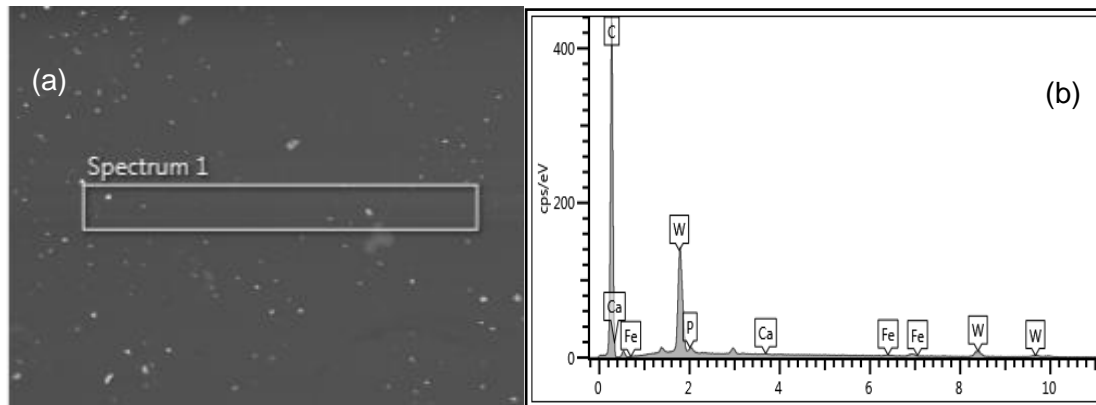


**Figure 4-18 SEM/EDX showing (a) Wear Track Morphology on a:C-H (b)EDX Spectra on Wear Track.**

#### 4.6.1.2. ta:C-H/CI SEM/EDX Results

Investigation of the SEM micrographs show multiple white striation marks in the track which indicate slight abrasive wear processes on the surface of the coated plates. SEM/EDX mapping reveals these to be Ti/Cr from the interlayer used in the coating. From the oil additives, a low concentration of phosphorus was observed on the surface. This suggests that minimal or no chemical reactions took place between the lubricant additives or that the films formed are heterogeneously dispersed after 12 hrs of testing on the taC-H DLC coated surfaces (Figure 4-18). However, it is important to remember that EDX probes to 1  $\mu\text{m}$  depth and so any very near surface changes may not be detected. Near surface analysis using XPS will aid in ascertaining the nature/states of the tribofilms.

Evaluation of the surface of the pin shows some interesting results. The surfaces appear rather rough, equally supporting an abrasive wear process. From the micrographs, this can be attributed to small wear particles from the coating which find their way to the rubbing track, thereby causing third body abrasive wear. The

presence of Mn from the plate substrate is still unclear as the coating does not appear entirely stripped off during the tribological tests.

Lubricant additive species of Ca, S, P and Zn were all observed in the wear track whereas Si, Ti or Cr from the coating interlayer were not seen in the spectra. In addition, the tribofilm on the pin does not appear to have a distinct tribolayer when compared with a:C-H/CI and Si1s/CI combinations.

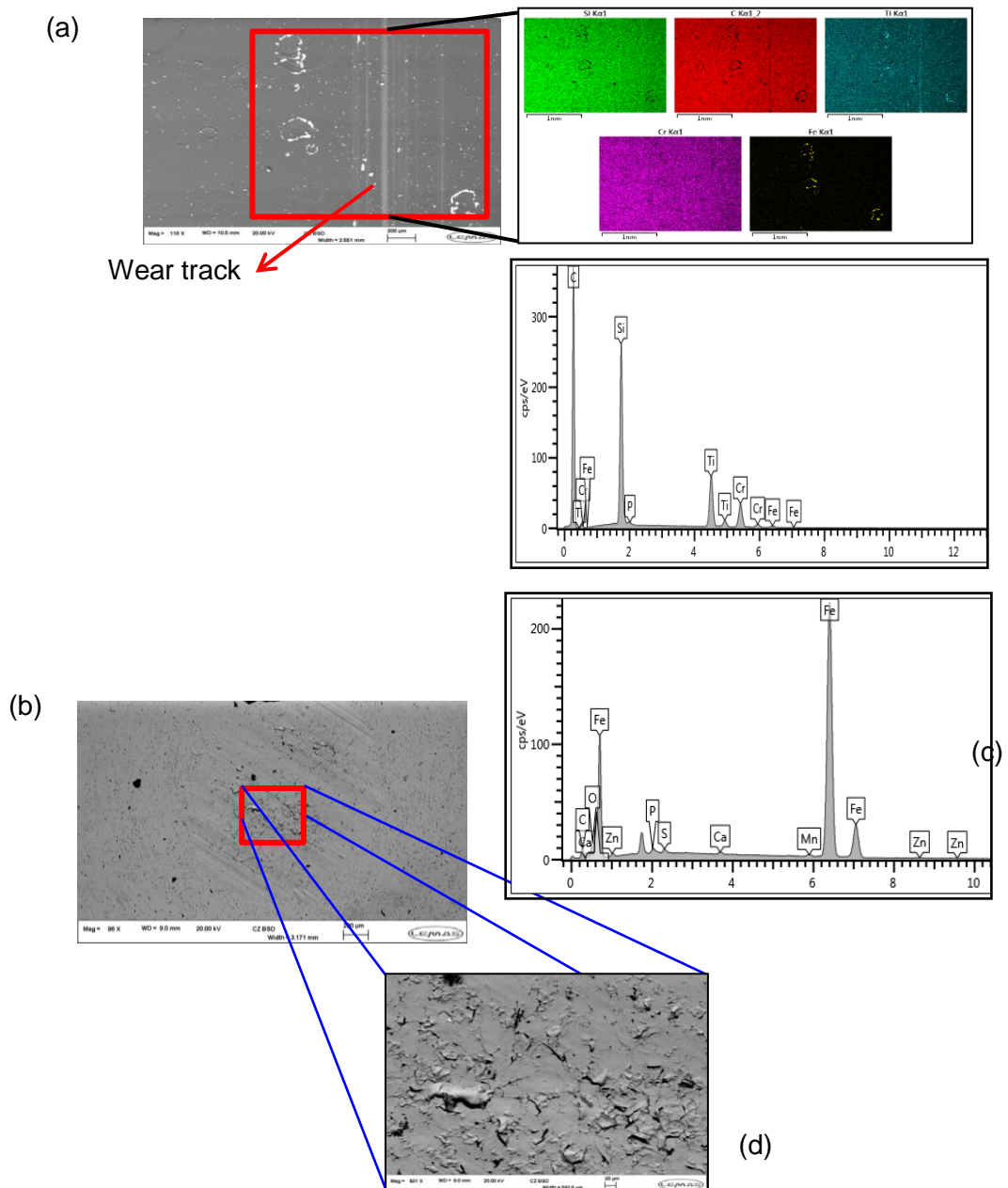
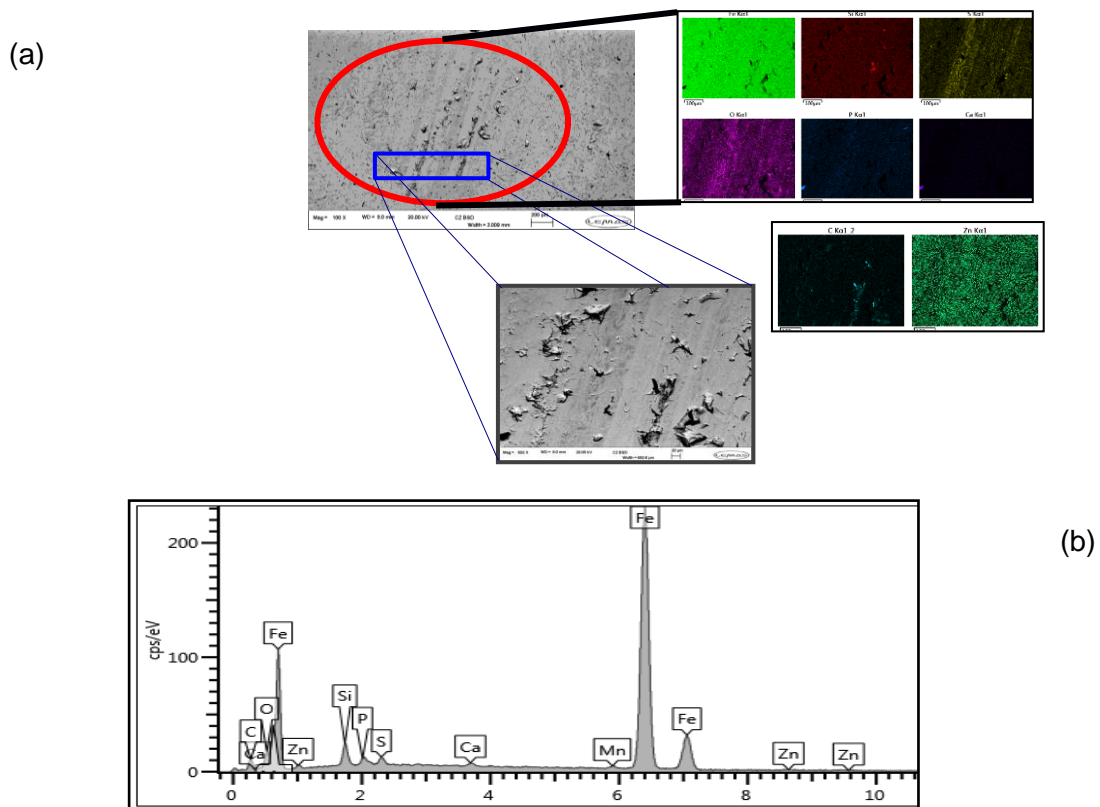


**Figure 4-19 SEM /EDX with FFB Showing (a) Morphology, Map and Spectra of Wear Track for taC-H (b) Wear on CI pin (c) EDX Spectra of Wear Track (d) Morphology Wear Track with Hard Particle from Coating Surface**

#### 4.6.1.3. Si1s/CI SEM/EDX Results

The CI pin surface appears rough with significant traces of silicon and carbon in the wear track. Regions that show grooves on pin surface correspond to silicon and carbon. These are clear indications of hard abrasive wear particles that plough out small chunks of the tribofilm. A smooth tribolayer of sulphur, silicon and oxygen was observed from EDX mapping. Since the lubricant additives were also observed on the pin surface, it can be said that the tribofilm is composed of a transfer coating material and reaction products from the lubricant additives when both FFA and FFB are used.

For the Si1s coating, SEM mapping shows coating failure was experienced with FFA. Similar results were obtained with oil FFB which had better wear prevention capabilities. The entire coating architecture was stripped off from the surface leaving the 16MnCr5 steel substrate. The traces of Cr seen in the mapping are those from the substrate metal as the Fe intensity clearly reveals that the region is entire Fe. Regions inside the wear track were also seen to be composed of a mixture of coating particles removed during tribological processes and reaction products of Ca,S, Zn and P in the lubricant (see Figure 4-20).





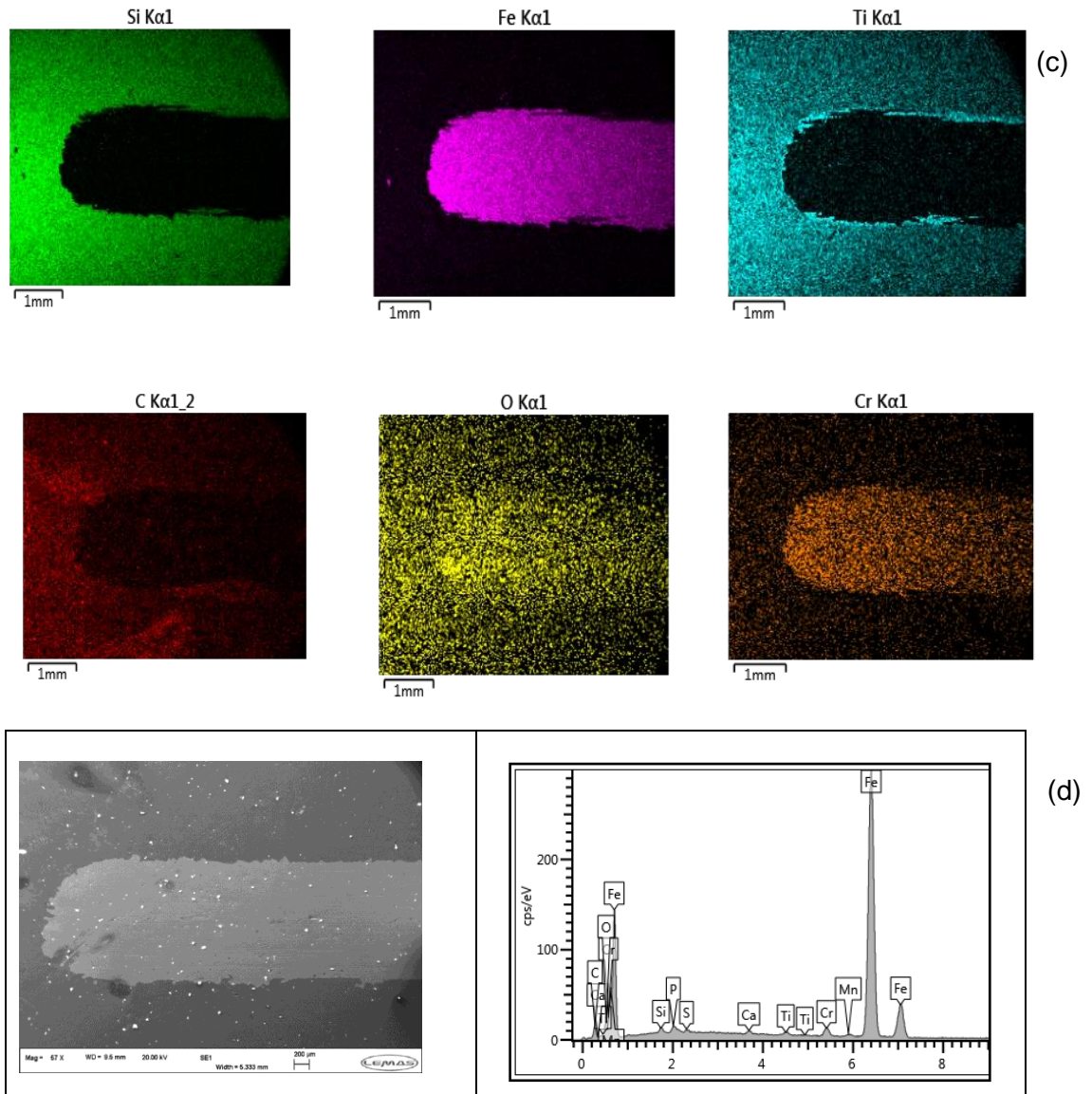


**Figure 4-20 SEM /EDX with FFB showing (a) Morphology, Map and High Magnification of Wear Track on CI Pins with Traces of Coating Wear Particle (b) EDX Spectra of Wear Track on CI pin (c) Mapping of Wear Track on Si1s Plate (d) EDX Spectra of Wear Track on Si1s Pin**

#### 4.6.2. XPS

XPS High resolution rescan of key elements was used to obtain better results since some coatings experienced delamination and it would be important to identify the states of the new species that had been formed. The new elements added include Si, Ti, Cr and W. Spectra were also taken inside and outside the track to enable distinctions to be drawn from those key compounds or species which may have been formed due to tribological reactions. Details of the outcome from each of the combination are briefly discussed in this results section with more extensive outline in the Chapter 9.

#### **4.6.2.1. XPS Results on DLC Coatings with FFA and FFB (a:C-H, Si1s and ta:C-H)**

The survey spectra on the a:C-H coating (see

Figure 4-21) reveal some interactions with Ca, P and S as opposed to the presence of P obtained from the EDX spectra. While this can be attributed to the heterogeneous nature of the tribofilm and the sensitivity of the technique, it may also indicate that the coating surface has more reactivity than its taC-H counterpart. However, both results suggest that an interaction with Ca, P and S occurs with both oils. Oil FFB does not have any S peaks and the high resolution rescan did not give any indication of this element on the surface. Presence of N can be attributed to the dispersants used in the oils. No Zn2p peaks were seen with both oils.

The XPS results from the taC-H are somewhat puzzling. In oil FFB, some phosphate films were formed on the surface of the plates. It thus means that the formulation of the oil have an effect on its interaction with the surface. Firstly, this oil has significantly higher concentration of antiwear additives than the oil FFA, thereby suggesting that the concentration may play a role in its reaction with non-ferrous surfaces. A closer look at the spectra does not reveal any peak of Zn3s. Further analysis of the Zn2p confirms that no Zn is adsorbed on the taC-H plate

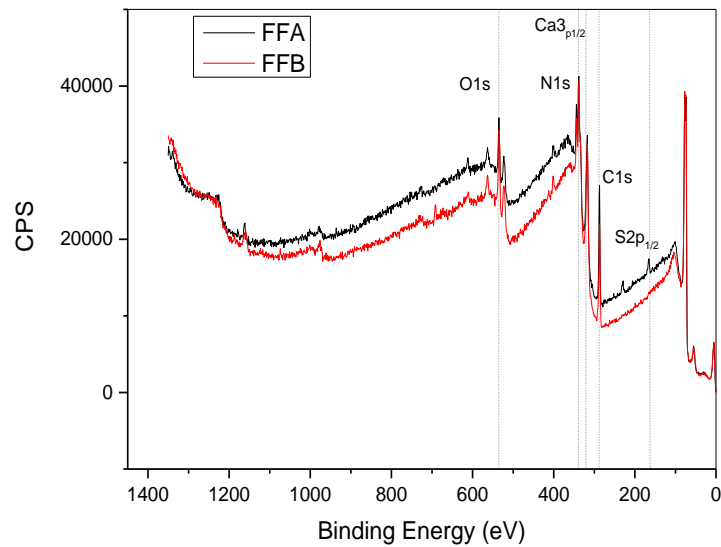


**Figure 4-21 XPS Survey Spectra on a:C-H Plates with FFA and FFB.**

This suggests that the presence of ferrous surfaces are necessary for the break-down of the ZDDP molecule before the Zn is then adsorbed on the surface [93]. This process is grossly lacking with taC-H as the Fe is replaced with carbon. Fe initiates the breakdown of the ZDDP molecule by replacing Zn. A reaction which cannot be started with carbon from the DLC. The only source of Fe will be from the pin which is why they form phosphate films in the wear track.

#### **4.6.2.2. XPS Results on Steel Plates and Cast Iron Pins (Counter body)**

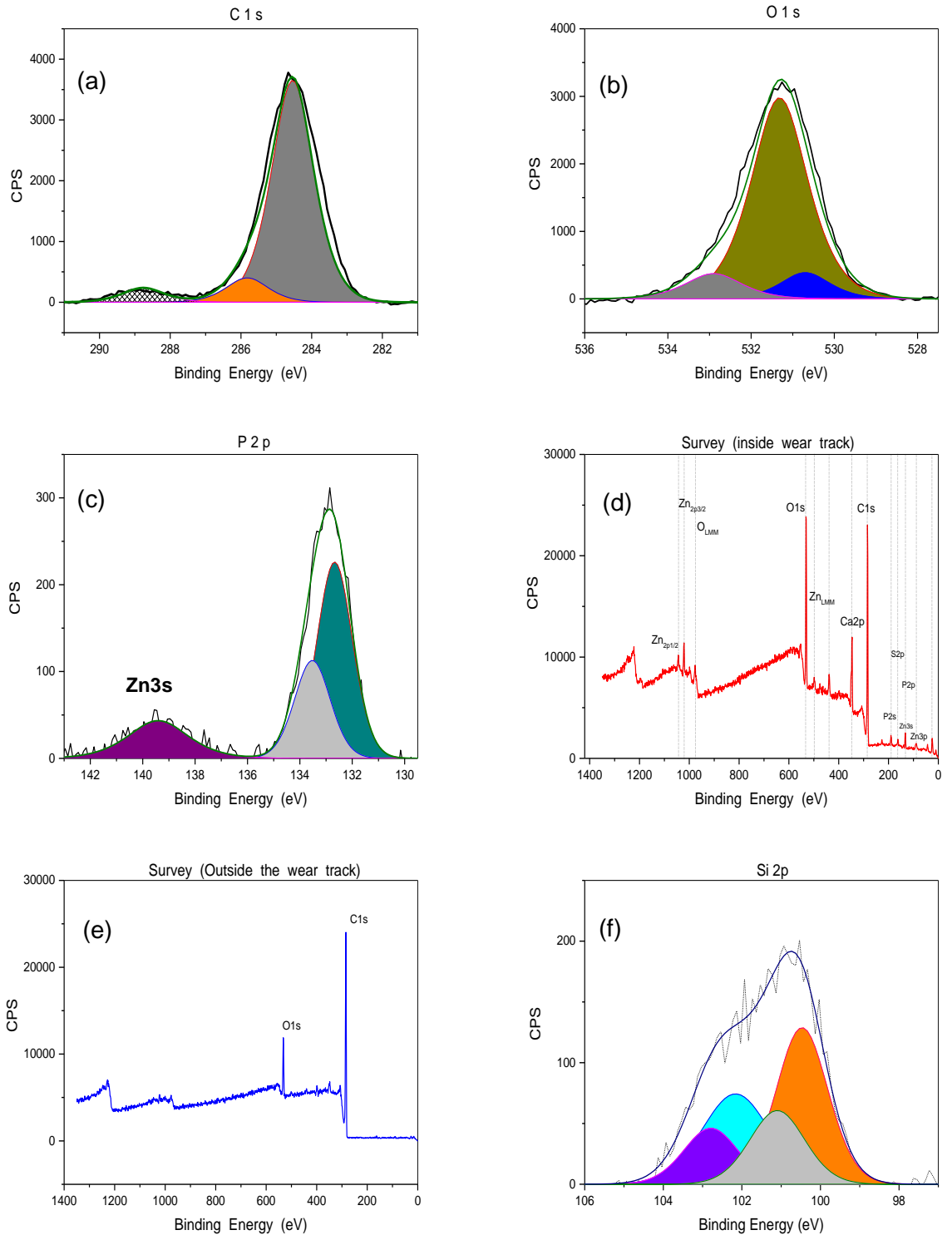
Figure 4-22 presents the XPS spectra of cast iron on regions both inside and outside the wear track. The survey spectra shows the distinction between both regions. In the wear track, significant phosphates, sulphur and calcium were observed in the wear track. Outside the track, only carbon and oxygen were seen. Some tungsten was also seen on the cast iron pin when rubbing against a:C-H (not shown). This indicates mild wear or a transfer layer from the coating surface. The O1s spectra was deconvoluted into three different components with the metallic oxides corresponding to ZnO. Chemical and molecular characterization of the phosphorus and calcium corresponds to short chain calcium phosphates. Outside the wear track, high resolution rescan show sulphides, sulphate and calcium with no trace of Zn.

On interaction with Si1s, silicon carbides (Si-C) and Silicones (Si-O-C) were formed in the wear track. SEM morphology show the track to be very rough due to the hard nature of the SiC/Si-O-C particles. The results confirm that particles of the coating are

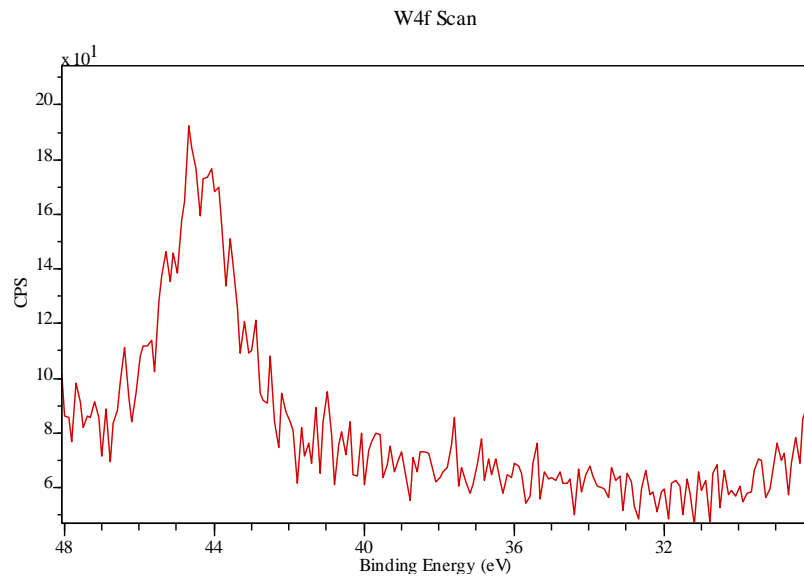


embedded in the contact and worsen the wear mechanisms. This is because Si-C are about 1.5 times harder than haematite which may have formed on the surface and about 3 times harder than ZnS or ZnO tribofilms.

On interaction with a:C-H, some tungsten was derived on the surface of the cast iron pin with oil FFA (See Figure 4-23), indicating that some delamination of the coating must have taken place during the tribological reaction and then transferred onto the pin. The Zn2p XPS spectra obtained on interaction with a:C-H are similar with those of steel and broader than those of the Si1s and taC-H. The absence of iron on the wear track also suggests that the tribofilm on the pin are dispersed and composed mainly of ZnS and ZnO. This is following deconvolution of the oxygen spectra into three components and further analysis of the S2p peaks.



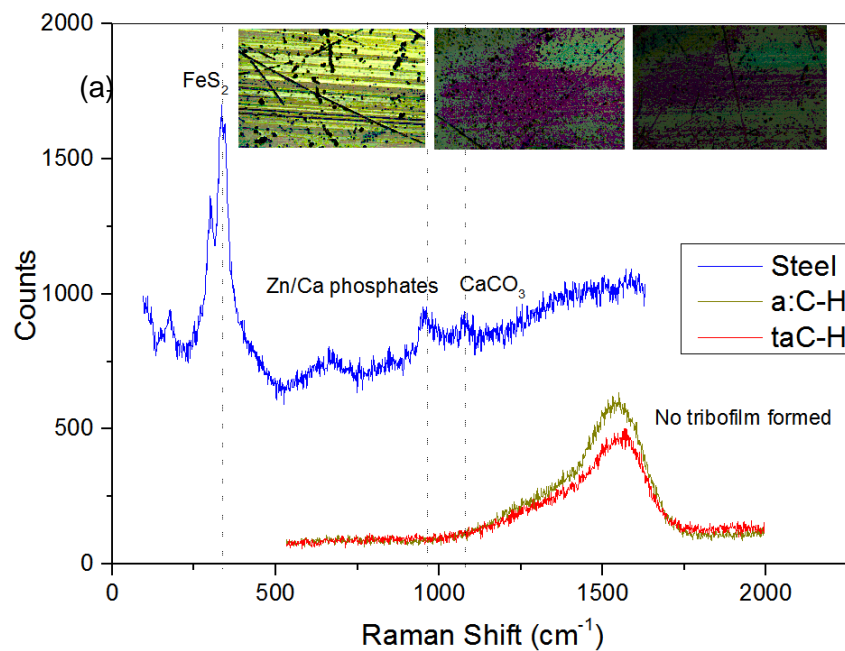
**Figure 4-22 XPS Analysis of Cast Iron Pins Inside and Outside Wear Track Showing (a) C1s Peaks (b) O1s Spectra (c) P2p Spectra showing Zn3s Peaks (d) Survey Spectra - inside wear track (e) Survey Spectra - Outside Wear Track and (f) Si2p Inside Wear Track.**



**Figure 4-23 XPS Spectra of W4f on a CI pin indicating transfer film from a:C-H**

#### 4.6.3. Raman Spectroscopy

The Raman spectra for the DLC coatings were taken at 5%, 10% and 50% laser power to prevent any damage on the DLC coatings. Tests were taken at the extended and full range with 1, 2, and 10 accumulations on the 488 nm laser wavelength. The samples were exposed for 5 secs and spectra were obtained both inside and outside the wear track.



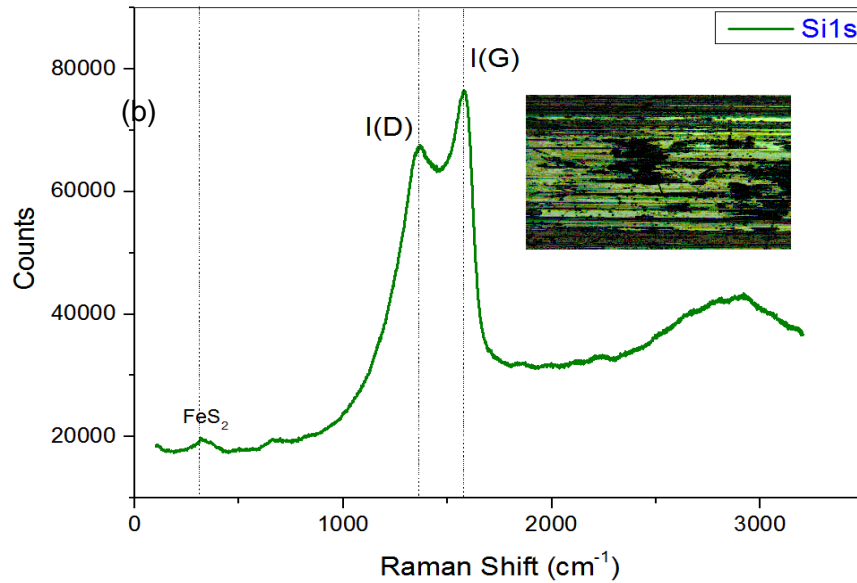


**Figure 4-24 Raman spectra of (a) coating surfaces and (b) Si1s with FFB**

Figure 4-24 shows the Raman spectra for the different coating surfaces investigated. The steel surface shows striations due to the abrasive wear processes taking place on the surfaces. With taC-H and a:C-H there were no tribofilms formed on the surface. In addition, the amorphous carbon DLC had a broad  $sp^2$  Raman cross section which overshadowed the  $sp^3$  peak. The Raman spectrum thus has a broad G peak at  $1580\text{cm}^{-1}$  which is due to the laser power of  $488\text{nm}$  used for the analysis [169].

Although the optical Raman images of a:C-H and taC-H shows brown patches close to the track, their physical appearance was unchanged. Peaks observed correspond to I(G)/ $sp^2$  i.e. the C-C bond on the DLC coatings. Steel surfaces show significant interaction with the coating with the formation of Ca/Zn phosphate and  $\text{CaCO}_3$ . Clear traces of  $\text{FeS}_2$  were also seen with peaks at  $330\text{-}341\text{ cm}^{-1}$  [168]. For the Si1s coatings, optical images show complete coating delamination with narrow shoulders of  $\text{Fe}_3\text{O}_4$  at  $675\text{-}680\text{ cm}^{-1}$  and sharp peaks of  $\text{FeS}_2$  [88]. The sharp clear I(D) and I(G) appear at  $1350\text{ cm}^{-1}$  and  $1580\text{ cm}^{-1}$  respectively and correspond to C-C and C-H bonding in the coating. This does not appear to have been changed by the coating when compared with regions outside the wear track (spectra not shown).

#### **4.7. Summary of Findings**

The friction, wear resistance and tribological interaction of polished steel,  $\text{MnPO}_4$ , Si1s, a:C-H and taC-H have been investigated in FFA, FFB and base oil solutions. It

was generally observed that lower friction coefficients were observed in base oils. The use of several surface analytical tools to determine the mechanical properties of the coating and the chemical films derived on interacting surfaces has shed more light on the key parameters which affect the friction, wear and nature of the tribofilms formed. Findings are summarized below;

- i. The ta:C-H and a:C-H showed exceptional wear characteristics. Raman, EDX and XPS studies revealed that the coatings a:C-H and taC-H are not very reactive with the oil, only Ca and S absorb on the surface with minor traces of Phosphorus when tested with oil FFA.
- ii. The oil type has a significant influence on the wear and friction behavior of the coating and pins. Base oil provided the lowest friction (a:C-H/Cl on base oil with  $\mu = 0.05$ ) with higher wear.
- iii. Wear analysis of the coating revealed that Si1s coating is less resistant to wear. Scratch test analysis reveals that the maximum Lc of the coating was about 19 N and complete coating failure occurred during testing. The hardness of the coating has an effect on its wear and that of the counter body.
- iv. The tribofilm seen on the pin surface is a mixture of transfer layers from the coating and the reactive products from the lubricant additives. In all cases, the presence of catalytic ferrous surfaces appear to be essential for the formation of tribofilms with certain DLCs

## **CHAPTER 5. SINGLE CAM RIG DESIGN, DEVELOPMENT AND EXPERIMENTAL PLAN**

### **5.1. Foreword**

This chapter of the thesis discusses the development and design of the single cam rig. The key features highlighted here are, the instrumentation and calibration of the test kit. While the focus of this research endeavour is to further understand tribochemical reactions that take place at the interfaces, it was equally important to develop a single cam rig that is capable of ranking lubricant chemistries and evaluating the performance of surface coatings. It focuses on interlayered lubricant films formed across the camlobe and on inserts. As such, the methodology used on the single cam rig should be suitable for tribochemistry studies and characterisation of the tribofilms formed on the cam and follower. The rationale was to link the component bench test to the pin-on-reciprocating plate tribometer (Chapter 9), mapping of the tribochemical films across the cam profile (Chapter 8) and resolving the torque as a function of cam angle (Chapter 5 and 8).

Tribochemistry studies are becoming very important because the nature of the inter-layered film formed during tribological reaction as well as their role in controlling the friction and wear of interacting systems. An understanding of the phenomenon will be very important to lubricant formulators in optimising system performance.

On another note, component level tests are crucial to the overall improvement of internal combustion engines. This is because they test the tribocomponents under practice oriented operating conditions and provides sound knowledge required for the enhancement of the tribopair. They also provide the tribologist with flexibility over operating conditions, interacting materials and ease of instrumentation. According to Czichos [80], certain test results can be related to the particular tribo-engineering structures. A prime example has been demonstrated by Mufti and Priest [5] with the inlet valve train in motored and fired conditions. It was observed that the friction response in the motored tests mirrored those in the fired tests. This can lead to huge monetary savings due to the extended test duration usually required for automotive engines components.

Another aspect where they could be particularly useful is when there have been new material/surface coating modifications where no prior test data or track records are available (typical example is DLC coatings). Conventional tribometers like the PoP

tribometer can also be used in this area but primarily to study specific tribological phenomena rather than to simulate tribo-engineering structures.

## 5.2. Development/Design of Single Cam Tribometer

The development of the single cam rig can be subdivided into three stages as shown below;

- Cylinder head modification – (Design stage 1)
- Components Calibration and Instrumentation (Stage 3)
  - Torque transducer
  - Electric Motor – ABB ACS 800
  - Shaft Encoder
  - Load Cell
  - Oil Bath
  - Thermocouples
- Noise filtering and friction/torque evaluation (Stage 3)

### 5.2.1. Modification of Engine Cylinder Head

This involves the sectioning of a 1.25 L 16 valves Dohc Ford Zetec (SE) engine cylinder head which will be termed as a 'SLICE' in the subsequent part of this report. It essentially consists of a single cam-lobe shaft driven by a 2.2 Horsepower dynamic braking motor in contact with a direct acting mechanical tappet which has removable inserts with diameter of 25mm and thickness of 2.65-2.70 mm. The lobes and tappets enjoy a clearance of 0.17-0.23 mm for the inlet camshaft and valve lift occurs in  $112^{\circ}$  revolution. The tappet is made out of trough hardened 16MnCr5 steel (See Figure 5-2) with thin film surface coating of Mn-Phosphate, hardness of 60-70 Rc and centreline average surface roughness ( $R_a$ ) of 0.35  $\mu\text{m}$ .

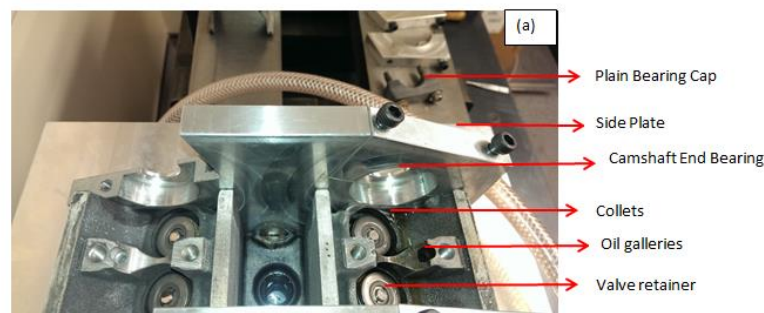


**Figure 5-1 Modified Cylinder Head (SLICE)**

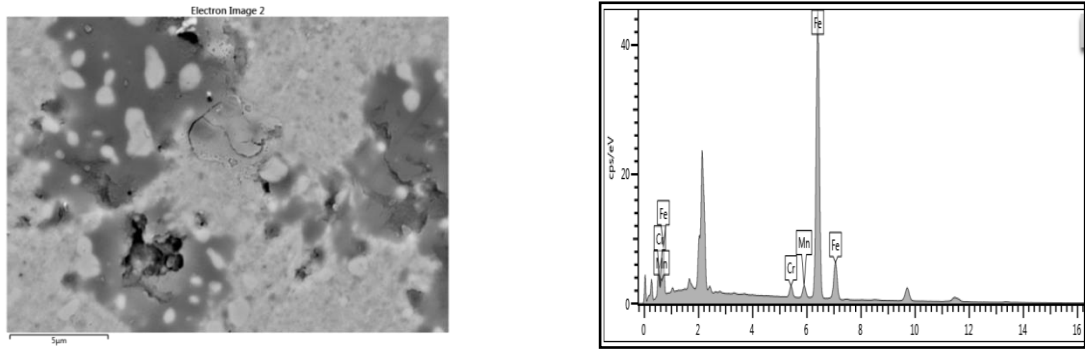


**Figure 5-2 SEM/EDX Spectra for Production Tappets of through Hardened 16MnCr5 Steel.**

### 5.2.2. Camshaft Modifications

The camshaft was slightly modified to accommodate the design configuration of the rig. This was achieved by sectioning the inlet camshaft into four bits in sets of 2 cam lobes each. At the ends of the modified camshafts, holes were made to fasten them to stud shafts. The modified camshaft assembly is shown in Figure 5-3b. Camshafts were made of induction hardened cast iron with hardness of 50-55 R<sub>c</sub>. This shaft was then connected to a high sensitivity torque transducer by means of flexible couplings to account for any misalignment. The plain bearings at the centre between the camlobes were grounded off to prevent any contact and eliminate friction at this point. The only bearing friction in the system are from two camshaft ball bearings.

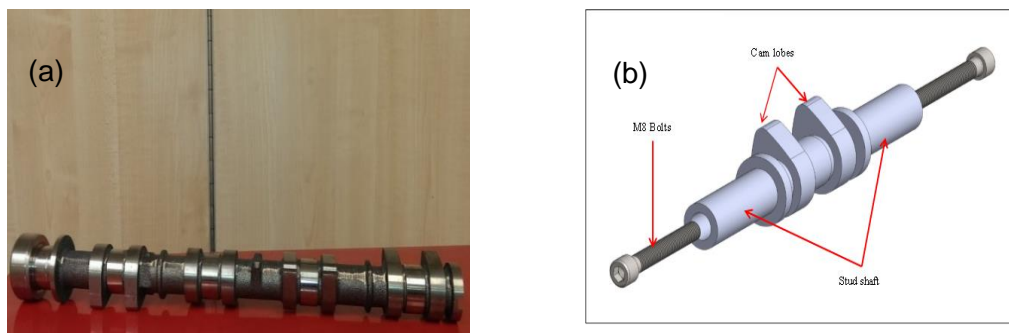


**Figure 5-3 (a) Standard Ford Fiesta 1.25L Engine Camshaft (b) Modified Camshaft Assembly with Stud Shaft and M8 bolts**

### 5.2.3. Side Plates and Dummy Shaft

Two side plates were machined to house the single cam rig assembly. Essentially, their initial design configuration is as shown below. Modifications along the top edges



were carried out to minimise weight. The forward end of the side plate holds the inlet camshaft to the SLICE by means of two end SKF bearings, while the aft region holds the dummy shaft in place. This dummy shaft is put in place to make the rig more compact and maintain rigidity as would have occurred in an engine.

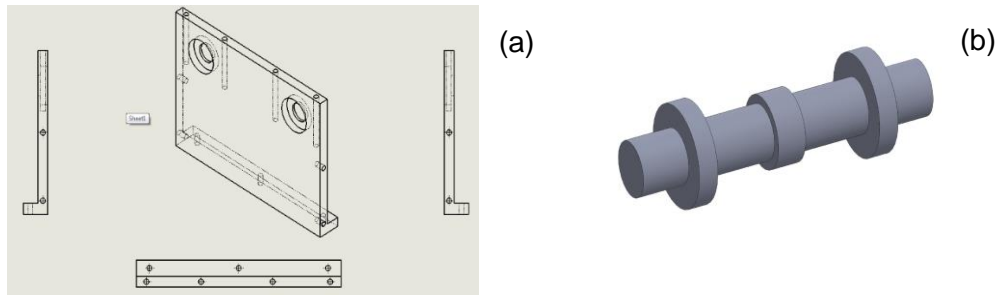


**Figure 5-4 (a) Side Plate and (b) Dummy camshaft**

#### 5.2.4. Displacement Transducer and Cam Follower Dynamics

Valve profile characteristics were determined with displacement transducer/dial indicator and protractor configuration (see Figure 5-5). This is to calculate the valve lift to corresponding cam angle. It involves mounting a displacement transducer/dial at the end of the valve. The valve profile will then be determined from the displacement values of the sensors. A typical example obtained with a digital dial indicator assembly is show in Figure 5-5. These values are then used to obtain the slide roll ratio and Hertzian Stress for corresponding cam angles.

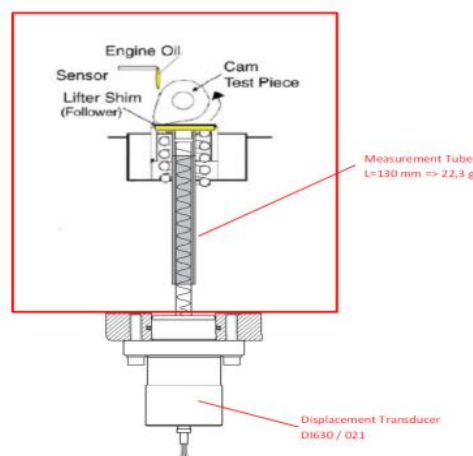


**Figure 5-5 Mounting of Displacement Transducer on Valve Train (Adapted from [32])**

### 5.2.4.1. Cam Lobe Profile and its Effects on Lubrication Films

The cam profile plays a significant role on the behaviour of the breathing and exhaust process in an engine. By controlling speed variations, level of vibrations/noise, lubrication regimes across profile, slide roll ratio and inertia loads on the systems are significantly varied. Figure 5-6 shows the effect of the camlobe profile on film thickness and entrainment velocity. For most cams where the action angle covers about one-third of the entire duration, these regions are expected to go through boundary (nose), mixed and elastohydrodynamic lubrications.

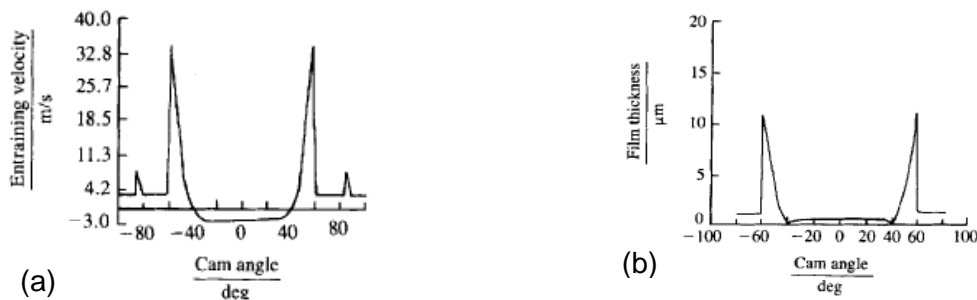


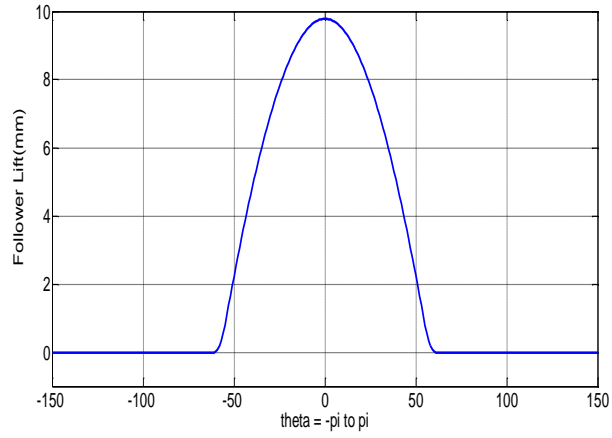
**Figure 5-6 (a) Effects of Camlobe Profile On Entrainment Velocity And (b) Film Thickness [12]**

### 5.2.4.2. Cycloidal Motion of Cam Profiles

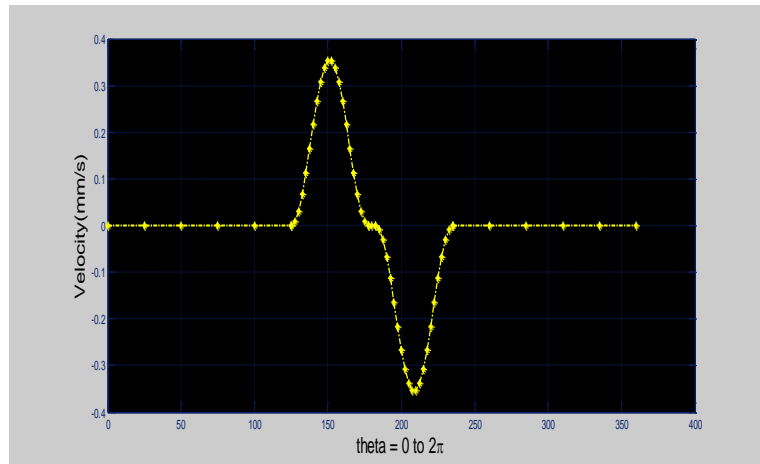
Cycloidal motion for cam profiles is one of the most widely used because it can accommodate high speed, gives smooth motion, produce minimum vibration/noise, improves the stability of the system and a unique clearance can be placed between the camlobes and tappets at the base circle region. Its values are best evaluated with **Equation 5-1**. This is to also minimize rolling friction. Its only disadvantage is in the development of high inertia forces in some cases due to greater accelerations generated by the profiles [180]. Description of some cam profiles and their applications are shown in Figure 5-7. The profile used in this work is from a modified cycloidal motion. Details of the its follower lift profile, velocity and Hertzian contact stress are shown in Figure 5-7

$$\text{Valve Lift } (L) = h \left[ \left( \frac{\theta}{\beta} \right) - \left( \frac{1}{2\pi} \right) \sin \left( \frac{2\pi\theta}{\beta} \right) \right] \quad \text{Equation 5-1}$$

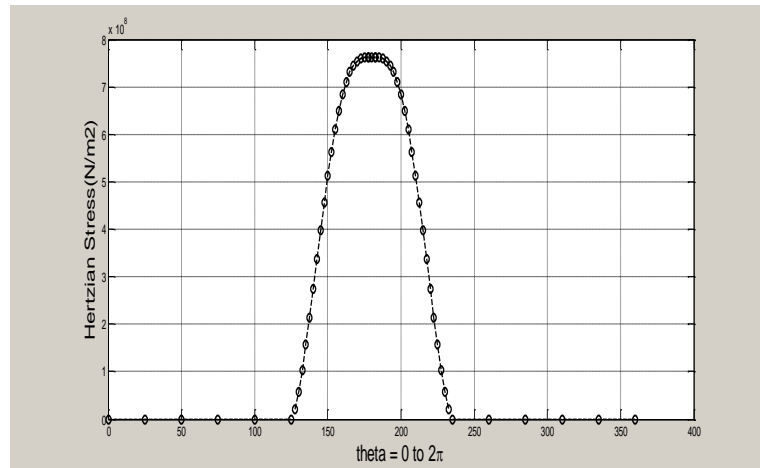
*h* is height,  $\theta$  is the cam angle,  $\beta$  is the linear displacement.



(a)



(b)



(c)

**Figure 5-7 (a) Cam-Follower Lift Profile (b) Cam Follower Velocity Profile (c) Hertzian Contact Stress Profile**

**Table 5-1 Comparison of some cam profiles used in engineering systems[13, 180]**

<b>Cam Profiles</b>	<b>Advantages</b>	<b>Disadvantages</b>	<b>Applications</b>
<b>Simple Harmonic Motion</b>	Can produce minimum acceleration than cycloidal profiles in certain conditions, thereby lowering inertia forces of the	Discontinuities of the acceleration at the end and beginning of the stroke	Used in combination with other cam profiles. Employed for moderate speed devices in textiles etc
<b>Double Harmonic</b>	Eliminates the discontinuities of the SHM at the dwell regions	Results in the production of bigger cam lobes	Medium/low speed applications.
<b>Cycloidal motion</b>	Smooth motion with no discontinuities of acceleration. Minimum noise and Vibration.	May produce High inertia loads than other profiles	High speed engines
<b>Cubic no. 2<sup>'''</sup></b>	No discontinuities of acceleration at the transition points.	Difficult construction method and discontinuities at the beginning and end of the acceleration stroke.	Significantly used in combination with other cam curves.

### 5.2.5. Shaft Encoder

A Hohner shaft encoder with a 720° pulse wheel of 25.4mm diameter was affixed to the end of the camshaft by means of a non-conducting bellow. This was to ensure that there was no thermal drift on the shaft encoder and enable accurate cam angle triggering. A tether was used to adapt the encoder to the rig surface by mean of set screws. Figure 5-8 shows the mounting arrangement for the shaft encoder.

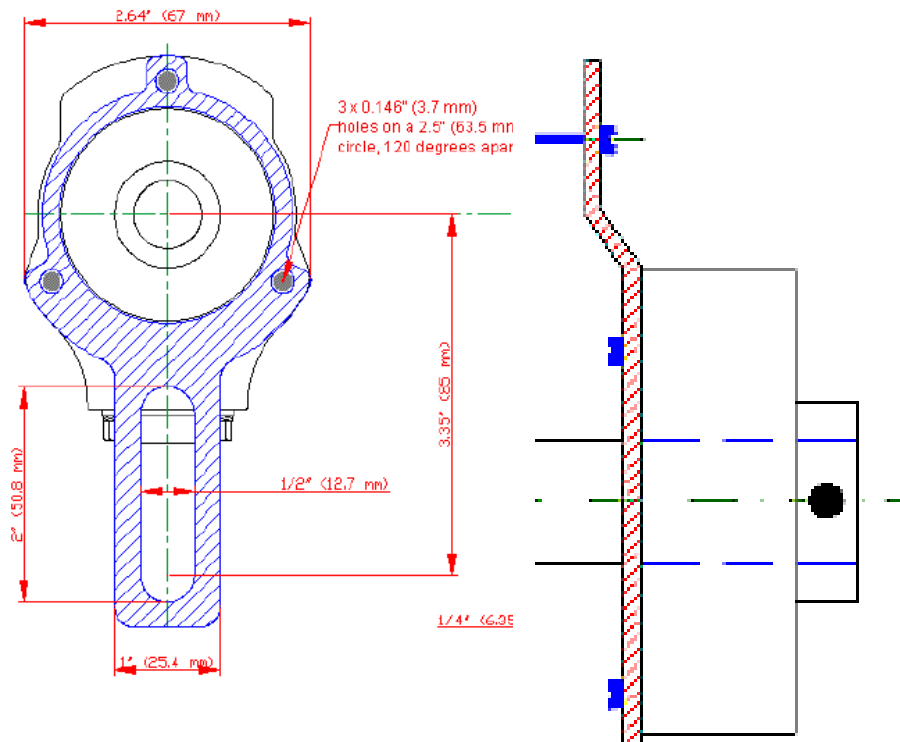


**Figure 5-8 Mounting Instructions for Shaft Encoder**

The encoder also aided in the determination of cam nose friction torque measurement upon completion of its calibration. Three different pulse states were generated from the cam rotation. Two reference pulses of A and B, were obtained with B as the lagging state, and a mean pulse O (see Figure 5-9). The encoder index channel was used to synchronise the instantaneous torque reading (from the torque sensor) with the cam angle. Incremental pulses were used for torque monitoring at each rising edge. Its split channel enabled the determination of torque data against cam angle for at least every 0.5° of camshaft rotation. In this condition, the rotation of the shaft is said to be in the clockwise direction. In anticlockwise motion, the pulse readings are inverted.

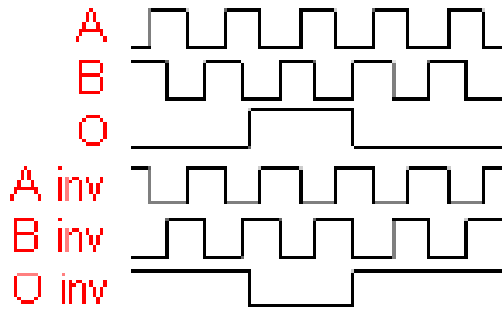


**Figure 5-9 Shaft Encoder Pulse Readings**

### 5.2.6. Torque Transducer Operation, Mounting and Calibrations

The sensor technology torque transducer measured the resonant frequency changes of surface acoustic waves device in a non-contacting manner when strain is applied to the shaft where the SAW is fixed (See Figure 5-10a). Essentially speaking, when a material is stress/strained, it emits an acoustic wave which is represented by the deformation of quartz substrate of the SAW device, which in turn causes changes in resonant frequency. In practice, the SAW acts as a frequency dependent strain gauge [181]. A typical fully assembled Sensor rotary torque transducer is shown in Figure 5-10b.

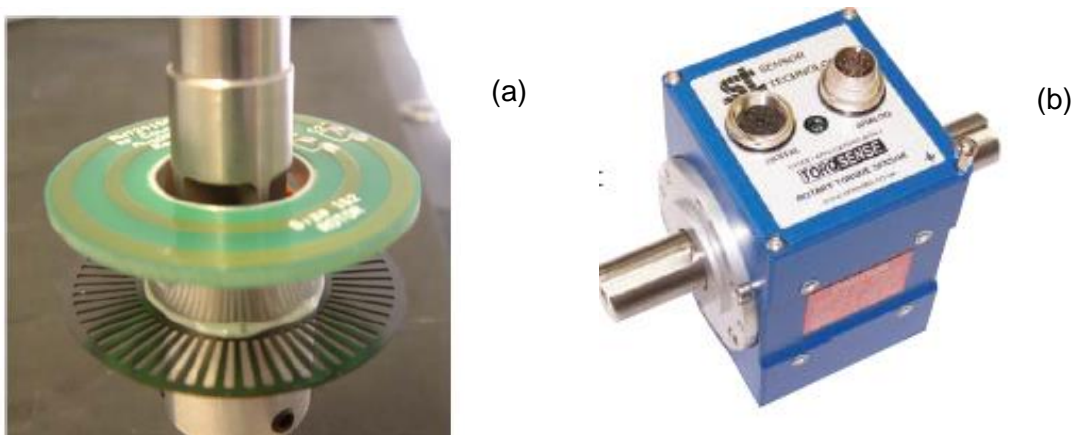


**Figure 5-10 (a) SAW assembly for Sensor Rotary torque transducer (b) Fully assembled of Sensor Rotary torque transducer [181]**

In mounting the torque transducer, suitable alignment coupling must be used. For highly loaded valve trains where the fluctuations of torques need to be measured to a good degree of accuracy, an alignment coupling with the right speed and torque rating was used. This is because an undersized coupling will not transmit the required

torque while the high inertia of an oversized coupling will produce high instantaneous peak torques far in excess of the applied torque. A schematic of the mounting arrangement for the newly developed single cam rig is shown in Figure 5-11

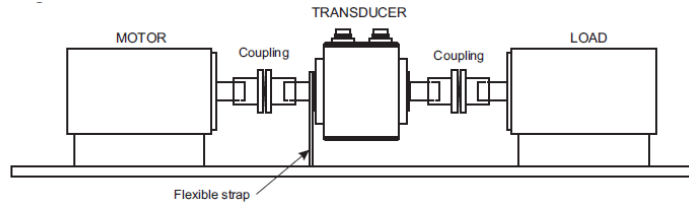


**Figure 5-11 Mounting arrangement of Torque transducer on single cam rig**

Although the device was calibrated by the manufacturer prior delivery, it was the objective of this research endeavour to determine the voltage vs. torque relationship. The calibration of the torque transducer was carried out by using known loads to determine the voltage generated by the electromechanical system. This will involve mounting a string along the end <sup>1</sup>shaft and increasing the load gradually while simultaneously measuring the voltage. The other end of the torque transducer will be supported by its hub. This is to check the linearity of the system. Once equation of linearity is determined, calibration of the device can be setup as reference points of the system will have been evaluated [182]. The typical calibration results are shown in Figure 5-12.

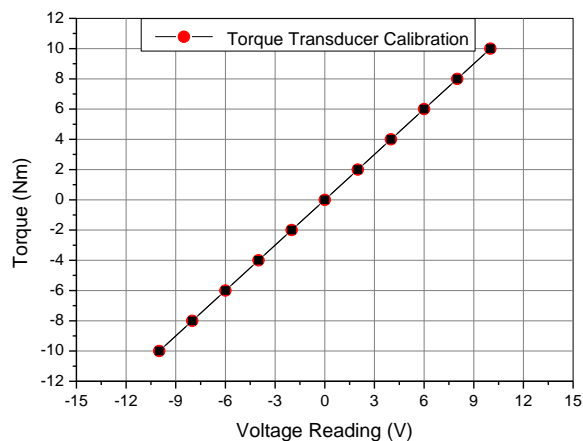


**Figure 5-12 Torque Transducer Calibration**

<sup>1</sup> [www.sensortechology.com](http://www.sensortechology.com)

### 5.2.7. Electric Motor – ABB ACS 800

The ABB ACS 800 motor (Figure 5-13a) was used to drive the camshaft assembly by means of a Hohner alignment couplings. It has a 12 mm radius spindle. Essential, one coupling was mounted with the motor and the other was connected to the camshaft with the torque transducer in between the arrangement. The motor runs from 250 to 3,000 rpm, which essential covers the speed range for a normal passenger vehicle. It can move in clockwise or anticlockwise direction. This drive has its inbuilt inertia and friction compensation as well as speed, torque, power and frequency evaluations. The drive is better adapted to provide a synchronous data in acceleration and deceleration motion. This enables the system provide a torque step rise in 5 ms and speed inaccuracy as low as 0.1% - 0.5% of nominal speed.

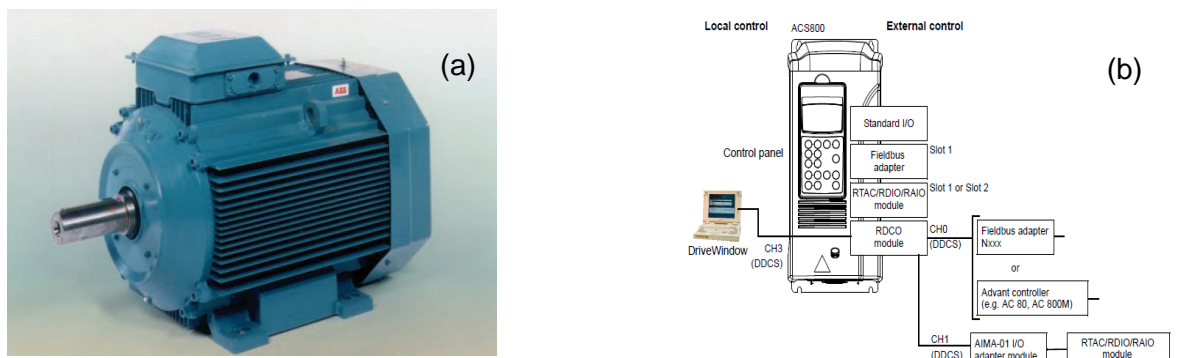


**Figure 5-13 (a) Image of ABB AC800 drive (b) Control Panel [183]**

Their self-adaptable external control shown in Figure 5-13b enables connection to a PC. This was achieved with an NI- USB 6212 device which delivers 400 Kilo-samples/sec with input voltage of 1:10 Volt which corresponds to the speed range of 300 – 3000 rpm. The unique speed automation system enables the ramping of the single cam rig to obtain friction characteristics at boundary, mixed and elastohydrodynamic regimes in a single test with minimal monitoring. The motor is also equipment with speed/torque ramping and flux braking to minimise noise.

#### 5.2.7.1. Speed Controller Tuning and Its Effect on Noise

The setting of the speed controller on the motor can affect the noise and dynamic response of the data obtained from the device. For the tests used in the report, the system was set in the autotuning mode. It is worthwhile mentioning that the difference between the manually tuning and autotuning is negligible. This is because of the 6 degree Buttwort filtering which was used to process the data.



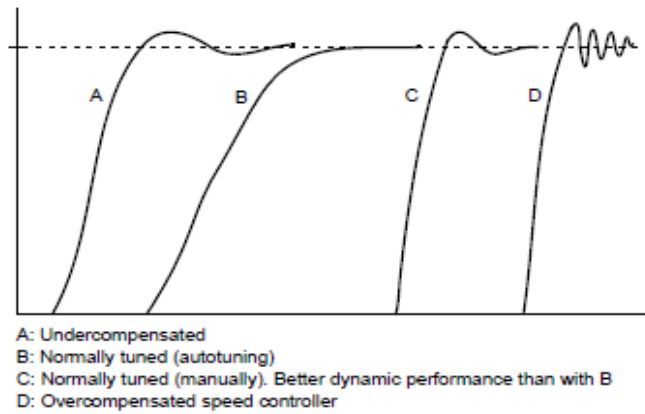


**Figure 5-14 Effect of Speed Tuning of Noise and Vibration of Motor/ Single Cam Rig Assembly [183]**

The system is equally applicable for the torque reference. In fact, speed controller output is the torque reference. This is achieved by taking the actual speed plus its error value and obtaining the derivatives of the acceleration compensation. The resultant output yields the torque reference. More details can be obtained from the ABB manual for ACS 800.

**5.2.7.2. Acceleration and Deceleration Ramps (Jogging)**

The ramping procedure employed during the testing of the single cam rig is the linear ramp. This is more suitable for steady acceleration and deceleration and for slow ramps. The S curve ramping procedure is more suitable for fragile systems carrying low loads and where a smooth transition is required. With the linear configuration, no data capturing was done during the ramping as the transition can be a bit erratic.

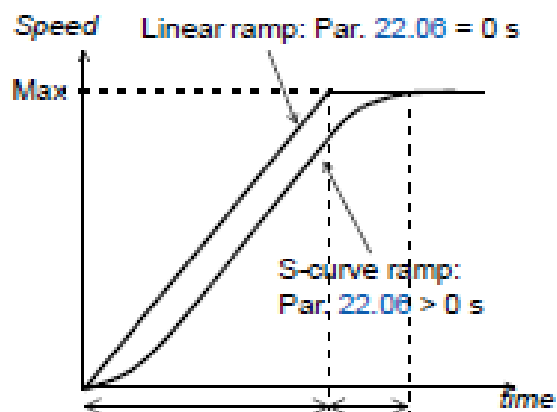


**Figure 5-15 Linear and S curve speed ramps of the motor**

The ramping procedure is programmable with the LabVIEW hardware (NI USB 6212) for set speeds with prescribed duration. Up to 22 different configurations or speed/time ranges can be set on the programmable configuration. The duration of reaching the set speed, ideally follows a linear ramp which is achieved in 10 ms but this can also be altered. For our testing protocol, it was maintained at 10 ms. An illustration of ramping profile for 16 different configurations is shown in Figure 5-16.

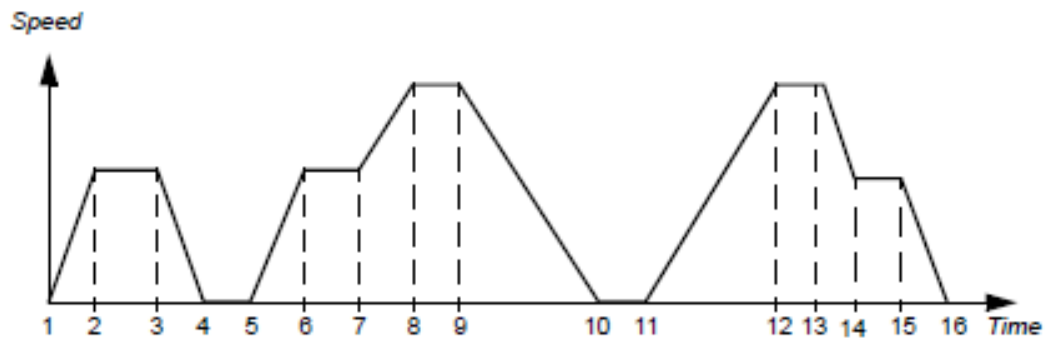


**Figure 5-16 A typical ramping (jogging) procedure[183]**

### **5.3. Lubricant Oil Bath and Temperature Monitoring**

In the single cam rig developed at the University of Leeds, the temperatures of the system typically range from 13 °C – 150 °C. The oil bath was used for temperature monitoring, circulation of oil to the cam tappet well and also for heating up the rig. The rig procedures are discussed in Chapter 6 (section 6.3.1).

#### **5.3.1. Lubricant Oil Bath with Flow Loop**

The oil bath used on the rig was a HAAKE AC 200 thermo Fischer PID temperature controller. Its temperature ranges from 14 °C to 200 °C with an accuracy of  $\pm 0.01$ . This temperature range typically covers those in the valve train assembly. It possesses 5 set channels for temperature control which can be adapted for specific applications. A flow test was also carried out with this device to observe the pressure at the cam tappet well, and the results were very promising. The lubricant flow rate through the rig was high and also had three control levels of low, medium and high which correspond to approximately 1.00 -1.73 g/min, 1.73 - 3.46 g/min and 3.46 - 5.30 g/min respectively. A throttle valve was also installed to control flow to the cam-insert contact by means of a 3 way flow block. The other two flow paths were basically used to heat up the rig. On the base tray of the rig, the system is slightly inclined and accommodates a lubricant retaining region, which is connected to the oil bath and

equally ensure that lubricant flows back due to gravity. The flow loop of the single cam rig is illustrated in Figure 5-17

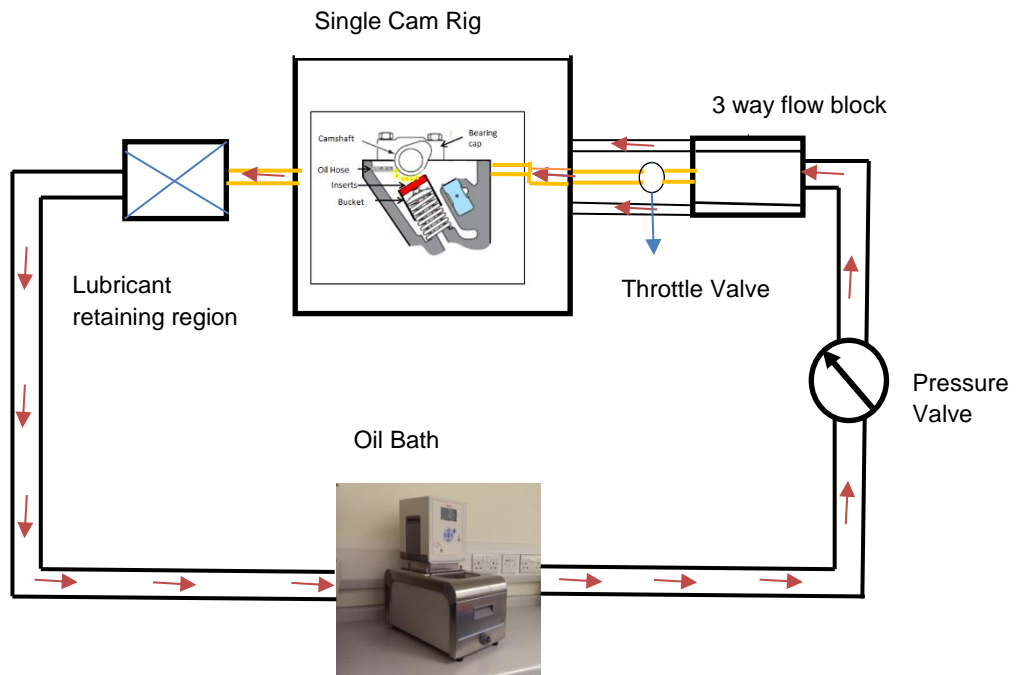


**Figure 5-17 Lubricant flow loop for single cam rig**

The device is equally fitted with remote port and lubricant level sensors. This is particularly useful if there is a leakage in the system as the alarm will alert the users of any inherent danger. Along with the alarms, several warnings and faults are usually displayed on its LCD for ease of troubleshooting.



**Figure 5-18 HAAKE DC 200 Thermo Fischer Oil Bath**

It has a minimum lubricant capacity of 5 Litres and can be used for a variety of 5 – 8 different lubricants with different temperature ranges. Its multi-purpose programmable

nature of Ethernet, USB, and RS232/RS485 has made the connectivity with PC simple and very adaptable. The booster pump on the device can also be used to achieve significantly higher flow rates than originally designed for. An external RTD thermocouple is also embedded with the device for evaluation of external temperature. These unique features made this oil bath our choice for the development of the single cam rig.

### 5.3.2. Thermocouples

Two mineral insulated thermocouples (as shown in Figure 5-19) with miniature plugs were used to monitor the temperature drop on the cam rig. One was mounted on the bearing cap of the rig while the other was installed close to the cam-insert housing. The objective was to investigate the temperature drop and recommend if an external source of heating will be needed. A drop of  $\pm 4$  °C was observed at the cam-insert housing while that on the cap was  $\pm 7$  °C. These results were suitable and since the rig heat-up took less than 15 mins, no additional heating was required.



**Figure 5-19 Mineral insulated thermocouples with miniature plugs**

### 5.4. Load Cell

The load cell used on the rig was a Kistler 9031A (Figure 5-20a) with a maximum load range of 60kN and capabilities of also measuring low forces of 1 N. Its calibration range typical employs load from 10 – 100 % and it has a maximum operating temperature range of up to 200 °C [184]. The maximum pre-tensioning on this device was set at 20kN and this was used as a guide in determining the dynamic perpendicular forces ( $F_z$ ) acting on the camlobes. The system was connected to a charge amplifier and read out from the NI 6212 onto a computer. Figure 5-20b shows the ordering information for the Kistler 9031A load cell.

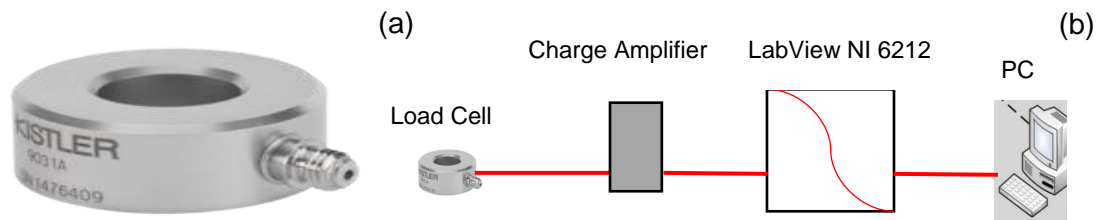


**Figure 5-20 (a) Kistler load Cell (b) Instrumentation for Kistler load cell**

### 5.5. Hohner Alignment Couplings

The alignment couplings used for the rig have customized dimensions to meet the specification of motor spindle, modified camshaft and torque transducer. The coupling fitted to the motor has a 24 mm diameter at B2 and 12 mm diameter at B1 while the coupling attached to the camshaft has a 20mm diameter at B2 and 12 mm diameter at B1. Figure 5-21a is used to illustrate the dimensional information. The couplings are made from Al Alloy 2104A T6 with a clear anodised finish (Figure 5-21b). Its light weight of 357 g ensures that it does not produced high inertia loads that exceed those within the system while it also transfers the required output torque.

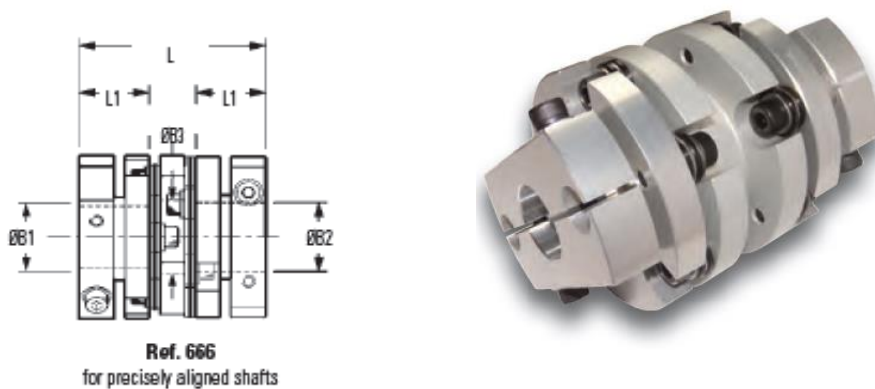


**Figure 5-21 (a) Specification of alignment couplings and (b) Pictorial view of coupling with M5 bolt assembly**

### 5.6. Newly Developed Single Cam Rig

The complete assembly of the single cam rig is as shown in Figure 5-22. An emergency stop button was also installed to the motor as a statutory requirement for machine systems. The single cam rig test block is essentially made up of the bearing

cap, camshaft, valve springs, buckets, inserts and an oil gallery (See Figure 5-23). On the base of the rig, 10 rubber stands were put in place to help damping any noise/vibration in the rig.

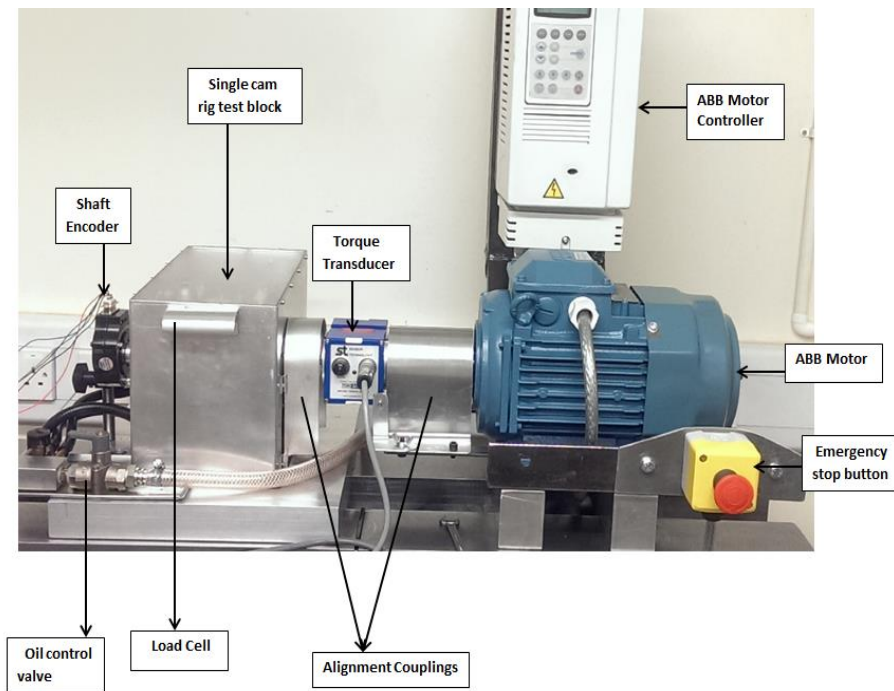


**Figure 5-22 Schematic of Single Cam Rig Assembly**

Upon running the newly developed rig, the novel features of the rig can be summarised as follows;

- Ability to determine friction torque for every  $0.5^\circ$  of camshaft rotation
- Ease of control with dynamic, programmable braking motor and oil bath
- Control over flow rate through check valve connected to cam tappet well
- Considerably lower weight, easy to use, clean and assemble
- High sensitivity to differentiate friction torque between lubricants with close chemistries and several different coatings/surfaces (this is discussed in more details in subsequent chapters)
- Provide data with high degree of accuracy
- Relatively short time to heat up
- Minimum noise and vibration
- Ability to resolve the friction torque with the cam angle by means of a rotary shaft encoder. This enables spot to spot correlation of tribological parameters with film properties

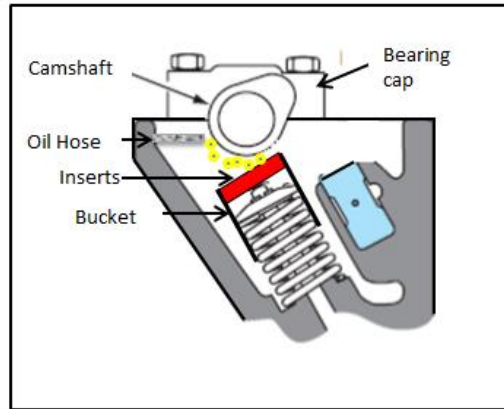


**Figure 5-23 Single cam rig test block**

With the system fully in place and operational, the objective was to check the durability of the assembly and evaluate the vibration within the system. This section is extensively discussed in CHAPTER 6.

## **5.7. Data Acquisition**

The data acquisition on the single cam rig consists of a combination of software and hardware instrumentations. The hardware which required instrumentation were; load cell, oil bath, torque transducer, shaft encoder and the electric motor. All components except the oil bath used LabVIEW software with an NI 6212 for data logging/DAQ device (Figure 5-24). This data logger was multiplexed with 8 channels at combined data capture of 400Kilo samples per seconds.

With this LabVIEW software, the routine for the interface provided the oil bath temperature, data samples captured per seconds, camshaft speed, and data capturing intervals, oil bath temperature and a graph showing the torque curves. Another window was also incorporated to give the minimum/maximum torque values, friction torque values, and also the display the duration of the test.

### **5.7.1. Rig Operational Procedure: Routine Checks and System Setups**

In order to prevent any damage to the apparatus, it was essential to embed a rig operation procedure with the software/hardware system. For instance, the maximum torque on the torque transducer is 10 Nm while that on the motor is 7.3 Nm. Torque values higher than 7.3 Nm will cause damage to the motor. This background checks were vital for the safety of the components and device. Therefore it was necessary to set some limits with the operational procedure by incorporating additional checks and setups instructions.

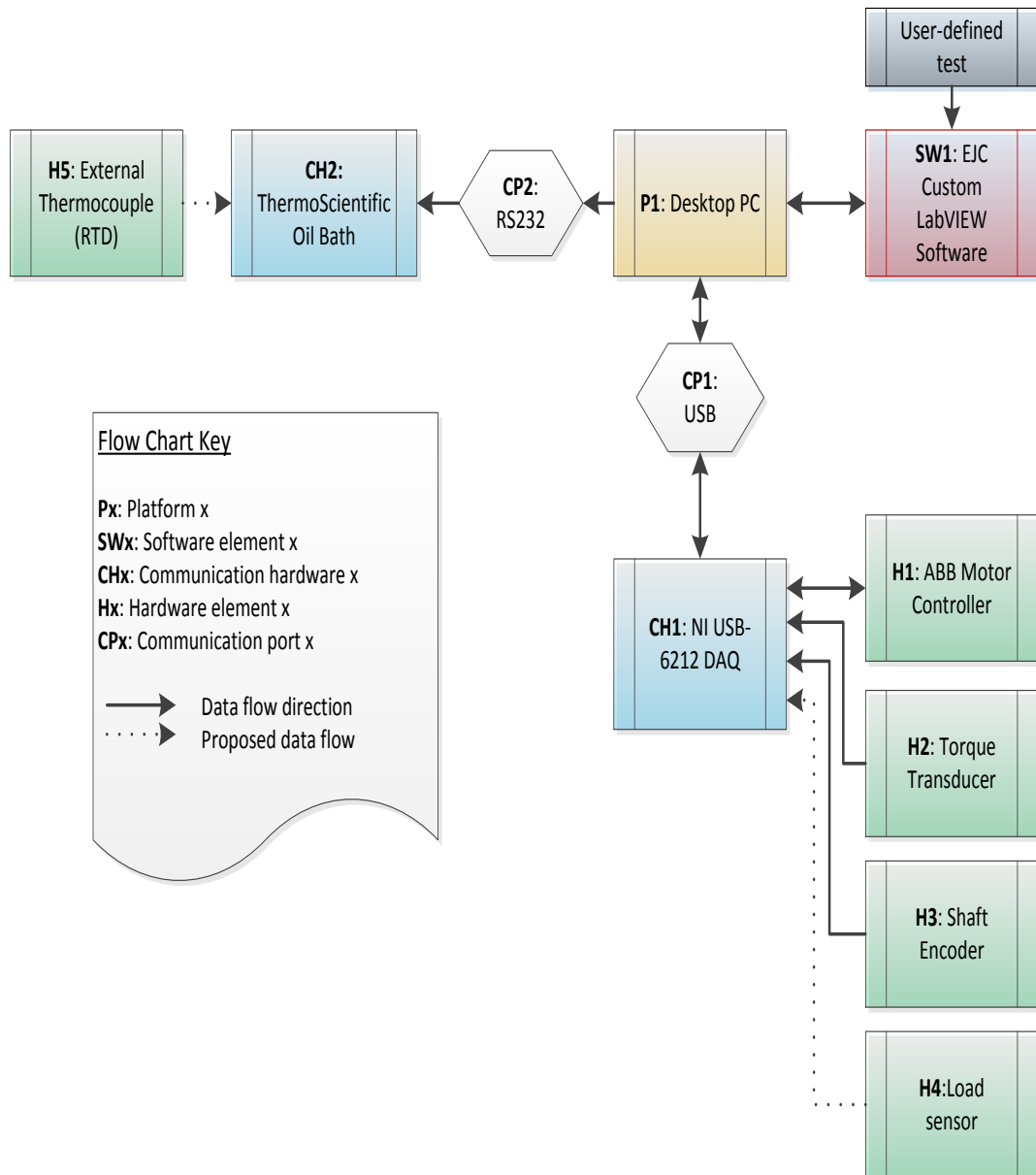


**Figure 5-24 Data logging for Newly Developed Single Cam Rig**

In practice, the software system does an ID check with motor, torque transducer and oil bath before operation. Once the ID checks are complete, it also ensures that the pre-set parameters of oil bath temperature and torque calibration are met. This is usually confirmed with light green bulb showing for all components and a pop-up showing checks complete. Only after these checks/setups are all carried out can a test commence on the device.

**Figure 5-25** shows additional information with the testing and data acquisition. The software possess inbuilt processing through a counting min/max and time stamping



sub VI's to determine the average friction torque. Data is stored with processed and raw data in separate files. The raw data enable us to plot the torque values with cam angle while the processed data facilitates the determination of friction torque against camshaft speed or (Stribeck curve).

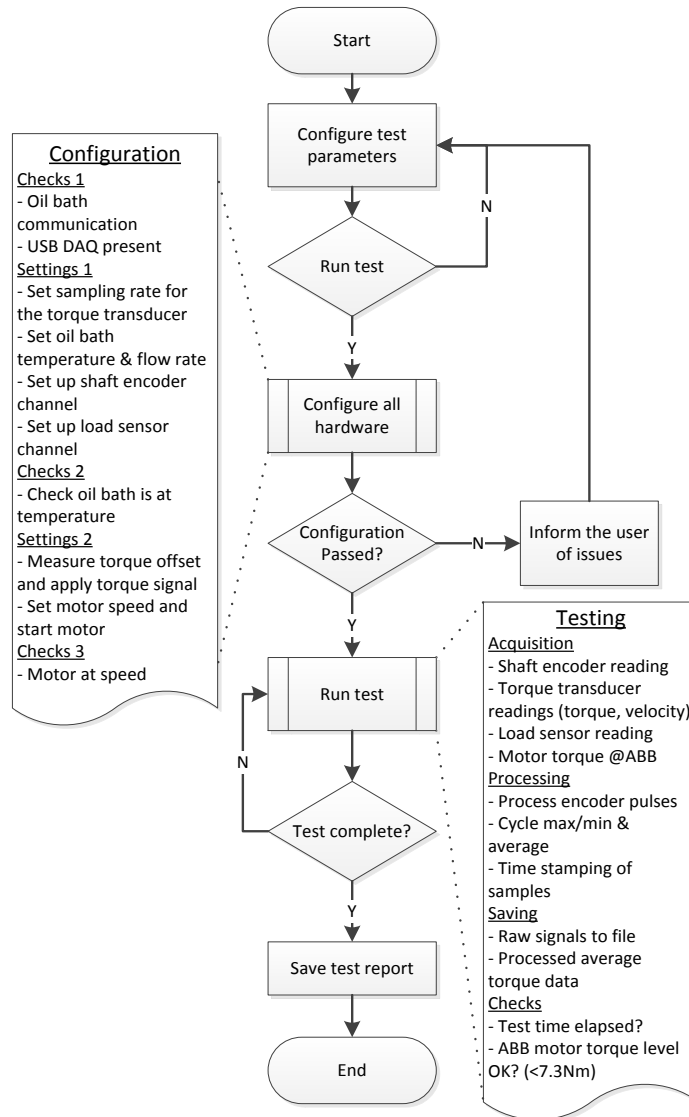


**Figure 5-25** Flow chart showing operational procedure for Single Cam Rig

### 5.7.2. Camshaft Positioning

The camshaft positioning was obtained by using the counting edge of the shaft encoder for indexing. This was attached with a non-conducting bellows to the test block to prevent any thermal drift. The maximum torque or load carrying point on the camlobes has been indexed at 73 °C [5, 182]. By setting the data capture per

revolution, this indexed region can be read off and corresponding angles on the cam profile determine with significant accuracy at a relative error of  $\pm 0.5^\circ$ .

### 5.8. Noise and Vibration Filtering on Newly Developed Single Cam Rig

In order to determine the noise or vibrational frequencies which have been superimposed on those of the original signal, it was necessary to evaluate the system without dynamic loads. This was carried out by pushing the spring and holding it in place with a split pin. The contact at the cam follower contacts was thereby eliminated while the noise amplitude due to other contacts/systems such as bearings, valve guide/valve stems, motor and oil bath was determined. Figure 5-26 shows amplitude from other contacts at 750 and 2800 rpm respectively.

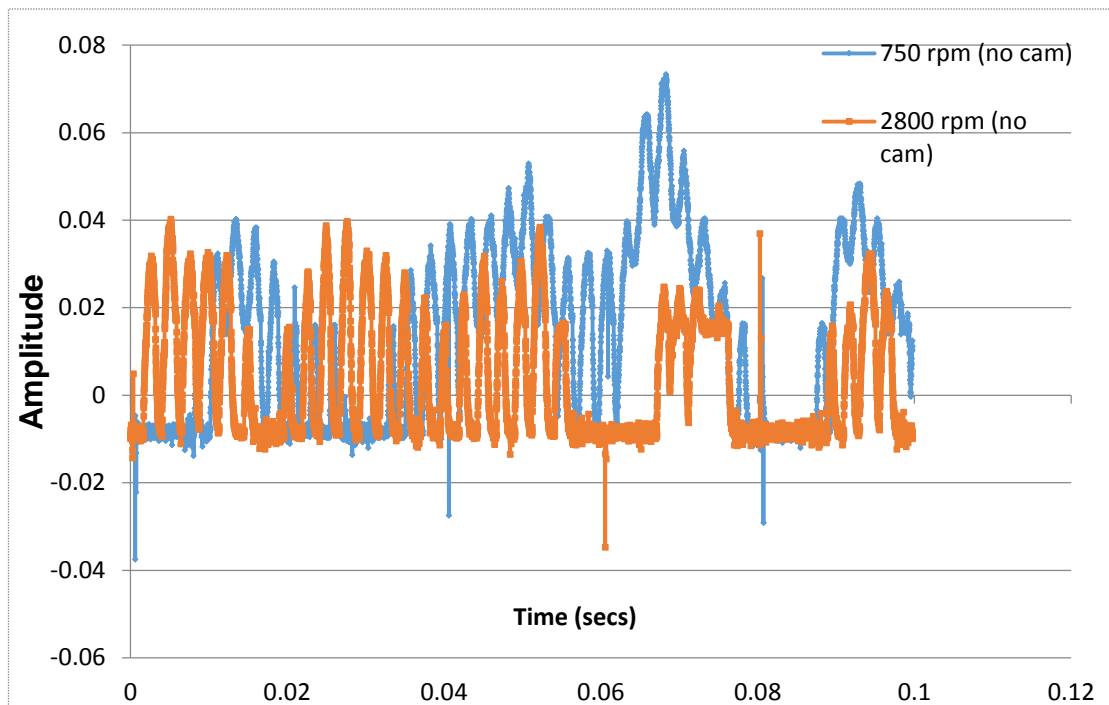


**Figure 5-26 Frequency/Noise Response Due to Bearing /Valve Guide Contact**

The process was also repeated with the cam-follower contact put in place and characteristic waveforms were obtained. Since the cam base circle enjoys a clearance of 0.17 – 0.23 mm with the camlobes, friction during this cam cycle can be attributed to support bearing. A closer look at the waveform at 750 rpm, reveal that there is minimal noise which rises to around 0.2 at 2800 rpm.

Frequency spectrum analysis of the torque signal under various camshaft speeds showed that peak amplitude appeared in the region between 395 Hz and 400 Hz.

This was attributed to the response from the torque transducer. At certain camshaft rotational speeds, the amplitude of the peak was found to be much higher than that of the other higher frequency components. Although the noise amplitude was far lower than the main signal, typical examples where significant perturbations were observed are 500 rpm, 900 rpm, 1350 and 2700 rpm. Under these conditions, the main rotational frequency and its higher order frequency components would excite severe torsional vibrations at a frequency close to the natural frequency of the sensor transducer.

This low frequency from the SAW of the torque transducer ensures that the rig could operate with low frequency/noise and provide data with a high degree of accuracy. While natural frequency within the test bench was about 400 Hz, filtering with a Butterworth filter to the 6<sup>th</sup> degree at a frequency of 395-405 Hz did not affect the maximum/minimum torque significantly. Deviations were in the range of  $\pm 5$  mNm. Figure 5-28 show the characteristic waveforms after filtering at 300 rpm and 2100 rpm. This was plotted against number of data points to observe the profile and noise impact. Due to the compact nature of the rig, it is clearly shown that the effect of noise is minimal. Going forward, it was also important to avoid carry out tests at the perturbation speeds mentioned above.

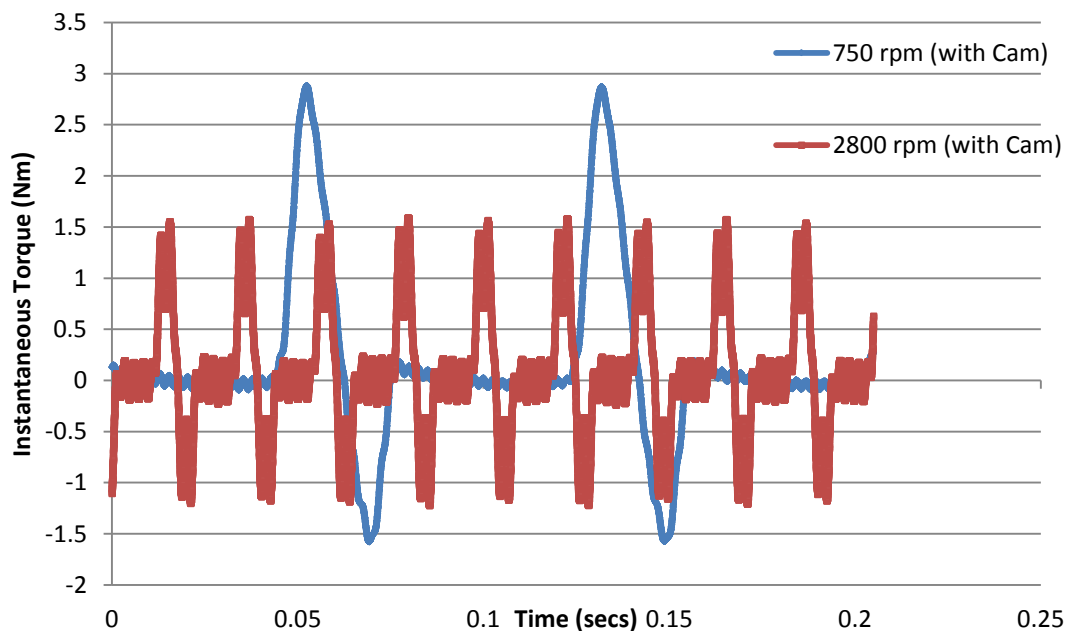


**Figure 5-27 Characteristic torque wave forms at 750 and 2800 rpm with camlobe**

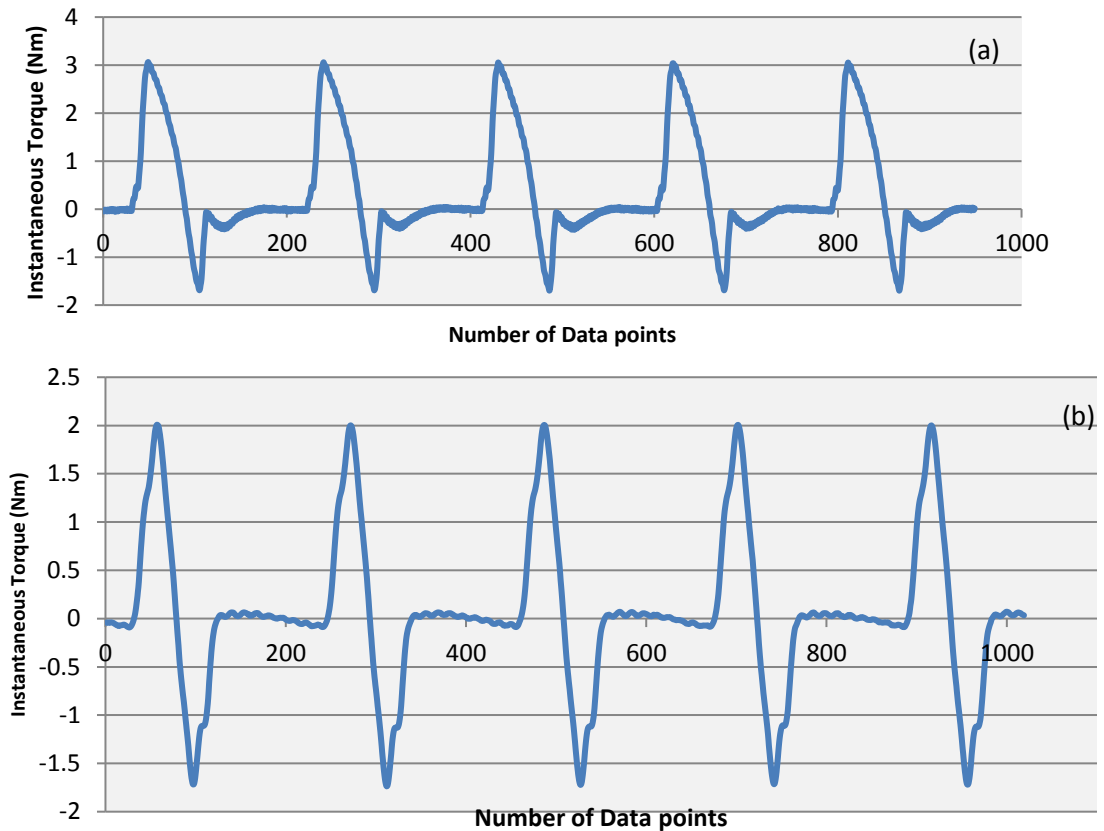


**Figure 5-28 Torque transducer output voltages at camshaft speed of (a) 300 rpm and (b) 2100 rpm**

## **5.9. Friction and Instantaneous Torque Measurements**

### **5.9.1. Valve Train Friction Torque**

The data collected from the analogue end of the torque transducer were passed into an NI-USB 6212 hardware giving characteristic waveforms that give information about the speed of the camshaft assembly. Similar findings have been reported by Mufti [182]. Essentially, the instantaneous torque is made up of friction and geometric components. During valve openings, energy is absorbed by the spring and this is released to the camshaft as torque. The friction component is very high during valve opening and has little or no components during valve closing. The inertia/geometric torque on the other hand have equal positive and negative components during valve opening and closing. Ideally, by taking mean torque values over the cam cycle, the inertia/geometric torque will be effectively cancelled out leaving the friction component [5, 185, 186]. The average friction torque was obtained by taking an average of the 200 data points obtained for each camshaft cycle. This corresponds to approximately 1 data point for every 1.8° of cam shaft rotation. This was then

averaged over the duration of the test in the steady state region.

Due to the compact and rigid nature of the modified camshaft and entire single cam rig assembly, the system was able to operate at high speeds (up to 3000 rpm) with limited noise. Figure 5-28a and 5-28b shows the output torque values at 300 and 2100 rpm respectively. Only 5 cycles were shown at 2100 rpm to demonstrate the low vibration of the rig at high speed. The asymmetric nature of the torque curve is due to work done by the camshaft during valve opening. This constitutes both geometric and the bulk of friction torque. On valve closing, work is done by the valve spring in maintaining contact with the camshaft which essentially consists of all geometric components. At high speed, the work done by the camshaft is slightly greater than those of the spring. This difference is proportional to the friction torque which is typically low at high camshaft speeds.

### **5.10. Experimental Work**

In this study, the experimental plan will be divided into pin-on-disk tests (Chapter 4) commissioning tests for the single cam rig (Chapter 6). Single cam rig tribochemistry (Chapter 7) and evaluation of coating and its effect on camlobe wear - Chapter 8. In Chapter 8, consideration will be given to the characterisation of the tribochemical films produced across the cam profile.

From Original Equipment Manufacturers (OEMs), most cam follower designs usually have a small clearance between the cam and shim, therefore, the base circle will not be considered in tribofilm characterisation. The shoulder, flank and ramp region will be determined from the LabVIEW data acquisition program of the shaft encoder and torque transducer.

The slide roll ratio, lubricant film thickness, and friction torque can be derived instantaneously. This will then be matched with the tribofilm studies (**done ex-situ**) at different points on the cam profile to give a detailed representation of the tribochemistry map across cam lobe.

Chapter 7 will investigate the tribology/tribochemistry of DLCs with a pin on reciprocating tribometer for further comparison with those of the bench test rig.

### **5.10.1. Procedure I – Validation Testing Procedure**

In this section, two oils referred to as FFA and FFB were used for the commissioning tests. The torque profile involves varying the speed from 300-2100 rpm. The profile is shown in **Figure 5-29**. Two surfaces of MnPO<sub>4</sub> and polished shims were used in conjunction with chromium chilled cast iron surfaces. A total of 24 tests were performed with each test having three repetitions. **Table 5-2** shows the test matrix.

### **5.10.2. Experimental Conditions Investigated on Single Cam Rig**

#### **5.10.2.1. Temperature**

Going through the review, it is evident that temperature has a significant role to play in terms of oil degradation, friction [25] and thermo-mechanical effects on wear. Temperatures values of **75, and 105 °C** were studied.

#### **5.10.2.2. Test Duration**

The duration of the test was 12 – 13 hrs. The friction torque values were recorded every 20 mins to observe when running-in was achieved. Between 4- 4.5 hrs was sufficient but it was better to run for longer hrs [25]. The test consist of a 5 – 5.5hrs breaking-in cycle before ramping to the required speeds. Duration at each speed was recorded for 1 hr. The procedure is illustrated in Figure 5-29

#### **5.10.2.3. Speed**

This will typically lie in the range of 300 – 2100 rpm for the validation tests. Speeds were varied but a large amount of time was spent on low speeds in boundary lubrication regimes. For the speed range tested, the oil film thickness was calculated using the Dowson equation for line contact and its lies between 0.06-0.20 µm while the composite surface roughness was 0.25-0.065 µm for the Mn-Phosphate coating and polished inserts respectively. The  $\lambda$  ratio was 0.24 µm at 300 rpm and about 3.75 µm at 2100 rpm.

#### **5.10.2.4. Oil Type**

For the commissioning tests, two commercial 5W30 oils of Normal and Mid SAPS will be evaluated for the performance on the newly developed single cam rig. Details of these oils have been described in Chapter 4. This oils have very close chemistry and they have been widely used in certain literatures. It will be vital to have a bench mark for comparison; this is why they were selected as the best choice for commissioning tests.

### 5.10.3. Anticipated Outcome

- To obtain a fundamental understanding of the behaviour of the newly developed single cam rig and assess the repeatability/reproducibility of the data obtained.
- Assess the Tribochemical films derived from Normal and Mid SAPS oil and compare this with literary results etc.
- To evaluate if the rig is sensitive enough to differentiate the friction responses between lubricants of similar chemistries.
- To assess the mechanisms of reduction of friction and wear under boundary/mixed and EHL lubrication regimes.

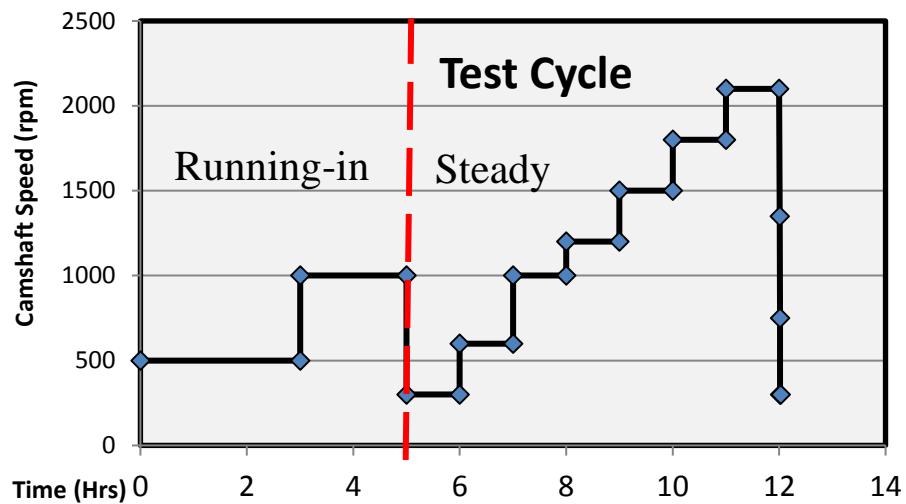


Figure 5-29 Camshaft test cycle

Table 5-2 Test Matrix for the Validation of Single Cam Rig Results

	Material/Coating	Temperature
Experiment 1	Mn-phosphate Coated Tappets	105 <sup>0</sup> C
Experiment 2	Polished Buckets	105 <sup>0</sup> C
Experiment 3	Mn-Phosphate Coated Tappets	75 <sup>0</sup> C
Experiment 4	Polished Buckets	75 <sup>0</sup> C

#### 5.10.4. Experimental Conditions For Procedure I

The experimental conditions to be investigated in **Procedure I** are outlined in **Table 5-3**. This aspect seeks to identify effects of sulphur and phosphorus reduction on a conventional material pair that will largely minimise engine friction and wear. Surface analytical test and mechanical test will be used to help identify the tribochemical reactions/modification of surfaces.

**Table 5-3 Test Materials, and Conditions for Procedure I**

System Components/Test Parameters	Materials/Values	Comments
Cam Material	Chilled Cr Cast Iron	
Tappet Substrate Material	Hardened Steel (16MnCr5)	
Tappet Coatings	MnPO <sub>4</sub> coating	Coating/lubricant interactions
Lubricants	Normal and Mid SAPS	FFA and FFB
Temperature (°C)	75, 105	Effect of Temperature
Motor Speed	300rpm – 2100 rpm (5Hz – 35 Hz)	Boundary lubrication is important for assessment of tribofilms.
Friction Modifier additives	FFA friction modifier oil Type – Ester type	To observe the reduction properties of this oil when compared with its counterpart FFB.
Duration (hrs)	12.5 hrs	Validation and testing of newly developed single cam rig
Surface Analysis	SEM/EDS, RAMAN, XPS, , Nano-indenter	
Mechanical Test	Hardness, Indentation Modulus	



## 5.11. Procedure II

Fully formulated Lubricant B (**B001 - Mid SAPS**) from **TOTAL**, which is a commercial generic **5W30** (multi-grade) lubricants will be used for the preliminary study of **a:C-Si-O and taC-H DLCs tappets, a:C DLC**. The aim is to use these coatings and select the best two in friction and wear performance for further study.

The further study will involve coating the camlobes. One of the objectives will be to observe if any significant advantage can be obtained from coating both the cam and the follower. With tribochemical investigation as the focus, surface analytical and wear examination will take place at  $\pm 14^\circ$ ,  $\pm 10^\circ$ ,  $\pm 4^\circ$  and  $\pm 0^\circ$  (cam nose) in line with ASTM 6891-09a standard. The wear scar is taken at the seven locations and the sum of all the wear scar at these location is used as the wear on the camlobes. According to ILSAC 4, the maximum wear acceptable by an oil should be 90  $\mu\text{m}$  in a 100 hrs tests.

### 5.11.1. Anticipated Goals

- To obtain information about the friction torque against cam angle, and wear of the cam follower in fully formulated oils.
- Investigated the durability of the coating in set conditions
- Obtain information about oil tribochemistry in boundary lubrication regimes of the cam nose.

### 5.11.2. Experimental Steps/Outline

1. Speeds were increased in a range of (300-2100 rpm) but a large extent of the experiment was at low speed (300-600 rpm)
2. No data capture took place at speed ramps as the rig was subjected to significant perturbation in speed/torque during speed change.
3. The test was composed of 4 cycles of 12.5 hrs each with 7.5 hrs spent at low speeds of 300 – 600 rpm.

**Table 5-4 Test Materials, and Conditions for Procedure II**

<b>System Components/Test Parameters</b>	<b>Materials/Values</b>	<b>Comments</b>
Cam Material	Chilled Cast Iron	To determine cam lobe wear, evaluate tribochemical films on cam nose
Tappet Material	Hardened Steel	
Tappet Coatings	taC-H, a:C and a:C-H-Si	Evaluate wear/friction performance of the coating
Lubricants	Fully formulated oils without Friction modifier additives	A001 (Normal SAP)
Temperature (°C)	105	Nil
Motor Speed	300 - 2100 rpm (5 - 35Hz)	This is to simulate a normal passenger vehicle.
Duration (hrs)	50 hrs	
Surface Analysis	SEM/EDS, RAMAN, XPS	Tribofilm Characterisation

### 5.11.3. Tribofilm Characterization across Cam Profile

The cam profile goes through three different lubrication regimes as illustrated in **Figure 5-30**. In boundary lubrication, the friction and wear properties are controlled by thin molecular boundary films obtained from the lubricant additives. Under this condition, the regions along the cam profile where boundary lubrication exist; predominantly the nose, should produce such films. The mixed lubrication regime should also produce tribochemical films since additives and lubricant viscosity are important. However, this should not be as conspicuous as those of boundary lubrication regime. The EHL is characterised by lowest friction with excessive pressure which leads to deformation of lubricant and solids.

Interestingly, to the best of our knowledge, no one has assessed the nature of the tribological films produced across the cam profile with steel and DLC coatings. Previous works [12, 187] have focused on film thickness and lubricant entrainment

speeds with significant success. Current studies look at surface coatings/architectures and films formed on the tappets [39, 79, 87, 88] neglecting the tribofilms formed on the cam.

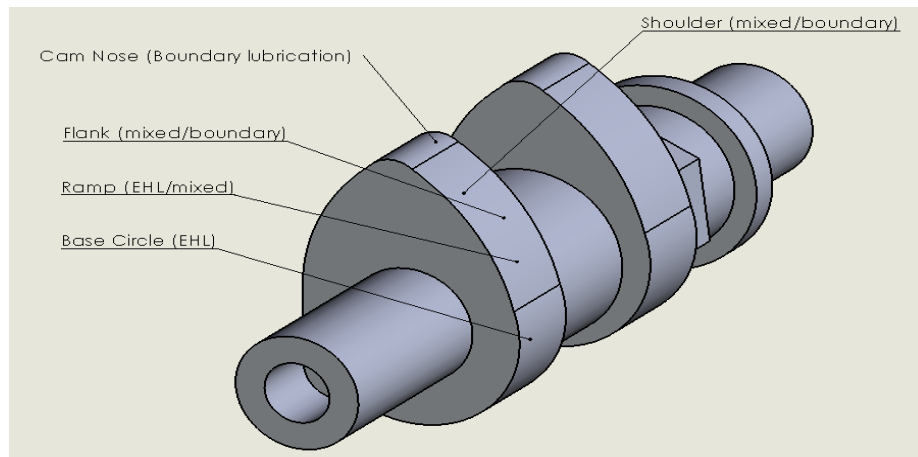


**Figure 5-30 Regions on Cam Profile**

## **CHAPTER 6. SINGLE CAM RIG VALIDATION AND COMMISSIONING TESTS**

### **6.1. Background**

Component bench tests are a crucial part of a tribology assessment experimental programme for most engines and subsystems. This is because they test the components under conditions simulating the operating characteristics of the system. These have become very important as they shed more light into the friction, wear, lubrication and importantly for this study, the tribochemistry of valve train systems. This section outlines the validation and commissioning test procedures used on the newly developed single cam rig (SCR) from a 1.25L FORD Zetec (SE) engine. Friction plots were used to validate the data obtained from the newly developed single cam rig with Mn-phosphate coated and polished follower against a cast iron camshaft.

### **6.2. Introduction of Single Cam Rig Commissioning Tests and Validation**

Environmental legislation calls for the use of engine lubricants with less impact on the environment in terms of exhaust emissions, while engine users demand more mileage per litre of fuel without any compromise on engine durability. From this standpoint, engine manufacturers require the optimum combination of materials, surface coatings and lubricant additive packages to minimize friction and wear in the piston, bearing and valve train components. The move from normal to mid and even ultra-low SAPS oils risks an increase in wear on engine tribocomponents. For this reason, there has been increased experimental work on the tribochemistry/tribology of 'low' SAPS containing oils against surface coatings, particularly DLC's and how they affect friction/wear of engine components-cam/follower tribopair.

Engine valve train friction contributions are typically from the valve guide/stem, camshaft bearings, bucket/tappet bore, and most importantly, cam follower interface, which accounts for approximately 80-85% friction contribution [32, 188]. Therefore, for improved engine efficiency, research into this tribopair is necessary. Accordingly, numerous authors have designed and used valve train rigs to study friction [185, 189-192], wear [40, 173, 193], film thickness [11, 12, 21, 51] and tribochemistry [22, 87] at the cam tappet contact. Historically speaking, Dyson and Naylor [189] were perhaps the first to investigate friction at the cam follower interface using a push rod

assembly where the tappets were held in place by a pair of flat springs, and the corresponding stresses measured by means of piezo electric gauges.

Ito et al [193] studied the friction with the use of two strain gauges mounted on a push rod and shaft. Using both the deformation on the shaft and the force on the tappet, the friction coefficient was evaluated with a good degree of accuracy. The final apparatus was mounted on an engine for wear testing. A modern configuration of the cam/follower is the direct acting mechanical bucket type with a somewhat high sliding. Pieprzak et al [185] used the configuration to develop a valve train rig for the evaluation of friction due to tappet/bore rotation. This was achieved by preventing the tappet/bore assembly from rotating with a rigid mechanical quill. High tappet/bore frictions of 13% were recorded at low speed with lower values at high speed. In our study, this approach was not ideal as tribofilms are affected by tappet/bore motion and lubricant entrainment velocity.

A vast majority of the cam follower studies involve the use of rigs with multiple cams. In these types of rigs, camshafts have lobes at  $90^{\circ}$  from each other thus making computation of torque and relating it to a specific cam location more difficult. This is also coupled with system instabilities [194]. In order to understand different regions on the cam profile where significant friction and wear benefits can be achieved, it was pertinent to develop a single cam rig where the friction torque is investigated with respect to cam angle. Some aspects of this have been published in the literature [54, 145]. The rig is equipped with high data recording and control with 1 data point for as low as  $0.2^{\circ}$  of camshaft rotation (1800 data points for one rotation of the camlobes). This will provide a better understanding of the cyclic processes in the cam follower contact and give us the ability to link the friction/wear properties to the tribochemical films across the camlobes and inserts.

Conducting tribochemistry studies of engine valve train systems is a very difficult task due to sliding/rolling motion, film thickness variation, and high loads/stresses experienced at the contact of interacting asperities. These dynamic variations cause a significant distinction on the tribofilm formation and removal across the cam profile and on the inserts. According to reports by Liu & Kouame [145], tribofilm investigations at seven locations on the cam profile ( $\pm 14^{\circ}$ ,  $\pm 10^{\circ}$ ,  $\pm 4^{\circ}$  and cam nose- $0^{\circ}$  degree) showed that the tribofilms were different at each location and were made

up of short and long chain polyphosphate films in which temperature had a significant effect on their tenacity. Long chain polyphosphates tribofilms were shown to have good antiwear characteristics [145]. The formation/or reaction kinetics of polyphosphate film are strongly influenced by temperature. It has been reported that the bulk of the films are composed of short chain with long chain at the topmost surface but this structure can be altered in fully formulated oils [98, 195]. Similar findings with engine oil on metal surfaces have been reported to contain films composed of low concentrations of Zn, P, S with Ca and O as the topmost layer of the tribofilm [87]. These species have been reported to affect the antiwear properties of tribofilms [94, 196]. Uy et al [168] also investigated the tribofilms formed on tappets with Raman and observed Ca/Zn orthophosphate ( $Zn_3(PO_4)_2$ ),  $CaCO_3$ ,  $Fe_3O_4$  with some undecomposed hydrocarbon on the surface.

Currently, coatings/surface treatments are finding increased application in valve train systems. For instance, super finishing before deposition of TiN achieved 40% reduction in friction torque with 1-2% achievements in fuel consumption [190]. Similar results were obtained in a motored cam rig by super carburizing inserts to  $R_a$  of 0.09  $\mu m$  [191]. The utmost in the use of coating architectures, is the sporadic increase in the use of DLC's in the improvement of cam follower friction/wear. DLCs have been touted for their low friction and wear-resistant properties in boundary/mixed lubrication. Friction coefficients as low as 0.006 have been reported in additivated oils [111]. However, due to vast DLC surface finishes available, these results are not general. DLC tribo properties are influenced by dopant elements, the quality of the oil, the submicron interlayers, and the need for adhesion of coating [33]. There is also a difference in their behaviour according to the interaction with oil additives which have conventionally been designed for ferrous surfaces [77, 87, 162].

It will be noteworthy to mention that the tribofilm removal rate, formation and stability are of utmost importance in highly loaded boundary/mixed tribological systems and so also in cam/followers. Gangopadhyay and coworkers [87] observed significant abrasive marks on DLC coated tappet in motored tests. This indicates a cyclic film removal process. There was also evidence in the tests performed on mixed sliding/rolling contacts by Haque et al.[194] on motored multiple valve train rig and MTM. SEM/XPS micrographs of the H-DLC coating revealed irregular polishing with the centre of the inserts showing high atomic species of the Cr interlayer while regions further from the centre revealed lower Cr in a ratio of 16.5:1. This indicates a high

wear towards the centre of the inserts. Polishing can be very detrimental to engine components as the surfaces may lack the retention of engine lubricant necessary for the optimal operation. This heterogeneous polishing could be because the centre of the insert is in direct contact with the cam, flank, shoulder and ramp positions of the cam while further from the centre, contact is more predominant with the nose. Also, huge contact pressures lead to coating damage and peeling. Similar results have been reported by Kodai [197] on non-metal doped DLC coating deposited by RF plasma.

Furthermore, in commercial applications, DLC coatings have been tested in fired engine conditions to ascertain their performance in realistic operating conditions. In a recent paper by Durham and Kidson [173], fired engine tests were performed for 300 hrs on four different DLC coated tappets where they reduce camlobe wear by as much as 50-75 folds in the inlet/exhaust camshafts when compared with standard steel. However, it was observed that only one of the coatings tested (HHS) showed resistance to polishing, spallation and pitting wear. A similar approach has been employed on motored tests by Haque et al [194]. Using a different deposition process (unbalanced magnetron sputtering) from [173] in the production of W-DLC [197], no spallation or peeling was observed but the coating was worn from the surface in motorcycle stand tests.

Component bench rigs examine the tribopair under practice oriented engineering structures, thus better simulating the operating characteristics of the engine [28]. For instance, the friction characteristics of the inlet camlobe in a motored single cam rig, though, not identical with the conditions in an engine, have been reported to mirror those of the fired engine [5]. Consequently, bench /motored cam follower tribometers have become vital as they shed more light into the friction, wear, lubrication and more importantly, the tribochemistry of valve train systems.

### **6.3. Experimental Methodology**

#### **6.3.1. Test Procedure**

The lubricant bath consists of a 5L reservoir which was filled with the set amount of lubricant for the test. The system was raised to the required test temperature by the oil bath. Two test temperatures of 75<sup>o</sup>C and 105<sup>o</sup>C were used for the validation testing

on the newly developed rig. The oil was maintained at the test temperature with a HAAKE DC200 oil bath with a sensitivity of  $\pm 0.10^{\circ}\text{C}$ . Instrumentation of LabView software via an RS 232 connection to the bath, was used to plot the temperature rise which typically took 3-5 minutes for the lubricant to reach the set temperature. The lubricant was pumped through the rig to heat up the entire setup, which generally took 25 mins to reach test temperature. The lubricant supply to the camlobe and follower well was controlled by check valves in contact with a 6 mm hose. Figure 5-22 shows a labelled photograph of the single cam rig setup. The flow rate was maintained at 7.5-8.0 g/minute with a pressure of 6.0 psi. The maximum load applied to the cam by the spring loaded valve/collet assembly was 1286 N which resulted in a mean contact pressure of 0.75 GPa. This was evaluated by taking into consideration the spring stiffness, inertia, damping effects associated with the parts, as well as the friction between components. Similar approach has been employed by Zhu [11]. The valve train friction torque was measured with the aid of a torque transducer which was in-line with the camshaft and motor spindle. This data was collected from the analogue section of the torque transducers at minimum of 1 data point for every  $1.8^{\circ}$  of camshaft rotation in 7.5 minutes intervals. This was achieved with DAQ 6212 hardware with a capacity of 400 K Samples/seconds. Further processing to obtain the average friction torque at specified interval was also achieved with LabView and this was transferred to the PC system. The average friction torque was recorded at camshaft speeds of 300, 600, 1000, 1200, 1500, 1800 and 2100 rpm but all data captured during ramping conditions were discarded due to fluctuations in torque values. Elimination of torque data at the instance of speed increase has also been used by Durham and Kidson [173]. This enabled the monitoring of the friction torque value until a steady state value was obtained, for about 45 minutes. Only then was the speed increased to the next level. The test profile can be divided into two sections; the running-in phase and the steady state phase as shown in Figure 5-29. Similar procedures have been used by Gangopadhyay [90] and Broda [33]. Numerical calculations using the Dowson and Higginson equation for line contact at the cam follower interface revealed that the oil film thickness lies between 0.06-0.20  $\mu\text{m}$ , based on the speed range used in the study. The composite surface roughness was 0.25  $\mu\text{m}$  and 0.065  $\mu\text{m}$  for the Mn-phosphate and polished insert respectively. This gave a specific film thickness ( $\lambda$  ratio) between 0.24-3.70  $\mu\text{m}$  (mixed regime).

Only one pair of camshafts and buckets was used during the test. After each test, the camshafts were cleaned with acetone to remove any tribofilm on the surface. This



was to ensure that the film will not affect the next result. This camshaft has also been used for past testing in the development of the rig. The used tappet/bucket had  $R_a$  value of  $0.025\ \mu\text{m}$ . Both camshaft and bucket were considered broken-in. Only the inserts were changed for each set of tests. The breaking-in period was typically between 4-5 hrs because the surfaces had similar  $R_a$  with those used in [90] . The test procedure had three basic objectives;

- 1) Observe if the newly developed rig had good sensitivity for differentiating the friction properties of two different oils and coatings.
- 2) Check for repeatability of the data produced from the new bench test apparatus.
- 3) Investigate the tribofilms formed on the inserts

### **6.3.2. Materials**

Tests were carried out using polished and standard production removable inserts of 16MnCr5 steel coated with soft running-in Mn-phosphate coating with thickness of  $0.5\text{-}2.0\ \mu\text{m}$ . SEM images of the polished inserts, Mn-phosphate inserts and chilled cast iron material are shown as **Figure 6-1a, b and c** respectively. **Figure 6-1d** shows removable inserts that are force fitted onto the buckets in the SCR assembly. Once the rig was heated up, they expand and remain tightly in place. Mn-phosphate and polished inserts had  $R_a$  of  $0.25\ \mu\text{m}$  and  $0.035\ \mu\text{m}$  respectively. The camshaft is chromium chilled cast iron with  $R_a$   $0.055\ \mu\text{m}$ .

Before changing the lubricant to be used on the SCR, the former lubricant was drained off, and the rig was first flushed with base oil at high pressure of 7 psi (20 L/m) for 2 hrs. This was to remove any residual oil within the hoses and cylinder head. The rig was then disassembled, and cleaned with iso-propanol and high detergency fluid. It was left to dry for 24 hrs before the bath was loaded with the next fresh oil.

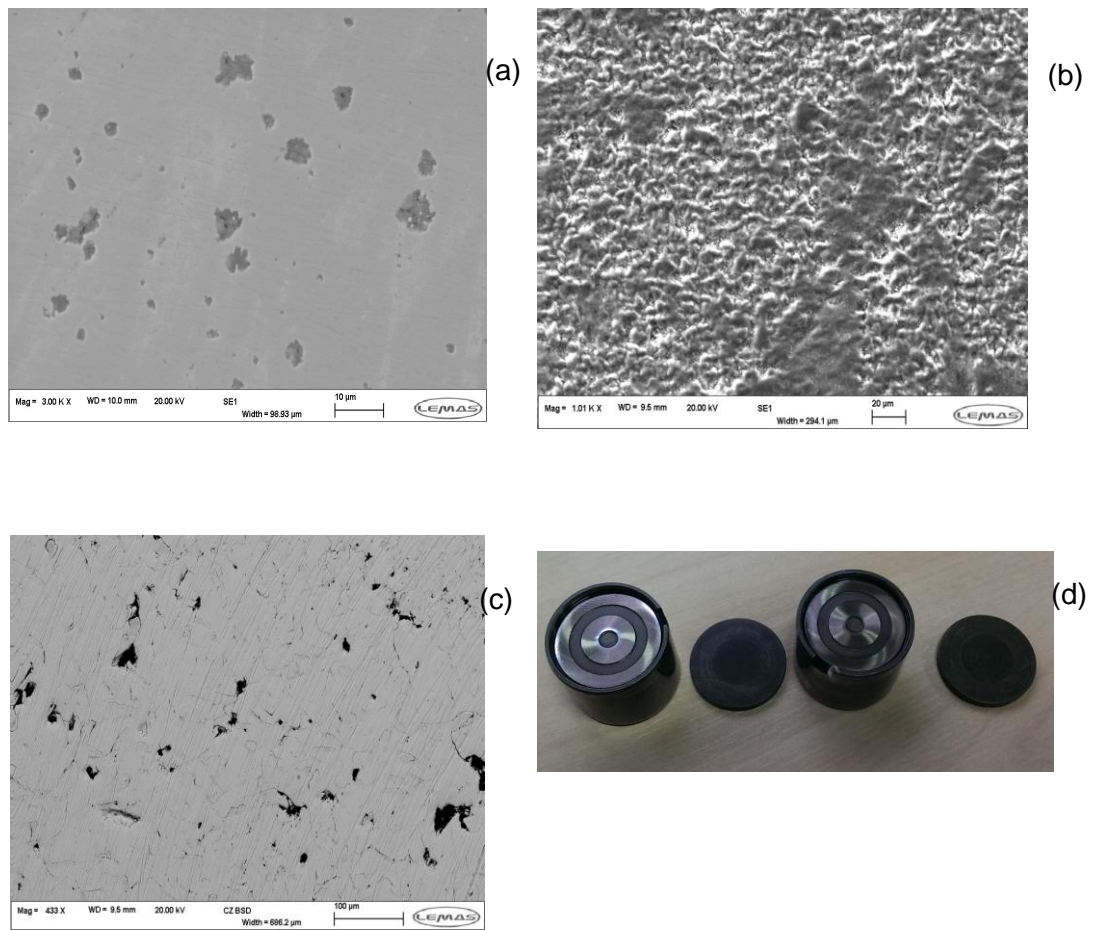


**Figure 6-1 SEM Image showing (a) Polished surface with  $R_a$  of  $0.025 \mu\text{m}$  (b) Polycrystalline structure of Mn-phosphate with  $R_a$  of  $0.35 \mu\text{m}$  (c) Chromium chilled cast Iron with  $R_a$  of  $0.055 \mu\text{m}$  (d) bucket and inserts**

### 6.3.3. Lubricants

Lubricants used for the tests are two European SAE 5W/30 fully formulated mid and normal SAPS oil from TOTAL, hereafter referred to as oil A and oil B respectively. Both are composed of a group III base stock. The engine oils essentially contained dispersant, detergents, antiwear additives, viscosity improvers, and antioxidant. In Oil A, the detergent is a mix of Mg/Ca overbased phenate and sulphonates with phenolic+arylamine based compounds as antioxidants. It also contains an OFM, olefin copolymers as VI improver and a secondary ZDDP. Whereas oil B, contains Ca/Mg overbased carboxylate type detergents. The antioxidant consists of arylamine based compounds, a primary ZDDP antiwear additive and no commercial friction

modifier. Further details of these lubricants can be found in our previous work [198]. Table 6-1 give details of the concentration of key elements in the engine oils.

**Table 6-1 Lubricant Composition**

Oil Code	Viscosity Grade	Additive concentration – Content (wt %)					Engine lubricant bulk properties					
		P	Zn	Mo	S	FM	Antiwear Type	KV40 (mm <sup>2</sup> /s)	KV100 (mm <sup>2</sup> /s)	Density (g/cm <sup>3</sup> )	Dynamic Viscosity (mPa.s)-ASTMD4684	
<b>Oil A - Mid SAPS</b>	SAE 5W-30	0.095	0.10	0	0.2	Yes	ZDDP 11	61.9	10.63	0.854	22120	
<b>Oil B - Normal SAPS</b>	SAE 5W-30	0.124	0.14	0	0.5	No	ZDDP 1	56.2	9.84	0.857	18040	

#### 6.3.4. Valve Train Friction Torque

The data collected from the analogue end of the torque transducer were passed into an NI-USB 6212 hardware giving characteristic waveforms that give information about the speed of the camshaft assembly. The natural frequency within the test bench was about 400 Hz and filtering with a Butterworth filter to the 6<sup>th</sup> degree at a frequency of 395-405 Hz did not affect the maximum/minimum torque. Deviations were in the range of  $\pm 5$  mNm. Similar findings have been reported by Mufti [182]. Essentially, the instantaneous torque is made up of friction and geometric components. During valve openings, energy is absorbed by the spring and this is released to the camshaft as torque. The friction component is very high during valve opening and has little or no components during valve closing. The inertia/geometric torque on the other hand have equal positive and negative components during valve opening and closing. Ideally, by taking mean torque values over the cam cycle, the inertia/geometric torque will be effectively cancelled out leaving the friction component [5, 185, 186]. The average friction torque was obtained by taking an average of the 200 data points obtained for each camshaft cycle. This corresponds to approximately 1 data point for every 1.8° of cam shaft rotation. This was then averaged over the duration of the test in the steady state region.

Due to the compact and rigid nature of the modified camshaft and entire single cam rig assembly, the system was able to operate at high speed (up to 3000 rpm) with limited noise. This has been discussed in section 5.8 of this thesis. Only 5 cycles were

shown at 2100 rpm to demonstrate the low vibration of the rig at high speed. The asymmetric nature of the torque curve is due to work done by the camshaft during valve opening. This constitutes both geometric and the bulk of friction torque. On valve closing, work is done by the valve spring in maintaining contact with the camshaft which essentially consists of all geometric components. At high speed, the work done by the camshaft is slightly greater than those of the spring. This difference is proportional to the friction torque which is typically low at high camshaft speeds.

## 6.4. Results

### 6.4.1. Friction Data

**Figure 6-2** and **Figure 6-3** show the good repeatability of the data obtained from the newly developed valve train rig with a standard cast iron camshaft against polished production inserts and Mn-phosphate inserts respectively. The difference in friction torque is a small fraction of the final insert finish observed between each sample. The variability observed at low temperature is slightly greater for all the speeds tested. Oil A was used for the test at an oil supply temperature of 105<sup>o</sup>C. All tests were performed three times and the average friction torque from all tests was used as the basis for comparison with other experimental conditions. The average friction torque reduces with increasing speed due to increased lubricant entrainment velocity into the cam follower contact region. The reduction profile also depicts the mixed lubrication regime of the Stribeck diagram which moves from a more boundary dominated regime at low speed to more elastohydrodynamic regimes at high speeds. An increase in friction torque is also observed with increasing temperature (**Figure 6-4**) and this has been reported in previous studies [53, 182].

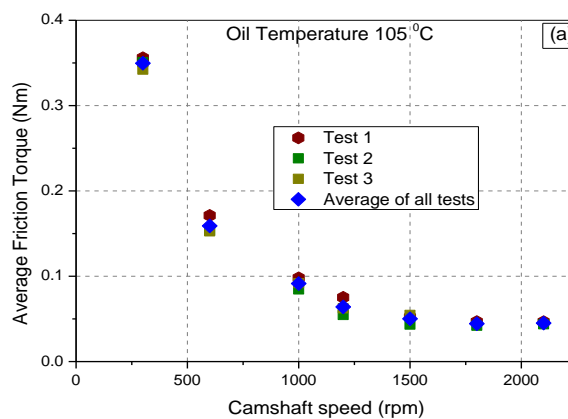


**Figure 6-2 Friction torque data on newly developed single cam rig showing good repeatability with oil A against polished inserts at 105<sup>o</sup>C**

At 2100 rpm, a noticeable increase in torque is observed. This can be attributed to a higher degree of hydrodynamic lubrication. The lubricant films are getting thicker which gives rise to higher friction with undoubtedly smaller applied forces.

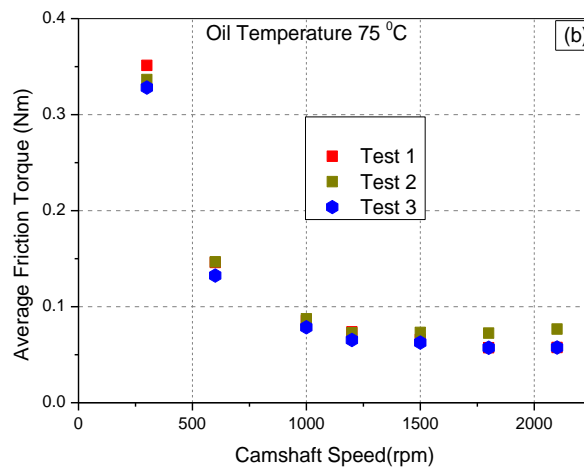


**Figure 6-3** Friction torque data on newly developed single cam rig showing good repeatability with oil A against Mn-phosphate inserts at 75°C

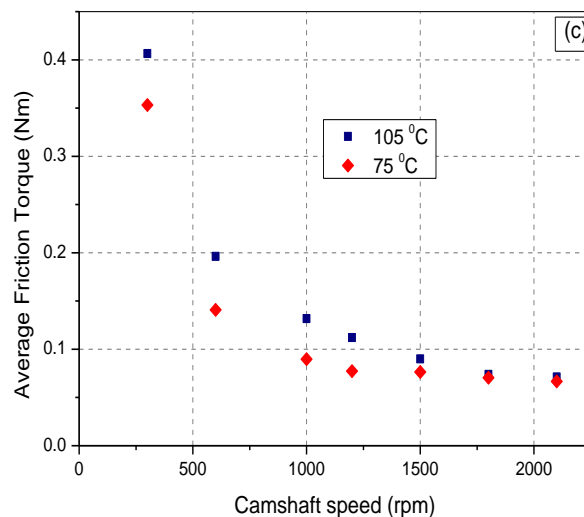


**Figure 6-4** Effects of temperature on newly developed single cam test rig with Mn-phosphate coating

#### 6.4.2. Effect of Surface Finish on Average Friction Torque

The effects of surface finish on the average friction torque are displayed in **Figure 6-5** (a) and (b). Friction torque benefits were achieved using the polished insert at higher temperature of 105°C for all speeds tested. At low temperature of 75°C, the frictional responses between these surfaces are marginally different for most speeds tested. This is particularly due to the viscosity of the lubricant which forms thick films between the interacting surfaces. At 105°C and 300 rpm, however, the polished insert and Mn-phosphate coating have specific film thickness ( $H_{min}$ ) 0.95 and 0.24  $\mu\text{m}$  respectively. At this speed, greater friction benefits are achieved due to boundary lubrication where the formation of molecular tribofilms controls the frictional response of the system. The effect of surface roughness is also an important factor for the improvement of friction because it controls the asperity contact which affects both friction and wear in boundary lubrication. Similar friction benefits have been observed when polished inserts were compared with Mn-phosphate coating [25]. Although, Mn-phosphate is widely used in cam/follower inserts and piston liners as soft running-in coatings [25, 45] and for adhesive wear prevention because the coating has a crystalline, porous, soft and rougher surface finish (See **Figure 6-1b**) which gives good oil wettability, absorbance and oil retention characteristics [56]. The high friction of the coating can be attributed to high asperity interaction between the insert and cam surface coupled with less reactivity with lubricant additives, which were conventionally designed for ferrous surfaces. For the speed range tested (300-2100 rpm), the Mn-phosphate coating had a specific film thickness ( $\lambda$ ) in the range from 0.24 -1.00. This is considerably lower than the polished insert which have a  $\lambda$  ratio from 0.95 – 3.7 for the speed range tested. It thus suggests that the polished insert is predominantly in the mixed regime. SEM micrograph discussed in section 3.5.1 also suggests that the  $\text{Mn}_3(\text{PO}_4)_2$  surfaces are less resistant to abrasive wear.

Comparing of Figure 6-5a and Figure 6-5b shows some conflicting behavior for the surfaces. This is due to the response of the oil at high temperature. It can be observed that the benefits seen at 75°C was marginal due to oil viscosity. At 105°C, however, the true behavior is revealed.

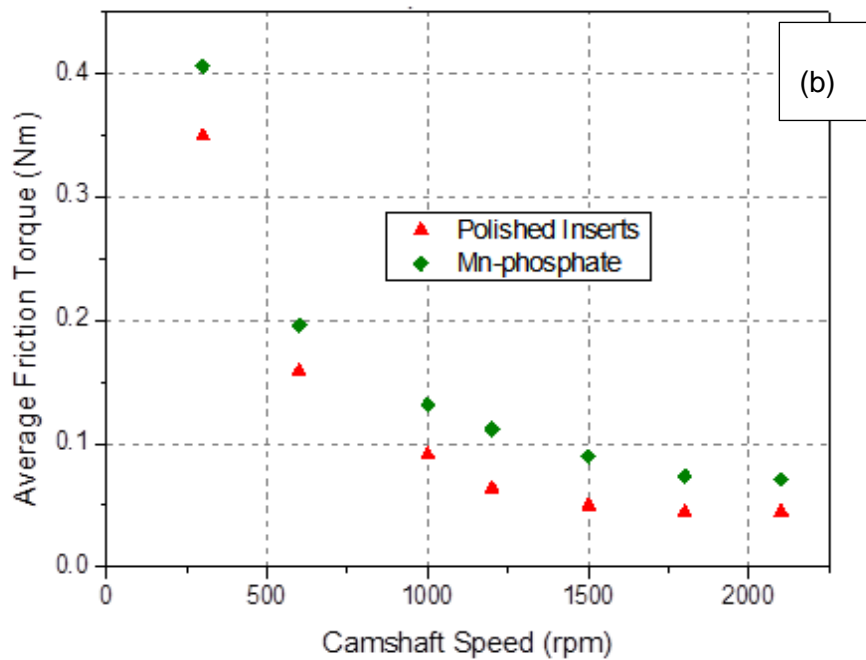
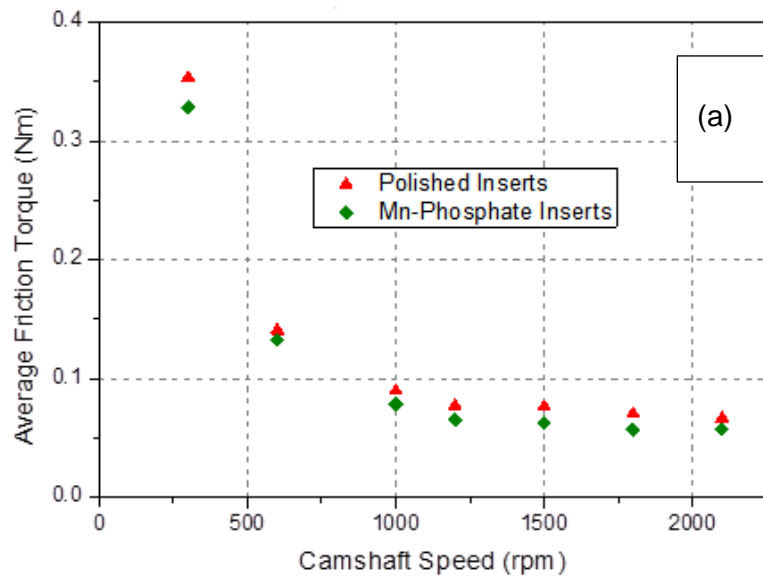
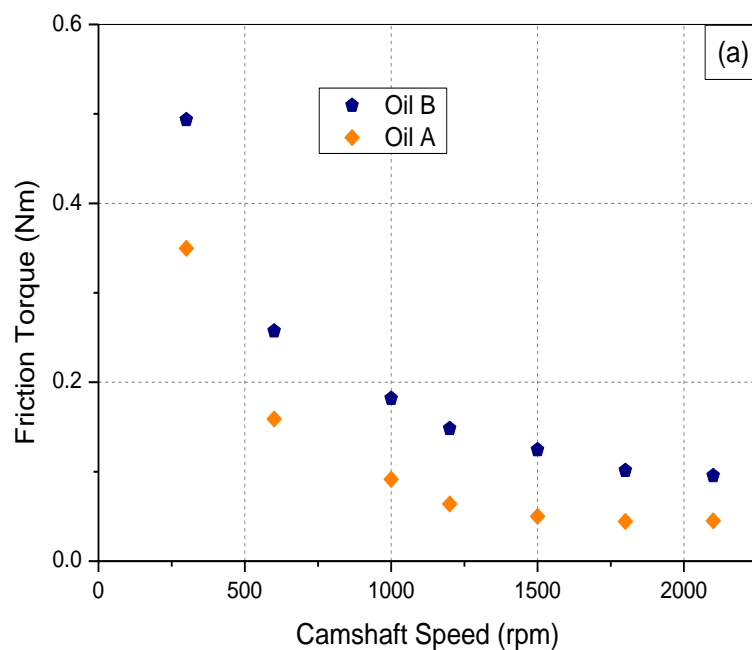


**Figure 6-5** Effect of surface finish on friction torque with the newly developed single cam rig with (a) Oil A at 75°C (b) Oil A at 105°C

### 6.4.3. Effects of Engine Oil Formulation

Oil formulations have a crucial part to play in the reduction of friction and wear in boundary/mixed lubricated contacts. Previous studies [90] have shown that fully formulated oil with 700 ppm of MoDTC reduced the friction torque by 29% and the friction torque were independent of camshaft speed/surface coatings. This was attributed to the formation of MoS<sub>2</sub> sheets which have weak Van der Waals interactions between layers and covalent bond between atomic species [86, 90]. These tribolayers control friction on interacting surfaces [90]. In our application, oil A was an ester-based friction modified fully formulated oil and the friction benefits (

**Figure 6-6a)** can be observed across the entire speed range although significant benefits are experienced at low speed. Improvements at high speed are due to the differences in the bulk properties of both lubricants particularly their viscosity [15]. Oil A was observed to reduce the friction in polished inserts by approximately 29 %.





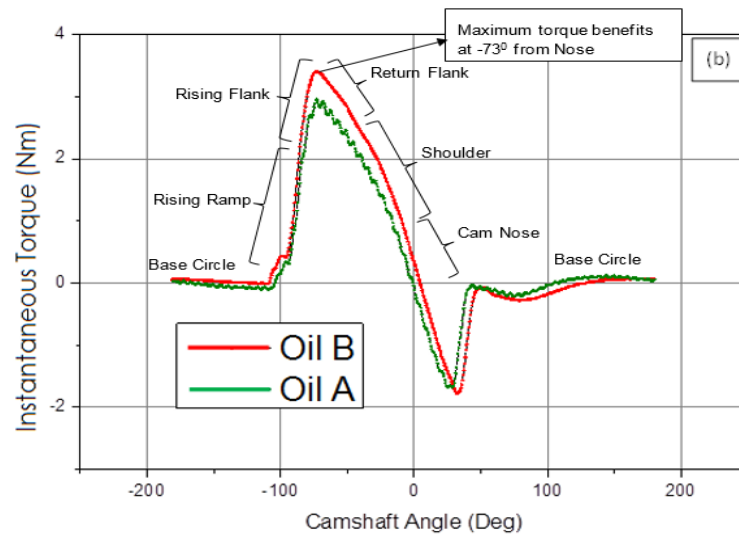


**Figure 6-6 Effect of oil type on friction torque (a) Polished inserts at 105 °C  
 (b) Instantaneous torque across cam profile at 300 rpm with polished Inserts  
 at 105 °C**

Ideally, the resultant of the forces on the follower, the inertia and spring forces should remain unchanged with the introduction of a new type of lubricant. Lower torque responses can therefore be attributed to the ability of the lubricant to reduce friction torque. Evaluation of the instantaneous torque across the cam profile revealed that significant friction torque benefits were achieved with oil A at all regions with maximum improvements at approximately  $-73^{\circ}$  from the cam nose. This is the region of high

loads and similar findings have been reported in [5] . The results were computed for the camshaft speed of 300 rpm in predominantly boundary lubrication (See

Figure 6-6b). The rising part of the cam showed more benefits as this is the region in which significant work is done by the camlobes. From

Figure 6-6b, oil A will result in a maximum of 14% reduction in power consumption at 300 rpm.

#### **6.4.4. Insert Wear Measurement**

At the end of the test, the wear on the insert was traced by an NPFLEX White Light Interferometry as shown in **Figure 6-7**. Significant wear regions were characterized by the presence of ridges on the inserts. At the edge of the insert, contact with the cam lobe occurs but this does not produce significant grooves or valleys on the surface of the inserts. At the centre, however, there are contacts with the cam nose, flank, shoulder and ramp regions, and as such, the wear depth (WD) was greatest in this region. The insert surface showed concentric circles with different width. Similar findings have been reported by [11]. This can be attributed to edge loading effects and tappet rotation within the tappet bore which allows circumferential rubbing action to take place on the inserts with dimensions greater than the camlobe width. The sum of the wear depth at the insert centre and the wear scar width was used to determine the maximum wear depth. These approaches have been employed by Kano [54] and Liu [145] for the evaluation of wear on camlobes.

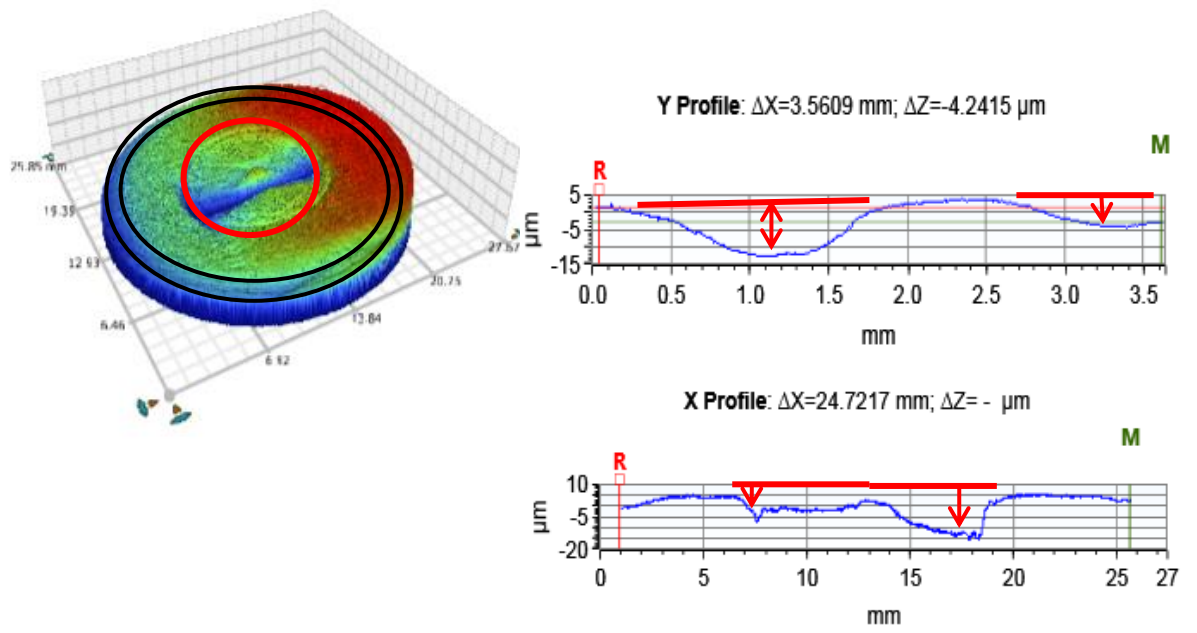
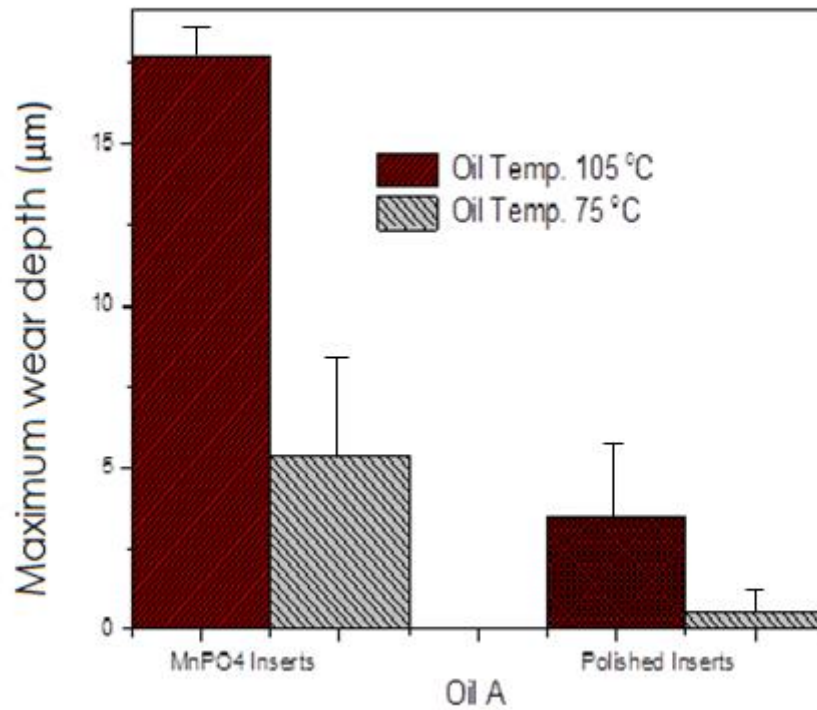
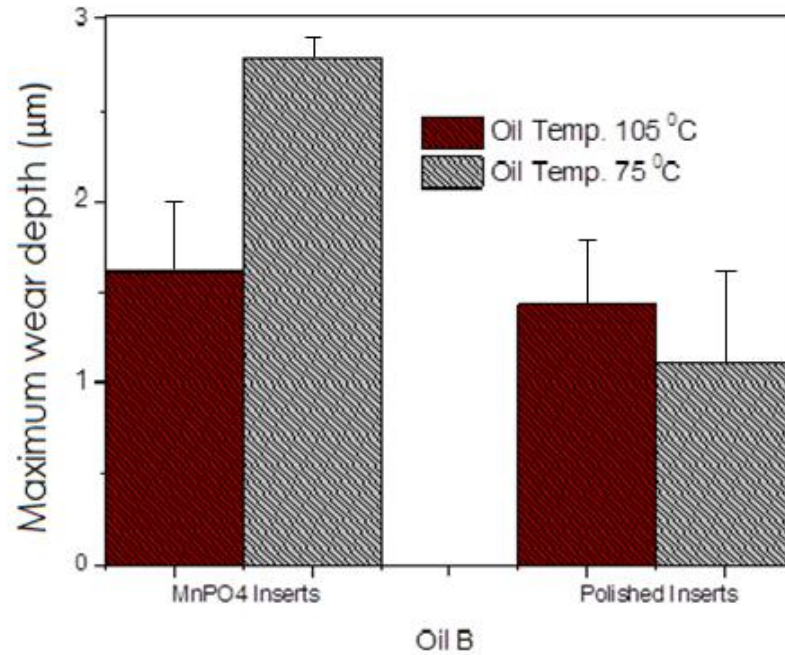


Figure 6-7 Wear scar measurement procedure from Inserts

(a)



(b)



**Figure 6-8 Maximum Wear Depths with (a) Mid SAPS Oil A & (b) Normal SAPS Oil B**

#### 6.4.5. Effects of Oil Type on Wear

Oil B was observed to reduce the wear for most of the conditions and material pairs tested. The surfaces of the inserts with oil B show a very distinct distribution of dark antiwear films on the surface which have good extreme pressure properties necessary to reduce wear. For the  $Mn_3(PO_4)_2$  the high wear could be due to the high temperature ploughing of the soft running-in Mn-phosphate coating during tribological tests (see Figure 6 8a & b). With oil A, high temperature affected both distribution and durability of the tribofilm. This was not observed with oil B which was composed of a primary ZDDP. On polished inserts, oil B produced a marginal difference in wear.

In fully formulated engine lubricants, synergistic, antagonistic and harmless interactions are all possible. In a paper by Fujita et al. [82], it was observed that antiwear films undergo antagonistic interactions in the presence of dispersant and load, with secondary ZDDP being more susceptible to attack. Film thicknesses could be as high as 80 – 120 nm in ZDDP additivated oils but could reduce to less than 20 nm in the presence of dispersant and load [82]. There have even been reports where no films were observed [2] due to antagonistic interactions with dispersants.

## **6.5. Conclusions**

- A single cam rig has been developed, that has high sensitivity to distinguish the frictional responses of surface coatings as well as fully formulated lubricants with very close chemistries.
- Good repeatability and consistency from the experimental protocol for the validation tests indicates that the newly developed rig, its instrumentation, data processing/acquisition and operational procedures are reliable. They can provide valid information with confidence.

## **CHAPTER 7. TRIBOCHEMISTRY STUDIES OF FILMS DERIVED FROM NEWLY DEVELOPED SINGLE CAM RIG**

### **7.1. Motivation for Tribocchemistry Studies**

The role of lubricant additives in forming adherent interlayered films on interacting surface is vital for the successful operation of most, if not all, machine components [10]. While these films are formed in boundary/mixed lubrication, they need to have the right mechanical and chemical properties to prevent scuffing, polishing and pitting on interacting surfaces. It is the objective of the chapter to investigate the composition of these films and correlate this to the wear/friction. In addition, since wear and friction are controlled on the molecular scale, the characteristics of these films are crucial to all lubricant formulators in identifying key additive that reduce friction/wear and generally improve the performance of internal combustion engines. The tribofilms formed using normal and mid Sulphated Ash, Phosphorus and Sulphur (SAPS) 5W-30 oils were evaluated and correlated to the friction and wear properties of the tribopair.

In terms of surface analysis, Raman, XPS, TEM and FIB-SEM/EDX investigations of the tribochemical films showed that the normal SAPS oil produced patchy, thick (80-100 nm) and well dispersed tribofilms with better wear prevention capabilities. It was observed that Mid SAPS oil had lower wear prevention due to loosely dispersed and thin tribofilms. TEM analysis also revealed that the tribofilms consists of dense matrix in regions with significant rubbing and a two layered structure in regions of less severe rubbing. The topmost layer is an oil rich layer while the lower section is the rigid tribofilm. XPS analyses revealed that oil B forms long chain polyphosphates at the top of the surface while oil A primarily forms orthophosphates in the core matrix of the tribofilm. Absence of tribofilms at the centre of the insert with this oil also suggests that formation and removal processes are an integral part of the wear mechanisms in highly loaded cam follower systems.

### **7.2. Raman Surface Test Procedure**

Raman spectroscopy is a very useful technique for the determination of the structure of the tribofilms which have been formed on the surface. Raman technique has a

probing depth of  $1\mu\text{m}$ , which is in excess of the thickness of the tribofilms, hence it will probe the substrate structure as well as the tribofilm. The change in counts due to increase in accumulation can be attributed to the re-ordering of the molecule while Raman shift indicates stretching of the molecules. The samples were exposed for 10secs at 488nm wavelength with laser power of 100 % at 2 accumulations. Higher accumulations help reveal narrow adsorption bands of molecules which may not have been seen at lower accumulations. Small spot sizes of  $20\mu\text{m} \times 20\mu\text{m}$  were chosen as the sampling region. Numerous spectra were obtained in this region to ensure the results were repeatable. Spectra of the wear scar were taken at three selected points approximately 0.5 mm from centre (P1), on the edge of concentric circles (P2) and at the edge of the inserts (P3), to identify the tribochemical films which were formed on the surface (see **Figure 7-1**. Based on the conditions used, the laser power reaching the surface was only a few milliwatts to prevent surface damage.

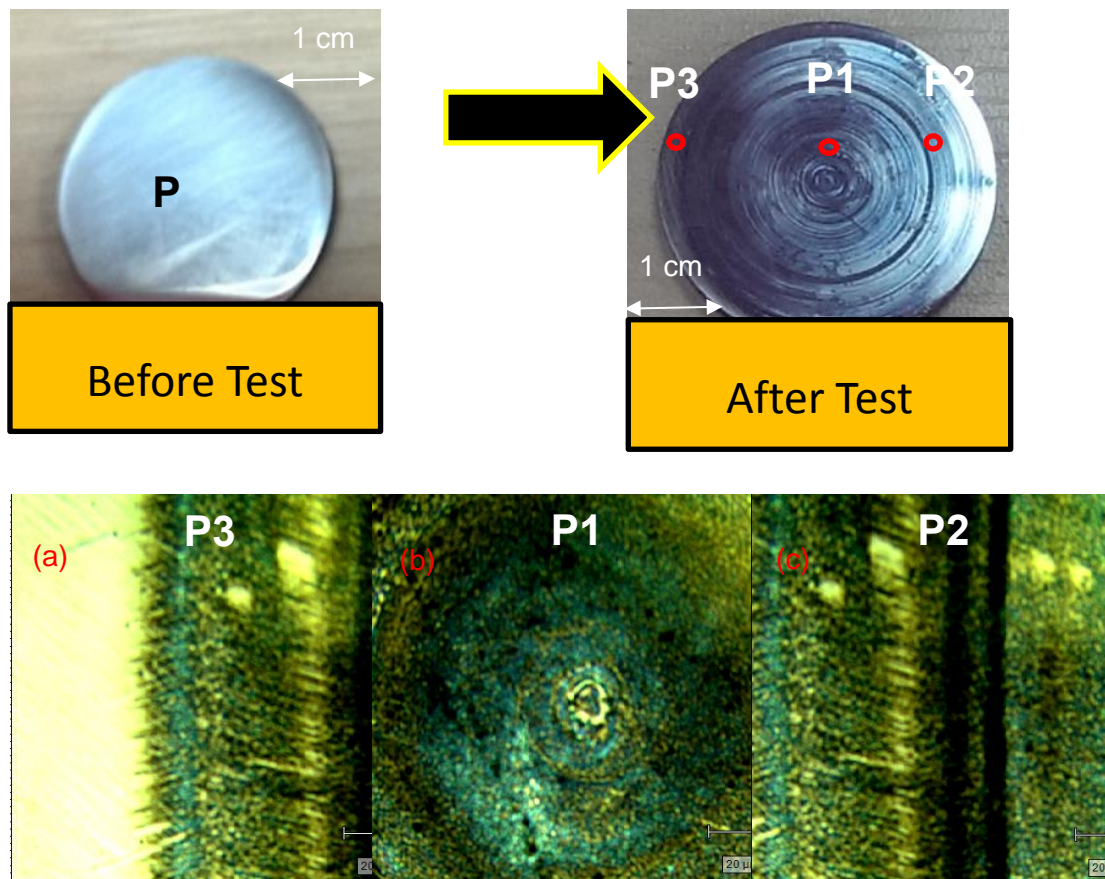


**Figure 7-1 Raman Image (a) Polished Insert Wear Scar – P1 (b) Polished Insert Wear scar - P2 (c) Polished Insert Wear Scar – P3**



### 7.3. FIB-SEM/TEM Imaging Procedure

This technique was used to observe the tribofilm on the surface before TEM surface analytical tests were carried out. The sample was prepared using an FEI Nova200 dual beam SEM/FIB fitted with a Kleindiek micromanipulator for in situ lift-out. The ion beam was operated at 30 kV with beam currents between 5000 and 100 pA. Platinum deposition of 10.00  $\mu\text{m}$  x 2.00  $\mu\text{m}$  x 1.00  $\mu\text{m}$  volumes was carried out at 0.3 nA. Bulk removal with an ion source of Gallium was carried out at 7 nA to create a volume of 10.00  $\mu\text{m}$  x 6.00  $\mu\text{m}$  x 3.00  $\mu\text{m}$ . Then a cleaning cross section was done at 1nA. Further cleaning cross sections were carried out at 0.3 nA with volume of 10.00  $\mu\text{m}$  x 0.5  $\mu\text{m}$  x 1.50  $\mu\text{m}$  to remove the curtaining effect and produce FIB-SEM images. TEM analysis was carried out using an FEI Tecnai F20 200 kV FEGTEM fitted with a Gatan Orius SC600 CCD camera and an Oxford Instruments XMax 80 mm<sup>2</sup> SDD EDX system. Figure 7-2 a & b highlights the images for FIB-SEM/TEM analysis where a distinguishable thick dark layer representing the tribofilm.

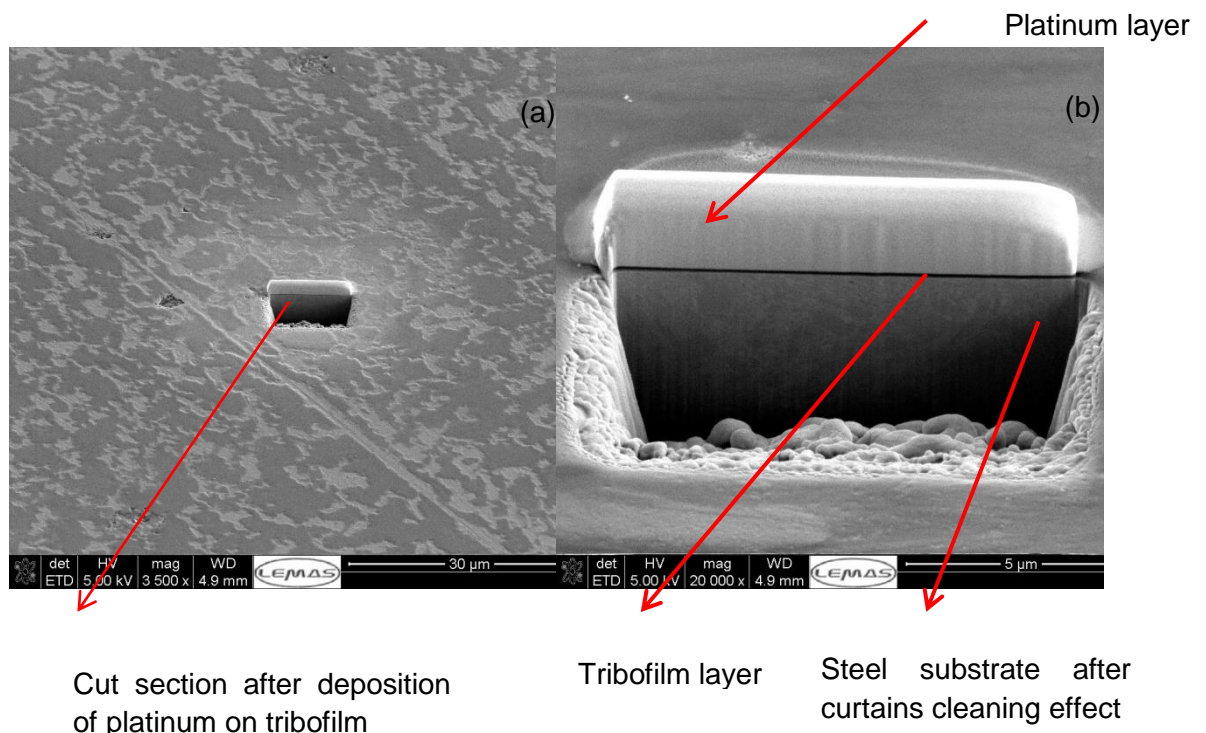


**Figure 7-2 Procedure for (a) FIB-SEM Investigation (b) TEM Sample Preparation**

### 7.4. XPS Tests and Imaging Procedure

XPS analysis was carried out in a Thermo theta probe. The background pressure was  $3 \times 10^{-7}$  mbar. The electrons were excited with a micro focused monochromatic Al-K $\alpha$



at X-ray energy of 1486.6eV. These were then detected after passing through the analyser. The spot size is an eclipse with dimensions of 200 $\mu$ m x 400 $\mu$ m. High resolution of the analyser was determined by the pass energy which was set at excitation energy of 200eV. High resolution rescans for the elements of interests (Zn, Fe, C, O, S, P, and Ca) were carried out at two regions on the inserts at 40 eV with a dwell time survey of 50 ms and charge neutralization times of 100ms. In the survey scan, the range was maintained at 0 – 1350 eV for all samples tested to identify major elements. For sputtering, Ar Mono atomic gun was used at 4KeV with a raster size of 1x2mm<sup>2</sup>.

The XPS spectra were processed using the CasaXPS software. The XPS spectra were calibrated by setting the binding energy of the major component of the C1s peak to 284.8 eV. The areas under the peaks were deconvoluted by curve fitting after appropriate background subtractions. Peaks were fitted with Gaussian Lorentzian line shapes. The binding energy of the fitted curves for all elements (P2p/Zn3s, O1s, Ca2p<sub>1/2</sub> and Ca2p<sub>3/2</sub>) was constrained within acceptable limits. Two locations were examined on the insert at 0.5mm and 6mm from the centre of the inserts which have been designated as points L1 and L2 respectively. This was done after following the procedure for Raman analysis, where location P2 and P3, were observed to have similar Raman spectra.

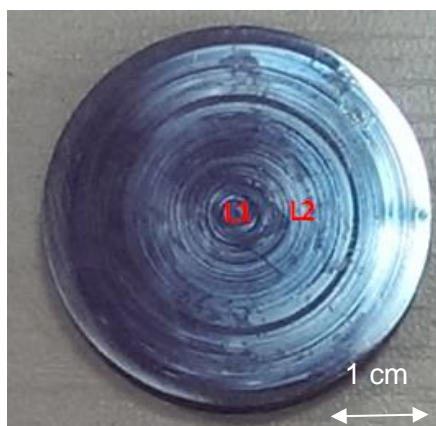


**Figure 7-3 Location P1 and P2 for XPS analysis**

## **7.5. Surface Analysis/Tribochemistry Results and Discussion**

### **7.5.1. SEM/EDX Results**

The significant difference between the surfaces of the inserts has to do with the polishing and abrasive wear of the inserts as well as the distribution of the tribofilm

on the surface. The polished shim in **Figure 7-4a** showed a heterogeneous distribution of the lubricant derived films with little/no scoring marks on the surface. White spots were identified as Ca concentrated areas, particularly CaCO<sub>3</sub> derived from the detergent/dispersant used in the oil with a matrix of phosphorus embedded underneath. This is shown at regions 5 & 6. The presence of CaCO<sub>3</sub> and phosphate has been supported by Raman analyses which are discussed in the next section. At higher temperature (**Figure 7-4b**), significant abrasive marks were observed on the worn surface with patchy phosphate films which appear to have been slightly removed due to rubbing action from the camlobe. These abrasive processes cause lots of third body wear particles due to plastic deformation and large nascent surfaces that can be quickly oxidised. In extreme cases, this can lead to catastrophic failures. EDX information revealed phosphorus concentrations (atomic %) of 0.70 % at regions 1, 2 and 3 respectively. At region 4 on the wear scar, the phosphorus concentration was 0.08 %. Zn concentration typically ranged from 0-0.24 % at regions 1-3, to 0.18 % at region 4. It is worthwhile to mention that at most regions of the wear track investigated, the Zn concentration was very low and even absent in some areas as shown in Table 7-1. This region was at the centre of the insert. This clearly illustrates the heterogeneous nature of lubricant derived tribofilms as well as the inherent surface sensitivity of this technique. Examination of the Mn-phosphate inserts showed parallel/horizontal scoring marks at both temperatures (**Figure 7-4c** & **Figure 7-4d**). At lower temperature, however, this resulted in a smoother surface while at high temperature, the surfaces were rougher consisting of ridges/grooves on the surface of the insert.

**Table 7-1** EDX Spectra of Regions on Polished Inserts at 75<sup>o</sup>C and 105<sup>o</sup>C with Oil A

Regions	Element (at. %)											Total
	P	Ca	Zn	Fe	S	C	Si	Cr	O	Mn	others	
1	0.7	0.1	0.0	32.4	0.0	58.1	0.1	0.7	7.6	0.3	0.0	100.0
2	0.7	0.1	0.0	32.0	0.0	59.5	0.1	0.6	6.7	0.3	0.0	100.0
3	0.7	0.0	0.1	32.2	0.0	59.2	0.1	0.6	6.7	0.3	0.0	100.0
4	0.1	0.1	0.1	60.3	0.0	38.1	0.3	1.1	0.0	0.0	0.0	100.0
5	2.7	0.1	0.3	41.6	0.4	41.7	0.0	0.8	11.1	1.3	0.1	100.0
6	2.9	0.0	0.0	50.9	0.5	38.1	0.0	0.8	5.2	1.3	0.3	100.0

The low levels of Zn, P, and S of the tribofilm on the wear track at points 1,2, 3, and 4 clearly reduces the antiwear properties on the inserts [196]. This could be as a result of the dispersant used in the oil. Certain dispersant particularly polyisobutyl succinimide polyamine (PIBSA PAM) have been reported to suppress the formation of antiwear films [2]. The absence of S on all regions examined on the insert at 105°C is still unclear. In addition, the high phosphorus concentration formed on the inserts at 75°C supports their good antiwear characteristics. These results suggests that the durability of antiwear films is strongly affected by temperature even though high temperature has been reported to favour the formation of thick padlike antiwear phosphate films [93, 199]. In addition, the efficacy of the tribofilm is influenced by the equilibrium between film removal, formation and associated mechanical properties [200].

Recent studies on camlobes [145] with secondary ZDDP have shown that high temperature affects the durability of these films, which supports the finding in this work. It will be worthwhile to investigate the mechanical and rheological properties of these films but this is beyond the scope of the present study.

Oil A produces tribofilms that are thin and sparsely distributed on the surface as shown in **Figure 7-4b**. These suggest that during rubbing, direct asperity interactions are more likely to occur, thus increasing the likelihood of insert wear. Using oil B, **Figure 7-4e** and **Figure 7-4f** show the SEM image of the tribofilm formed on the surface of the polished insert. Continuous padlike layers that are separated by craters were observed on the insert surface although this was more conspicuous at 105°C. This has been reported for model oils containing ZDDP [101]. The tribofilms are significantly thicker and more evenly distributed on the surface than oil A. These minimizes the asperity contact and clearly helps improve wear on the inserts.

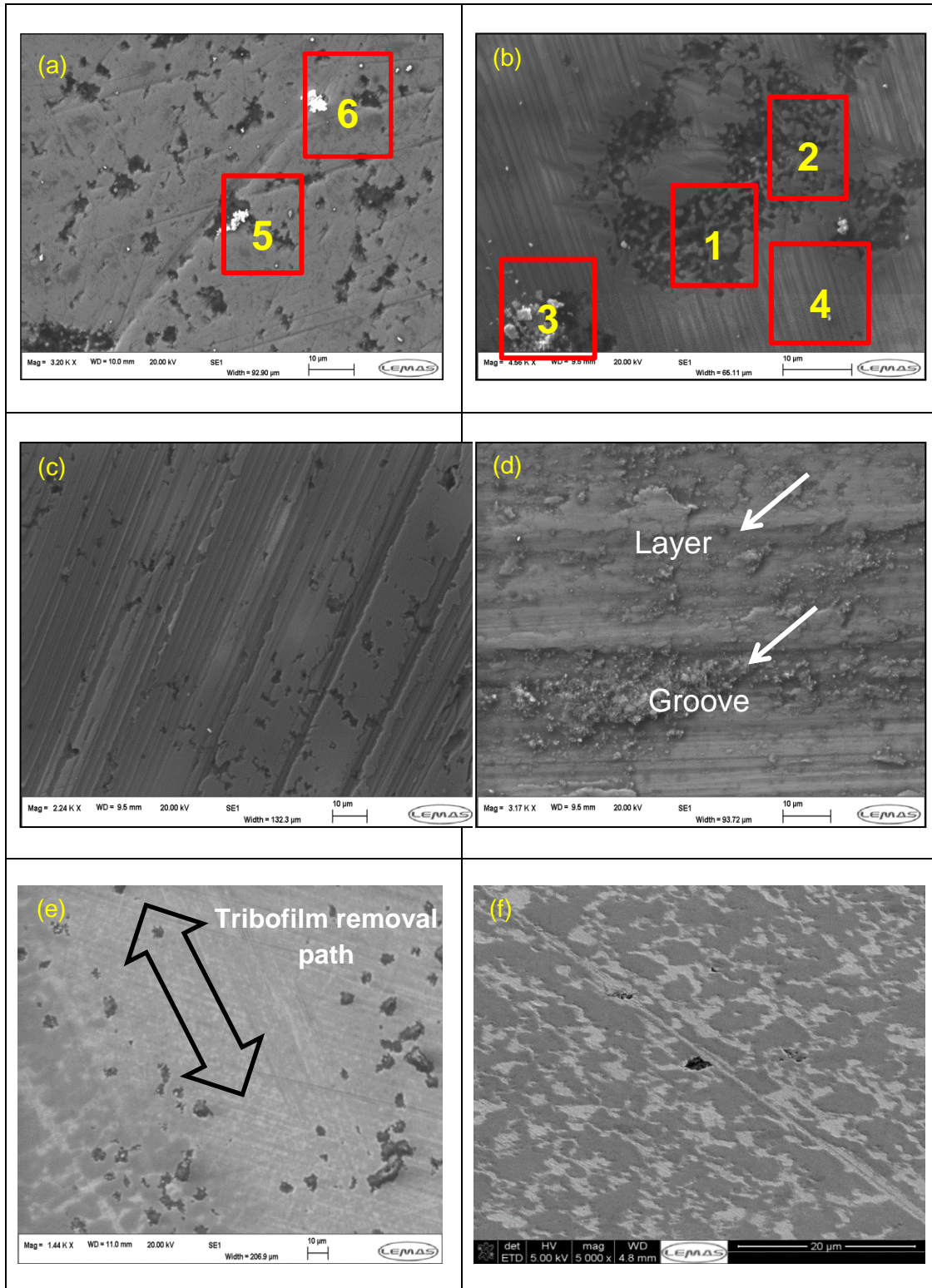


**Figure 7-4 Scanning Electron Micrograph (a) Oil A with Polished inserts at 75 °C – Top left (b) Oil A with Polished inserts at 105 °C – Top Right (c) Oil A with Mn-phosphate at 75 °C – Mid left (d) Oil A Mn-phosphate at 105° – Mid Right (e) Polished inserts against Oil B at 75 °C – Bottom left (f) Polished inserts against oil B at 105.**



### 7.5.2. Raman Spectroscopy – Investigation of Film Structure

Figure 7-5a, b and c illustrate the points where spectra were taken. Similar points were used for the FIB-SEM images. Figure 7-5, Figure 7-6a & b showed the Raman spectra of the films formed on the wear track of the polished inserts at 105°C using oil A and oil B. Raman spectra of an unused sample was shown as P for comparison. The tribofilm from both oils have similar characteristics or film structures at P2 and P3. The narrow shoulders at 964-975  $\text{cm}^{-1}$  are fingerprints of zinc/calcium orthophosphate [88]. These are more obvious at 105°C than 75°C, suggesting thicker films at higher temperature (Raman spectra's at 75°C are not shown). Other components of the tribofilm within the wear scar are  $\text{FeS}_2$  with peaks at 330-341  $\text{cm}^{-1}$ . Narrow bands at 527-530  $\text{cm}^{-1}$  may be internal vibrations of  $\text{PO}_4^{3-}$  [201] or an iron oxide [88]. The peaks at 901-920  $\text{cm}^{-1}$  are due to bending of the phosphate from the secondary antiwear additive. At 1040-1105  $\text{cm}^{-1}$ , calcium carbonate peaks were observed from the detergent used in the oil. Spectra of oil A at P1 showed some fingerprints  $\text{Fe}_3\text{O}_4$  at 675-680  $\text{cm}^{-1}$  which was not observed at other points. Minor peaks of phosphates and carbon were also seen on the contact region at 960  $\text{cm}^{-1}$  and 1350/1550  $\text{cm}^{-1}$  respectively. Peaks at 2736-2748  $\text{cm}^{-1}$  are due to undecomposed hydrocarbon on the insert surface.

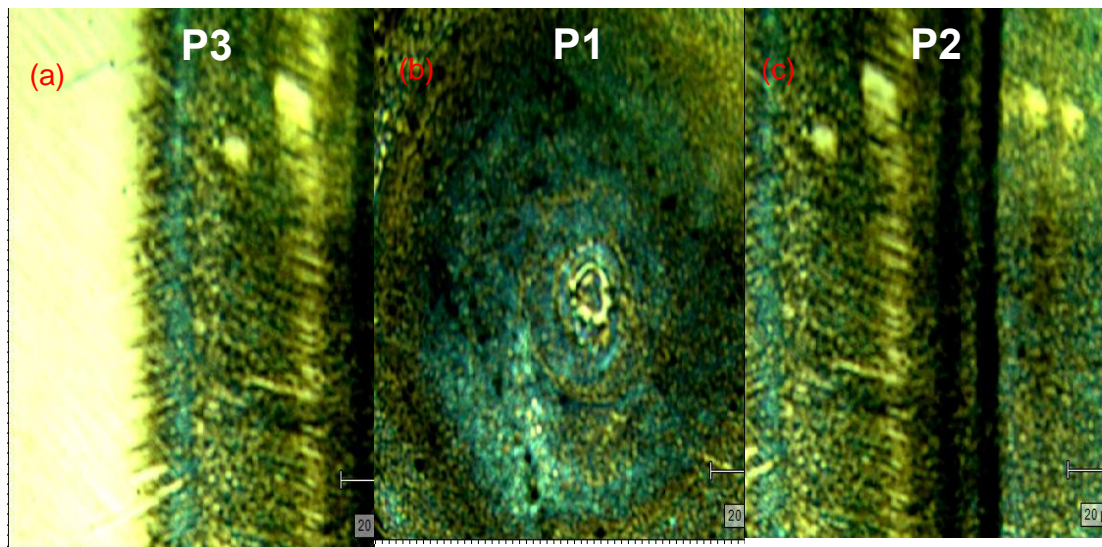


**Figure 7-5 Raman Image (a) Polished insert wear scar – P1 (b) Polished insert Wear scar - P2 (c) Polished insert wear scar – P3**

At the centre of the inserts (P1), oil B produced tribofilms which had similar spectra with points P2 and P3. Oil A had a different spectrum at the centre of the insert at

105°C. The films comprises of Fe<sub>3</sub>O<sub>4</sub> and FeS<sub>2</sub> with no indication of phosphate films. These have been supported by FIB-SEM images (see Figure 7-7). These suggest that the tribofilms derived from oil A are easily removed at the centre of the insert due to rubbing action from the camlobes in highly loaded non-conformal valve train contacts.

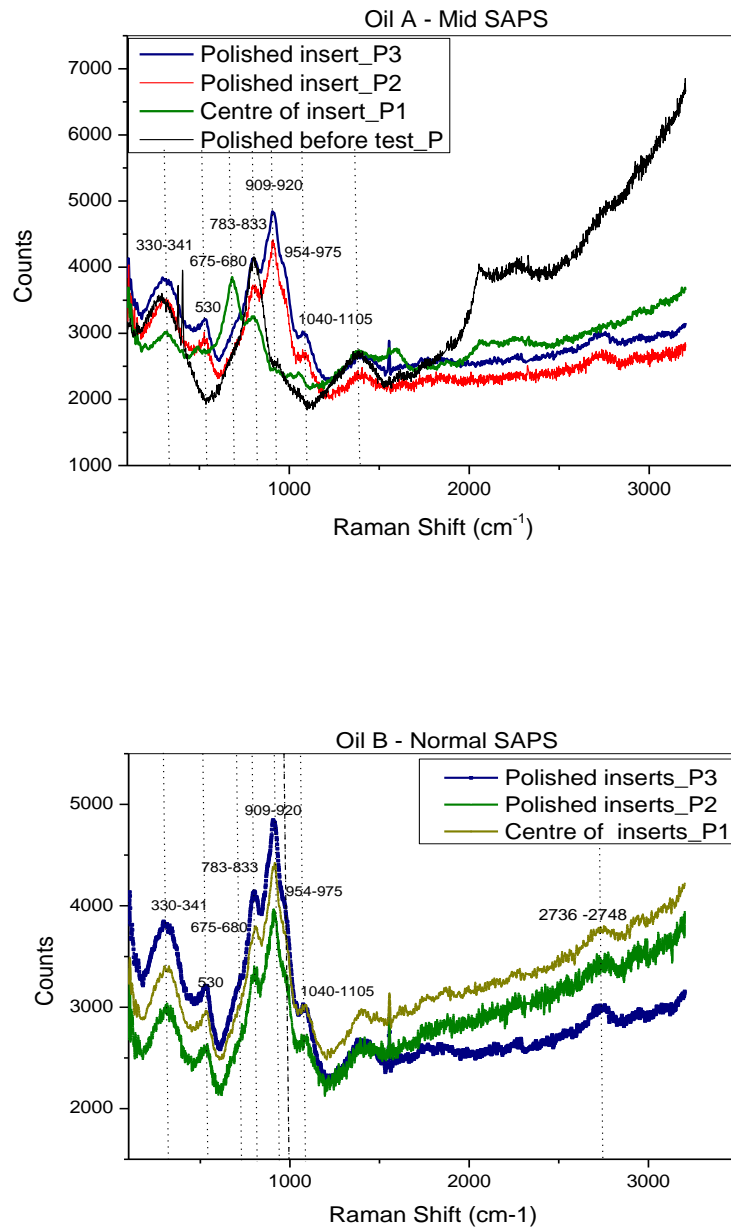


**Figure 7-6 Raman spectra of films formed on polished inserts at P1, P2, and P3 at 105 °C by (a) Oil A – Mid SAPS and (b) Oil B – Normal SAPS**

### 7.5.3. FIB-SEM Results

Oil A produced a very thin film (ca.2-5 nm) at the centre of the inserts while ca. 54-68 nm thick tribofilm was formed at P2. This huge discrepancy can be attributed to the removal action due to high pressure rubbing action (from the ramp, flank, shoulder and nose) of the camlobe at the centre of the insert. The presence of subsurface cracks at the centre of the insert was also observed which indicates that the deformation process extends beyond the thin nanoscopic films into the base of the material and suggests that the tribofilm has low tenacity. This also indicates that the film thicknesses influences the wear as this has been reported by Zhang et al [2]. At other points, no cracks were seen since the films formed reduced and modified the wear processes. At P2, intermittent rubbing occurs due to edge loading and rotation of the tappet in the tappet bore.

Oil B forms significant tribofilms at both the centre of the inserts (P1) and at P2 (See Figure 15). The thickness of the tribofilm formed by oil B is considerably higher than those observed with oil A. At the centre, oil B formed tribofilms about ca. 80-86 nm thick which was about 16-40 times thicker than oil A. This clearly supports the initial Raman investigation of the presence of the tribofilm at the centre of the inserts. At P2 however, oil B formed films ca. 100nm thick while oil A produced tribofilms ca. 68 nm thick. Going through the wear depth on the inserts and SEM micrographs, the development of stable, uniform and well dispersed tribofilms is an essential requirement for low wear rates. Difference in thickness of these tribofilms at P1 and P2 supports a removal and formation process. This may be due to load/pressure variations, flash temperatures and reactivity/or interaction with the oil on the substrate.

While film thickness appears to be one of the causes of the differences in wear of both oils, tribofilm dispersion on the surface also plays a vital role in the prevention of wear on interacting surfaces. This is because the asperities are covered by an antiwear film that offers significant protection. Figure 7-8 shows the distribution of the tribofilm on the surface of the inserts at 105 °C. Oil B produces a well dispersed tribofilm that covers the entire rubbing surfaces on the inserts. In oil A, the tribofilm appears to be widely dispersed on the surface. This difference in film coverage can

be attributed to the type of detergents/dispersants used in the formulation of the oil. It has been widely reported that Sulphonates and Phenates type detergent modifies the surfaces during rubbing and in solution, thereby inhibiting or blocking the sites for ZDDP antiwear film formation [139, 141, 142, 148].

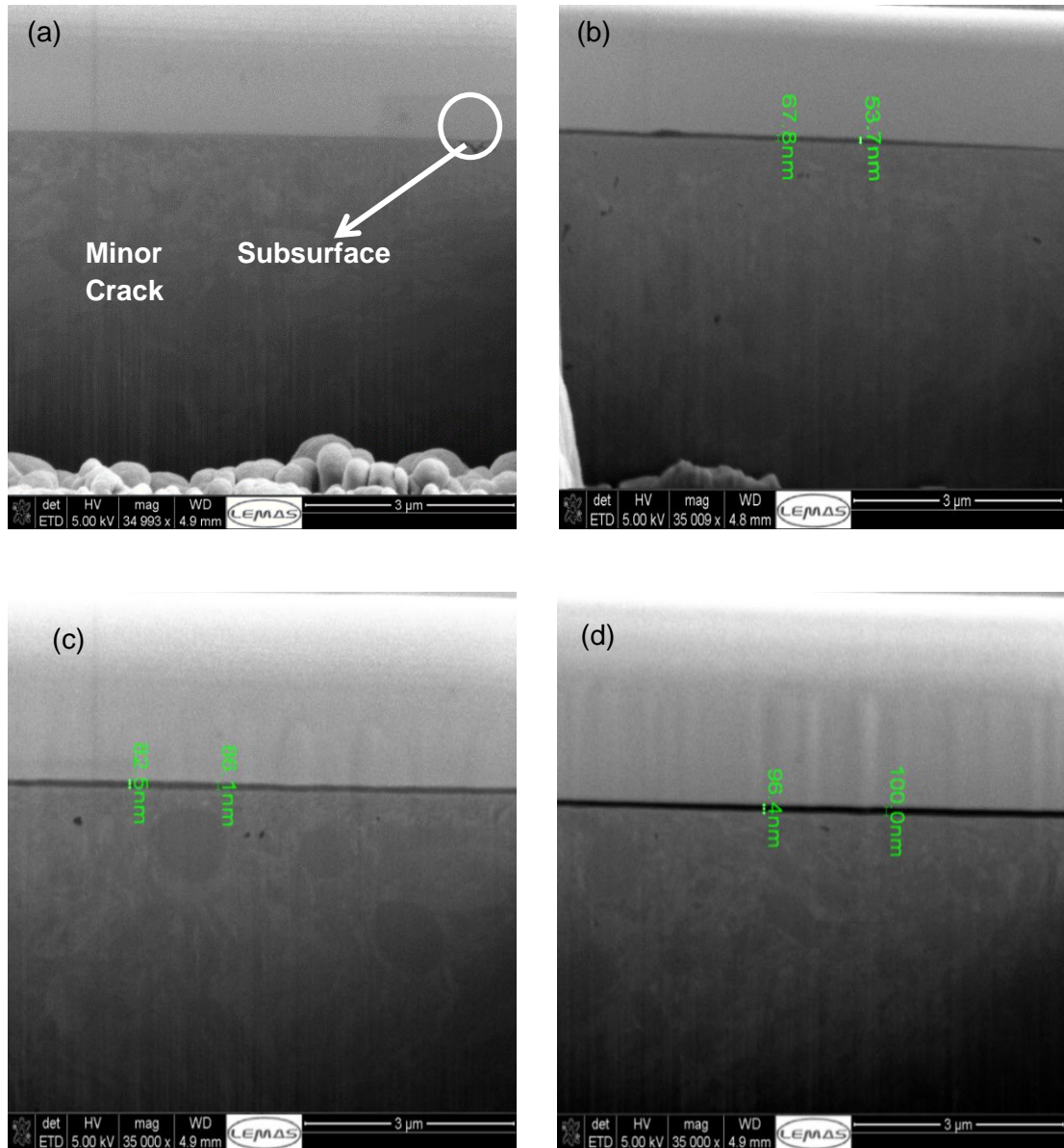


**Figure 7-7 FIB-SEM showing tribofilm thickness with (a) Oil FFA at P1- top left (b) On track P2 – top right (c) Oil B at P1 –bottom left (d) Oil B at P2 – Bottom right**



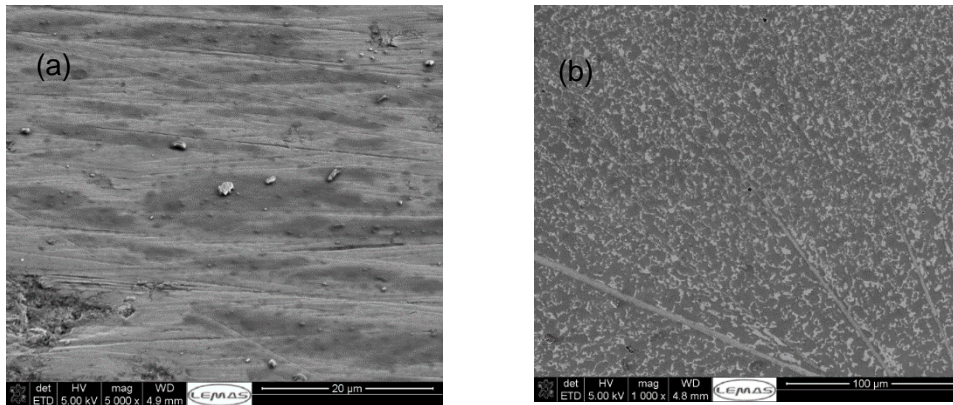


**Figure 7-8 FIB –SEM Image showing dispersion of tribofilm with (a) oil FFA and (b) oil FFB at 105 °C**

#### 7.5.4. TEM Results

The characterisation on the surfaces of the inserts with both oils has revealed so many unique properties on the tribofilm. At the centre of the insert with FFB, the films are composed of a dense matrix with nano-crystallites of  $\text{Fe}^{2+}$ ,  $\text{Zn}^{2+}$  and  $\text{Ca}^{2+}$  in a phosphate glassy network as illustrated in Figure 7-9. On analysis with high beam current, the sizes or spatial distances of these crystals was observed to increase. These tribofilm properties are significantly different from those obtained at 6mm from the cam centre (i.e. location P2/P3). In this region, the tribofilm has a two layered structure. This is better illustrated in Figure 7-10. By visual examination, nano-crystallites are observed at the centre of the insert which can be attributed to the severe rubbing action taking place.

Essentially, the two layered structure consist of a white looking oil rich layer with small fractions of Fe. This is also supported by its XPS spectra (Not shown here). The dark grey area is the tribofilm which is made of  $\text{Ca}^{2+}$ ,  $\text{Zn}^{2+}$ , P, and Sulphur. Gallium is the source of the device while copper is the grid which enable the samples to be held in place. The platinum layer is coming from the deposition prior to cutting in the FIB-SEM.

This varying structure of the tribofilm on the surface has a significant effect on the wear as well. In CHAPTER 6, the wear profile shown clearly suggests that the oil rich section of the surface is soft and can be easily worn away while the nano-crystallites can improve the wear, as long as the particles are not very hard, thereby causing third body abrasive wear by themselves.

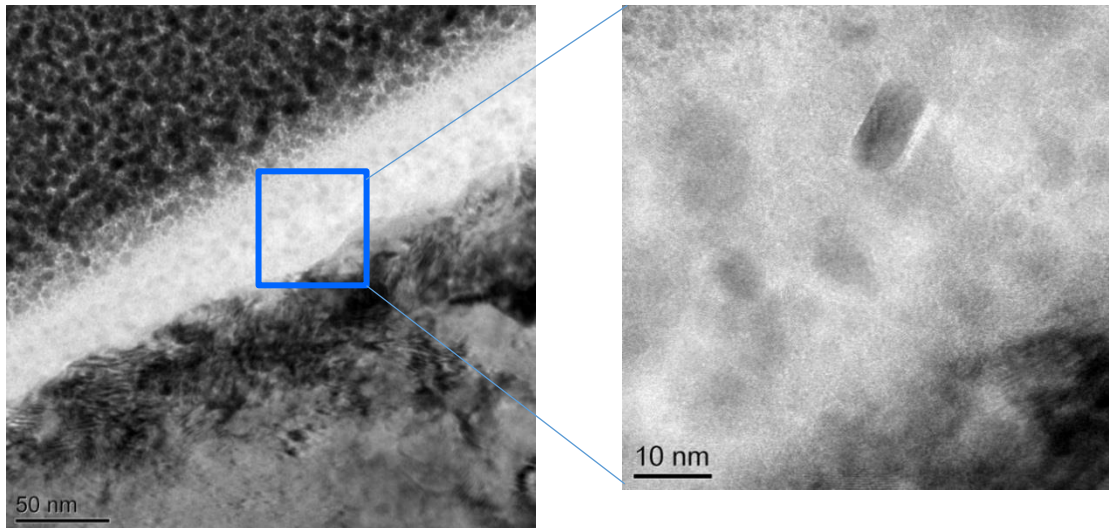


**Figure 7-9** TEM Image showing tribofilm at centre with nano crystallites formed on interaction with Oil FFB at 105 °C

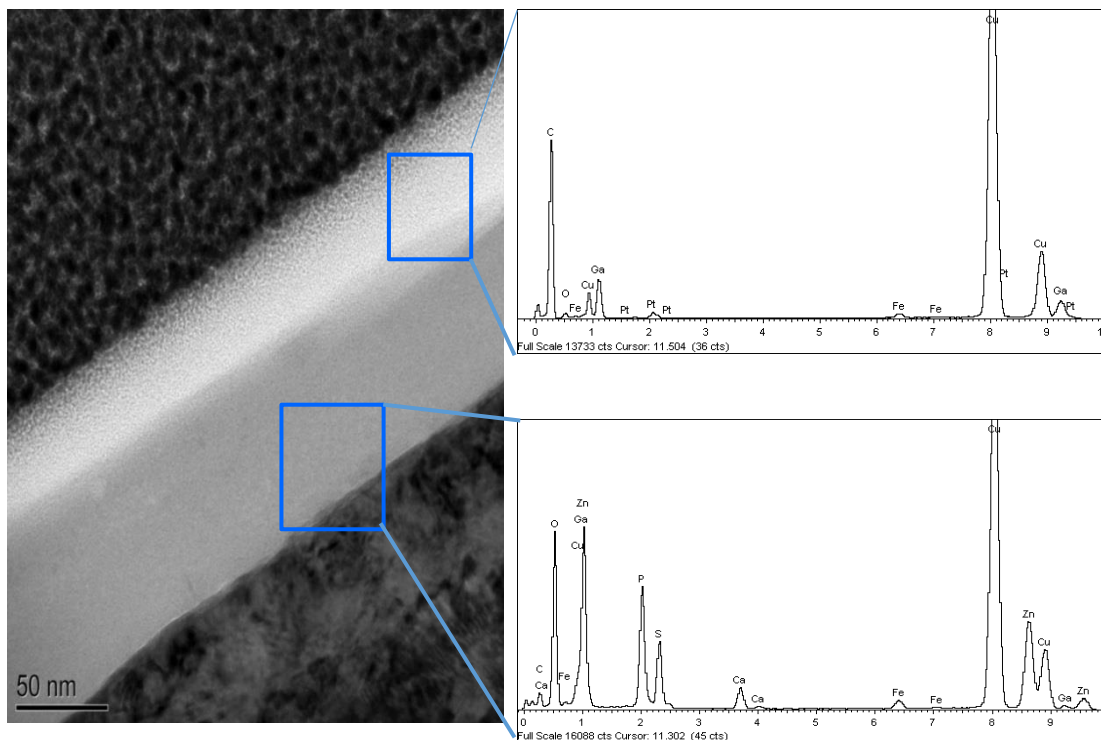


**Figure 7-10** TEM Image showing two layered structure of tribofilm at 105°C – P2 (6 mm from insert centre) with FFB

Although the tribofilm derived by oil A was not efficiently dispersed on the surfaces, in regions where they appeared, some similar characteristics were observed. Similarities lie at location P2/P3 where the tribofilm still exhibits its two layered

structure. At the centre of the insert, the tribofilm contained bigger metallic crystals than those of oil B. Diffraction patterns of this crystals show them to be composed of mainly  $\text{Al}^{3+}$  and  $\text{Fe}^{3+}$  oxides. The  $\text{Al}^{3+}$  originates from the modified cylinder head and the  $\text{Fe}^{3+}$  or  $\text{Fe}_2\text{O}_3$  (haematite) are from the wear of the insert surface. While haematite are significantly harder than  $\text{ZnO}$ , it is important to note that  $\text{Al}_2\text{O}_3$  is about 1.5 times harder than haematite (in terms of Mohs circle). Abrasive wear processes generate a lot of wear particles as the hard (third) body  $\text{Al}_2\text{O}_3$  and  $\text{Fe}_2\text{O}_3$  entrained in the interfaces ploughs the softer surfaces of the inserts. Thus, these combinations of hard particles are responsible for severe damage by abrasive wear of the film which exposes the surface. This is revealed by the pattern of scratches seen on the surface of the insert in section 7.5.1.

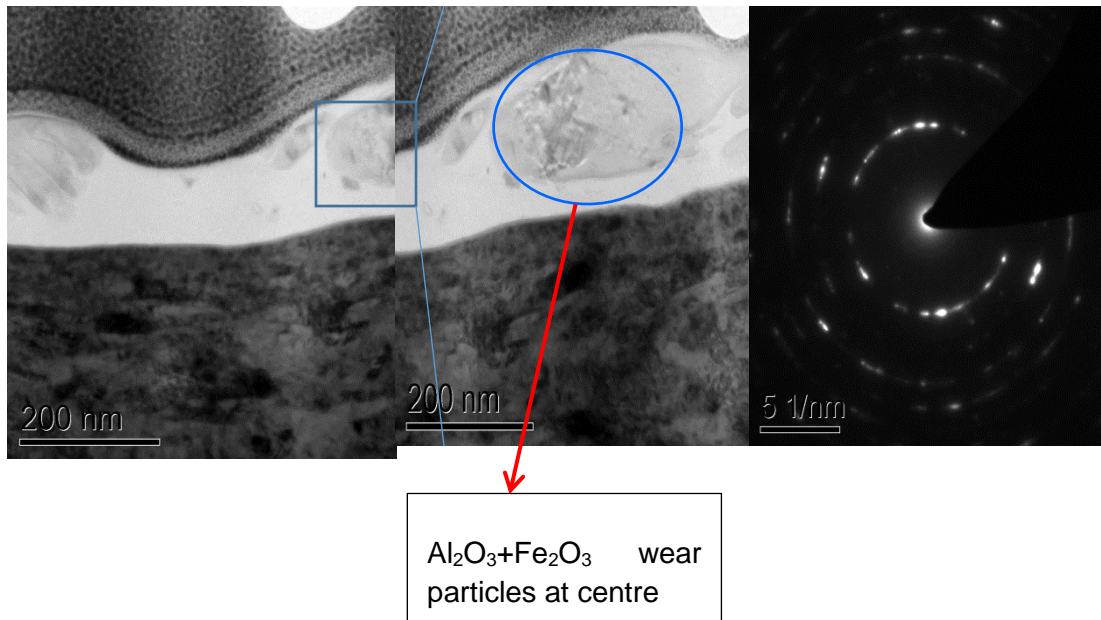


**Figure 7-11 TEM Image showing the Diffraction pattern and large size of metallic wear particle in the tribofilm**

### 7.5.5. XPS Results

The O1s peaks were deconvoluted into three peaks consisting of the bridging oxygen (BO), non-bridging oxygen (NBO) and metallic oxides (MO) with corresponding binding energies of  $532.4 \pm 0.2 \text{ eV}$ ,  $531.2 \pm 0.3 \text{ eV}$  and  $529.5 \pm 0.2 \text{ eV}$  respectively. This is shown in Figure 7-12. These binding energies are in close agreement with a vast majority of the literature [86, 145, 166, 195, 202]. In addition, the area ratio of the BO/NBO is widely used for the determination of phosphate chain length even though the difference between the linewidth of the peaks and the chemical shift may not be entirely distinguishable. In a recent paper by Crobu [202], the difference between the

Zn3s and P2p binding energies was used as a complementary means for the determination of polyphosphate chain length in complex tribological systems. This is because they possess the unique advantage of not been altered by severe chemical shifts. A greater BO/NBO is indicative of long chain polyphosphate which can be used to determine the polymeric number  $n$  by Equation 2. Larger binding energy differences between Zn3s and P2p also support long chain phosphate glasses.

$$\frac{BO}{NBO} = \frac{(n - 1)}{2(n + 1)} \quad \text{Equation 2}$$

Both parameters (BO/NBO and  $\Delta\text{Zn3s-P2p}$ ) will be used to investigate the phosphate films formed on an insert at locations P1 and P2. This was then correlated to the wear on the inserts.

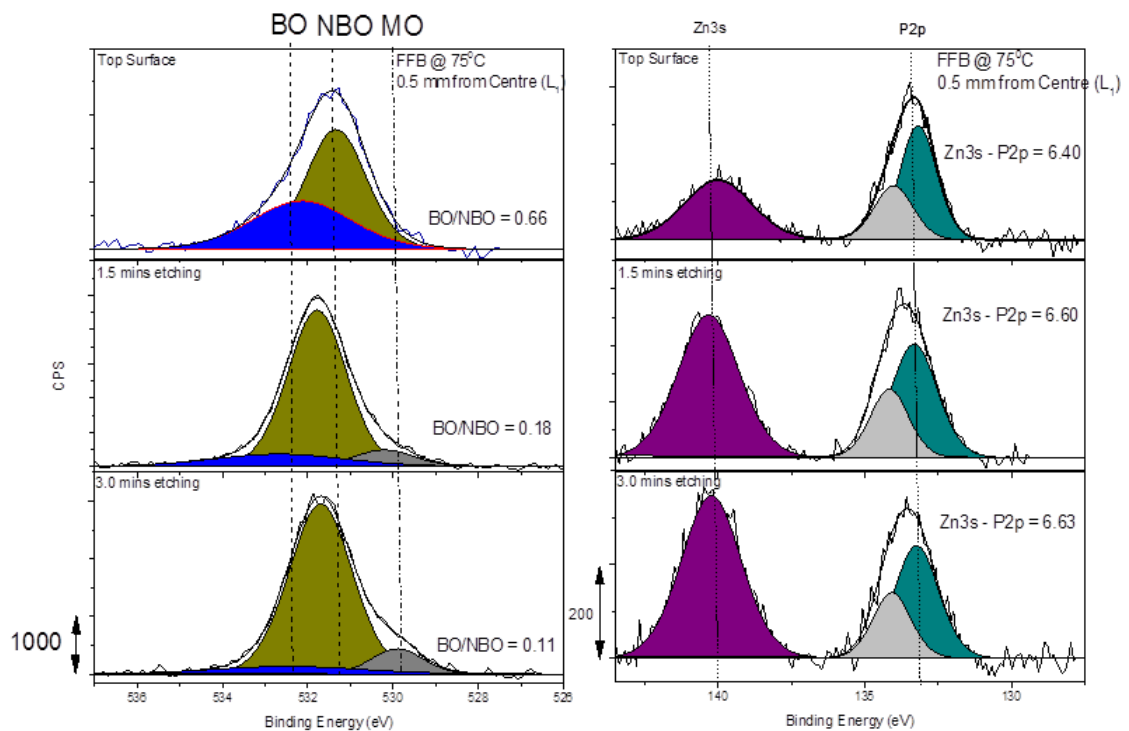


**Figure 7-12** XPS High resolution rescan on P2p, Zn3s and O1s with etching time showing the ratio of BO/NBO and binding energy difference of  $\Delta\text{Zn3s-P2p}$

Analysis of P2p and O1s high resolution spectra from both oils FFA and FFB showed some significant distinction in their characteristics. Chain length determination of the antiwear film formed by oil FFB reveals that they are made up of long chain polyphosphates which is gradually degraded to pyro & orthophosphates close to the bulk. Table 7-2 also shows that the chain has a direct correlation with the wear observed on the surface of the inserts. Region with no phosphate films and short chains generally produced less wear (except at 75 °C with polished inserts). Oil FFA produced tribofilms at small sites, essentially, they consists of ortho/pyrophosphates. Liu and Kouame [145] have shown in a valve train rig, that the longer the chain length of the phosphate film, the better the wear prevention capabilities. Several surface analytical tests also shed more light on the key mechanisms responsible for the wear characteristics observed.

Oil FFA essential forms minute fragments of pyrophosphates, Fe<sub>2</sub>O<sub>3</sub>, carbonates, Iron sulphides and sulphates while oil FFB forms well disperse calcium polyphosphates, ZnO, FeS<sub>2</sub>, no sulphates and Fe<sub>2</sub>O<sub>3</sub>. Details of the chemical components of the film are shown in **Table 6-4**.

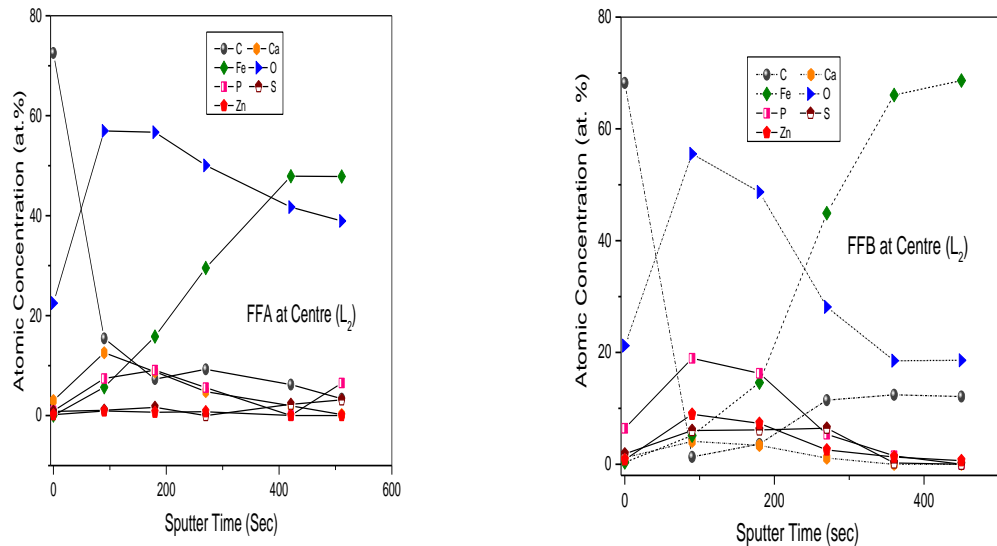


**Figure 7-13 XPS depth profiling at same location with Oil FFA and FFB at 105 °C**

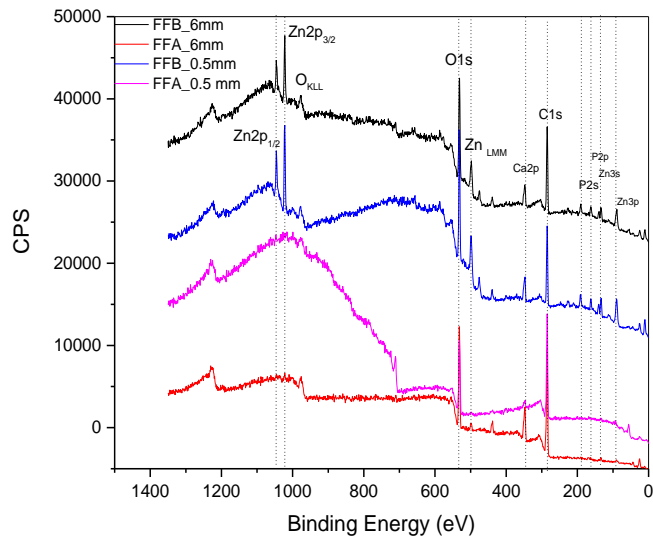


**Figure 7-14 XPS survey spectra showing key elements in the tribofilm with both oils FFA & FFB at 105 °C**

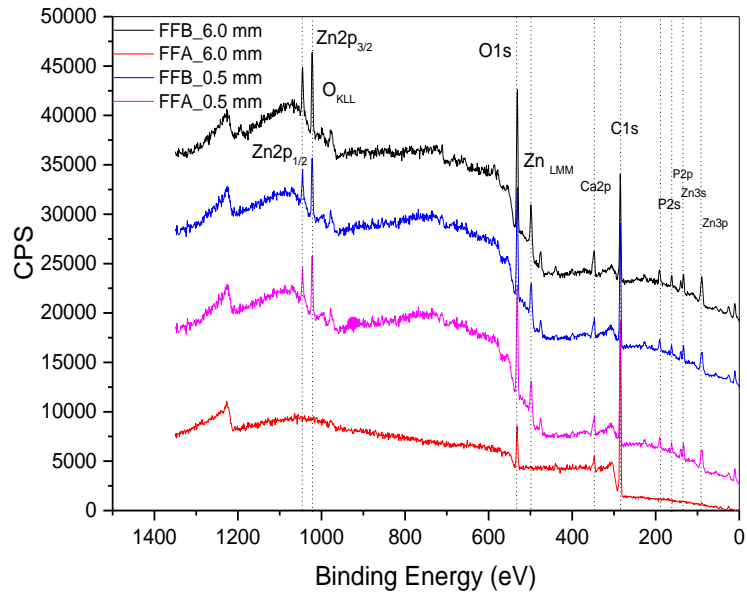


**Figure 7-15 XPS Survey spectra showing key elements in the tribofilm with both oils FFA & FFB at 75 °C**

A closer look at the XPS depth profiling (Figure 7-13) and survey spectra (Figure 7-14 & Figure 7-15) reveals that the film derived from oil A do not possess significant concentration of Zn, S and P. They also do not form significant tribofilms for most



regions investigated. This supports our earlier investigation with SEM/EDX and Raman analysis where no significant tribofilms was observed at the centre (0.5 mm) on the inserts at 105 °C. Depth profiling of the film shows that the concentration of these elements are significantly lower as we approach the substrate. It does suggest that this oil does not promote the formation of antiwear phosphate films on steel surface. For both locations investigated, the film formed is essentially made of carbonates, Fe<sub>2</sub>O<sub>3</sub> and carbon, which will cause an increased wear due to absence of antiwear phosphate films as well as third body abrasive wear from the haematite particles.

These results are equally in agreement with FIB-SEM images of both oils at 105 °C. FFB showed a very well dispersed and distinct tribofilm while the films obtained from FFA were sparsely distributed and loosely bounded to the surface. These suggest a film inhibiting mechanism by one or more of the additives in the oil particularly the detergents. Sulphonate and phenate type detergents are very surface active and will arrive on the metal surface before the ZDDP additives, thereby modifying the surfaces and blocking the sites which are necessary for the breakdown and eventually formation of ZDDP antiwear films. Another mechanism involves the formation of complexes in solution which ultimately reduces the performance of the ZDDP on rubbed surfaces [139, 141, 142].

#### **7.5.5.1. Effects of ZDDP Type and Concentration on Wear**

It is widely accepted in the tribology community that there is a dependency of ZDDP type and concentration on the antiwear effectiveness [93, 203, 204]. While oil A contains a secondary ZDDP with superior antiwear capacity and thermal stability, its antiwear properties in the single cam rig tests showed significant wear. Although the concentration (oil A contains 870 ppm Zn to Oil B 1190 ppm Zn) is slightly lower, the corresponding effect on the antiwear performance is immense. At high temperature of 105 °C, XPS survey spectra and FIB-SEM/EDX of Oil A was no observed to form significant or well dispersed tribofilm on the surface.

**Table 7-2 Oil type BO/NBO ratios, BE  $\Delta$ (Zn3s-P2p), intensity ratios P2p/Zn3s and their effects on wear at different points of an insert in a single cam tribometer**

Test Temperature	Oil Type	Position on insert	$\Sigma$ Wear	BO/NBO (eV)	$\Delta$ Zn3s-P2p (eV)	P2p/Zn3s (eV)	Remarks
75	Oil A	Centre	(0.20 $\mu$ m) [1.76 $\mu$ m]	0.29 $\pm$ 0.02	6.89 $\pm$ 0.2	1.5 $\pm$ 0.30	Phosphate film observed
		P2/P3	(0.34 $\mu$ m) [3.64 $\mu$ m]	-	-	-	No significant phosphate film observed.
	Oil B	Centre	(0.22 $\mu$ m) [1.89 $\mu$ m]	0.35 $\pm$ 0.02	6.39 $\pm$ 0.05	2.48 $\pm$ 0.02	Same as below with FeS <sub>2</sub>
		P2/P3	(0.32 $\mu$ m) [0.90 $\mu$ m]	0.30 $\pm$ 0.03	6.36 $\pm$ 0.05	2.48 $\pm$ 0.02	Calcium phosphate observed with Fe <sub>2</sub> O <sub>3</sub>
105	Oil A	Centre	(3.10 $\mu$ m) [15.50 $\mu$ m]	-	-	-	No significant phosphate film observed
		P2/P3	(0.34 $\mu$ m) [2.17 $\mu$ m]	0.25 $\pm$ 0.01	6.91 $\pm$ 0.2	-	Minor traces of pyrophosphates
	Oil B	Centre	(0.75 $\mu$ m) [1.52 $\mu$ m]	0.32 $\pm$ 0.03	6.35 $\pm$ 0.05	2.50 $\pm$ 0.20	Polyphosphates
		P2/P3	(0.69 $\mu$ m) [0.18 $\mu$ m]	0.51 $\pm$ 0.03	6.58 $\pm$ 0.03	2.10 $\pm$ 0.10	Meta - polyphosphates

(\*) – Polished inserts, [\*] Manganese Phosphate coating



**Table 7-3 Binding energies of XPS spectras of S2p, O1s, and P2p spectra at two temperatures (75 °C and 105 °C) and the corresponding species formed on top surface.**

Test Temperature	Oil Type	Location on insert	S2p (eV)	P2p (eV)	O1s (eV)	Ca2p (eV)	C1s (eV)	Remarks on species observed with XPS and Raman spectroscopy.
75	Oil A	Centre	161.9	133.1	531.1 (NBO) 532.5 (BO) 530.2 (MO)	347.27	284.8 (C-C) 286.00 (C=O) 288.40	Pyrophosphate, CaCO <sub>3</sub> , sulphite, ZnO  No significant phosphate film observed. Film composed of CaCO <sub>3</sub> from the detergent
		P2/P3	-	-	531.1 (NBO) 532.5 (BO) 530.2 (MO)	342.3	284.8 (C-C) 286.60 (C=O) 288.50	
75	Oil B	Centre	161.8	133.4	531.1 (NBO) 532.5 (BO) 530.2 (MO)	342.4	284.8 (C-C) 286.60 (C=O) 288.50	Calcium phosphates observed with Carbonates, Fe <sub>2</sub> O <sub>3</sub> and FeS <sub>2</sub>
		P2/P3						
105	Oil A	Centre	-	-	532.2 531.1(NBO) 529.30 (MO)	347.27	284.8 (C-C) 286.60 (C=O) 288.50	No antiwear phosphate films observed, Fe <sub>2</sub> O <sub>3</sub> , Carbonates, ZnO  Carbonates, Minor traces of Ca-pyrophosphates, Iron sulphide, and sulphates
		P2/P3	168.5 162.2	133.30	530.9 (NBO) 532.6 (BO) 530.6 (MO)	347.27	284.8 (C-C) 286.00 (C=O) 288.40	
105	Oil B	Centre	161.9	133.52	531.1 (NBO) 532.3 (BO) 530.3 (MO)	347.30	284.8 (C-C) 286.00 (C=O)	Well dispersed film of FeS <sub>2</sub> , Carbonates, Ca-Polyphosphates, low conc. Fe <sub>2</sub> O <sub>3</sub> were observed on regions analysed.
		P2/P3	161.7	133.1	530.9 (NBO) 532.0 (BO) 529.5 (MO)	347.20	284.8 (C-C) 285.6 (C=O) 288.4	

Tribofilms were derived at lower temperature of 75 °C. This is quite contrasting, bearing in mind secondary ZDDP's are more thermal stable than the primary types. One fundamental reason for this process could be the role of the detergents. Since they are more surface active, they absorb on the surface first, block the sites necessary for polyphosphate film formation and high temperature facilitate the completion of the carbonation process. This results have been supported by TEM/EDX were large carbonation crystals were seen in the tribofilm.

#### **7.5.5.2. Type of Detergent and Its Role on Film Dispersion/Morphology**

The detergent plays a significant role on the effectiveness of the ZDDP tribofilms derived on rubbing surfaces. Oil A contains overbased calcium sulphonated and phenate type detergents which have been reported to have antagonistic effects on the film forming characteristics of ZDDP.

According to Rounds [146], ZDDP peaks were slightly distorted following infrared spectra in two component systems of ZDDP/OBCaSu. This gives some evidence of a slight interaction in the liquid phase. While it is widely accepted that OBCaSu are surface active, they retard the decomposition rate of the ZDDP by raising its decomposition temperature. Following this action, they (detergent) tend to firstly adsorb on the surface and subsequently block or modify the sites necessary for ZDDP to form its padlike films. A prime example was shown using adsorption isotherm plots. Inoue [142] and Plaza [147] demonstrated that Ba/Ca sulphonates effectively reduce the adsorption of ZDDP on metallic powders. The bifilm has been reported to have a paste-like structure forming basal islands that prevent the agglomeration of the antiwear films [146, 148].

Essentially, the films derived from oil A consists of short Ca phosphate films which are sparsely distributed with increased wear than oil B. These have been reported by [148, 149]. When these detergents are used in combination with succinimide dispersant, the decomposition temperature is increased thereby leading to scuffing on valve train systems [141]. These reports are supported by FIB-SEM images were subsurface scuffing were observed on the surface of the insert.

#### **7.5.6. Effects of Tribofilm Thickness, Film Dispersion and Polyphosphate Chain Length on Insert Wear.**

This study has shown that there is a correlation between tribofilm dispersion, film composition/thickness, the polyphosphate chain length and their effect on wear. The

tribofilms generated on the insert with thicker, well dispersed and longer polyphosphate chain generally produced less wear. Table 7-2 shows the film formed at different locations on the insert and their corresponding wear. It clearly reveals that the wear was similar at 75 °C due to the presence of antiwear film. However, these values are more significant as the temperature increases due to the inability of oil A to form significant tribofilms. Liu and Kouame [145] proposed that high temperature has a means of distorting the stability of the antiwear phosphate film in fully formulated oil. Another influencing factor is the promotion of the carbonation process at high temperature. Under this condition, big calcium carbonate crystals would be formed which ideally with alter the antiwear process and may cause third body abrasive wear. Information from the TEM/EDX micrographs gives reveal that third body abrasion phenomenon is responsible for the high wear.

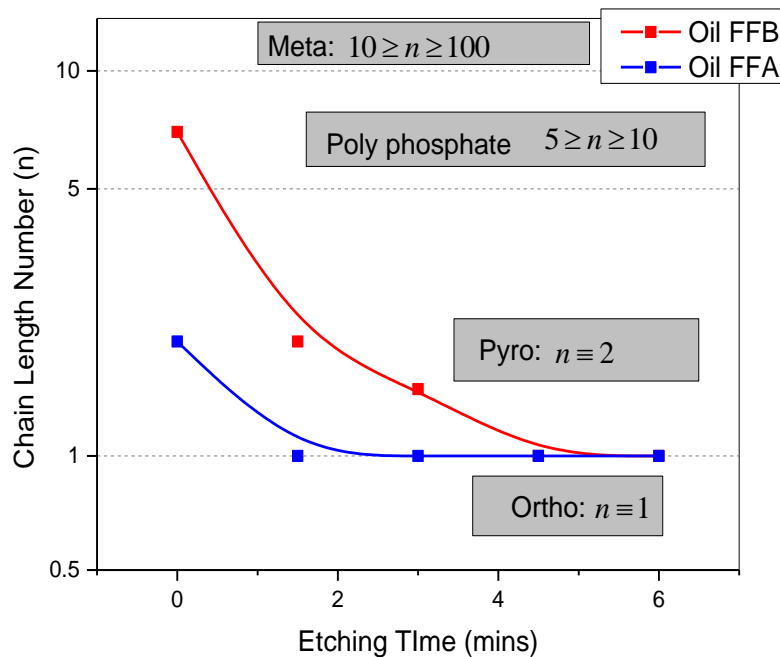


**Figure 7-16 Polyphosphate chain length obtained on Insert with Fully Formulated Oil A & B**

Oil B generally produced lower wear than oil A. The reasons are due to the oil formulation with a carboxylate type detergent with a better interaction with the primary ZDDP additive used in the oil. Under this condition, the surfaces are not modified and the antiwear additives can absorb on the surface and form well dispersed extended basal islands of long chain meta/polyphosphate glasses. These padlike basal islands reduce direct asperity contacts. The film also contains significant amounts of Phosphorus, Zn and S which help improve the tenacity of the film. As shown in Figure

7-7, the topmost layer of the film contains ZnS and Calcium polyphosphate. With oil B, the films are between 60 – 100 nm thick while oil A produces scattered films that are 5 – 60 nm thick with very low concentration of Zn, S and phosphorus.

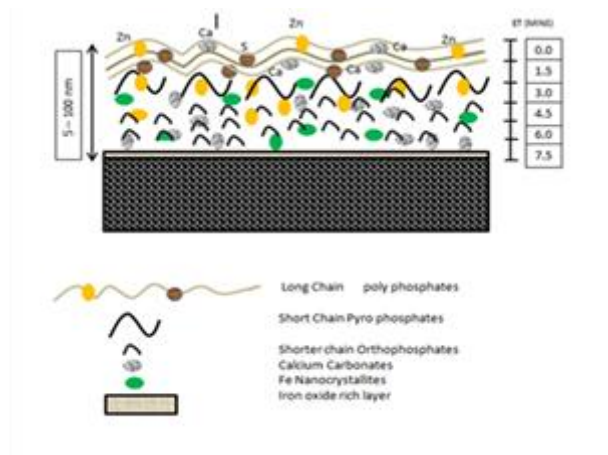


**Figure 7-17 Interatomic layered arrangement for tribofilm**

## 7.6. Conclusions on Rig Development, Validation and Testing Protocol

Tribological tests and post mortem surface analytical tests of Raman, XPS, TEM and FIB-SEM/EDX have been used to investigate the structure, film thickness and composition of the tribofilms formed by oils with the coating architectures of Mn-phosphate, and polished inserts. The use of these techniques helped shed light on the composition of the tribofilms on the surface of inserts and enables correlation with the wear mechanisms to be established. The findings of this work can be summarised as follows;

- Tribochemical investigations of the inserts are in close agreement with previous studies. Temperature and additive concentration appear to affect the distribution of phosphate films on the inserts. More densely packed and well dispersed films were observed at 75°C & 105°C on inserts tested with oil B which has a higher concentration of primary ZDDP additives. This resulted in better wear prevention.
- The composition and structure of the tribofilm has a huge impact on the friction and wear response of the system. The presence of Zn, P and S were shown to have significant impact on the antiwear properties of the tribofilm. They have been shown to affect the durability of the films on the surface.
- The films of oil B consist of long chain polyphosphates of chain length between 5-10 in the uppermost surface which is gradually degraded to pyro and

orthophosphates in the bulk. Oil A primarily consists of short chain calcium pyro and orthophosphates. TEM diffraction patterns reveal some third body abrasive particles of aluminium oxides (from engine block) and haematite trapped in the wear track. Aluminium oxides are harder than haematite and this will surely aggravate the wear processes observed with oil A.

- The tribofilm consist of a two-layered structure in regions on the tappets with limited rubbing action. The first layer consists of an oil rich phase followed by dense tribofilm. In the insert centre where rubbing with the nose, flank, shoulder and ramp of the cam occurs, the tribofilm does not show a two-layered structure. It shows a dense matrix with significant metallic oxides as well.

## **CHAPTER 8. THE ROLE OF DLCs IN CAM FOLLOWER APPLICATIONS – A FRICTION WEAR AND TRIBOCHEMISTRY STUDY**

### **8.1. Introduction to the Application of DLC For Cam Follower Systems**

Various original equipment manufacturers (OEM) employ different designs and configuration of valve train mechanisms. All having distinct merits and demerits which engineers/tribologist must try to get the right compromise. Based on the uniqueness of the design, the valve train may accounts for 10% to 25% of the total energy required to power an internal combustion engine [188]. These energy consumptions are split between the tappet/tappet bore, valve stem/guide, support bearings, push rods, rocker arms and the cam/follower; which accounts for approximately 50 – 80 % of the energy consumed [205].

One mechanism of interest and which is the focus of this study is the direct acting mechanical bucket configuration. This mechanism helps provide good induction and exhaust processes for the engine due to its high rigidity. They are equally suitable for high speed applications and provide good lubrication [17]. Despite its advantage, the tribological challenges are extensive and range from metallurgy, wear, additive package, boundary lubrication, surface layers, surface coatings, design considerations, and even cost.

Surface coatings, particularly DLC are by far the most commonly used approach to reduce friction and wear on cam follower systems, although the use of lighter materials have also received some attention. A prime example was demonstrated by Kanzaki and coworkers [192] where tappets and spring retainers were replaced with lighter aluminium materials and a 40% reduction in friction torque was achieved in the valve train. Ahn et al [191] and Masuda [190] have also developed super carburised and TiN surfaces respectively, these are capable of reducing friction at the cam follower contacts with 1-2% fuel economy.

Despite the advances by lighter materials, DLC coatings have superior friction, wear and running-in properties in cam-follower applications which has been demonstrated in [32, 33, 67, 87, 197]. Reports by Schamel and coworkers [206] have shown that W:C-H performed better than other surface coatings in pin on disk tests and a motored cylinder head rig. Gangopadhyay et al [25] have also shown that

considerable friction benefits can be achieved with DLC coatings in a valve train rig. The values were close to those observed for polished steel at 100 °C and 120 °C. In a similar research by Broda [33], a:C-H was observed to reduce the friction in a cylinder head test which was performed at 90 °C. 50 % reductions were achieved in conditions with oils containing higher Mo concentrations. Another form of DLC containing C and H were also used by Kodai [197] to evaluate cam followers for motor cycle application and these performed better than W-DLC and Cr-DLC.

Si has also been incorporated into several DLC's to reduce friction, the coordination number, induced stress, improve thermal stability [207] and increase its interaction with oxygen (air) or water [177, 208-213]. It was observed that increase in the concentration (between 0 – 10) of Silicon in the DLC leads to a reduction in friction coefficient [213] with the tribofilm composing mainly of SiO<sub>2</sub> due to interaction with the humid environment. Similar findings have been observed by Oguri et al [176]. Another variant of Si doped DLC was able to reduce friction to values as low as 0.04 in relative humidity of 70 % but these coatings also had a significant amount of hydrogen. These friction reduction properties are also not valid for static friction as predominantly high values are reported by [212]

In reducing the stress, Si has been observed to form Si-H, Si-C and Si-O bonding with the coating. This causes a reduction of the three dimensional rigid structure of the coatings [211] which will alter the ratio of sp<sup>2</sup> to sp<sup>3</sup> hybridization of the coating. Consequently, the wear responses for Si doped DLC's are not entirely promising as they are comparatively higher than their fellow counterparts. According to Gilmore [72], a 20 fold increase was observed in Si of 20 at. % DLC when compared with doped Ti and F DLC. Based on the deposition technique, the failure mechanisms consist of low spalling rates at low bias to conformal cracking at high bias voltages [210].

However, by tweaking the interlayer and growing them to the right thicknesses, an improved Si doped DLC coating can be obtained with superior wear and friction properties similar to those of a:C-H [177]. Their interaction with the environment can also be modified. Unfortunately, the deposition technique/rates, precursor, temperature and bias voltage greatly affect the mechanical properties of essentially, "all" DLC coatings which will ultimately affect their interaction with the oil.

Thus, the tribochemical interaction of DLC coatings with lubricant additives in the oil is also widely varied in the tribology community. This is due to the diverse properties

and reactivity of the coatings as well as the different experimental conditions used in tribological tests. Some DLC coating however, particularly ta-C are widely known for their chemical inertness, hardness and stability [32, 158].

Recent studies of Mo additive showed that they do not absorb on a:C-H-Si-O or a:C-H surfaces [214] even though earlier reports suggested that some interactions take place [64]. Haque and coworkers [77] revealed that Mo were absorbed on a:C-H composed of 15 at % H even though the Mo was reported to have aggravated the wear mechanisms of the DLC with significant spalling of the coating. Contrary to this, Podgornik [70] has shown that certain DLC coatings do not interact with extreme pressure and antiwear (ZDDP) additives.

While this chapter systematically evaluates the tribochemical behaviour of Si1s, a:C-H and ta:C-H in a single cam rig, one novel aspect of this study is mapping the tribochemical films across the cam profile in regions where the contact pressure accurately promotes the formation of boundary films. The locations are  $\pm 14^\circ$ ,  $\pm 10^\circ$ ,  $\pm 4^\circ$  and at  $0^\circ$  (cam nose). This gives a good insight on how the additives in the oil are functioning and if they can withstand highly loaded valve train systems. This study then takes it further by evaluating the effect of coating both the cam and the follower. Although, this is used for high performance engines like Formula 1, it will be interesting to observe what level of friction and wear benefits can be achieved with this procedure.

The objective of this chapter is to look at three different surface coatings and to assess their performance in the direct acting mechanical bucket configuration. It is the aim of this study to understand the following;

- wear and friction behaviour of the coatings
- interaction of the coating with the oil additives. i.e. surface layers, tribofilm
- the effect of coating hardness on the cast iron camshaft counter-body
- effects of coating both cam and follower
- mapping the tribochemical films across the camlobes and correlating this to the wear using ASTM 6891-09a standards.



## 8.2. Experimental Methodology for DLC Coatings

### 8.2.1. Test Procedures

The friction reduction properties of three coatings were evaluated in a motored single cam rig shown in Figure 5-22. All coatings had similar centre line average roughness ( $R_a = 0.02 \mu\text{m}$ ) to ensure that the friction/wear and tribochemical responses were due to the coating properties and not the roughness. Rough surfaces have been reported to increase friction [174] and wear [175] of DLC coatings. The cast iron camlobes were first cleaned by a sand blasting thermomechanical process before polishing in a Sulzer Sorevi automechanical camshaft polisher to an  $R_a$  of  $0.02 \mu\text{m}$ . These very smooth surfaces are useful for high performance engines such as Formula 1. The test was performed for 50 hrs with 4 cycles, each cycle lasts for 12.5 hrs typical ranging from 300 rpm to 2100 rpm, from a predominantly boundary to elastohydrodynamic regime. Data capture was recorded every 20 mins and data obtained during speed were usually ignored due to vibration and to give the system time to stabilize [173]. The test conditions are shown in Table 8-1 with a test cycle/ramping sequence as shown in Figure 8-1. New camlobes and tappets were used for each 50 hrs test.

**Table 8-1 Test Parameter for Tribological Test with DLC Coatings**

Test Parameters	Conditions
Test Duration	50hrs
Lubricant	FFB
Coating	Si1s, taC-H, a:C-H and Steel
Lubrication regime	Boundary/Mixed/EHL
Oil temperature	105 <sup>0</sup> C
Speed	300 – 2100 rpm

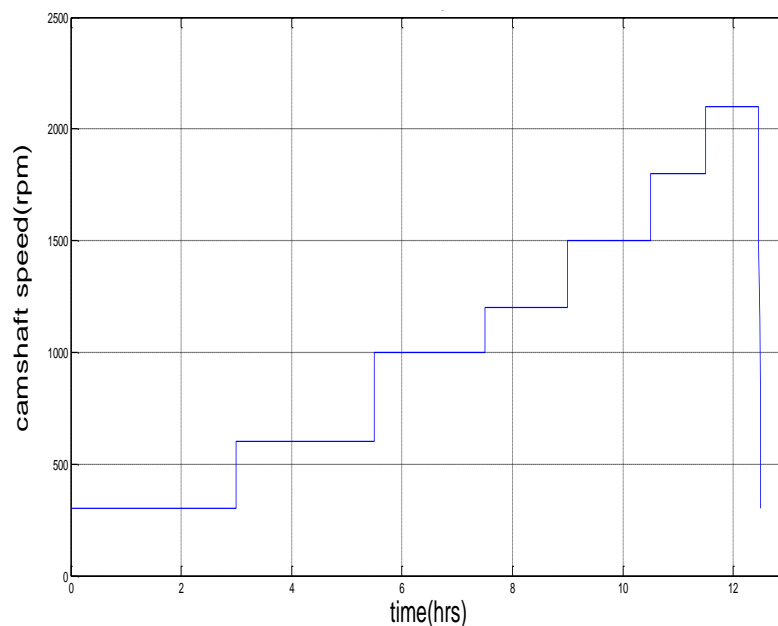


**Figure 8-1 Single Cam Rig Test Cycle and Ramping Procedure**

An identical procedure was used when both the cam and the inserts were coated. This is to give room for comparison on friction performance, wear and tribofilm. Each experiment was carried out three times. In all cases, good repeatability was observed and the average friction torque values was used in the final results.

The flowrate used in this investigation are similar to those developed in the works of Ofune et al. [198] with a 15 mins rig heat, to reach the test temperature before being maintained at  $105 \pm 0.10$  °C. This was monitored by two sets of thermocouples, one connect to the cylinder block and the other to oil vent just above the cam follower contact.

### 8.2.2. Breaking-in

In our in-house tests, the smooth surfaces on the camlobes and inserts significantly reduce the running-in period for the newly polished camlobe and inserts. This can be achieved by running the rig for a longer duration at low speed of predominantly boundary/mixed lubrication regimes. Bearing this in mind, the friction torque for the first cycle was adequately compared with those of the final cycle to evaluate any deviation which may have arose due to the chemo-mechanical running-in process. No significant deviations of friction torque were seen between the first cycle and the

fourth cycle while the temperature was maintained at  $105\pm 0.10$  °C throughout the test.

### **8.2.3. Wear Methodology**

A profilometry trace was taken before and after the tribological test to determine the wear depth or scar that occurred due to sliding rolling motion of the single cam rig contact. Figure 8-2a shows the profilometry trace for the camlobe before the test. This clearly falls well within the expected value of 20 nm for the polished camlobes which were used for the test.

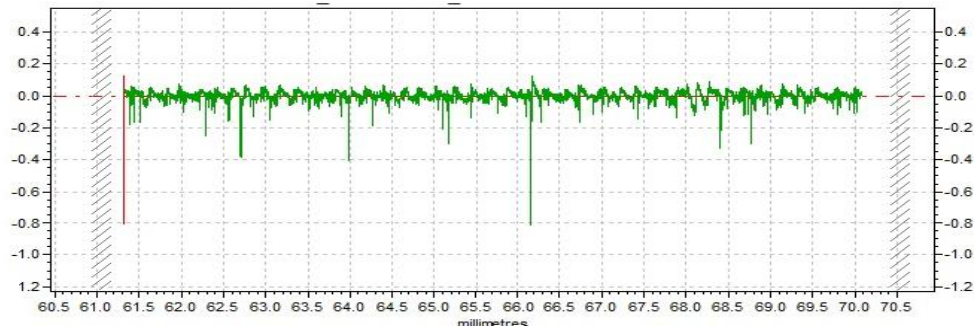
This was done at seven locations as shown in Figure 8-2b and in accordance with ASTM 6981-09a standards. These positions were suitable as the contact pressures ensures the formation of boundary lubricated films which can be derived from the lubricant additives in the oil. In addition, based on the configuration of the rig and the clearance between the cam base circle and the follower, there was no need to investigate the films formed on this region. Firstly because there was no contact and any films formed would have been chemisorbed or be a thermal film without any form of rubbing. That is beyond the scope of this research endeavour.

The cam nose ( $0^\circ$ ) was used as the reference and other locations were indexed with respect to this location. In all locations, a line trace of  $11\pm 0.5$  mm (which corresponds to the cam-width) was used. This will give a better insight about the wear morphology across the cam surface. The contact pressures (Table 8-2), lubricant entrainment velocity (Figure 8-2d) and load per unit length (Figure 8-2d) at these regions were also calculated using the Dowson and Higginson equation for line contacts, to correlate these values to the wear mechanisms.

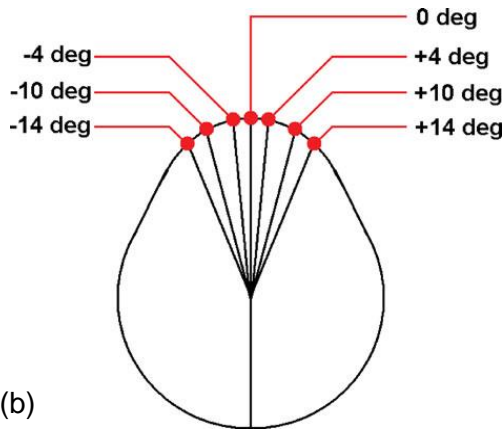
For instance, the negative entrainment speed at the rising edge of the cam nose indicates that lubricants are being forced out of the contact and gradually flow back to the contact during valve closing. These numerical velocity values coupled with the load/contact pressures will further enable the wear mechanism taking place across the camlobes to be elucidated.

These positions were measured with an angular digital dial and protractor which was affixed on the camlobes with an accuracy of  $\pm 0.5^\circ$ . This enabled the wear scar along a unique line which was traced with our dial/protractor configuration to be mapped. At all locations, three distinct traces were taken and the average was used as the wear scar for the camlobe. This straight line trace also enables a clearer evaluation of the

camlobe wear and prevents any ambiguity which may have been experienced when tracing along edges.



(a)



(b)

Table 8-2 Contact Pressure across camlobe

Angle	Pressure
0°	0.76GPa
±4°	0.70GPa
±10°	0.62GPa
±14°	0.59GPa

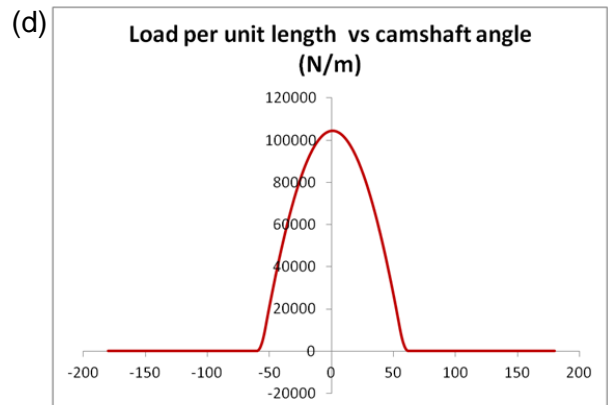
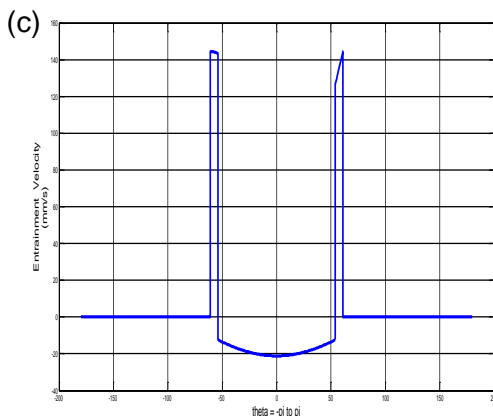


Figure 8-2 (a) Cam Nose profile before tribological test (b) Location for wear analysis (c) Lubricant entrainment velocity (d) Load per unit length (Adapted from [145])

### 8.3. Materials

Each of the coatings were deposited on a 16MnCr5 material with a  $25\pm 0.02$  mm diameter and  $2.60\pm 0.03$  mm thickness. Thereafter, the phosphate coatings were removed by a chemo-mechanical cleaning process before polishing to an  $R_a$  value of 20 nm. The samples were then sand blasted and further surface cleaning was carried out before the deposition of the coatings. Coating thickness and other details are shown in **Table 8-3**. The taC-H has a hydrogen content between 5 – 10 %. Tests were also conducted with polished steel surface with similar roughnesses as a reference.

**Table 8-3 Properties of Lubricants/ DLC coatings**

Oil Code	Viscosity Grade	Content (wt %)				FM	Antiwear Type
		P	Zn	Mo	S		
<b>Oil B</b>	SAE5W-30	0.124	0.140	0	0.5	No	ZDDP 1
Coatings		Hardness (GPa)		Thickness ( $\mu\text{m}$ )		Surface Energy (mN/m)	
	Si1s	18-22		2.0 – 2.5		25 - 30	
	taC-H	27 - 35		1.2-1.5		35 – 40	
	a:C-H	20 – 30		1.5 – 2.0		25 – 32	
Cast Iron Camlobe	Microstructure	Hardness substrate		Reduced Elastic Modulus		Ra ( $\mu\text{m}$ )	
	C 3.0%, Si 2.0%, Mn 0.4%, Cr 0.1%, Cu 0.3% , 0.005 max, 0.003 max	4.0-4.5Pa		155 GPa		0.02 – 0.03	

Figure 8-3 shows the micrograph of the coatings which were tested. Si1s shows a slightly rougher surface with dimples. ta:C-H reveals some trace of ridges but the surface appears smoother than the a:C-H and Si1s.

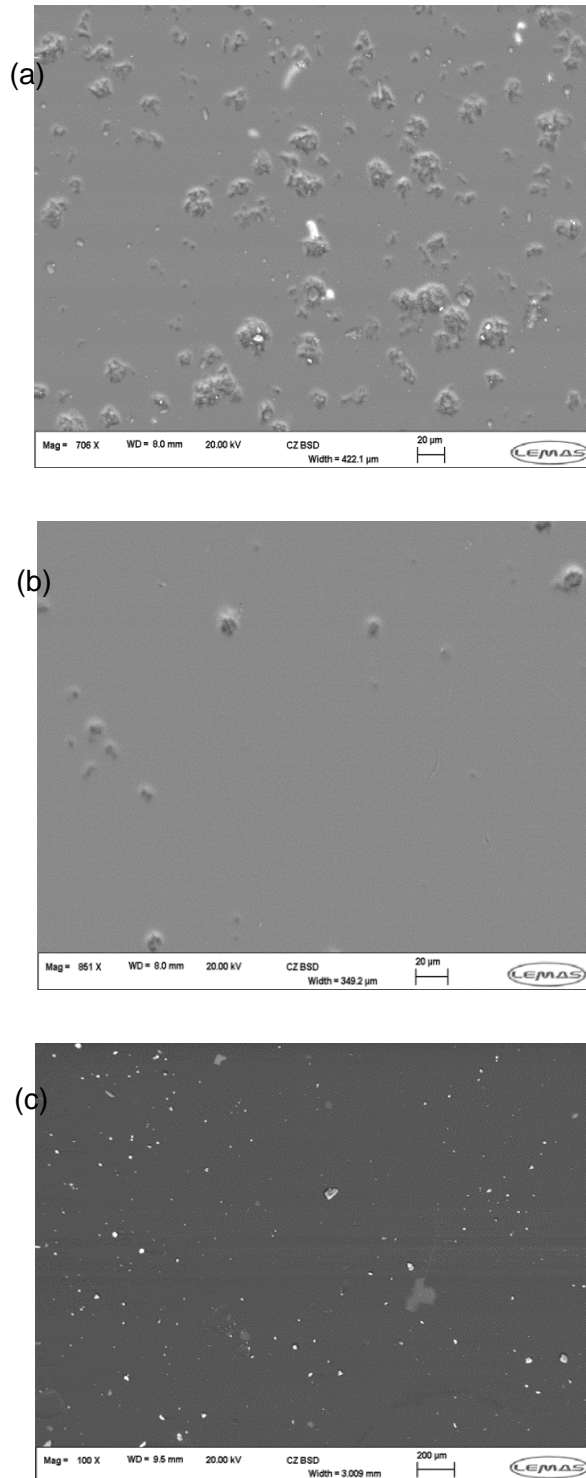


**Figure 8-3 SEM Micrograph of (a) Si1s (b) ta:C-H (c) a:C-H as deposited**

## 8.4. Surface Analysis

### 8.4.1. XPS Analysis

XPS measurements were performed using a PHI 5000 Versa Probe™ spectrometer equipped with a monochromatic Al K $\alpha$  source (1486.6 eV). Tiny areas of X-ray Photoelectron spectra were collected with a beam size of 100  $\mu$ m and a power of 25 W in the fixed analysed transmission mode selecting a pass energy of 46.95 eV and an energy step size of 0.1 eV for the acquisition of the detailed spectra. Survey spectra were collected with a pass energy of 117.0 eV and an energy step size of 1 eV. The residual pressure was always lower than 10<sup>-7</sup> Pa.

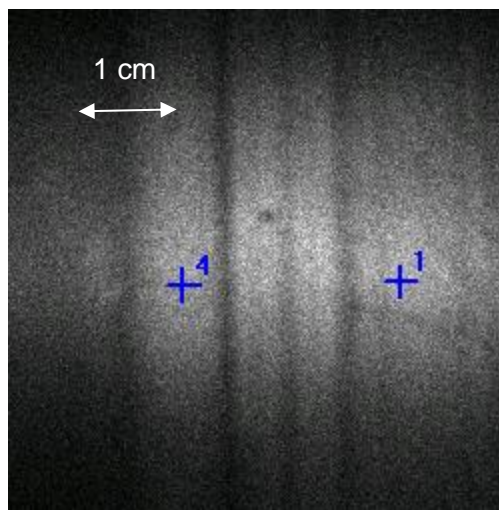


**Figure 8-4 Scanning X-ray Images on Camlobes**

Regions on the camlobes have been indexed and the identification of the tracks were performed using scanning X-ray images (as shown in Figure 8-4), allowing the identification of the different analysis locations inside and outside the tribological tracks. XPS data were processed with CASAXPS software. The photoelectron spectra were fitted with Gaussian–Lorentzian curves after Shirley background subtraction. Slight shifting was observed and calibrated by referring the aliphatic C-C carbon bonding to 284.8 eV [215].

## 8.5. Results

### 8.5.1. Friction Results

Figure 8-5 shows the repeatability of the results obtained with taC-H DLC coated shims tested at oil temperature of 105 °C for 50 hrs. Due to the good quality assurance/unique batch processing procedure used in the production of the coatings,

there was little variability in roughness and structure. This helped in reducing the variability between each tests.

The friction responses from all the coated inserts against a non-coated cast iron camshaft are shown in Figure 8-6. These data points were the average from three tests that were performed on new coated cam and inserts. On the average, a:C-H was observed to reduce the friction torque by about 25 – 40 % (from 0.51Nm – 0.32 at 300 rpm) for all the speed range tested. Higher friction benefits were experience in the boundary lubrication regime which decreased progressively as the regime changed from mixed to EHL regimes. This lower friction torque values can be attributed to the properties of the coating and the boundary lubricated films derived from the lubricant additives. In the mixed regime, both the boundary films and lubricant properties play a significant role in the friction reduction. This is because some portion of the contacts are separate by the lubricant. In the EHL regime, the properties of the lubricant particularly viscosity becomes very important in separating the interacting surfaces which theoretically should ensure that the friction torque responses are very similar. They are comparatively closer in this regime than any other regime in the graph.

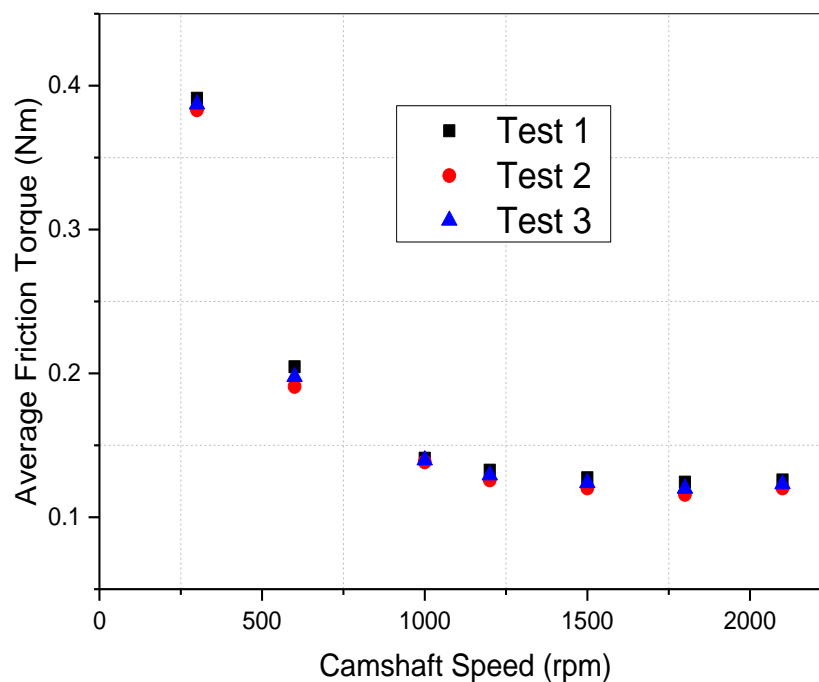


**Figure 8-5 Average Friction Torque Showing Repeatability of Data From the Single Cam Rig After 50 hrs Testing with ta:C-H**



Friction response for the taC-H and Si1s coating have similar friction torque responses throughout the speed range tested but their wear properties are entirely different and were discussed in section 8.6.1. 18 – 22 % reduction in friction were experienced with taC-H and Si1s coating. The values obtained for all the coated surfaces are largely lower than those for the steel surface in boundary and mixed regimes indicating that these coating have superior friction performances than an uncoated surface. Mn- phosphate coatings were investigate earlier in this thesis but not under the same ramping procedure or test duration. The surface mechanism of lubrication of  $Mn_3(PO)_4$  can be attributed to its polycrystalline surface and minute pore sizes which trap or retain the lubricant in small/tiny inclusions. In comparison the DLC coated insert with the result for Mn- phosphate coated inserts earlier discussed, it was decided to remove this as the values are close with the polished inserts. The mechanism of lubrication is still unclear but surface analysis show that some aspect of the coating can be transferred to the camlobe surface (see section 8.6.1.1 for XPS). Under this condition, the system would be similar to DLC sliding against DLC which could account for the low friction values seen.

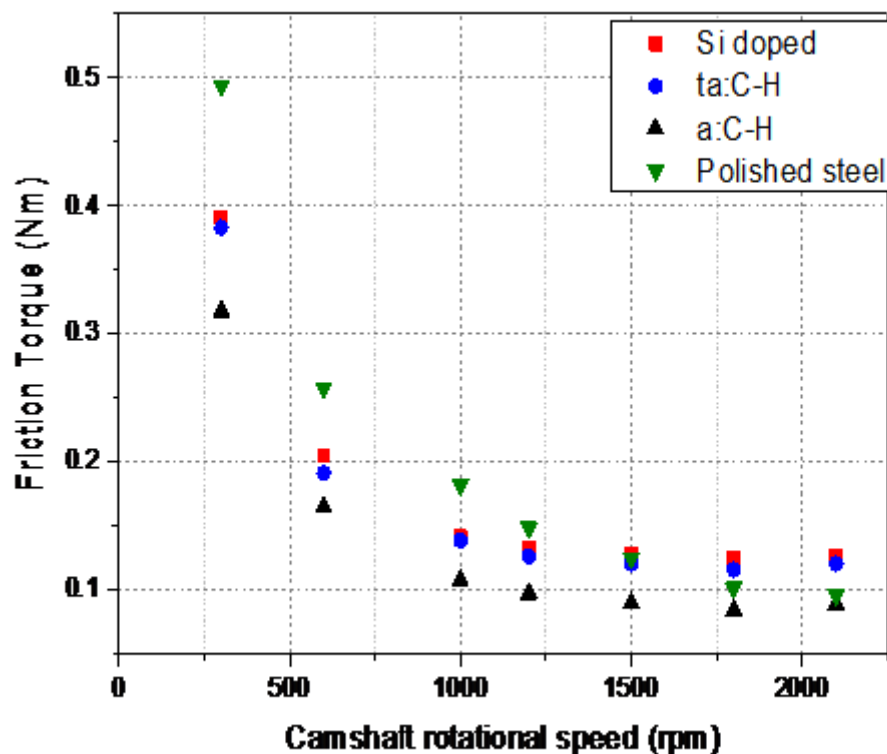


**Figure 8-6 Effect of Surface Coating on the Friction Torque with Fully formulated oil B (FFB) after 50 hrs testing.**

### 8.5.2. Friction Response from Coating both Cam and Tappet/Inserts

In Figure 8-7, the ta:C-H frictional responses from coating both the cam and tappet with those of coating only the tappet are compared. All tests were performed under identical conditions and fresh set of oil was used for each test. The graph shows that huge friction benefits can be obtained from coating both the cam and the follower. An average of 35 – 40 % friction reduction was achieved when both components were coated with ta:C-H and this was obtained for all the speed range tested. The surface roughnesses were the same as those of the uncoated surfaces and thus roughness had no role to play on the friction benefits shown. These can be attributed to the properties of the coating itself.

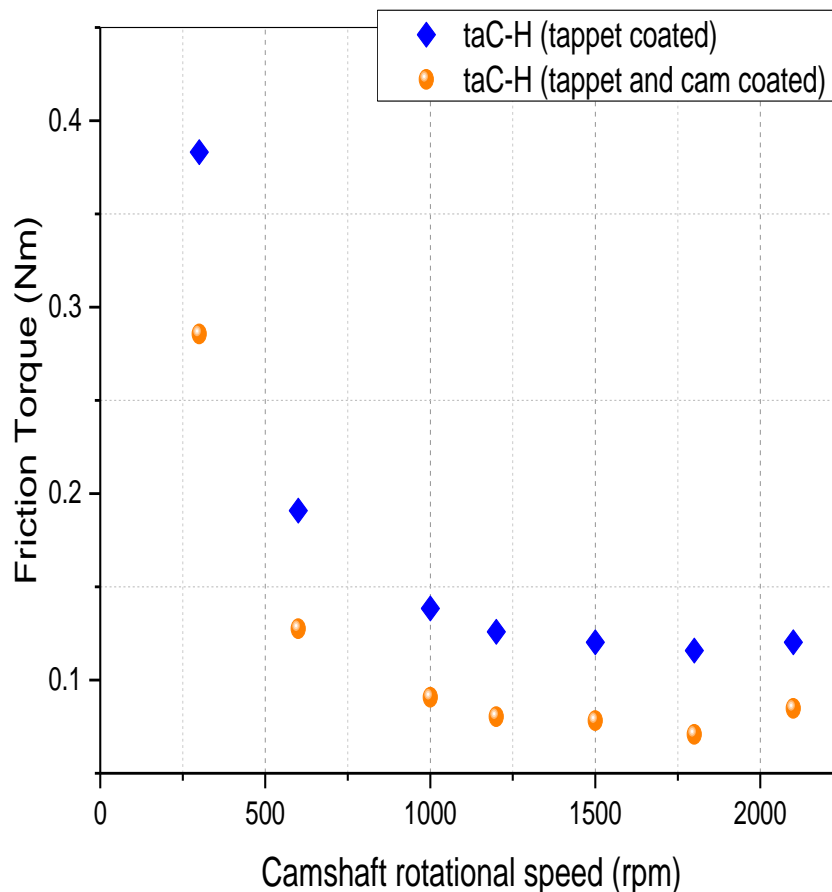


**Figure 8-7 Effect of Coating Both Cam and Follower with taC-H on Single Cam Rig**

According to **Figure 8-8**, no clear friction benefits can be achieved by coating the cam and tappets with the a:C-H coating. Friction benefits were achieved at 300 rpm during the first 3-4 hrs of the test. While this suggests a breaking in period, the responses from there onwards are similar with those of coating only the tappets. A closer look at the ta:C-H/ta:C-H and a:C-H/a:C-H interaction shows that ta:C-H/ta:C-H tribopair of cam and tappet have a better friction performance than the latter but the same cannot be said on their wear properties.

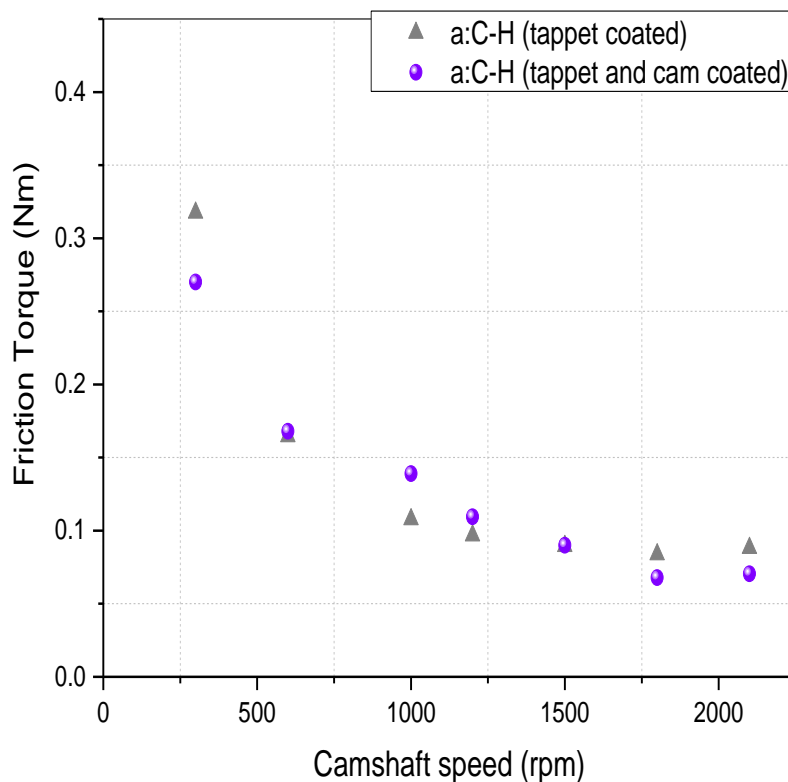


**Figure 8-8 Effects of Coating both the Cam and Tappets with a:C-H on Single Cam Rig.**

### 8.5.3. Torque Profiles

One unique feature of the single cam rig developed at the University of Leeds (unlike multiple cam rigs) is the ability to determine the instantaneous torque at specific locations on the cam lobes. From Figure 8-9, it was observed that both coatings ta:C-H and Si1s have similar torque effect on the single cam rig system. The instantaneous torques are significantly higher than the a:C-H coating but the steel surface is the highest. The larger positive profiles represents the opening of the valves and the area

of this region can be viewed as the work done is opening the valves. A system which utilizes less work in opening the valves will therefore have significant friction benefits on the overall system. The lower negative section in the profiles accounts for the return of the valves and this is identical for all the surfaces tested. This suggests that little or no friction is expended during the valve closing action. The minor profile after the return are just due to noise/vibration with the valve seat. Theoretically speaking, these can be filtered off but they have been left here for a better appreciation of the system.

Close comparison of the torque profiles suggests that a:C-H reduces friction by 6-8 % than taC-H and Si1s while the values are about 12-15 % when compared with steel surfaces. With Si1s, it is noteworthy to mention that significant coating delamination was observed by optical investigation.

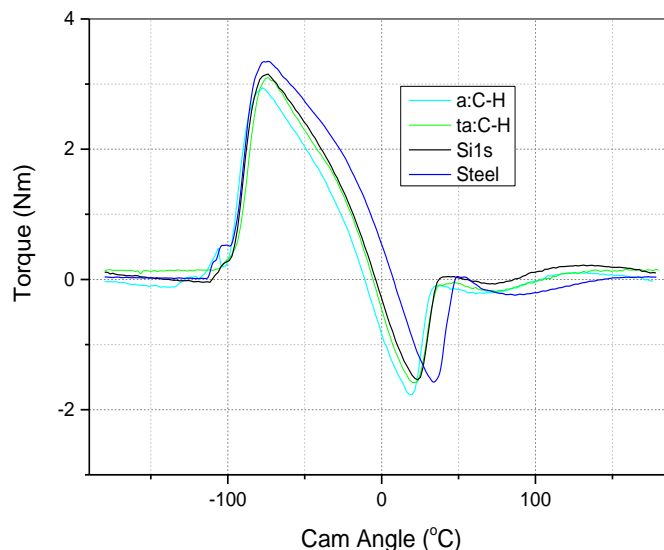


**Figure 8-9 Torque Profile of different surfaces at 300 rpm**

On comparison with ta:C-H coated surfaces, it was observed that the torque values had a mirror reflection of each other at the camlobe base circle due to the clearance between the cam and the inserts. However, during the opening of the valves, it was observed that significant torque reductions were seen with the ta:C-H/ta:C-H tribopair (see Figure 8-10). The torque benefits are directly proportional to less energy expended in opening or operating an engine valve train system. Consequently less energy is lost due to friction. In a a:C-H/a:C-H tribopair (not shown), a minor friction benefit were seen at 300 rpm when compared with the CI/a:C-H tribopair and this

performance diminished as the speed was increased. In essence, it thus appear that coating both surfaces can help improve the friction significantly however, same cannot be said for the wear properties of the system. This is due to the fact that delamination of the taC-H coating on the camlobe were identified by visual inspection. This result, although puzzling, suggests that the coating, despites its high hardness, cannot withstand edge loading in non-conformal contacts.

Hence, making the coating harder may not be the solution in solving the issues of edge loading on highly loaded cam follower contact since the taC-H is considerably harder that the a:C-H or Si1s coating. It thus suggests, that a threshold of coating hardness will help improve the cam follower wear and friction. Tribological interactions with the oil is also of paramount interest, since the coating (ta:C-H) was not observed to interact effectively with the Zn/S additives in the oil. Improving the reactivity of the surfaces of the coating will help improve its resistance to edge loading in a valve train system.

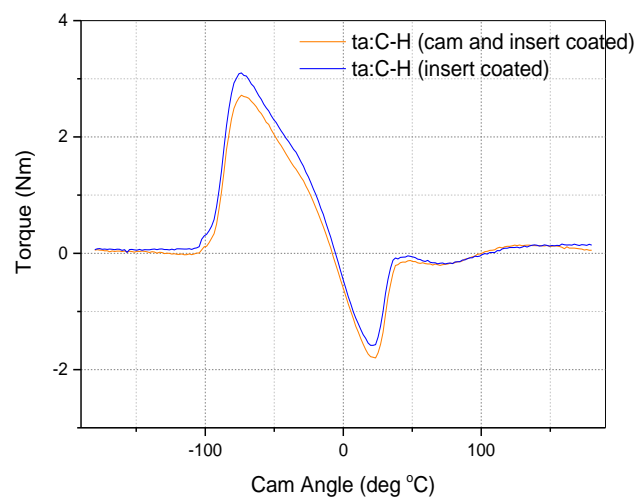


**Figure 8-10 Torque profiles at 300 rpm with ta:C-H coatings showing effects of coating both cam and follower**

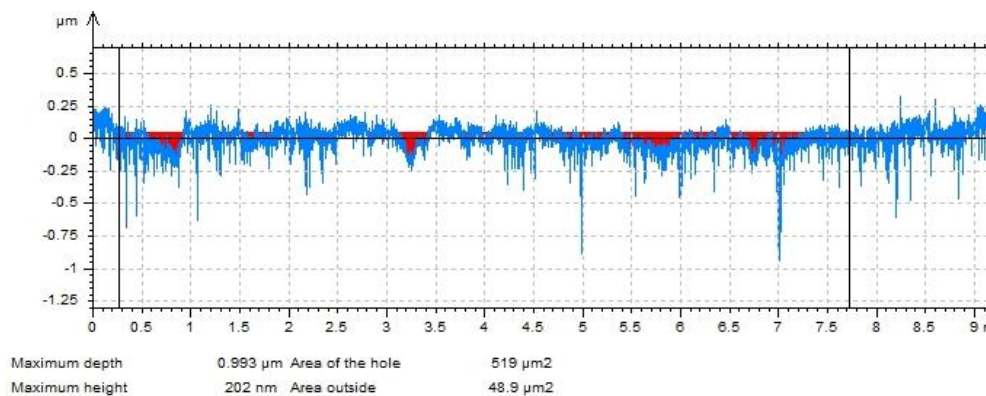
#### **8.5.4. Wear Results**

Figure 8-11 and Figure 8-12 show the cast iron cam nose profile against a Si1s, and ta:C-H tappet. These were measured with the contact talysurf before and after the test and the wear volume/depth were determined by the in-built software of the device. The images help reflect the wear depth and volume along the cam nose. These values are then used to obtain the wear depth/area at the 14 locations

specified according to the key methodology used in ASTM 6891-09a for the evaluation of lubricant for cam follower wear.

Optical images (see Figure 8-13) of the Si1s, ta:C-H and a:C-H coated inserts show that Si1s is changed after 50 hrs of testing while taC-H and a:C-H remain the same throughout the 50 hr testing procedure. This indicates that the durability (wear) of the Si1s coating is considerably lower than the corresponding coating. This finding is in agreement with the pin on plate reciprocating tests that were carried out in Chapter 4.

In this thesis, it was also observed that the coating has a counter effect on the wear of the camlobes. Another important observation was the increase of wear during valve opening as indicated in Figure 8-14. In essence, significant deformation of the surface occurred during the opening of the valve perhaps due to greater energy/work which is expended during valve opening actions. Similar findings have been reported by Durham et al [173]



**Figure 8-11 Cam Nose profile against Si1s coating**

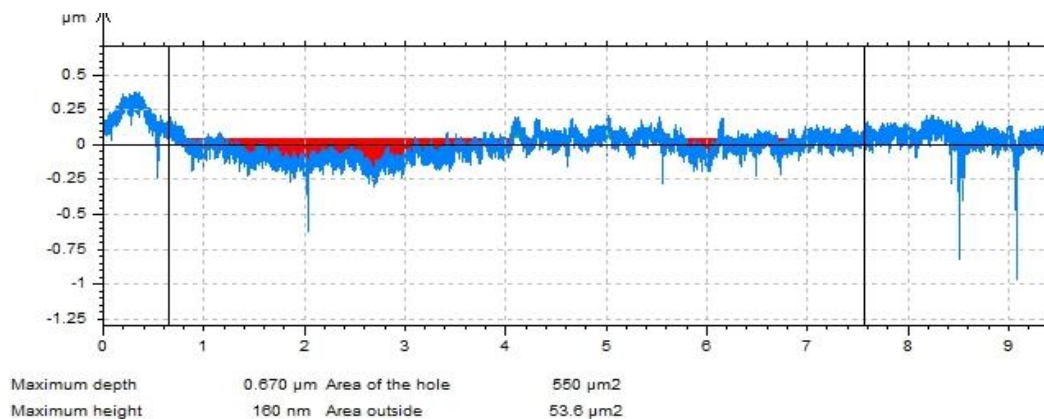


**Figure 8-12 Cam Nose Profile against taC-H Coating**

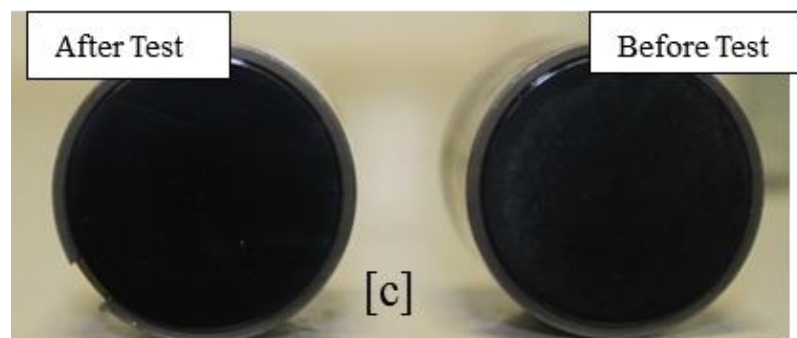
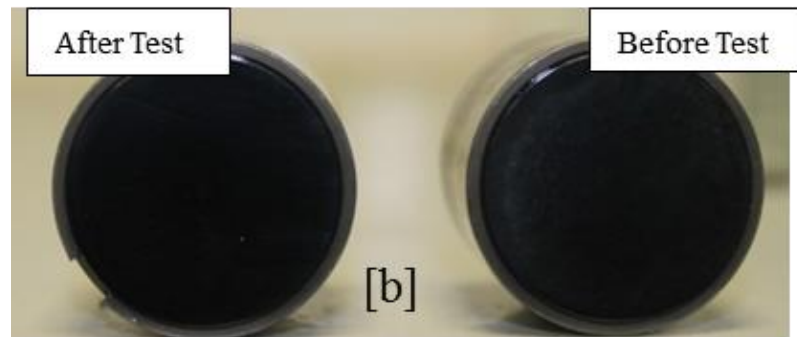
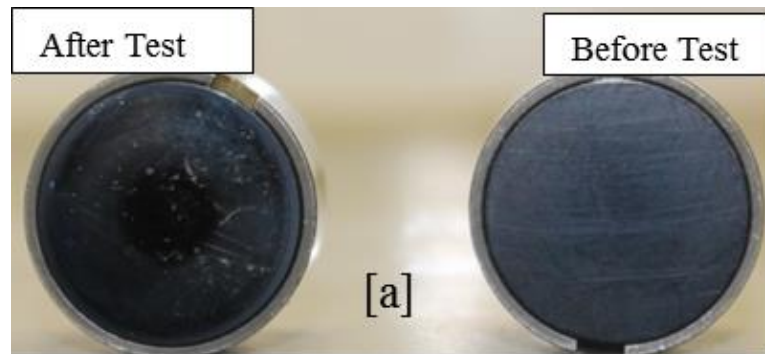


**Figure 8-13** Optical Images of (a) Si1s coated inserts, (b) ta:C-H coated inserts, (c) a:C-H coated inserts

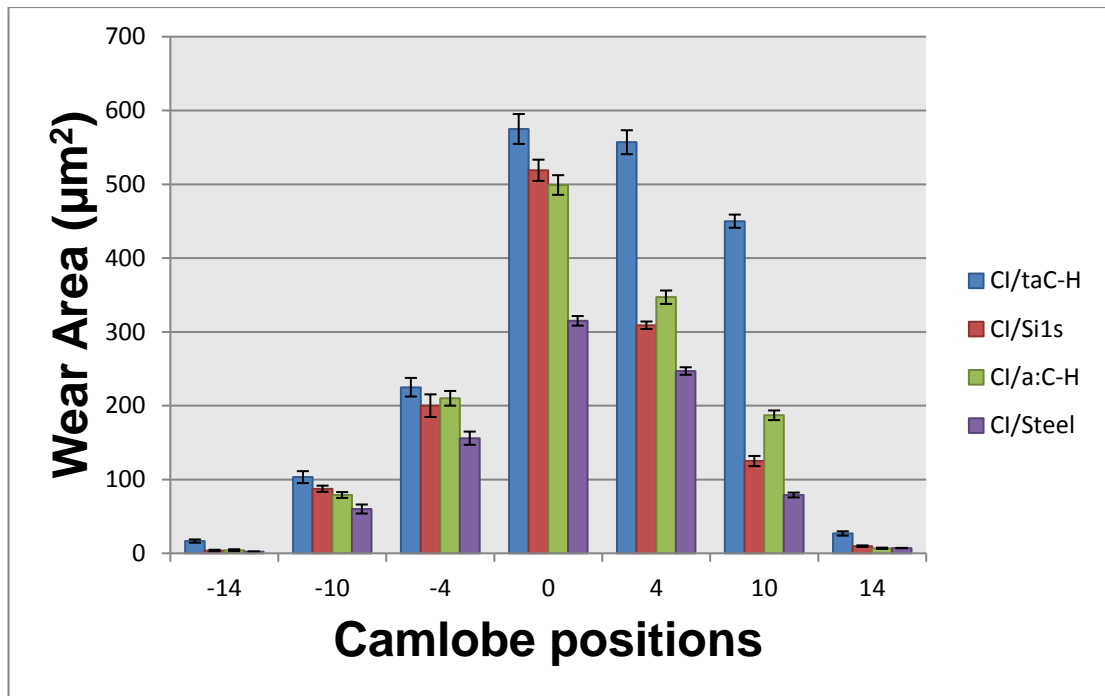


**Figure 8-14 Camlobe position and corresponding wear area**

On coating both the cam and the follower, only ta:C-H and a:C-H were considered for analysis in the rig due to their superior performance. The ta:C-H showed significant wear at a specific location on the cam nose area (See Figure 8-15a & Figure 8-15b). The wear is also confined to a particular location on the cam nose (toward the edge) [216, 217]. This is called edge loading and the results indicate that ta:C-H as a valve train coating is not capable of withstanding such harsh highly loaded pressure conditions on the nose. Optical investigation shows the coating to be completely stripped off from the surface revealing the steel substrate. By comparison of the load/pressure and entrainment conditions illustrated in Figure 8-2, we can observed that in addition to the harsh conditions, lubricants are also been forced out of the contact during the valve opening processes and the corresponding surface has no means of retaining the lubricant. Earlier studies in CHAPTER 4 also showed that the coating form loosely bonded tribofilms that are easily removed by the rubbing action of the cam during each cycle. This is also predominant at the cam nose due to boundary lubrication and sliding action. With the a:C-H coating, the camshaft appears unchanged after the test and no significant wear was observed on the cam nose. Although both coatings were exposed to identical test conditions, a:C-H has shown remarkable wear characteristics as a valve train coating with ability of withstanding edge loading effects that do not lead to the complete removal of the coating.



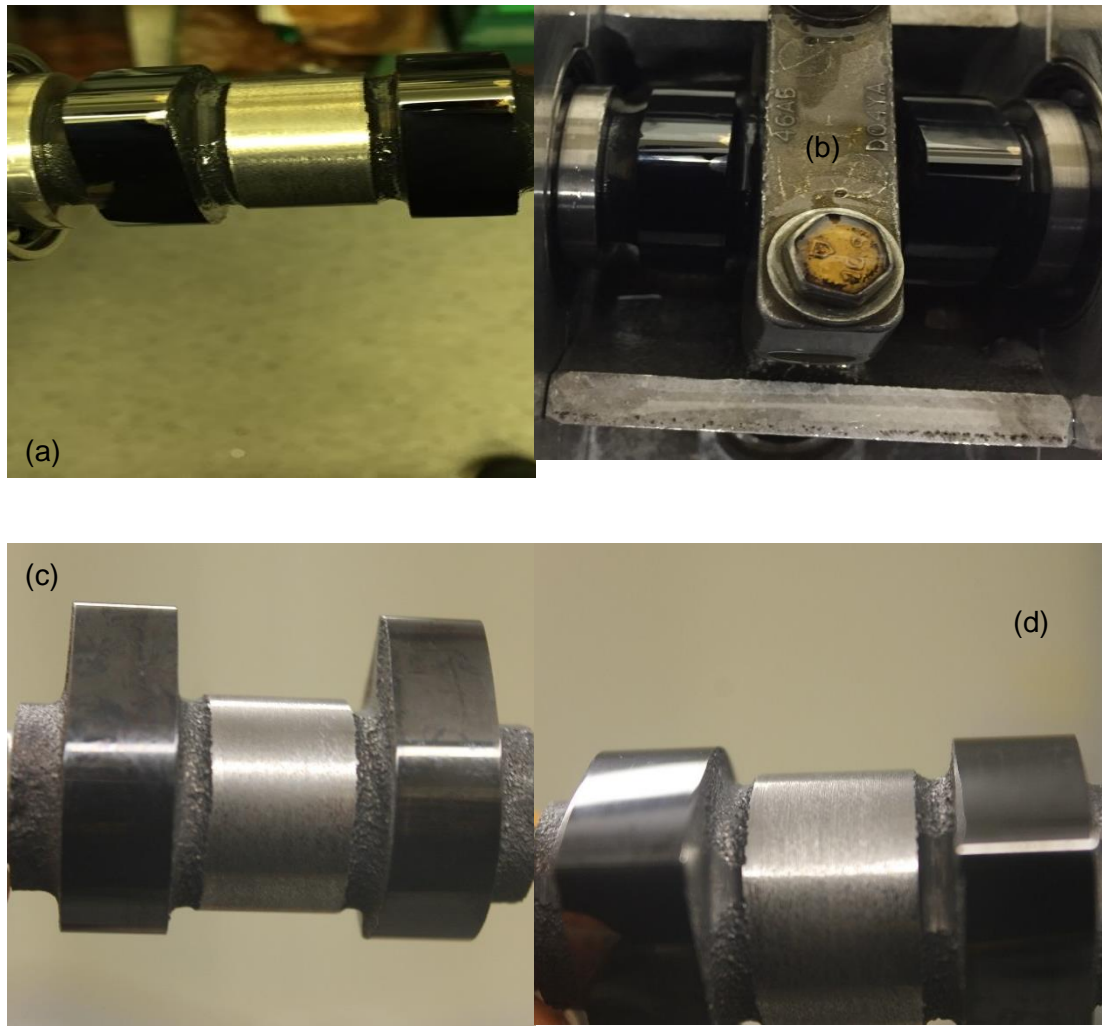


**Figure 8-15 Optical Images of Coated Camshaft after 50 hrs testing on a Single Cam Rig.**

### **8.5.5. Wear Comparison with Standard Engine Tests**

In an attempt to compare the wear on camlobes with standard engine tests, summing of the wear scars was taken at 7 locations as specified in sequence IVa, and in accordance with ASTM 6891-09a standard. This method has been used by [218]. In this procedure, a threshold value of 90  $\mu\text{m}$  is acceptable as the maximum wear on the camlobes. This is depicted by the red line shown in Figure 8-16. In this test profile, although the threshold value was not exceeded, the coating hardness appear to play a significant factor on the wear performance of the camlobes. Similar results have been reported by Durham and coworkers [173]

In addition, the tests performed have about 60 % of the experimental time on low speed with predominantly boundary lubrication which will accelerate asperity contacts or wear on the camlobes. The oils used are also in compliance with ILSAC GF5 as opposed to GF 4 which was investigated by Okuda and coworkers [218]. These new oils have reduced sulphur and phosphorus concentrations which tend to reduce the durability of engine components. While these tests have been used to compared the level of wear which can be expected on the engine, it will still be ideal to carry out an engine stand test before any conclusion can be drawn. There are several reasons why these additional tests may be required.

Firstly, the presence of unreacted carbonaceous products referred to as soot will have a role to play at the interface. The effects of these substances at the interface is still unclear as they have been reported to aggravate wear in some cases [60, 219, 220] while other papers have reported an improvement in wear. According to Gauthier [221], there is no correlation between camlobe wear and soot concentration but a threshold value of soot in the oil can lead to undesirable behaviour. This value however, depends on the overall composition of the oil.

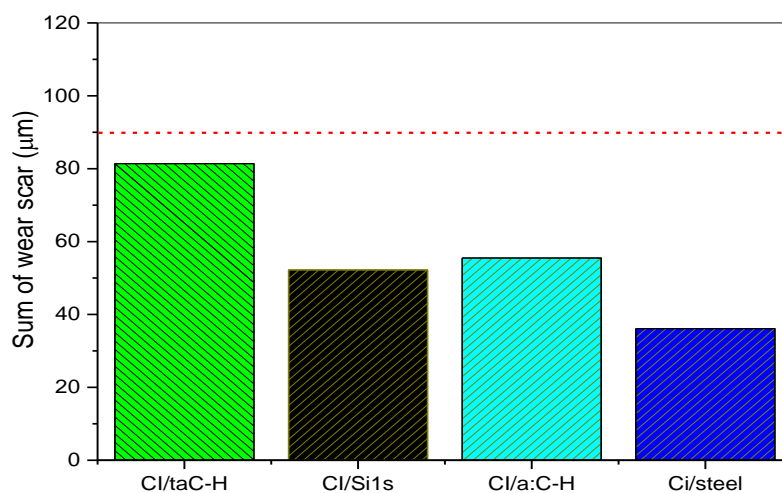


**Figure 8-16 Sum of Wear Scar on Cast Iron Camlobes when interacting with several coated follower (red line denotes 90 µm threshold value above which the oil will be deemed unsatisfactory in service).**

Thermal and oxidative decomposition of the additives in the oil will also play a significant role in engine fired tests. During the rubbing actions, and due to thermal

degradation, the additive will be depleted in the lubricants, thereby reducing their performance and efficacy. The presence of soot will cause some co-absorbance with dispersant/detergent in the oil, all of which will take place at high temperature and lead to the formation of complexes. Hence, in an engine fired test, the lubricant deterioration/composition is grossly affected with time/running hours. This will significantly affect the tribofilm formation as well as the friction/wear of the entire engine valve train system.

Other important notes to consider are the engine drive cycle, direct ignition configuration, exhaust gas recirculation and stop-start phenomena used in modern engines. For the exhaust gas recirculation system, unburnt gases are passed into the combustion chamber by means of a turbocharger. This reduces exhaust gas emission but increases the soot concentration in the vents, pores, orifice and other tribo-contact in the engine. The high level of soot concentration can affect these contact and this is why several research works have focused on its effect on tribological systems.

With the differences in the component bench test – single cam rig, we have been able to show that the coatings cause cam wear to levels that are far beyond those of the steel counterparts. They equally give an insight on the regions on the camlobes where the wear is high. For instance, earlier results (shown in Figure 8-14) has revealed that wear on the camlobes are most severe during the opening action of the valves and are lesser during the closing action. This is a relevant information which has not been revealed in the literature and can give new design insights of how the rising edge and the entire camlobes can be redesigned to eliminate this uneven wear.

In DLC coatings, it was observed that taC-H/taC-H tribopair of the camlobes and inserts have huge friction benefits with some delamination of the coating on the camlobes. This happened at a specific location which suggests that the contact mechanism/pressure experienced were significantly higher than those which the coating can withstand. Another possible cause of the coating delamination can be adhesion although this was not experienced for a:C-H coated camlobes. The results are interesting since the taC-H coating are considerably harder than their counterparts and should be able to withstand wear. It thus follows that increasing the hardness of the coating may not be the best means of improving the wear of valve train systems. Interaction of the coating with the oil and a threshold hardness may be

required for optimal performance. This can be achieved by a suitable experimental system with single cam rig

Another important factor to note (although this has not been discussed in the literature), is the precision engineering which have been used for the surfaces. The a:C-H (ca. 2 $\mu$ m) coating are considerably thicker than those of ta:C-H (ca. 1.5 $\mu$ m). This would alter the clearances between the cam and the insert. This alteration can affect or minimize tappet rotation which will increase the wear on the cam or the tappet.

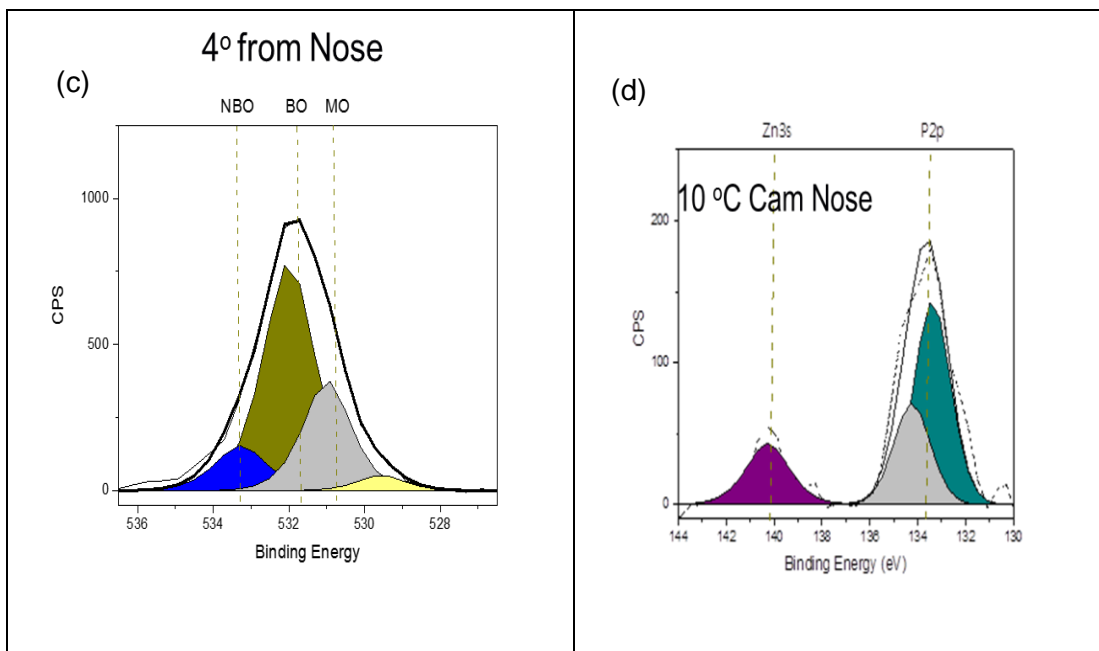
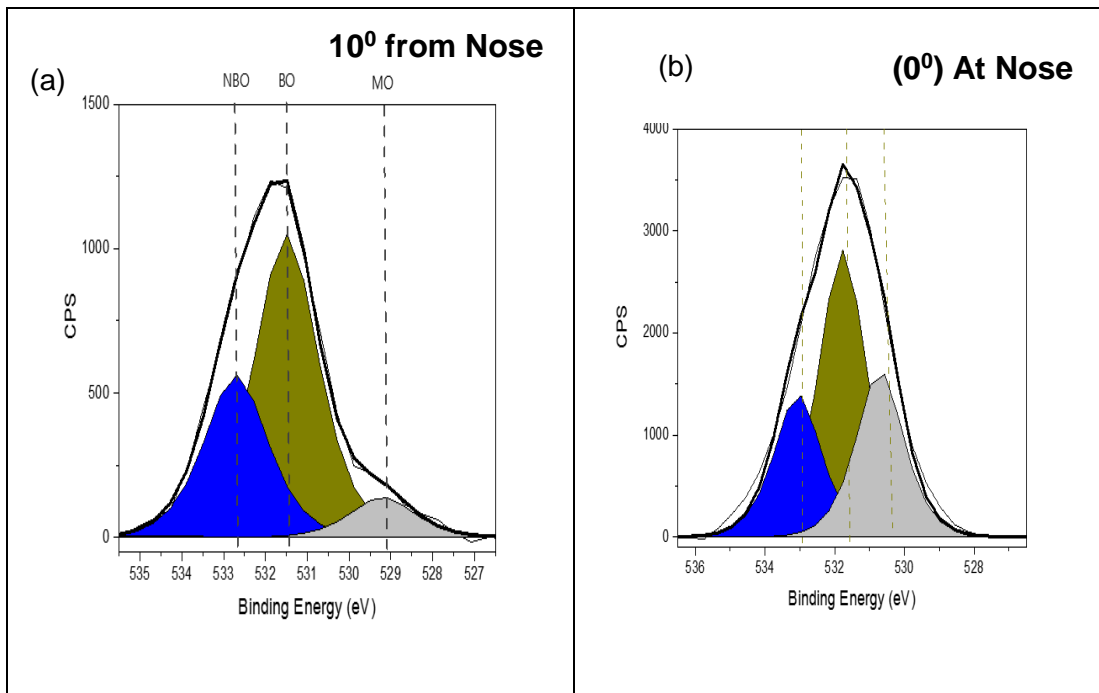
## **8.6. Surface Analytical Results**

### **8.6.1. XPS Analysis (Tests were carried out only on the camlobe)**

The investigation of the coated tappet showed the tribofilm to be identical with those of the pin on plate reciprocating tribometer discussed in Chapter 4. Basis the above, analyses were concentrated on the tribofilms derived on the cast iron camlobes.

#### **8.6.1.1. Si1s/Cl Combination**

In the evaluation of the cast iron camlobes on interaction with Si 1s DLC coating, it was observed that the tribofilm derived across the 7 locations on the camlobes had distinct characteristics owing to the differences in load, contact pressure and lubricant entrainment velocity at the contact of the asperities. Photoelectron peaks of the O1s spectra (see Figure 8-17) at 10° from the nose reveal that the tribofilm is composed of metallic oxide of Fe<sub>2</sub>O<sub>3</sub> while those at the 0° and 4° are made up of predominantly ZnO. At 14°, no significant films were observed. Although this is quite puzzling, the high pressures at these location will definitely favour the formation of tribofilms and consequently lead to the deformation/wear of the solids. It is equally possible that these are third body abrasive wear particles that may have moved during the tribological sliding action at the cam nose. The Zn 3s and P 2p peaks also show that the phosphate chain lengths obtained at 0° and 4° are comparatively shorter than those derived at 10°. Evaluation of the  $\Delta P2p - Zn3s$  reveals that the films are composed of short chain calcium phosphates at 4° and 0°.



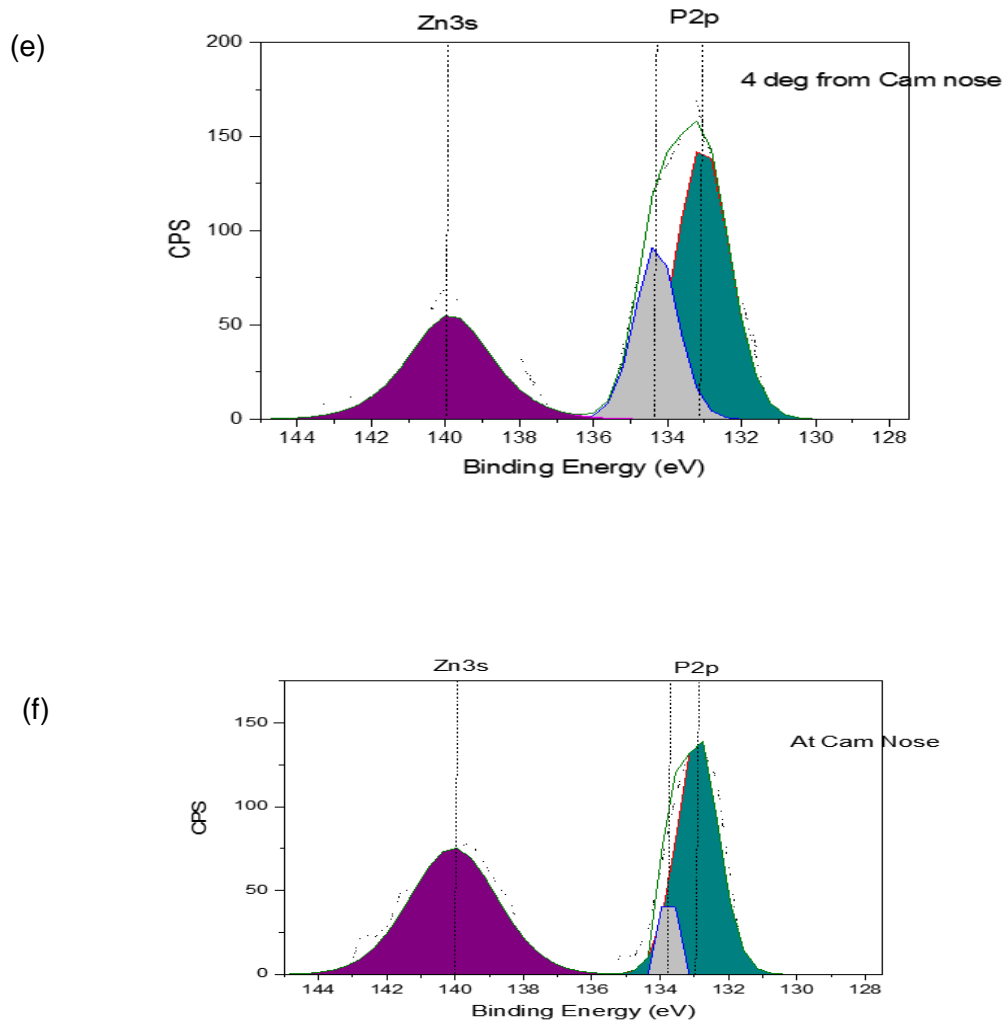


**Figure 8-17 XPS Photoelectron spectra for (a) O1s 10° from can nose (b) at cam nose (c) 4° from the nose (d) P2p spectra 10° from the cam nose (e) P2p spectra 4° from the cam nose and (f) at the cam nose**

Details of the S2p (See Figure 8-18) peak also reveals that the films are similar and composed of some ZnS and FeS<sub>2</sub>. At 4° from the cam nose, significant silicon was observed on the tracks of the camlobes which indicates that a delamination process of the Si1s coating was already taking place. Visual inspection of the coating confirms that a discoloration and slight shiny flakes were already seen on the surface. Shiny particles are traces of TiC used for the interlayer of the coating. Si2p photoelectron spectra show the chemical states to be composed of Si-O-C, Si-C and possibly Si-H. SiC are considerably as hard as diamond in terms of Mohr's Circle and the presence of these particles in the wear track will cause severe third body abrasive wear for both the cam and the follower (tappets). In regions investigated, no sulphates were observed on interaction with Si1s coatings.

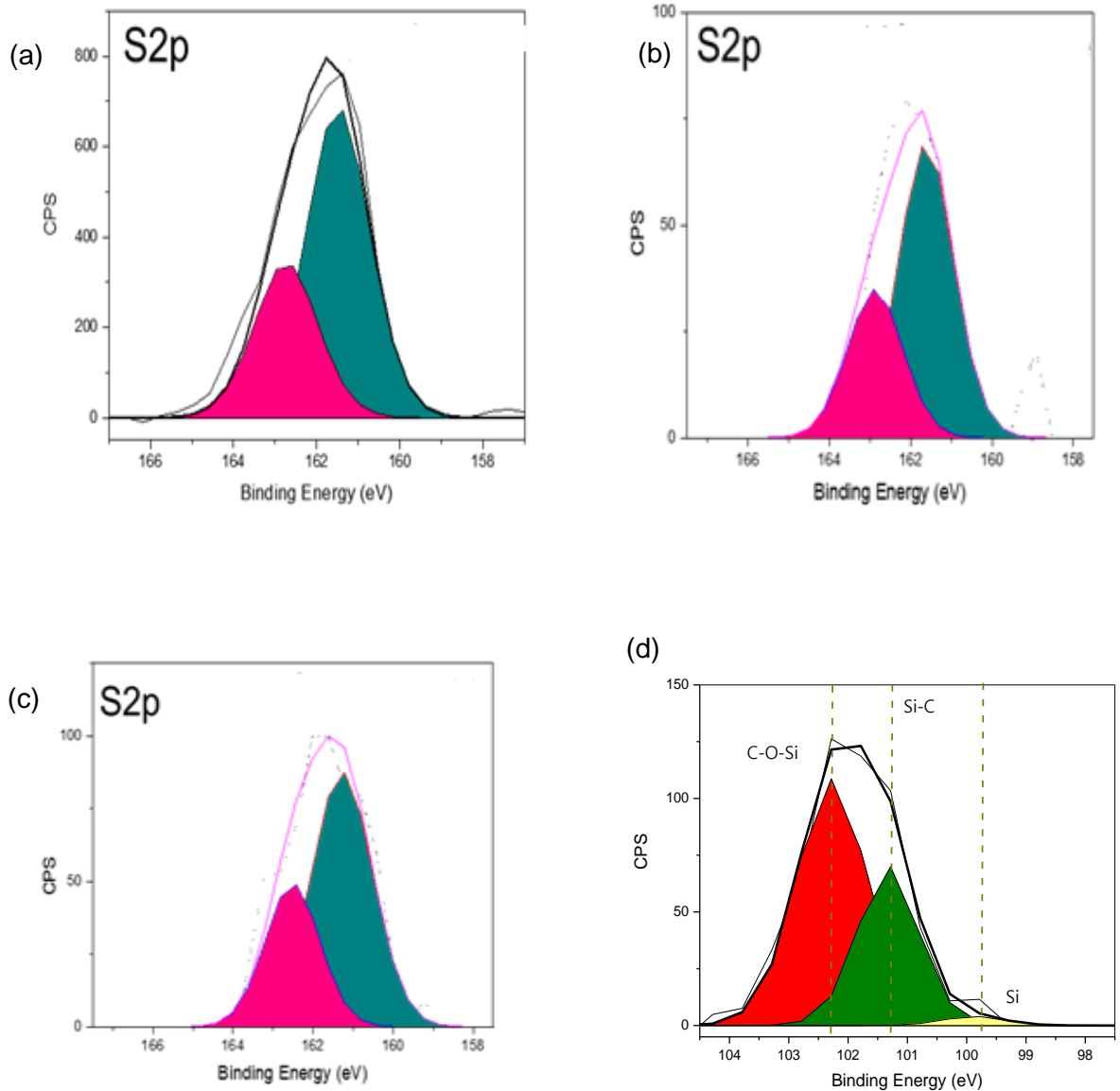


**Figure 8-18 XPS Photoelectron spectra for (a) S2p at Nose (b)S2p at 10° from nose (c) S2p at 4° from Nose (d) Si2p at 4° from the cam nose.**

#### 8.6.1.2. ta:C-H/Cl Combination

On analysis of the cast iron camlobes, the O1s spectra that were derived at 0° and 4° suggests that the film characteristics are similar to those obtained at 10° (as shown in Figure 8-19). However, significant sulphate films were detected at 0° and 10° from the cam nose. These films have been reported to be very corrosive. In addition, no clear/distinct phosphorus peak were detected at these location. These reasons may be responsible for the high wear rates that occurred at these points on the camlobe.

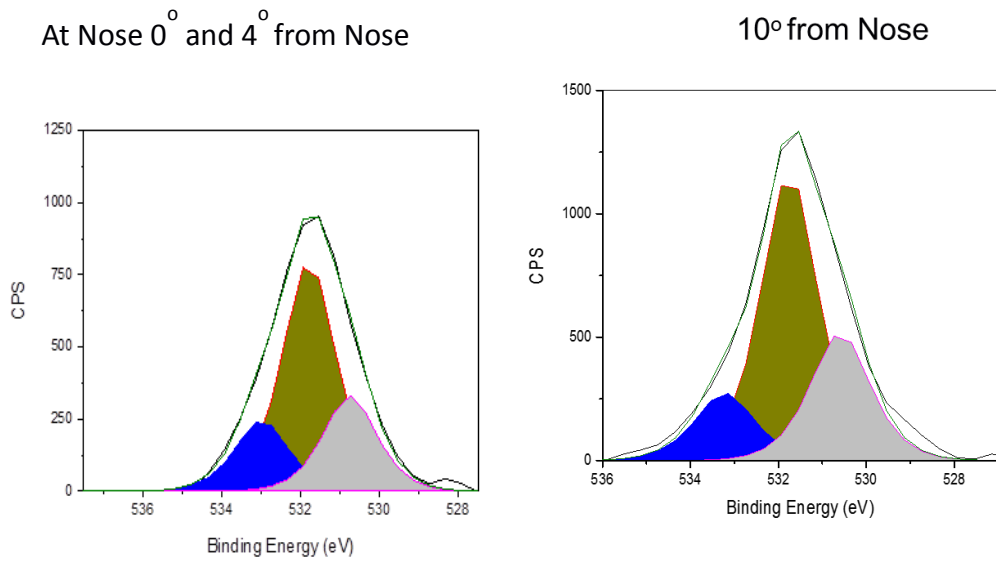


**Figure 8-19 O1s spectra for Cl/taC-H interaction**

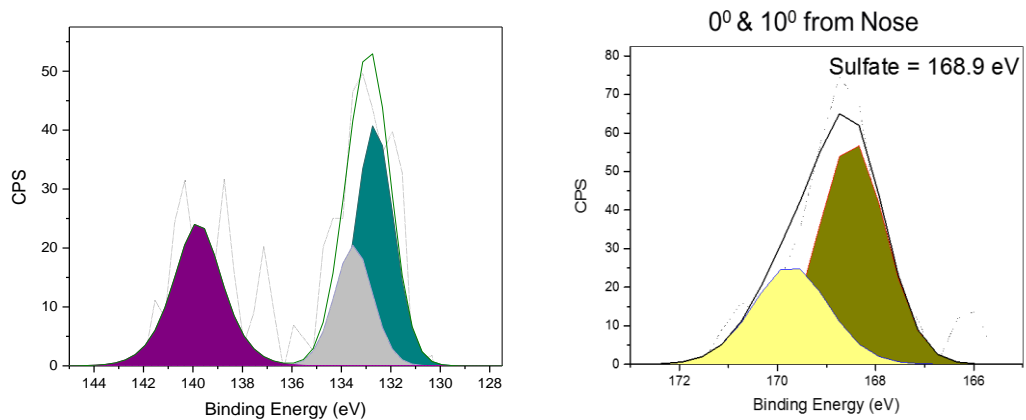


**Figure 8-20 Showing (a) P2p spectra at 4° from cam nose (b) S2p spectra at 0° and 10°**

The presence of sulphates, less dense phosphate film on the camlobe and the hardness of the counter body are responsible for the high wear values that was obtained on the cam nose area.

### 8.7. Consequences of DLC Coated Cam and Follower on Valve Train Friction and Cam Wear

While these DLC coatings have been shown to improve valve train friction when only the tappet was coated, they have also given good results when the counter body is coated. Significant friction benefits of up to 40 % (1-2% engine efficiency) was achieved with a:C-H. This coating is also the most comparative with the steel surface



in terms of camlobe wear. Its exceptional attributes in withstanding edge loading on the camlobe are vital for the system to perform optimally.

Essentially, while these coatings significantly reduce the friction, they tend to increase the wear than conventional steel materials. In the selection of a coating for camlobe application, care should be taken in selecting the right coating which minimises the cam wear. In addition, it might be worthwhile to coat both component for more comparative analysis.

## **8.8. Conclusions**

Evaluation of the tribochemistry across the cam profile reveals that the films have different composition and structure.

- Si1s showed no sulphate on the camlobe while taC-H revealed some sulphate peaks. They have been reported to be corrosive and increase wear.
- The absence of visible phosphate peaks at the nose and 10° away are also responsible for the increased wear on the camlobes. This tribofilm absence can be attributed to a removal action by the taC-H coated follower.
- The cam nose is a region of significant wear and the antiwear phosphate film compose of short chain calcium orthophosphates.
- Increased wear is observed on the rising edge of the cam i.e. the section responsible for the opening of the valves.
- The hardness of the insert/follower affects the wear on the camlobes.

## CHAPTER 9. DISCUSSION

### 9.1. Outline of Discussion

This aspect of the thesis explains different aspects of the single cam rig development, lubricant additive chemistries, PoP tribometer and surface coatings/material behaviours. It can be broadly divided into five sections as follows;

- Newly designed SCR – novel features
- Coating performance on SCR
- Coating performance on PoP tribometer
- Correlation between PoP tribometer and SCR
- Level of prediction and economic significance of valve train tests

### 9.2. Newly Designed Single Cam Rig - Novel Features

#### 9.2.1. Instrumentation: Data Capture, Torque Profiles & Dynamic Load Determination

In this study, the presence of the shaft encoder and controllable data capture of up to **10<sup>5</sup> samples/seconds** have made the rig unique for investigation of friction torque across the cam profile. This data capture gives better resolution across the cam profile. A large number of single [33, 39, 90, 133] and multiple cam rigs [40, 87] have been developed for valve train studies with most of them capturing only speed, torque, temperature and oil pressure [222]. Some have also been designed to determine the real-time measurement of wear with surface layer activation techniques [25, 90, 193, 221]. However, very few of the rigs have the ability to determine the friction torque as a function of cam angle. Another important factor lacking in these rigs is the ability to determine the dynamic load over one cam cycle. This approach was first investigated by Hamilton [21] but the load gauge used were unsatisfactory. In this rig, the load cells used for the determination of dynamic load gave satisfactory results but after successive testing, a phase drift was identified. The shift is not based on any aspect of the development of the rig itself but some intrinsic properties of the load cell. The next approach will be to use a load cell with cycle/phase shift compensation which would produce representative results.

A controllable oil bath with three different set flow rates of low, medium and high has a sensitive of 0.01 °C. The choke valve on the rig also gives additional control of lubricant to the cam tappet contact. Using both system, lubricant starvation systems

typical in stop-start phenomena of the engine can be simulated with no difficulty. These unique features make the rig very versatile to study various conditions in a typical valve train system.

### **9.2.2. Noise Levels**

Valve train noise is an important factor to consider in the development of a single cam rig. The noise or vibration can be characterized as periodic impulsive, whining, friction and rumble noise, all having varying magnitudes [223]. At low speed during valve opening and closing, this vibration can be attributed to impact which is periodic impulsive noise [224] but can be suitably avoided with the choice of an appropriate clearance between the cam and follower system [223, 225]. In the development of the rig used in this study, the clearance between the cam and the follower was modified by using slightly thinner inserts. This involved changing the thickness from 2.70 – 2.65 mm thereby giving the valve guide a somewhat slower impact and allowing time for the system to recover.

Secondly, noise levels can be reduced by optimizing the cam profile or using relevant material with acoustic damping characteristics [226]. The objective of the research was to test steel surfaces hence no material change was required but Aluminum tappets have also been reported to reduce inertia loads on engine components [192, 226]. Since we could not modify the cam profile, acoustic dampers were placed underneath the rig base to dampen the vibration.

Another aspect used to minimize the noise was the surface finish on the camlobes. Camlobe profile accuracy and surface finish are vital to wear and noise reduction as the presence of minute craters, pore, grooves or valleys give rise to significant vibration [224]. All camlobes used in this study were polished by Oerlikon Balzers to a surface finish of 20 – 30 nm. They were also degreased and stored in a good environment to ensure that the vibration in the system was kept to a minimum.

Figure 9-1 reveals that the newly developed single cam rig has significantly low noise levels at high speed and little or no recognisable noise/vibration of 700 rpm than those of [223] and [11] (not shown). This is due to the design modification and noise reduction methods which were taken during its development.

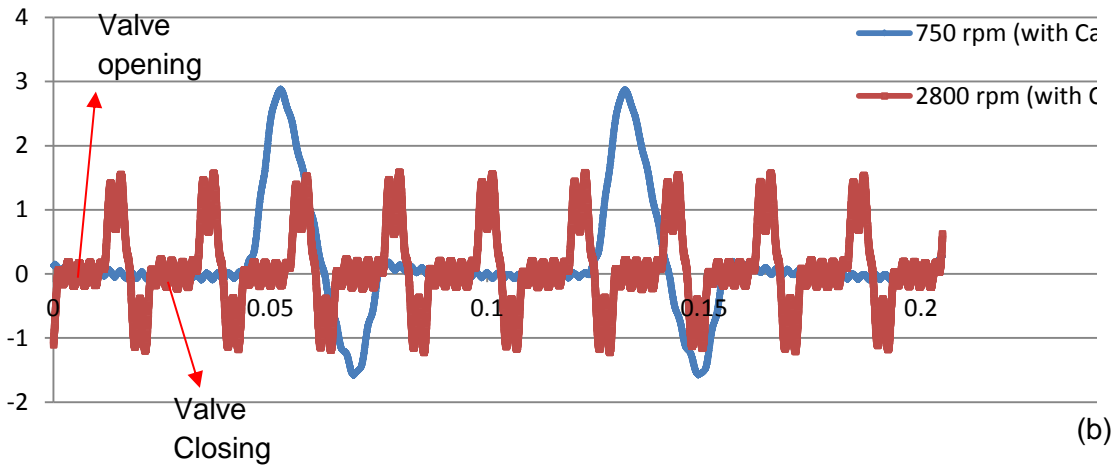
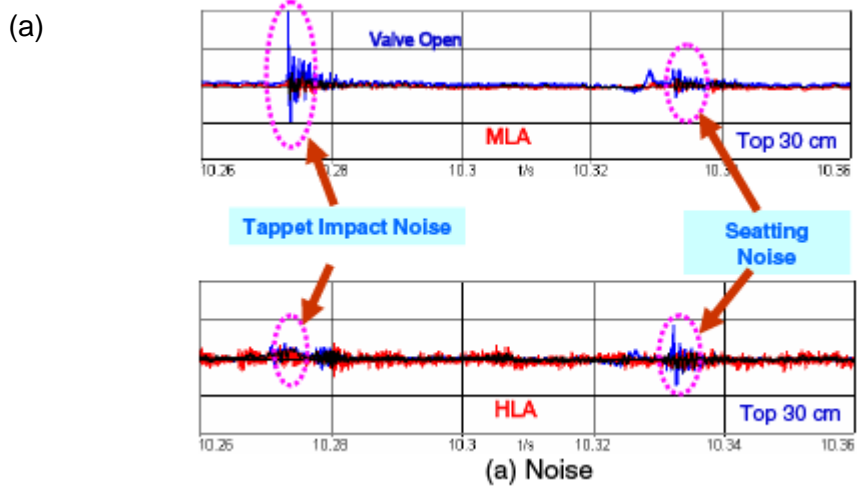


**Figure 9-1 Noise level with (a) Hwang et al [223] (b) Newly Developed Single Cam Rig**

### 9.3. Coating Performance on SCR – Wear and Friction

Coatings have reduced the friction or power consumption in valve train systems by several folds. In this study, the single cam rig has shown that reduction as high as 38 % can be achieved by changing the surface from steel to a:C-H. Within DLC coatings, a 5-25 % reduction range was experienced over the speeds tested. These results are in similar agreement with the works of [32, 33, 218]. The friction torque response from a:C-H and taC-H against a cast iron counterpart with commercial 5W30 oils are also very similar. The results support those presented by [32]. Oil A is composed of an ashless friction modifier as proposed in [218]. It equally achieved a 25% friction reduction. The DLC was used to achieve 5-25 % reduction in friction when compared with CrN. CrN surfaces are prone to polishing which makes engineering surfaces lack the ability to retain lubricant necessary for its optimal performance. Under this condition, starvation may occur and the significant wear

occurs [45]. When compared with the values obtained between oil A and oil B over the validation testing for the single cam rig, a 29 % reduction in Friction was achieved.

As per wear, coating can improve the wear but it appears a balance between hardness, and oil composition must be met. According to McGeehan and Ryason, [227] increasing the cam hardness improve the wear on the camlobes. This ideology have also been touted by Kano [54]. High hardness was observed to improve the fatigue resistance and ploughing on interacting components [62]. It is worthwhile to mention that each of these works focus on the hardness of the substrate material [54, 62, 227]. However, results obtained in this thesis suggests otherwise. Coating a cam with ta:C-H with hardness around 35 GPa aggravated the wear on the camlobes. Significant spalling of the coating was observed. The same cannot be said for a:C-H coating with slightly lower hardness of 25 GPa. a:C-H gave a satisfactory performance in single component and bi-component coating combinations. The results obtained with the a:C-H coatings are in agreement with the works of Kodai [197]. It was envisaged that higher hardness coatings will not conform to the rig configuration. Further test with WC-H DLC of considerable hardness also gave good results for valve rig systems. These results are in agreement with those presented in this thesis – Chapter 8.

Likewise, as the coatings were polished to a surface finish of 20 nm with very smooth profiles, the surface roughness was eliminated as a source of wear [224]. This lead us to suggest two different phenomena known as edge loading [216] and rig misalignment [227]. However more test showed that the results were repetitive and the coating could not withstand the edge loading phenomena in the rig. In addition, the oil type will have a role to play in this process. Coating only the insert resulted in higher wear on the camlobes. These results are also in contrast to [173], however it should be mentioned that different oils were used. The wear of the camlobe/a:C-H inserts are close to those of steel and may indicate that a threshold value of coating hardness and oil interaction can ultimately improve the friction and wear in valve train components.

#### **9.4. Coating Performance on PoP Tribometers – Friction and Wear**

The a:C-H and ta:C-H coatings generally improved friction and wear on the PoP tribometer that conventional steel materials. A 15 – 57 % reduction from fully formulated oil to base oil was observed. These values are in agreement with the works of [32, 35, 87, 111, 179, 197]. The lower friction of the a:C-H/CI and ta:C-H/CI

system in base oil is due to the formation of a transfer layer on the CI surface [73]. At the onset of sliding there is a high interaction between the CI surface and the DLC which leads to the build-up of transfer layer. For the a:C-H and ta:C-H it takes about 2-3 hrs for the transfer layer to sufficiently build up and the surfaces begin to behave like a ta:C-H/ta:C-H and a:C-H/a:C-H tribopair. This gives the low friction seen in the PoP and supported by the works of [76, 179]. For fully formulated lubricants, the protective film produced by the lubricant additives in the oil retard the movement of transfer layer to the counter-body. Going through the optical micrographs shown earlier, it can be observed that traces of the transfer film are seen but they do not build up to significantly dispersed thick carbon films on the wear tracks.

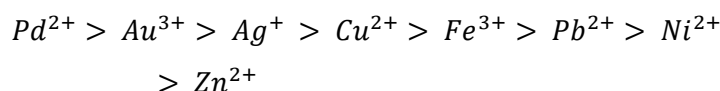
Tests with Si1s coating did not give any friction benefits. At the beginning of the tests, the friction was low but sharply rose to a high value as the coating was been removed during the rubbing action. The final friction values are similar to a CI/Steel tribopair in-lubro test conditions [72, 207]. The friction response of Si1s coatings have been reported to be strongly dependent of Si concentration and moisture or relative humidity [72, 207]. According to Gilmore, a threshold value of 6% Si concentration produce optimal performance. However, based on the information from the manufacturers, this coating contains between 12-18 % silicon. This is responsible for the high wear experienced in the tests. Notwithstanding some silicon DLC coatings produced by ion beams have been resulted in friction values of 0.05. This implies that the low friction also depends on the processing routes [228].

Mn-phosphate coatings have a crystalline and porous structure that permits the spreading and absorbance of the oil on the surface [45], its friction characteristics on the reciprocating tribometer has not provided any benefits. This is perhaps due to its high roughness which gives rise to asperity interactions, thereby leading to high wear and friction [56]. Based on the results, roughness play a vital role on the friction response. In addition to that, coating interaction with the counter-body and oil are crucial to friction and wear performance.

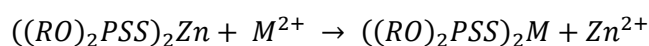
#### **9.4.1. Interaction of Additives with the DLC Surfaces**

In this study, the EDX, XPS and Raman spectroscopy shows that DLC coatings do not interact with lubricant additives in the same way or extent as ferrous surfaces do. Certain components of the additives necessary for the formation of boundary nanoscopic films may be inhibited in the process. In addition, analysis of the steel samples show that Fe have a significant role to play in the formation of these films.

The mechanisms for the formation of tribofilms with DLC coating is very different from those of Fe. In ferrous surfaces for instance, Fe is necessary for the breakdown of the ZDDP molecule by a cation displacement reaction, which takes place on metal surface during tribological tests. These were observed on the steel and cast iron surfaces with the formation of ZnO, Fe<sub>3</sub>O<sub>4</sub> and short chain polyphosphates. Displacement order and reaction steps are shown in Equation 9-1 and Equation 9-2 [93]



**Equation 9-1**



**Equation 9-2**

Further breakdown of the intermediates take place during rubbing to Ca phosphates, ZnO, haematite and Iron sulphides (depending on the additives in the oil). On ferrous surfaces, SEM micrographs show the corresponding tribofilms to be strongly adherent to the cast iron pin or steel surface while those on the coating appear to be loosely bound to the surface and are composed of mainly the dispersant/detergent in the oil. These films are have been reported to be easily removed by cleaning in cyclohexane [162] with supports the results here.

With the DLC coatings, this process (Equation 9-2) is grossly lacking or completely inhibited. No Zn peak was visible on taC-H and a:C-H surfaces except for Si1s. Some traces of Zn were seen on the Si1s wear track. The reason, however, can be attributed to the delamination/removal of the coating to the point where the nascent iron surfaces react with the lubricant additives to form boundary films. These are further supported by EDX analysis/mapping on the plate which show that reaction take place in the wear scar due to the presence of iron.

The low electron affinity/reactivity of a:C-H and taC-H make them very unreactive with the oil additives. Ca and S species which appear on the surface may have been physisorbed from the detergent/dispersant used in the lubricant. Whereas certain literary studies have reported them to be reactive with MoDTC and ZDDP/MoDTC combinations [64, 115], current studies from De Feo and coworkers [229] show that the interaction of these coatings with MoDTC do not occur and the additive has an

antagonistic effect on the wear mechanism of the coating. With a:C-H, it has equally been shown that ZDDP has no effect on its wear or friction characteristics as no derived films were observed on the surface [70]. This has also been demonstrated by Haque et al [194]. It was confirmed that the interaction seen on the surface depends on the dopant element of the coating.

#### **9.4.2. Mechanism of Friction Reduction by DLC Coating**

The investigations show that there is a correlation between the smoothing of the surface and the wear/friction properties observed between the tribopair. For a:C-H, it has been shown that the friction/wear is low at high temperature and considering smoothing of the surface takes place. These are in agreement with the works of [69, 71]. Also, despite the hardness of the coating and the presence of wear particles on the pin surface, no abrasion of the pin surface is observed.

The reason for this phenomena can be a slight transformation or microstructural change of a very thin layer on the topmost surface, perhaps due to hydrogen effusion [71, 73]. This makes the surface considerably softer thereby, ensuring the CI pin slides over a softer counter body, promoting low friction and eliminating or reducing the chance of third body abrasive wear although the overall wear are higher on the pin surface [33].

With taC-H, this process does not appear to take place but the surface of the counter body appear significantly rougher. Due to its hardness, ta:C-H has exceptional wear performance. Assessment of the micrographs on the pin show that an abrasive wear mechanism takes place with the hard coating ploughing the soft CI pins.

The Si1s forms significant tribofilms in the wear track but complete coating failure was observed. XPS spectra on the track reveal presence of Si-C and Si - O - C which are extremely hard. In fact, as hard as diamond in terms of Mohs circles. This particle aggravate the wear process both on the coating and the pin. Micrographs on the pin have shown significant chunks of material being removed from the track despite the formation of well dispersed antiwear film. It thus shows that this coatings are not suitable for tribological applications.



## **9.5. Correlation between Tribometer and SCR Test**

In both tests, the contact pressures, load, operating temperature, material combination and lubricants were very similar to give room for comparison. Although the cam follower system has a sliding-rolling contact, tribofilm assessment was carried out  $\pm 14^\circ$ ,  $\pm 10^\circ$ ,  $\pm 4^\circ$ , and  $0^\circ$  (Cam nose) which is predominantly in the sliding regime of the camlobes. The material of the plates were sectioned from a standard insert material to eliminate any deviation due to material variability. These makes the film comparison with the pin on reciprocation plate tribometer more realistic.

### **9.5.1. Tribochemistry – Comparison of Tribofilms Structure and Composition on Ferrous surfaces**

#### **9.5.1.1. Inserts**

The films observed on the steel tappets/inserts vary based on the oil formulation. For oil B (FFB), a well dispersed film is seen which covers the surface and prevents plastic deformation of the asperity. This unique property of film dispersion can be attributed to the detergents/dispersants which were used during the formulation of the oil. Oil A contains a mix of Mg/Ca based phenates and sulphonated type detergents while oil B contains a mix of Mg/Ca overbased Carboxylate type detergent. Phenate and sulphonate type detergent are very surface active and are quickly absorbed on the surface of the steel, thereby covering the sites necessary for the breakdown of the ZDDP molecule [141, 142]. In essence, the surface active detergents inhibit the direct contact of the ZDDP molecule with ferrous surfaces which significantly reduce its decomposition.

When the ZDDP molecule manages to gain access to the steel surfaces, the growth is also reduced and there are minimal nucleation sites. In addition, the growth mechanism will have been distorted [147]. Another important factor for the low dispersion of the ZDDP film is their ability to form complexes with detergents/dispersants. These suggest that some of the ZDDP molecules will have been consumed/modified in solution before the tribological reaction [146]. Concentration of ZDDP in oil FFB is also more than oil FFA. This facilitates the antiwear formation. These are some of the reasons why Oil FFB produce well dispersed films

Furthermore, oil FFB goes a long well in withstanding the high loads in the cam follower system due to its composition of long chain phosphate film which have good mechanical strength. On oil FFB, nano-indentation data which was carried out within

20 nm depth from the surface of a 10 $\mu$ m\*10 $\mu$ m area show the Hardness and reduced modulus to be around 9.1GPa and 135GPa respectively (Shown in APPENDIX C). Those obtained with oil FFA did not have significant dispersion on the surface and the hardness and reduced modulus was around 6.0 GPa and 117 GPa

SEM and XPS analysis of the films derived with oil FFA shows that the film has a low concentration of phosphorus, sulphur and Zn. In fact, for most of the locations examined with XPS, Oil FFA did not form significant tribofilm. O1s and Fe2p spectra with oil FFA reveal that the film observed contains metallic oxide particularly haematite. TEM analysis also identifies Aluminium oxides with oil FFA. In terms of Mohs circle, Al-oxide is almost as hard as diamond. These particles are very hard and worsen the wear by a third body abrasive wear process. FIB-SEM and TEM was used to evaluate the thickness of the tribofilm. FFA was observed to have a thickness as thin as 5 nm in regions of significant rubbing to around 55 nm while oil FFB had a thickness of 80 nm in region of significant rubbing to around 100 nm.

Thus, the combined effects of oil formulation, film thickness, tribofilm composition and mechanical strength have been used to show why oil FFB have a superior performance in terms of wear. Despite the fact that this oil does not contain a friction modifier, its performance is comparable with those of Oil FFA in the sliding contact. This are shown with the pin on reciprocating plate.

#### **9.5.1.2. Cast Iron Pins**

The tribofilms derived from the pin are similar with those obtained on the steel inserts/plates. These film are slightly different from those on the camlobes even though the single cam rig tests are much longer (50 hrs compared to 12 hrs for the pin on reciprocating plate). This can be attributed to the sliding-rolling action on the camlobes.

A careful review from Chapter 4 shows that film morphology is dependent on the nature of the counter-surface and the engine oil. While it has been established in the major part of this thesis that oil B forms well dispersed films of Ca phosphates, ZnS, carbonates and FeS<sub>2</sub> on steel surfaces, these film dispersion and morphology are affected by the wear process exhibited by the counter-body. In a Ci/Steel contact, the tribofilm derived on the CI and steel plates are well dispersed when oil FFB is used. These are similar on interaction with the a:C-H where the CI surface has a thick layer

of Ca phosphates. These observations equally matches those which were observed on the steel inserts.

On comparison of the CI surface from a CI/taC-H and CI/Si1s tribopair, it was observed that the films were not properly dispersed on the surface. The taC-H hard particles from the coating made the cast iron surface rougher and no distinct tribofilm dispersion was observed. For the CI/Si1s tribopair, the film was slightly dispersed although with rough groove consisting of Si and Carbon. Traces of SiO<sub>2</sub> were identified with XPS on pins and steel plates. These particles are very hard and tend to remove the tribofilm during the rubbing action.

#### **9.5.1.3. Camlobes**

Although SEM/EDX investigation of film morphology was not carried out, information obtained with XPS suggests that the films are not as well dispersed like the pure sliding contact obtained on the pin on reciprocating plate. X-ray photoelectron spectroscopy was carried out at three to five times for each locations. At the cam nose, the films are similar with those obtained from the steel surface but the intensities are considerably weak. At  $\pm 14^\circ$  the film appear to be very thin and loosely dispersed as only a single phosphate peak was observed during five examination at different locations on the camlobes.

#### **9.5.1.4. Tribofilms Derived on DLC Coatings – Inserts, Plates and Camlobes**

The tribofilms derived on DLC surfaces are very different from those obtained on ferrous surfaces [87] in some cases, no interaction occurs [70]. For most of the DLC surfaces studied, no interaction was observed with Zn additives except for Si1s. For Si1s coatings, tribofilms were seen on the wear scar after the coating had been removed and there was direct interaction between the oil and the substrate metal - Steel. The films were composed of Ca sulphur and phosphorus with some traces of WC, Titanium and Si1s which are from the coating. The wear properties of the system are strongly dependent on the coating itself as the film appeared sparsely dispersed and loosely bonded to the surface. As per the mechanism of formation, for the dissociation process for the ZDDP molecule, it has been reported that Fe is required for the initial breakdown of the ZDDP molecule [93]. Based on this, the absence of Fe, which has been replaced with Carbon, indicates that the reaction step will take an entirely different route.

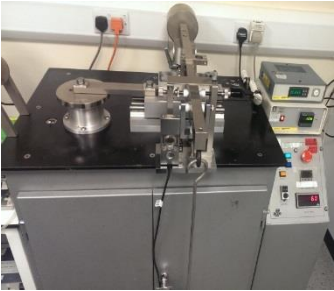
On the cast iron pin surface, significant breakdown of the ZDDP molecule were seen on the interacting surface. This is why significant well dispersed Ca phosphate films were seen with XPS and the morphology was determine with EDX. By comparing the surface analytical results, we can conclude that the detergent/dispersant in the additive are slightly absorbed on the DLC surface and film morphology further reveal that an abrasive wear mechanism took place on the pin surface on all CI/DLC tribopairs.

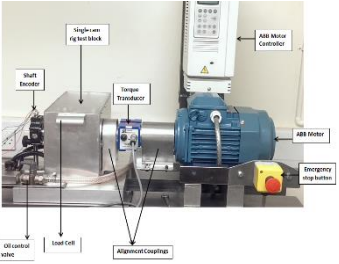
For the single cam rig system, this morphology was not visible due to the nature of the contact. Only concentric circle and minor flakes were seen with Si1s. Other tests involving coatings on the inserts did not show wear but the tribofilm formed were essentially the same. Then only marked difference was the location were the tribofilm were dense. This was towards the centre of the insert were significant rubbing from points on the cam were taking place. The comparison of the tribofilm from a reciprocating tribometer and single cam rig can be summarised as shown in Table 9-1

#### **9.5.2. Effect of Oil Type/Composition of Tribofilm and formation Mechanisms**

Engine oil formulation plays a critical role in the durability and performance of IC engines components particularly cams and followers. According to the works in this study, two commercial 5W30 lubricants were used and the film characteristic obtained were widely different from one another. Although the concentration (oil A contains 870 ppm Zn to Oil B 1190 ppm Zn) is slightly lower, the corresponding effect on the antiwear performance is immense. Oil B was observed to form well dispersed and thick tribofilm on the steel surfaces than oil A. This was attributed to the concentration of ZDDP in the oil, type of detergent/dispersant used as well as the antagonistic interaction between ZDDP/detergent and ZDDP/dispersant [93, 140, 203, 204].

**Table 9-1 Showing the comparison of tribofilms with a Pin on reciprocating plate tribometer and Single Cam Rig**

System – tribometer test Tribofilm derived from Pin on reciprocating tribometer				
	Material/Surface Coating	Tribofilm	Remarks	
<p><b>Component/tribopair</b></p> <p><b>Pin on reciprocating plate</b></p> 	Cast Iron Pins	Ca phosphates, FeS <sub>2</sub> , Carbonates, ZnS	Similar with those on the cam nose but more dispersed.	
	Steel Plate	Ca phosphates, FeS <sub>2</sub> , ZnO/ZnS	Similar with those on the inserts. Oil FFA formed some sulphates	
	DLC Coated plates	taC-H	No significant tribofilm observed, minor traces of phosphorus were seen with no Zn absorbed on the surface	Similar with those of the coated inserts. No coating delamination were seen.
		Si1s	Films composed of SiO <sub>2</sub> , CaCO <sub>3</sub> , ZnS, Calcium phosphates	Coating delamination was observed.
		a:C-H	Ca Phosphates, no Zn observed with both oils, Sulphides seen with oils FFA. Tungsten Sulphide peaks were seen in XPS	Very mild wear not visible with the eye.

System – Component bench test	Tribofilms derived from Single Cam rig		
<p data-bbox="347 376 549 409"><b>Single Cam Rig</b></p> 	Steel Inserts	Ca phosphates, FeS <sub>2</sub> , Carbonates ZnS	The tribofilms were well dispersed at the centre due to rubbing from cam flank/shoulder/ramp and nose
	Cast Iron Camlobes	Ca phosphates, FeS <sub>2</sub> , Carbonates ZnS	Tribofilms concentrated around the nose with little or no films at ±14° from cam nose
	DLC Coated Inserts	There are little or no changes observed with the coating on the single cam rig	<p data-bbox="1241 864 1485 1025">Si1s coating showed some delamination but not to the same extent as was observed on the pin on reciprocating plate tribometer.</p> <p data-bbox="1241 1088 1485 1391">ta:C-H coated cam lobes experienced delamination of the coating. This coating was removed and the base material can be seen with the naked eye. This occurred on the cam nose. It however produced very low friction.</p> <p data-bbox="1241 1453 1485 1615">a:C-H showed exceptional friction and wear performance. Tribofilm characteristics remained the same.</p>

Detergent and dispersant are generally accepted to affect the antiwear properties of ZDDP [2, 141, 142, 146, 147]. According to Rounds [146], the interactions takes place in the liquid phase, where OBCaSu distorts the ZDDP structure when observed with

infra-red (IR) systems, with more changes expected during tribological test. It thus indicates that some of the ZDDP are consumed or modified in solution thereby minimizing the efficacy even before the tests. The mechanism involves retarding the decomposition rate of ZDDP by raising its decomposition temperature which increases the affinity of the detergent to the metal surface. Upon adsorption of the detergent to the surface, they modify it, thereby inhibit the adsorption of antiwear ZDDP molecules or depriving them of access to Fe which is essential for the initial break down of the ZDDP molecule.

This phenomena has also been supported by the works of Inoue [142] and Plaza [147] using adsorption isotherms. They showed that the adsorption of ZDDP is greatly reduced when Ca/Ba overbased sulphonates are used with the situation deteriorating further when phenate. type detergents are used – as in the case of Oil A [139]. Under this scenario, the detergents are firstly adsorbed on the surface and block the sites necessary for antiwear film formation. The corresponding bifilm has been reported to form a jelly like structure of basal islands that prevent the agglomeration of padlike antiwear films. The compounding reason for oil A forming heterogeneous and dispersed film has to do with the presence of the phenate detergent, lower ZDDP concentration and the type dispersants.

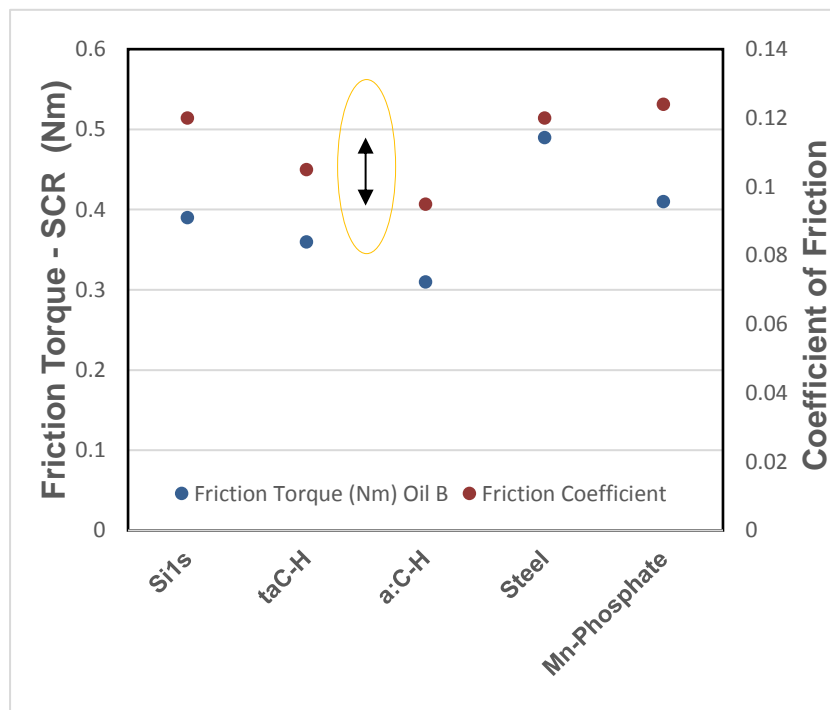
Dispersants consume the ZDDP molecule in solution by the formation of complexes. According to Ramakumar [139] and Galloupolos [150], additional infrared peaks were seen when dispersant were blended into ZDDP containing oils. The amino acid chain from the dispersant could coordinate with the ZDDP molecule to form N=P or C=P, C=N affecting the P=S bonding which inhibit the ZDDP antiwear film formation on tribological surfaces.

To prevent wear, the film derived should have the right composition and mechanical strength to minimise asperity-asperity contact [200]. FIB-SEM images of Oil B reveal that the film has a thickness ca 70 -100 nm and they are well dispersed than their counterpart (Oil A) which has a heterogeneous film and thickness ranging from ca 5-60 nm. The thick film may arise from regions of the surfaces that were not modified or adsorbed by the detergent or dispersant additives used in the oil. Nevertheless, film thickness have been reported to minimise wear on interacting surfaces [93, 145] but the concept of film dispersion and its role on interacting surfaces is still not completely understood. This work has shown that the dispersion of the film is equally important and it is grossly affected by detergent and dispersant.

Nano-indentation results have also shown that the mechanical properties of oil B are more durable for coverage area of the 10 x 10  $\mu\text{m}^2$  investigated. The hardness and reduced modulus of oil A as  $9.1 \pm 2.0$  GPa and  $135 \pm 25$  GPa respectively which is in line with the works of [230]. The hardness of the film is about 1.5 times better than those of oil A which is responsible for its superior wear properties.

### 9.5.3. Friction and Wear Comparison

Very few research works have compared the friction in a PoP tribometer and SCR owing to the different scales in which the friction parameters are obtained. Vast work in comparing reciprocating tribometers and SCR systems have been carried out by Gangopadhyay and coworkers [87]. Similar works are ongoing at the University of Leeds. In this research, we plotted the Friction torque for predominantly boundary lubrication regime (300 rpm) with the coefficient of friction. This should give some insight on the behavior of the systems.



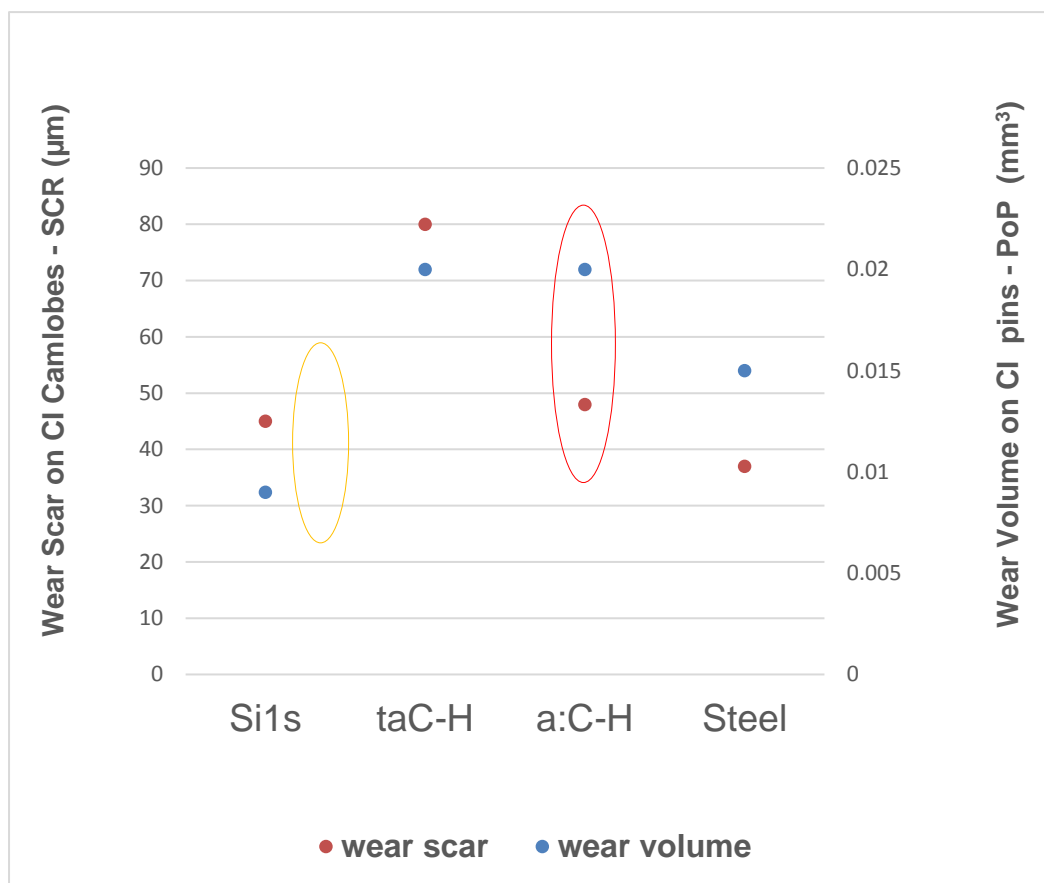
**Figure 9-2 Friction Comparison for SCR and PoP Tribometer Showing The Effects of Different Coatings When Tested Against a CI Counter-body With Oil B**

Figure 9-2 shows that the systems, behavior are only a mirror reflection of one another in boundary lubrication regime. This gives good credibility of the level of representation that can be obtained with the PoP tribometer for simulation of SCR system in boundary lubricated regime. The width difference also follows a particular



threshold except for steel perhaps due to the high reactivity of the surface with the lubricant additives. This results also supports the works of Mufti [5] and Torii [231] for more complex systems. Nonetheless, the results explains why both tribosystems are key to the development of engine valve train components.

Comparison of the wear data on the pin in a PoP and the camlobe in a SCR test have been used to reveal the effects of coating architectures on the counter-body. Both systems show a similar trend for all the coatings investigated but the effects are more severe on the pins. These values are in contrast to those obtained by [173]. Going through the data, it appears that the coating hardness affects the wear on the CI camshaft and pins. The Si1s and a:C-H (yellow and red circles gives an indication that it should be possible to design a coating surface that should improve the wear on both the CI camshaft and pin or perhaps a threshold hardness will be required to achieve optimum performance.



**Figure 9-3 Wear Comparison for CI Camlobes and Pins against Different Coatings When Tested with Oil B**

#### **9.5.4. Friction and Wear Mechanisms**

The mechanisms of friction and wear on interacting surface are summarized in Figure 9-4. The discussions of these mechanisms will be split with respect to the oil type.

##### **9.5.4.1. Oil B – Friction and Wear Mechanisms**

Oil B reduces wear by forming a well dispersed and thick tribofilm on the interacting surfaces [198]. The film equally has the right composition and mechanical strength to reduce asperity contacts. Based on its composition of a salicylate type detergent, surface analytic tests with XPS, FIB-SEM/EDX and HRTEM have shown that this type of detergent does not large distort the antiwear characteristics of the ZDDP additives when related to the film observed on the surfaces [146]. In PoP tests, well dispersed Ca –phosphate pads were seen on the CI surface supporting the results observed on the SCR tests.

The mechanism proposed for its formation of antiwear film has to do with the adsorption of the additives on steel surfaces. For sulphonated Salicylate type detergent, although they are very surface active and adsorb on the surface before the ZDDP [142], they also have good antiwear properties [141]. Likewise, in solution, they interact with the ZDDP molecule but have not been reported to form complexes. Nonetheless, they do not entirely inhibit the ZDDP molecule from having access to the ferrous surface, thereby increasing the formation of a complex Ca-phosphate/CaCO<sub>3</sub> wear resistant film on the surface[141]. Hence its mechanisms has to do with a co-adsorption of the additives. Simply speaking, this detergent has a unique antiwear characteristics and the degree to which it affects ZDDP molecule in solution and on interacting surfaces is minimal when compared with other detergents within its group.

On interaction with DLC coatings, few of the additives, particularly Ca and small amounts of Phosphorus have been observed to adsorb on the coating surface. These value are in agreement with [70]. This low level of adsorption of lubricant additives on the DLC suggests that the friction and wear properties are strongly controlled by the coatings. Similar results were obtained with oil A

##### **9.5.4.2. Oil A – Friction and Wear Mechanisms**

Oil A is a mixture of Ca/Mg sulphonates and phenate detergent with slightly lower ZDDP concentration. However, the phenate and sulphonates detergent combination are more antagonistic to ZDDP than salicylate type detergent [198]. FIB-SEM/EDX,

XPS and HRTEM reveal that the film is loosely dispersed on the surface and very thin (ca 5-60 nm). On inserts, in SCR, high surface wear have been observed when this oil is used[198].

In singular additive systems, OBCaSu are better antiwear additives than OBCaPh with the same or slightly lower concentration [141]. Essentially speaking, the phenate and sulphonates combination appear to have an antagonistic reaction within since OBCaSu are good antiwear additive. Likewise, the lower wear resistance of the oil appear to come from the phenate detergent. They are first adsorbed on the surface, where they modify it and prevent the co-adsorption of ZDDP. The lower concentration of the ZDDP should also make adsorption difficult. This strongly inhibit the dispersion of antiwear film on the surface.

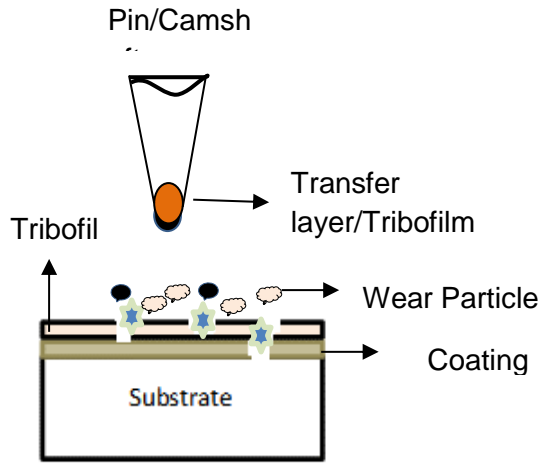
Hence, in highly loaded contacts like the valve train system, the surface modifying loosely bound antiwear films are removed during the rubbing action while the ZDDP molecule does not have direct access to the ferrous surfaces. These lack of access to 'pure' ferrous surfaces makes the film very heterogeneous while the modifying nature of the phenate additives prevent both the growth and agglomeration of the ZDDP pads.

#### **9.5.4.3. Base oil – Friction and Wear Mechanisms**

The group III base oil was only tested on the PoP tribometer to have a reference for comparison. Going through the optical micrographs it was observed that during rubbing with a:C-H and ta:C-H, a transfer layer was seen on the wear track. A closer look at the friction plot suggests that these films take about 2 hrs to fully build up for a:C-H and about 5 hrs for ta:C-H. After the build-up of the film on the cast iron pins, the surfaces are similar to a tribopair of a:C-H and ta:C-H. The friction values are in agreement with the works of [32, 35, 179].

These mechanisms are different from what was observed for the Si1s coating. From the friction plots, the coating appeared to be stripped off after 2 hrs of testing and the friction values rose to that of steel. SEM/EDX reveal Si1s in the wear track and on the CI pins. Figure 9-4, has been used to show the mechanism with base oil. Significant wear particles were trapped in the wear scar for Mn-phosphate and Si1s. These particles are harder than the substrate thereby increasing the wear by an abrasive mechanism. For steel, the base oil did not form a protective film which had the ability to withstand the loads of the system. For a:C-H and ta:C-H, a thick transfer layer which takes about 1-2 hrs to build up reduced the friction to a DLC/DLC tribopair.

Under the DLC/DLC developed interaction, the wear was considerably lower as both surfaces exhibited close hardness



Plate/Inserts

Based on oil type  
For both PoP and DLC's

Base oil

- Significant transfer layer from plate to pin.
- Friction is controlled by these transfer layer and the interacting surface exhibit coefficient of friction similar to DLC/DLC tribopairs.
- Not similar for Si1s due to coating strip off. Surfaces exhibit CI/Steel coefficient of Friction.
- Increase wear due to large amount of third body abrasive wear particles

Based on oil type

For both PoP and SCR

Oil B

- Significant oil spreading on metal surfaces.
- Thicker tribofilms.
- Tribofilms possess good mechanical strength due to balanced composition of Zn, P, Ca and S.
- Lesser wear particles thereby reducing third body abrasive wear.

Based on DLC coating  
Tribological/Tribochemistry

Different oils

- Loosely bonded film
- Certain lubricant additives particularly Zn and P, do not adsorb on the coating surface but when they do, they appear loosely bonded to the coated surface.
- The type of the oil and coating hardness are the two key parameters that influence the wear

**Figure 9-4 Mechanisms of Friction and Wear for Different Oils and Coating Combinations**

## 9.6. Level of Prediction & Economic Significance of Valve Train Tests

Valve train rigs can lead to huge monetary savings when the tests are properly designed. According to the reports from Mufti [5], the friction responses in valve train rigs mirrored those observed in fired tests. Torii [231] has also shown that more can be achieved at low speed, constant and cyclic test conditions. Following these results, tests our study showed that Si1s coatings did not perform satisfactorily in the valve

train system, thereby making further fired engine tests unnecessary. This could help minimize extended engine tests carried out on engine components thereby leading to lower costs for original equipment manufacturers. Another compelling results was obtained when the friction torque from oil A and oil B were compared.

Using the same scale from [218], we can suggest that a 1-2% fuel economy can be achieved with the oil A. These values are similar for those from the a:C-H when compared with [32, 33, 197]. For the ta:C-H coating, a 0.8-1.2 % fuel economy can be estimated when only the insert is coated. On coating the cam and follower with ta:C-H, the values are slightly higher (around 2.5). However, care should be taken as coating the cam and follower with ta:C-H have produced some unfavorable durability issues where the coating delaminates on the cam after 50 hrs testing. This suggests that during extended tests, the system will lose the coating necessary for its optimal performance and the high friction benefits will be greatly reduced. In fired conditions, the process could be more rapid than expected due to hot exhaust gases.

Nonetheless, valve train components tests are crucial to the overall develop of the engine and should been given due attention as they more closely mimics the operating conditions of the system in service. The results provide significant insights into coating and lubricant additive performance.

## **CHAPTER 10. CONCLUSIONS AND FUTURE WORK**

### **10.1. Conclusions**

The conclusions in this thesis can be split into two broad groups of Single cam rig and pin on plate tribometers. For the single cam rig tests, the conclusions are divided into the different aspects of rig development, tribochemistry results on the inserts (steel surfaces) and the effects of coating both on the cam and the follower

#### **10.1.1. Single Cam Rig Development**

- A single cam rig has been developed, with high sensitivity to distinguish the frictional responses of surface coatings as well as fully formulated lubricants with very close chemistries.
- Good repeatability and consistency from the experimental protocol for the validation tests indicates that the newly developed rig, its instrumentation, data processing/acquisition and operational procedures are reliable. They can provide valid information with confidence.
- The rig is capable of providing data that can accurately reveal the torque benefits that can be achieved at different location on the camlobes. This can go a long way in identifying regions on the camlobe where torque reductions are of paramount interest to the design engineer.

#### **10.1.2. Single Cam Rig Tribochemistry**

- Tribochemical investigations of the inserts are in close agreement with previous studies. Temperature and additive concentration appear to affect the distribution of phosphate films on the inserts. More densely packed and well dispersed films were observed at 75°C & 105°C on inserts tested with oil B which has a higher concentration of primary ZDDP additives. This resulted in better wear prevention.
- The composition and structure of the tribofilm has a huge impact on the friction and wear response of the system. The presence of Zn, P, and S were shown to have significant impact on the antiwear properties of the tribofilm. They have been shown to affect the durability of the films on the surface.
- Nano – indentation test with oil B show that the films are considerably harder and well dispersed than oil A.
- The films of oil B consist of long chain poly phosphates of chain length between 5-10 in the topmost surface which is gradually degraded to pyro and

orthophosphates in the bulk. Oil A primarily consists of short chain Calcium pyro and orthophosphates. TEM diffraction patterns reveal some third body abrasive particle of aluminium oxides (from engine block) and haematite trapped in the wear track. Aluminium oxides are harder than haematite and this will surely aggravate the wear processes observed with oil A.

- The tribofilm consist of a two layered structure in regions on the tappets with limited rubbing action. First layer consist of an oil rich phase followed by dense tribofilm. In the insert centre where rubbing with the nose, flank, shoulder and ramp of the cam occurs, the tribofilm does not show a two-layered structure. It shows a dense matrix with significant metallic oxides as well.

### **10.1.3. Consequences of Insert Coating**

- Increased wear is observed on the rising edge of the cam i.e. the section responsible for the opening of the valves. These were determined with the talysurf contact interferometry where the positive section (+14°, +10°, +4°) showed higher wear than the negative section for all the camlobes tested.
- The cam nose is a region of significant wear and the antiwear phosphate film compose of short chain Calcium orthophosphates.
- Although significantly marked reduction in friction was achieved, the hardness of the coated insert/follower affects the wear on the camlobes. This was seen to contribute a marked difference to the wear on the cam-nose with little effect at ±14°.
- Si1s showed no sulphate on the camlobe while taC-H revealed some sulphate peaks. They have been reported to be corrosive and increase wear.
- The absence of visible phosphate peaks at the nose and 10° away are also responsible for the increased wear on the camlobes. This tribofilm absence can be attributed to a removal action by the taC-H coated follower.

### **10.1.4. Consequences of Coating Both the Cam and the Insert**

The conclusions from coating both the cam and the follower are not entirely direct. It appears a trade-off between friction and wear/tribofilms must be made before any choice can be drawn.

- By coating both the cam/follower with taC-H/taC-H, huge reduction in friction was achieved but delamination of the coating on the follower was seen by visual inspection. This delamination also took place a specific location on the

- cam nose which indicates, a loading mechanism. This is called edge loading and the taC-H coating cannot withstand this phenomena despite its hardness.
- Making the coating harder will not solve the problem as a:C-H (which has lower hardness) did not delaminate. The outcome suggests that a threshold between hardness and reactivity with lubricant additives must be obtained for the optimal coating performance in a valve train system.

## 10.2. Future Work

This aspect of the thesis itemises areas that were not adequately covered or investigated during this research project. It was divided into three main sections of;

- Single cam rig development: Essentially, this section give some modifications which can be made to the rig and its components and/or (samples) that will improve the tribological and tribochemical understanding of the system.
- Tribochemistry of valve train systems: While this work has discussed the tribochemical interaction of two commercial lubricants, with three industrial coating architectures, it was observed that interaction between these two are grossly lacking as lubricants were ideally designed of ferrous surfaces. Research into lubricant additives that interact with oil additives while improving the friction and wear is of paramount interest for the automotive industry particularly; in sliding rolling contacts.
- Modelling of the single cam rig.

### 10.2.1. On Single Cam Rig Development

In order to determine the dynamic load variation with camshaft speed, a kistler load cell was mounted on the camlobe holder in the newly developed single cam rig. This was to enable us evaluate the force transmitted during the opening and closing of the valves and also to perhaps determine the coefficient of friction according to the Equation 10-1 (from the energy balance or principle of virtual work).

$$T = P \left[ \frac{\dot{s}}{\omega} + \mu(s + r_b) \right]$$

**Equation 10-1**



Where  $T$  is the torque,  $P$  is the normal load on the cam,  $r_b$  is the radius of base circle,  $s$  is the cam lift,  $\mu$  is the coefficient of friction, and  $\omega$  is the cam angular velocity.

Unfortunately, the load cell was observed to be influenced by dynamic input with significant phase shift [232]. This caused the amplitude in the voltage profile to significantly increase and the values could not be readily retraced to the initial position. Hence, the result obtained with such load cells were deemed spurious and could not be used in the determination of the friction loads. One method of overcoming this problem would be to install load cells that have phase shift compensation. With such load cells, the voltage amplitude would be significantly diminished or eliminated thereby ensuring that the values obtained are reflective of the properties of the system. According to the works of Sun and Rosenberg [232], one load cell was selected for steady state test and another for dynamic load test in a single cam rig. One fundamental challenge with this process is that the load in the single cam rig system is a variable. According to Equation 10-1,  $P$ , is the resultant of the weight and loading of the follower, the resistance inertia and the spring forces. This relationship can only be determined with experimental data and perhaps well-developed models. Once the relationship is obtained, the coefficient of friction at corresponding points on the camlobe can be accurately evaluated [13].

### **10.2.2. Effects of Tappet/Insert Rotation on Tribochemistry**

In the literatures studied [186, 233, 234], the focus has been on the effect of tappet rotation on friction and wear with no consideration of the effect of tappet rotation on the tribofilm. Thus information on the tribofilms which are derived on the interacting surfaces are grossly lacking. Controlling the rotation of the tappet is not easy but by measuring its free rotation, valid information of the rolling velocity, oil film thick, wear and tribofilm can be adequately investigated. According to Bona and Ghilardi [233], increased tappet rotation improve the surface finish which ideally should reduce pitting, but this can also increase the likelihood of fatigue. Certain additives have been reported to increase pitting [93] and it will be very interesting to observe the role of lubricant additive on the tappet rotation.

### **10.2.3. SLA Technique for Cam Wear Measurements.**

Surface layer activation (SLA) is a widely used technique for the investigation of camlobe wear [90, 221, 235]. It can also be used at specific locations on the cam

lobes (e.g. the cam nose) [221]. Evaluation of the wear rates at the breaking-in and steady state periods of the valve train operation can also be accurately determine [235]

Practically speaking, it involves the bombardment of the wear regions on the camlobe with energetic particles of ion (particularly  $^{56}\text{Co}$  or  $^{57}\text{Co}$ ) from a linear accelerator. This induces a nuclear reaction which leads to the formation of radionuclides. These radionuclides which are formed on the surface of the camlobes usually possess a thickness between 10 – 300  $\mu\text{m}$  and do not alter the metallurgical structure of the substrate metal. This technique permits a real time online monitoring of the wear on the camlobes by the use of radio-nuclide isotopes which are read off from the lubricant sumps. A Geiger counter is used to trace or read off these particles at different times and the wear rate can be accurately determined. However care should be taking when using this technique as it can only record data during abrasive wear processes. For an adhesive wear mechanism where the wear particles are transferred to the counter body, the Geiger count will detect a zero result when wear has actually taken place. A similar phenomena may be experienced with polishing and scuffing which are wear mechanisms which are particular to valve train system.

Notwithstanding, a more compact SLA system has been developed at the Austria Centre for competence in Tribology (AC2T) and it will be worthwhile to incorporate this system into the single cam rig for real time online monitoring of wear on the camlobes.

#### **10.2.4. ECR for Indirect Determination of Film Thickness**

Although this technique has been used in previous studies [12, 168, 236], it would be vital to have the rig equipped with the method of film thickness evaluation. Gao and coworkers have shown that increased phosphorus concentration in the oil provide thicker films which are read off from the electric contact configuration. Although there is no direct contact between electrical properties and film thickness, Uy [168] has also employed this same method with significant findings. In their configuration, a zero contact voltage was indicative of a metal to metal contact and the presence of an electrically insulating film between asperities. The presence of a conducting film gave rise to a voltage drop which can be read off from a voltmeter to give the voltage drop across the cam profile or contact point. The most notable advance of this technique was demonstrated by Dowson [12] using an electrical resistivity technique to

determine film state across a cam profile). The technique can be explore for novel additives with electrical conductivity.

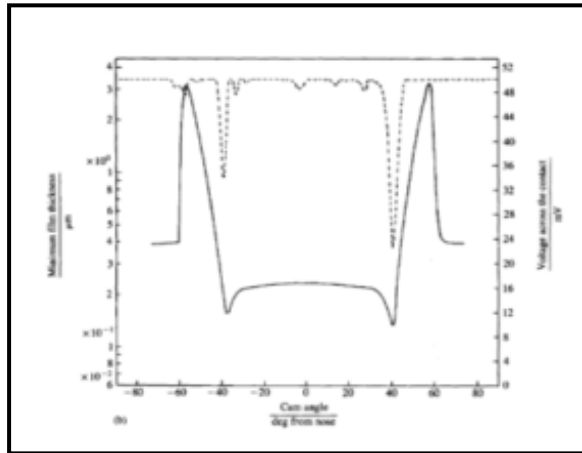


**Figure 10-1 Film state measurement across cam profile using ECR [12]**

### **10.2.5. Lubricant Additive Investigation**

Evaluation of additive performance, reaction kinetics and tribofilm composition are of significant interest to both the tribologist and lubricant formulators. However, assessing these additive in systems that closely mimic their operation in service is a bit of a challenge. In the literature, perhaps only [51, 102, 141] have investigate additive components in valve train systems. The current changes in additive concentration and environmental legislation, call for further research work in new formulation as well as the identification of novel additives. This additivated packages should have the right properties for tests on the single cam rig.

For instance, during round trials on the rig, base oil have been used for cleaning processes and short runs with the rig was observed to produce some noise. However, further tests with ZDDP additive oil from TOTAL have been investigated and the noise levels were eliminated. Therefore, with the right viscosity, it will be very interesting to investigate model oils with singular or multiple additives in a sliding-rolling contact. Unique and new additive packages can also be investigated to determine their friction/wear benefits as well as the tribofilms derived on the interacting surface.

### **10.2.6. Single Cam Rig Modelling**

#### **10.2.6.1. Friction and Wear Models**

Modelling the friction on the cam profile requires an understanding of the cam profile and the entire valve train system. The lubrication regime across the cam profile

exhibits boundary lubrication at the nose, mixed lubrication at the flank/ramp with EHL at the shoulder. Each lubrication regime are governed by different principles which makes modelling more complicated. According to Hu [237] and Hol [238], the change in surface topography was used to determine the wear and evolution of surface friction in boundary lubrication. In EHL where the high pressures lead to the deformation of solids, this procedure will not be ideal. Hence, a different friction and wear model will have to be developed for each lubrication regime. Due to the transient nature of the contact in the cam follower systems, it will be unique to develop models for micro displacements of surfaces subject to transient sliding. This will be suitable for simulations of the cam nose and some insights can be obtained from [239]

In Mixed regime, part of load is shared between the asperities and the lubricant film. Therefore, most models for this regimes have utilized a load sharing concept [237, 240] with due consideration of the surface topography. In all these studies, the focus has been on sliding contact. In a valve train system, the contact is of a sliding-rolling nature and models covering these systems are still lacking. Investigation into such systems while considering the laws governing the lubrication regime, a unique model can be developed which can give a better understanding into the friction and wear at specific locations on the camlobe – be it the nose, flank, shoulder, base circle or ramp.

#### **10.2.6.2. Tribochemistry Models in Valve Train Systems**

In order to develop a suitable friction and wear model, significant consideration should be given to the tribochemical films which are few tenth of nanometres thick.

In the literature, there are few works in tribochemistry models, According to Bosman[241], he modelled tribochemistry evaluating the growth of the tribofilm and its removal using a diffusion reaction. Ghanbarzadeh et al [242], used a non-equilibrium thermodynamics of tribochemical reactions to develop a tribofilm growth model based on local properties of contact on rough surfaces. This model is able to consider the effect of antiwear tribofilm on the localised wear of boundary lubricated systems. It was a valid stating point to look at macroscale measurements with microscale simulation of rough surfaces.

These tribofilm models can be extended to study rolling sliding contacts in the mixed lubrication regime in order to simulate valve train tribochemistry

## APPENDIX A

### Properties and Definitions

#### Molar Mass

Molecular mass is defined as the sum of the atomic masses of a molecule. It has its SI units in kilogram but scientifically, the atomic mass is the preferred units.

#### Concentration of Mixtures

A lubricant is made up of various additives blended in unequal proportions. Suppose we have an engine lube with mass  $M$  and volume  $V$ , the concentration of species with mass  $m_i$  is given by;

$$C_i = \frac{m_i}{V} \quad \text{Equation A- 1}$$

$$\sum_{i=1}^n m_i = M \quad \text{Equation A- 2}$$

$$\sum_{i=1}^n C_i = \rho \quad \text{Equation A- 3}$$

Where  $C_i$  is the concentration of additives,  $m_i$  mass of additives,  $M$  mass of engine lubricant and  $\rho$  is the density of the lubricant. Chemists usually express this in mole per  $\text{dm}^3$  but tribologists prefer to represent this in ppm or more commonly in mass fractions. It is worthwhile to mention that the concentrations are temperature and pressure dependent.

#### Molar Fraction

This is the ratio of the number of moles of an additive ( $n_i$ ) to the total number of moles in the engine lubricant mixture. A lubricant mixture of mass  $M$  is composed of  $n_1$  moles of additive 1,  $n_2$  moles of additive 2 and  $n_i$  moles of additive  $i$ , the molar fraction can be written as ;

$$x_i = \frac{n_i}{n_1 + n_2 \dots n_i} = \frac{n_i}{\sum n_i} \quad \text{Equation A- 4}$$

$$x_1 + x_2 + \dots x_i = \sum_i x_i = 1 \quad \text{Equation A- 5}$$

#### Mass Fraction

This is the ratio of mass of additive specie (say  $m_i$ ) to the total mass of the engine lubricant mixture  $M$ . it is mathematically represented as;

$$w\% = m_f = \frac{m_i}{M} = \frac{m_i}{\sum_i m_i}$$

Equation A- 6

## APPENDIX B

### Lubricant Categories based on Phosphorus and Ash Levels

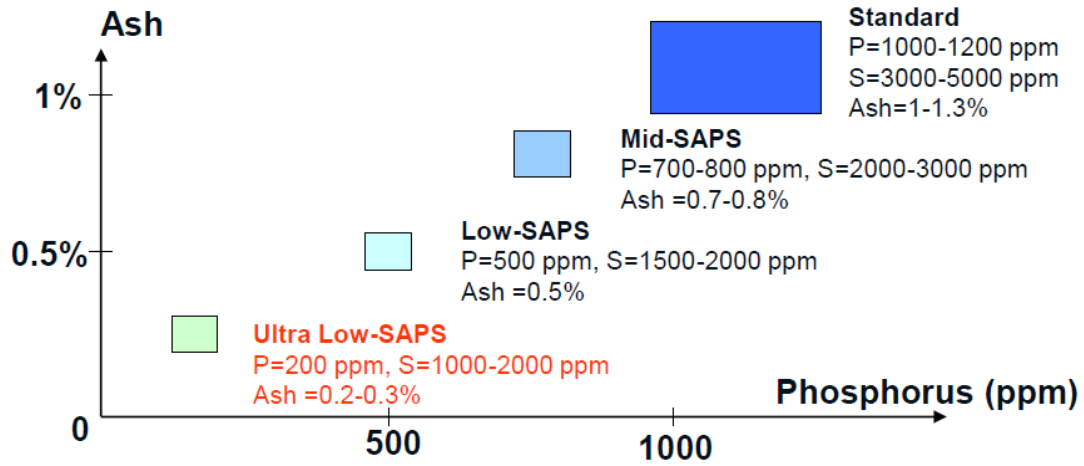


Figure B- 1 Engine Lubricant Classification

## Engine Cylinder Layout

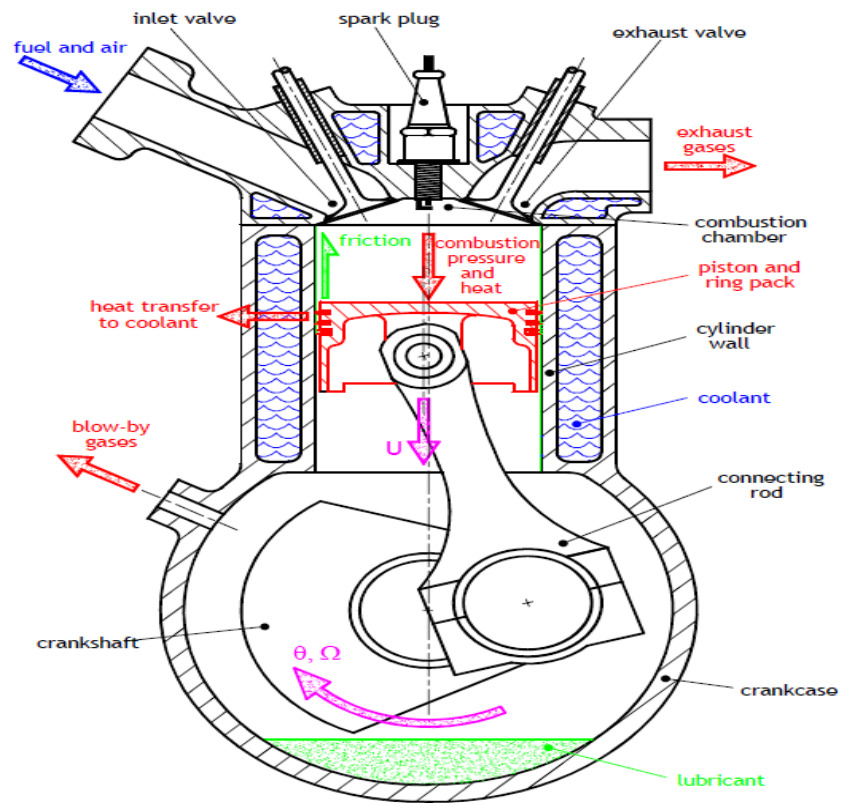
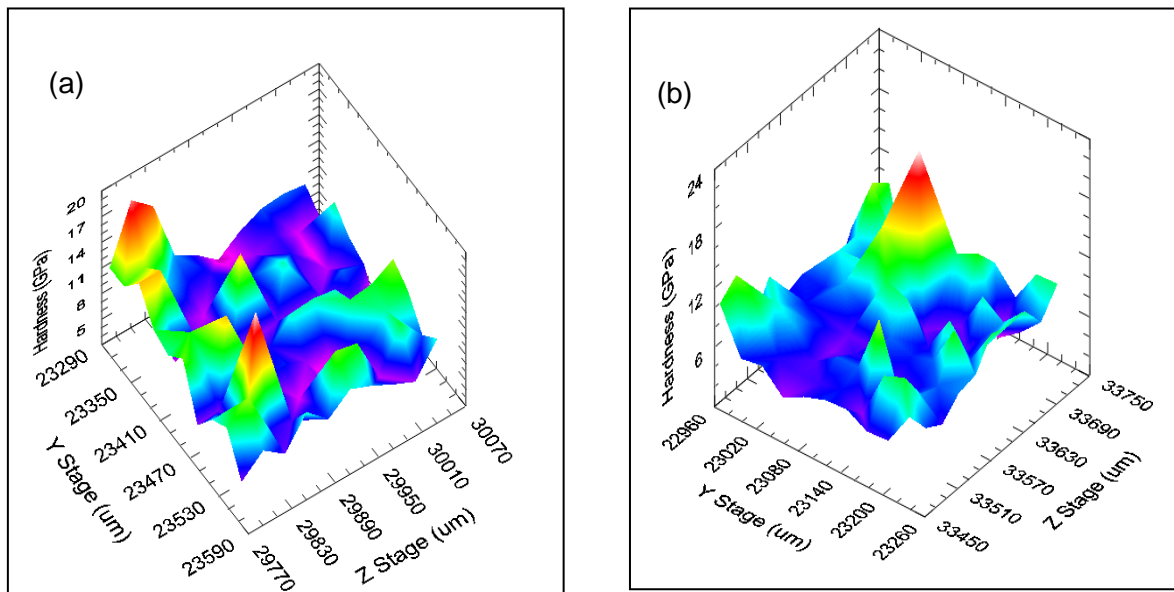


Figure B- 2 Typical Four Stroke Gasoline Cylinder Engine Layout

## APPENDIX C



C. 1 Hardness of tribofilm formed (a) Oil FFB (b) Oil FFA

## REFERENCES

- [1] M. T. Costello and R. A. Urrego, "Study of surface films of the ZDDP and the MoDTC with crystalline and amorphous overbased calcium sulfonates by XPS," *Tribology Transactions*, vol. 50, pp. 217-226, 2007.
- [2] J. Zhang, E. Yamaguchi, and H. Spikes, "The Antagonism between Succinimide Dispersants and a Secondary Zinc Dialkyl Dithiophosphate," *Tribology Transactions*, vol. 57, pp. 57-65, 2014/01/02 2013.
- [3] A. Morina, J. H. Green, A. Neville, and M. Priest, "Surface and Tribological Characteristics of Tribofilms Formed in the Boundary Lubrication Regime with Application to Internal Combustion Engines," *Tribology Letters*, vol. 15, pp. 443-452, 2003/11/01 2003.
- [4] A. Gangopadhyay and D. G. McWatt, "The Effect of Novel Surface Textures on Tappet Shims on Valvetrain Friction and Wear," *Tribology Transactions*, vol. 51, pp. 221-230, 2008/03/25 2008.
- [5] R. Mufti and M. Priest, "Effect of cylinder pressure on engine valve-train friction under motored and fired conditions," *Proceedings of the Institution of Mechanical Engineers, Part J: Journal of Engineering Tribology*, vol. 226, pp. 306-314, April 1, 2012 2012.
- [6] T. Kanzaki, N. Hara, A. Mori, and K. Ohtsubo, "Advantage of lightweight valve train component on engines," SAE Technical Paper 0148-7191, 1998.
- [7] K. Hanada, Y. Murakami, Y. Shoji, H. Aihara, and A. Hirose, "Development of a Valve Train Wear Test Procedure for Gasoline Engine Oil," SAE Technical Paper 0148-7191, 1994.
- [8] I.-S. Suh and R. H. Lyon, "An investigation of valve train noise for the sound quality of IC engines," SAE Technical Paper 0148-7191, 1999.
- [9] D. M. Beloiu, "Modeling and analysis of valve train, part I -conventional systems," *SAE International Journal of Engines*, vol. 3, pp. 850-877, 2010.
- [10] C. M. Taylor, "Valve Train - Cam and Follower:Background and Lubrication Analysis, in engine tribology," *Tribology Series 26*, pp. 159 -182, 1993.
- [11] G. Zhu, "A Theoretical and Experimental Study of the Tribology of a Cam and Follower," Doctor of Philosophy, Mechanical Engineering PhD Thesis, University of Leeds 1988.
- [12] D. Dowson, P. Harrison, C. Taylor, and G. Zhu, "Experimental observation of lubricant film state between a cam and bucket follower using the electrical resistivity technique," in *Proceedings of the Japan international tribology conference*, 1990, pp. 119-124.
- [13] F. U. Chen, "Mechanics and Design of Cam Mechanisms," *Book*, vol. 1, 1982.
- [14] S. Günsel, H. A. Spikes, and M. Aderin, "In-Situ Measurement of ZDDP Films in Concentrated Contacts," *Tribology Transactions*, vol. 36, pp. 276-282, 1993/01/01 1993.
- [15] M. Priest, "Introduction to Tribology," *University of Leeds, Teaching Manual*, vol. 1, pp. 1 -76, 2011.



- [16] A. Dyson, "Kinematics and wear patterns of cam and finger follower automotive valve gear," *Tribology International*, vol. 13, pp. 121-132, 1980.
- [17] C. Taylor, "Fluid film lubrication in automobile valve trains," *Proceedings of the Institution of Mechanical Engineers, Part J: Journal of Engineering Tribology*, vol. 208, pp. 221-234, 1994.
- [18] A. Ito, L. Yang, and H. Negishi, "A study on cam wear mechanism with a newly developed friction measurement apparatus," SAE Technical Paper 0148-7191, 1998.
- [19] P. S. Y. Chu and A. Cameron, "Flow of Electric Current Through Lubricated Contacts," *A S L E Transactions*, vol. 10, pp. 226-234, 1967/01/01 1967.
- [20] G. Williamson B.P, I.R. and Benwell, S., "Measurement of Oilfilm thickness in the Elasto-Hydrodynamic contact between a cam and Bucket follower in a Motored Cylinder Head: Newtonian Oils int. Fuels and Lubricants Meeting and Exposition, Baltimore, Maryland, USA.,," *SAE Int. J. Engines*, vol. 1, p. 11, 1989.
- [21] G. M. Hamilton, "The hydrodynamics of a cam follower," *Tribology International*, vol. 13, pp. 113-119, 1980.
- [22] A. K. Gangopadhyay, R. O. Carter, S. Simko, H. Gao, K. K. Bjornen, and E. D. Black, "Valvetrain Friction and Wear Performance with Fresh and Used Low-Phosphorous Engine Oils," *Tribology Transactions*, vol. 50, pp. 350-360, 2007/06/26 2007.
- [23] E. Yamaguchi, P. Ryason, and T. Hansen, "Electrical contact resistance studies on zinc dithiophosphates," *Tribology Letters*, vol. 3, pp. 27-33, 1997.
- [24] E. S. Yamaguchi, P. R. Ryason, S. W. Yeh, and T. P. Hansen, "Boundary Film Formation by ZnDTPs and Detergents Using ECR," *Tribology Transactions*, vol. 41, pp. 262-272, 1998/01/01 1998.
- [25] A. Gangopadhyay, D. G. McWatt, R. J. Zdrodowski, S. J. Simko, S. Matera, K. Sheffer, *et al.*, "Valvetrain Friction Reduction through Thin Film Coatings and Polishing," *Tribology Transactions*, vol. 55, pp. 99-108, 2012/01/01 2011.
- [26] A. Katoh and Y. Yasuda, "An analysis of friction reduction techniques for the direct-acting valve train system of a new-generation lightweight 3-Liter V6 Nissan engine," SAE Technical Paper 0148-7191, 1994.
- [27] E. Ciulli, B. Piccigallo, and D. Vela, "Experimental study of engine cam-followers," in *Proceedings of the XIX Congresso AIMETA, Ancona*, 2009, pp. 14-17.
- [28] J. R. Davis, "Friction and Wear of Internal Combustion Engine Parts," *ASM Handbook*, vol. 18, pp. 553 - 560, 1992.
- [29] M. Masuda, M. Ujino, K. Shimoda, K. Nishida, I. Marumoto, and Y. Moriyama, "Development of titanium nitride coated shim for a direct acting OHC engine," SAE Technical Paper 0148-7191, 1997.
- [30] B. Hanula, J. Radeckzy, R. Ernst, S. Weinzierl, and M. Fuchs, "The Potential of the Ceramic Valve in IC Engines," SAE Technical Paper 0148-7191, 2003.

- [31] S. G. Ahn, H. O. Ban, B. L. Jo, S. C. Kim, and S. C. Jung, "Development of supercarburized tappet shim to improve fuel economy," SAE Technical Paper 0148-7191, 2000.
- [32] M. Kano, "Super low friction of DLC applied to engine cam follower lubricated with ester-containing oil," *Tribology International*, vol. 39, pp. 1682-1685, 2006.
- [33] M. Broda and R. Bethke, "Friction Behavior of Different DLC Coatings by using Various Kinds of Oil," *SAE Int. J. Mater. Manuf.*, vol. 1, pp. 832-840, 2008.
- [34] A. Kodai, T. Mori, and T. Inukai, "Applying Hard thin coatings to tappets to reduce friction," SAE Technical Paper 0148-7191, 2001.
- [35] B. Vengudusamy, J. H. Green, G. D. Lamb, and H. A. Spikes, "Tribological properties of tribofilms formed from ZDDP in DLC/DLC and DLC/steel contacts," *Tribology International*, vol. 44, pp. 165-174, 2011.
- [36] S. Okuda, T. Dewa, and T. Sagawa, "Development of 5W-30 GF-4 fuel-saving engine oil for DLC-coated valve lifters," SAE Technical Paper 0148-7191, 2007.
- [37] M. Woydt and J. Ebrecht, "Testing friction and wear of the tribosystem piston ring and cylinder liner outside of engines," *Tribotest*, vol. 14, pp. 113-26, 2008.
- [38] J. C. Bell and T. A. Colgan, "Critical physical conditions in the lubrication of automotive valve train systems," *Tribology International*, vol. 24, pp. 77-84, 1991.
- [39] K. Mistry, A. Morina, and A. Neville, "Single cam tribometer for evaluating tribological parameters and tribochemistry of DLC coated valve train follower," *Tribology - Materials, Surfaces and Interfaces*, vol. 6, pp. 31-37, 2012.
- [40] J. E. Booth, T. J. Harvey, R. J. K. Wood, and H. E. G. Powrie, "Scuffing detection of TU3 cam-follower contacts by electrostatic charge condition monitoring," *Tribology International*, vol. 43, pp. 113-128, 2010.
- [41] E. W. Schneider and D. H. Blossfeld, "Real-Time Measurement of Camshaft Wear in an Automotive Engine-a Radiometric Method," SAE Technical Paper 0148-7191, 1990.
- [42] A. Gauthier and T. Delvigne, "Soot induced cam wear in diesel engines: An investigation using thin layer activation," SAE Technical Paper 0148-7191, 2000.
- [43] L. L. W. H. Shaub, "Real Time Radioactive Marker Technique for Measuring Valve Train Wear , ," *SAE 872156, International Fuels and Lubricants (Toronto)*, , vol. 1, Nov, 1987.
- [44] I. Minami, T. Kubo, H. Nanao, S. Mori, T. Sagawa, and S. Okuda, "Investigation of Tribo-Chemistry by Means of Stable Isotopic Tracers, Part 2: Lubrication Mechanism of Friction Modifiers on Diamond-Like Carbon," *Tribology Transactions*, vol. 50, pp. 477-487, 2007/10/23 2007.
- [45] T. S. Eyre and B. Crawley, "Camshaft and cam follower materials," *Tribology International*, vol. 13, pp. 147-152, 1980.
- [46] A. Dyson, "Scuffing - a review," *Tribology International*, vol. 8, pp. 77-87, 1975.

- [47] A. Neville, A. Morina, T. Haque, and M. Voong, "Compatibility between tribological surfaces and lubricant additives—How friction and wear reduction can be controlled by surface/lube synergies," *Tribology International*, vol. 40, pp. 1680-1695, 2007.
- [48] Y. Enomoto and T. Yamamoto, "New materials in automotive tribology," *Tribology Letters*, vol. 5, pp. 13-24, 1998.
- [49] J. Michalski, J. Marszalek, and K. Kubiak, "An experimental study of diesel engine cam and follower wear with particular reference to the properties of the materials," *Wear*, vol. 240, pp. 168-179, 2000.
- [50] E. P. Becker, "Trends in tribological materials and engine technology," *Tribology International*, vol. 37, pp. 569-575, 2004.
- [51] M. Soejima, Y. Ejima, Y. Wakuri, and T. Kitahara, "Improvement of Lubrication for Cam and Follower," *Tribology Transactions*, vol. 42, pp. 755 - 762, 2008.
- [52] H. Izumida, T. Hishioka, A. Yamakawa, and K. Matsunuma, "A Study of the Effects of Ceramics Valve Train Parts on Reduction of Engine Friction Evaluation of High Strength Si3N4 Tappet Shims by Motoring Apparatus," *JSAE Review*, vol. 16, pp. 326-326, 1995.
- [53] D. Zhu and H. S. Cheng, "Vehicle Tribology - Tribological Performance Ceramic Roller Followers/Camshaft System in Automobile Valve Trains," *Tribology Series 18*, vol. 18, pp. 149 - 156, 1991.
- [54] M. Kano and I. Tanimoto, "Wear mechanism of high wear-resistant materials for automotive valve trains," *Wear*, vol. 151, pp. 229-243, 1991.
- [55] S. Fukuoka, N. Hara, A. Mori, and K. Ohtsubo, "Friction loss reduction by new lighter valve train system," *JSAE Review*, vol. 18, pp. 107-111, 1997.
- [56] B. J. Taylor and T. S. Eyre, "A review of piston ring and cylinder liner materials," *Tribology International*, vol. 12, pp. 79-89, 1979.
- [57] D. Scott, A. I. Smith, J. Tait, and G. R. Tremain, "Materials and metallurgical aspects of piston ring scuffing — A literature survey," *Wear*, vol. 33, pp. 293-315, 1975.
- [58] C. Verpoort, K. Bobzin, F. Ernst, K. Richardt, T. Schlaefer, A. Schwenk, *et al.*, "Thermal spraying of nano-crystalline coatings for Al-cylinder bores," SAE Technical Paper 0148-7191, 2008.
- [59] S. Johansson, P. H. Nilsson, R. Ohlsson, and B.-G. Rosén, "Experimental friction evaluation of cylinder liner/piston ring contact," *Wear*, vol. 271, pp. 625-633, 2011.
- [60] J. J. Truhan, Q. Jun, and P. J. Blau, "The effect of lubricating oil condition on the friction and wear of piston ring and cylinder liner materials in a reciprocating bench test," *Wear*, vol. 259, pp. 1048-55, 2005.
- [61] P. Kodali and N. Stanley, "Exploring PVD coatings for cylinder liner applications," SAE Technical Paper 0148-7191, 2001.
- [62] M. Kano and Y. Kimura, "Quantitative analysis of cam follower wear in relation to various material properties," *Wear*, vol. 162–164, Part B, pp. 897-905, 1993.

- [63] S. Miyake, T. Saito, Y. Yasuda, Y. Okamoto, and M. Kano, "Improvement of boundary lubrication properties of diamond-like carbon (DLC) films due to metal addition," *Tribology International*, vol. 37, pp. 751-761, 2004.
- [64] M. I. De Barros'Bouchet, J. M. Martin, T. Le-Mogne, and B. Vacher, "Boundary lubrication mechanisms of carbon coatings by MoDTC and ZDDP additives," in *Boundary Lubrication*, 2005, pp. 257-264.
- [65] A. Erdemir, "The role of hydrogen in tribological properties of diamond-like carbon films," *Surface and Coatings Technology*, vol. 146–147, pp. 292-297, 2001.
- [66] J. Andersson, R. A. Erck, and A. Erdemir, "Frictional behavior of diamondlike carbon films in vacuum and under varying water vapor pressure," *Surface and Coatings Technology*, vol. 163–164, pp. 535-540, 2003.
- [67] S. Lawes, M. Fitzpatrick, and S. V. Hainsworth, "Evaluation of the tribological properties of DLC for engine applications," *Journal of Physics D: Applied Physics*, vol. 40, p. 5427, 2007.
- [68] T. Horiuchi, K. Yoshida, M. Kano, M. Kumagai, and T. Suzuki, "Evaluation of DLC coating damage in the delamination and wear test," *Tribology Online*, vol. 5, pp. 129-135, 2010.
- [69] B. Podgornik, S. Jacobson, and S. Hogmark, "DLC coating of boundary lubricated components—advantages of coating one of the contact surfaces rather than both or none," *Tribology International*, vol. 36, pp. 843-849, 2003.
- [70] B. Podgornik and J. Vižintin, "Tribological reactions between oil additives and DLC coatings for automotive applications," *Surface and Coatings Technology*, vol. 200, pp. 1982-1989, 2005.
- [71] A. Vanhulsel, B. Blanpain, J. P. Celis, J. Roos, E. Dekempeneer, and J. Smeets, "Study of the wear behaviour of diamond-like coatings at elevated temperatures," *Surface and Coatings Technology*, vol. 98, pp. 1047-1052, 1998.
- [72] R. Gilmore and R. Hauert, "Control of the tribological moisture sensitivity of diamond-like carbon films by alloying with F, Ti or Si," *Thin Solid Films*, vol. 398, pp. 199-204, 2001.
- [73] A. A. Voevodin, A. W. Phelps, J. S. Zabinski, and M. S. Donley, "Friction induced phase transformation of pulsed laser deposited diamond-like carbon," *Diamond and Related Materials*, vol. 5, pp. 1264-1269, 1996.
- [74] Y. Liu, A. Erdemir, and E. I. Meletis, "A study of the wear mechanism of diamond-like carbon films," *Surface and Coatings Technology*, vol. 82, pp. 48-56, 1996.
- [75] H. Ronkainen, S. Varjus, and K. Holmberg, "Friction and wear properties in dry, water- and oil-lubricated DLC against alumina and DLC against steel contacts," *Wear*, vol. 222, pp. 120-128, 1998.
- [76] S. Kosarieh, A. Morina, E. Lainé, J. Flemming, and A. Neville, "Tribological performance and tribochemical processes in a DLC/Steel system when lubricated in a fully formulated oil and base oil," *Surface and Coatings Technology*, 2012.

- [77] T. Haque, A. Morina, A. Neville, R. Kapadia, and S. Arrowsmith, "Effect of oil additives on the durability of hydrogenated DLC coating under boundary lubrication conditions," *Wear*, vol. 266, pp. 147-157, 2009.
- [78] E. Rabinowicz, "Friction and Wear of Materials," *Wiley, New York*, 1965.
- [79] A. Gangopadhyay, D. Mc Watt, P. Willermet, G. M. Crosbie, and R. L. Allor, "Effects of Composition and Surface Finish of Silicon Nitride Tappet Inserts on Valvetrain Friction," in *Tribology Series*. vol. Volume 36, M. P. C. M. T. P. E. T. H. C. C. G. D. Y. B. L. F. J. M. G. D. Dowson and A. A. Lubrecht, Eds., ed: Elsevier, 1999, pp. 635-644.
- [80] H. Czichos, "Design of Friction and Wear Experiments," *ASM Handbook*, vol. 18, pp. 480-488, 1992.
- [81] H. Czichos, S. Becker, and J. Lexow, "Multilaboratory tribotesting: Results from the Versailles Advanced Materials and Standards programme on wear test methods," *Wear*, vol. 114, pp. 109-130, 1987.
- [82] H. Fujita, R. P. Glovnea, and H. A. Spikes, "Study of Zinc Dialkydithiophosphate Antiwear Film Formation and Removal Processes, Part I: Experimental," *Tribology Transactions*, vol. 48, pp. 558-566, 2005/10/01 2005.
- [83] K. Topolovec-Miklozic, T. Reg Forbus, and H. A. Spikes, "Film thickness and roughness of ZDDP antiwear films," *Tribology Letters*, vol. 26, pp. 161-71, 2007.
- [84] A. Morina, A. Neville, M. Priest, and J. Green, "ZDDP and MoDTC interactions and their effect on tribological performance—tribofilm characteristics and its evolution," *Tribology Letters*, vol. 24, pp. 243-256, 2006.
- [85] T. Haque, A. Morina, A. Neville, R. Kapadia, and S. Arrowsmith, "Non-ferrous coating/lubricant interactions in tribological contacts: Assessment of tribofilms," *Tribology International*, vol. 40, pp. 1603-1612, 2007.
- [86] A. Morina, A. Neville, M. Priest, and J. H. Green, "ZDDP and MoDTC interactions in boundary lubrication-The effect of temperature and ZDDP/MoDTC ratio," *Tribology International*, vol. 39, pp. 1545-1557, 2006.
- [87] A. Gangopadhyay, K. Sinha, D. Uy, D. G. McWatt, R. J. Zrodowski, and S. J. Simko, "Friction, Wear, and Surface Film Formation Characteristics of Diamond-Like Carbon Thin Coating in Valvetrain Application," *Tribology Transactions*, vol. 54, pp. 104-114, 2010/12/01 2010.
- [88] D. Uy, S. J. Simko, R. O. Carter lii, R. K. Jensen, and A. K. Gangopadhyay, "Characterization of anti-wear films formed from fresh and aged engine oils," *Wear*, vol. 263, pp. 1165-1174, 2007.
- [89] P. A. Willermet, D. P. Dailey, R. O. Carter lii, P. J. Schmitz, W. Zhu, J. C. Bell, *et al.*, "The composition of lubricant-derived surface layers formed in a lubricated cam/tappet contact II. Effects of adding overbased detergent and dispersant to a simple ZDTP solution," *Tribology International*, vol. 28, pp. 163-175, 1995.
- [90] A. Gangopadhyay, E. Soltis, and M. Johnson, "Valvetrain friction and wear: influence of surface engineering and lubricants," *Proceedings of the Institution of Mechanical Engineers, Part J: Journal of Engineering Tribology*, vol. 218, pp. 147-156, 2004.

- [91] P. A. Willermet, R. O. Carter Iii, and E. N. Boulos, "Lubricant-derived tribochemical films—An infra-red spectroscopic study," *Tribology International*, vol. 25, pp. 371-380, 1992.
- [92] M. Teodorescu, D. Taraza, N. A. Henein, and W. Bryzik, "Simplified elastohydrodynamic friction model of the cam-tappet contact," SAE Technical Paper 0148-7191, 2003.
- [93] H. Spikes, "The history and mechanisms of ZDDP," *Tribology Letters*, vol. 17, pp. 469-89, 2004.
- [94] H. Spikes, "Low-and zero-sulphated ash, phosphorus and sulphur anti-wear additives for engine oils," *Lubrication Science*, vol. 20, pp. 103-136, 2008.
- [95] A. M. Barnes, K. D. Bartle, and V. R. A. Thibon, "A review of zinc dialkyldithiophosphates (ZDDPS): Characterisation and role in the lubricating oil," *Tribology International*, vol. 34, pp. 389-395, 2001.
- [96] M. A. Nicholls, T. Do, P. R. Norton, M. Kasrai, and G. M. Bancroft, "Review of the lubrication of metallic surfaces by zinc dialkyl-dithiophosphates," *Tribology International*, vol. 38, pp. 15-39, 2005.
- [97] J. J. Dickert Jr and C. N. Rowe, "Thermal decomposition of metal O, O-dialkyl phosphorodithioates," *The Journal of Organic Chemistry*, vol. 32, pp. 647-653, 1967.
- [98] M. L. S. Fuller, M. Kasrai, G. M. Bancroft, K. Fyfe, and K. H. Tan, "Solution decomposition of zinc dialkyl dithiophosphate and its effect on antiwear and thermal film formation studied by X-ray absorption spectroscopy," *Tribology International*, vol. 31, pp. 627-644, 1998.
- [99] Y. L. Wu and B. Dacre, "Effects of lubricant-additives on the kinetics and mechanisms of ZDDP adsorption on steel surfaces," *Tribology International*, vol. 30, pp. 445-453, 1997.
- [100] B. Dacre and C. H. Bovington, "The Effect of Metal Composition on the Adsorption of Zinc Di-Isopropyldithiophosphate," *A S L E Transactions*, vol. 26, pp. 333-343, 1983/01/01 1983.
- [101] M. Aktary, M. T. McDermott, and J. Torkelson, "Morphological evolution of films formed from thermooxidative decomposition of ZDDP," *Wear*, vol. 247, pp. 172-179, 2001.
- [102] P. A. Willermet, D. P. Dailey, R. O. Carter Iii, P. J. Schmitz, and W. Zhu, "Mechanism of formation of antiwear films from zinc dialkyldithiophosphates," *Tribology International*, vol. 28, pp. 177-187, 1995.
- [103] Z. Yin, M. Kasrai, M. Fuller, G. M. Bancroft, K. Fyfe, and K. H. Tan, "Application of soft X-ray absorption spectroscopy in chemical characterization of antiwear films generated by ZDDP Part I: the effects of physical parameters," *Wear*, vol. 202, pp. 172-191, 1997.
- [104] J. Martin, "Antiwear mechanisms of zinc dithiophosphate: a chemical hardness approach," *Tribology Letters*, vol. 6, pp. 1-8, 1999/01/01 1999.

- [105] J. S. Sheasby, T. A. Caughlin, A. G. Blahey, and K. F. Laycock, "A reciprocating wear test for evaluating boundary lubrication," *Tribology International*, vol. 23, pp. 301-307, 1990.
- [106] M. Suominen Fuller, L. Rodriguez Fernandez, G. Massoumi, W. Lennard, M. Kasrai, and G. Bancroft, "The use of X-ray absorption spectroscopy for monitoring the thickness of antiwear films from ZDDP," *Tribology Letters*, vol. 8, pp. 187-192, 2000.
- [107] Z. Yin, M. Kasrai, G. M. Bancroft, K. F. Laycock, and K. H. Tan, "Chemical characterization of antiwear films generated on steel by zinc dialkyl dithiophosphate using X-ray absorption spectroscopy," *Tribology International*, vol. 26, pp. 383-388, 1993.
- [108] G. Pereira, D. Munoz-Paniagua, A. Lachenwitzer, M. Kasrai, P. R. Norton, T. W. Capehart, *et al.*, "A variable temperature mechanical analysis of ZDDP-derived antiwear films formed on 52100 steel," *Wear*, vol. 262, pp. 461-470, 2007.
- [109] J. C. Bell, K. M. Delargy, and A. M. Seeney, "Paper IX (ii) The Removal of Substrate Material through Thick Zinc Dithiophosphate Anti-Wear Films," in *Tribology Series*. vol. Volume 21, C. M. T. T. H. C. C. M. G. D. Dowson and G. Dalmaz, Eds., ed: Elsevier, 1992, pp. 387-396.
- [110] M. Crobu, A. Rossi, F. Mangolini, and N. D. Spencer, "Tribochemistry of Bulk Zinc Metaphosphate Glasses," *Tribology Letters*, vol. 39, pp. 121-34, 08/ 2010.
- [111] M. Kano, Y. Yasuda, Y. Okamoto, Y. Mabuchi, T. Hamada, T. Ueno, *et al.*, "Ultralow friction of DLC in presence of glycerol mono-oleate (GNO)," *Tribology Letters*, vol. 18, pp. 245-251, 2005.
- [112] M. De Barros Bouchet, J. M. Martin, T. Le Mogne, P. Bilas, B. Vacher, and Y. Yamada, "Mechanisms of MoS<sub>2</sub> formation by MoDTC in presence of ZnDTP: effect of oxidative degradation," *Wear*, vol. 258, pp. 1643-50, 2005.
- [113] A. Morina, A. Neville, M. Priest, and J. H. Green, "ZDDP and MoDTC interactions and their effect on tribological performance - Tribofilm characteristics and its evolution," *Tribology Letters*, vol. 24, pp. 243-256, 2006.
- [114] C. Grossiord, K. Varlot, J. M. Martin, T. Le Mogne, C. Esnouf, and K. Inoue, "MoS<sub>2</sub> single sheet lubrication by molybdenum dithiocarbamate," *Tribology International*, vol. 31, pp. 737-743, 1998.
- [115] M. I. De Barros Bouchet, T. Le Mogne, J. M. Martin, and B. Vacher, "Lubrication of carbon coatings with MoS<sub>2</sub> single sheet formed by MoDTC and ZDDP lubricants," *Lubrication Science*, vol. 18, pp. 141-149, 2006.
- [116] D. N. Khaemba, A. Neville, and A. Morina, "New insights on the decomposition mechanism of Molybdenum DialkylthioCarbamate (MoDTC): a Raman spectroscopic study," *RSC Advances*, vol. 6, pp. 38637-38646, 2016.
- [117] J. Graham, H. Spikes, and S. Korcek, "The friction reducing properties of molybdenum dialkylthiocarbamate additives: part I—factors influencing friction reduction," *Tribology Transactions*, vol. 44, pp. 626-636, 2001.

- [118] Y. Yamamoto and S. Gondo, "Environmental Effects on the Composition of Surface Films Produced by an Organo-Molybdenum Compound©," *Tribology Transactions*, vol. 37, pp. 182-188, 1994.
- [119] A. Morina and A. Neville, "Tribofilms: aspects of formation, stability and removal," *Journal of Physics D: Applied Physics*, vol. 40, p. 5476, 2007.
- [120] J. W. Schick and J. M. Kaminski, "Lubricant composition for reduction of fuel consumption in internal combustion engines," ed: Google Patents, 1981.
- [121] R. Dhein and K.-H. Hentschel, "Carboxylic acid esters and their use as a base lubricating oil," ed: Google Patents, 1979.
- [122] a. S. T. O. R.M. Mortier, "Chemistry and Technology of Lubricants , pub. Blackie Academic and Professional," *Book* vol. 2 pp. 51 - 72, 1997.
- [123] P. W. Brewster, C. R. Smith, and F. W. Gowland, "Glycerol esters as fuel economy additives," ed: Google Patents, 1987.
- [124] R. W. Begland and E. E. Sommers, "Friction, Wear and Blending Benefits of Dodecanedioate Diest ers in Automotive Lubricants," SAE Technical Paper 0148-7191, 1982.
- [125] I. Minami, S. Mori, Y. Isogai, S. Hiyoshi, T. Inayama, and S. Nakayama, "Molecular Design of Environmentally Adapted Lubricants: Antiwear Additives Derived from Natural Amino Acids," *Tribology Transactions*, vol. 53, pp. 713-721, 2010/08/20 2010.
- [126] J. B. J.Denis, J.C. Hipeaux, "Lubricant Properties, Analysis and Testing " *Institut Francais Du Petrole Publication (Book)*, vol. 1, pp. 1 - 400, 2000.
- [127] J. T. Carey and H. Oumar-Mahamat, "Friction reducing additives for fuels and lubricants," ed: Google Patents, 1998.
- [128] L. Cizaire, J. Martin, T. Le Mogne, and E. Gresser, "Chemical analysis of overbased calcium sulfonate detergents by coupling XPS, ToF-SIMS, XANES, and EFTEM," *Colloids and Surfaces A: Physicochemical and Engineering Aspects*, vol. 238, pp. 151-158, 2004.
- [129] K. Topolovec-Miklozic, T. R. Forbus, and H. Spikes, "Film forming and friction properties of overbased calcium sulphonate detergents," *Tribology Letters*, vol. 29, pp. 33-44, 2008.
- [130] H. Hong and J. Vinci, "The Chemistry of Sulfonates as Metalworking Additives@," *Journal of the Society oi Tribologists and Lubrication Engineers*, 1993.
- [131] J. Mansot, M. Hallouis, and J. Martin, "Colloidal antiwear additives 2. Tribological behaviour of colloidal additives in mild wear regime," *Colloids and Surfaces A: Physicochemical and Engineering Aspects*, vol. 75, pp. 25-31, 1993.
- [132] N. Han, L. Shui, W. Liu, Q. Xue, and Y. Sun, "Study of the lubrication mechanism of overbased Ca sulfonate on additives containing S or P," *Tribology Letters*, vol. 14, pp. 269-274, 2003.



- [133] A. Greenall, A. Neville, A. Morina, and M. Sutton, "Investigation of the interactions between a novel, organic anti-wear additive, ZDDP and overbased calcium sulphonate," *Tribology International*, vol. 46, pp. 52-61, 2012.
- [134] T. Kubo, S. Fujiwara, H. Nanao, I. Minami, and S. Mori, "TOF-SIMS analysis of boundary films derived from calcium sulfonates," *Tribology Letters*, vol. 23, pp. 171-176, 2006.
- [135] T. Kubo, S. Fujiwara, H. Nanao, I. Minami, and S. Mori, "Boundary film formation from overbased calcium sulfonate additives during running-in process of steel–DLC contact," *Wear*, vol. 265, pp. 461-467, 2008.
- [136] T. Palermo, S. Giasson, T. Buffeteau, B. Desbat, and J. Turlet, "Study of deposit and friction films of overbased calcium sulphonate by PM-IRRAS spectroscopy," *Lubrication Science*, vol. 8, pp. 119-127, 1996.
- [137] A. Van de Ven, P. Johal, and L. Jansen, "The characterisation of synthetic sulphonate and phenate detergents by nuclear magnetic resonance and infrared spectroscopy," *Lubrication Science*, vol. 6, pp. 1-19, 1993.
- [138] S. O'connor, J. Crawford, and C. Cane, "Overbased lubricant detergents—a comparative study," *Lubrication Science*, vol. 6, pp. 297-325, 1994.
- [139] S. Ramakumar, A. M. Rao, and S. Srivastava, "Studies on additive-additive interactions: Formulation of crankcase oils towards rationalization," *Wear*, vol. 156, pp. 101-120, 1992.
- [140] H. Spikes, "Additive-additive and additive-surface interactions in lubrication," *Lubrication Science*, vol. 2, pp. 3-23, 1989.
- [141] S. Shirahama and M. Hirata, "The effects of engine oil additives on valve train wear," *Lubrication Science*, vol. 1, pp. 365-384, 1989.
- [142] K. Inoue and H. Watanabe, "Interactions of Engine Oil Additives," *A S L E Transactions*, vol. 26, pp. 189-199, 1983/01/01 1983.
- [143] A. Morina, A. Neville, J. H. Green, and M. Priest, "Additive/additive interactions in boundary lubrication—a study of film formation and tenacity," in *Tribology and Interface Engineering Series*. vol. Volume 48, M. P. G. D. D. Dowson and A. A. Lubrecht, Eds., ed: Elsevier, 2005, pp. 757-767.
- [144] M. Kasrai, J. N. Cutler, K. Gore, G. Canning, G. M. Bancroft, and K. H. Tan, "The Chemistry of Antiwear Films Generated by the Combination of ZDDP and MoDTC Examined by X-ray Absorption Spectroscopy," *Tribology Transactions*, vol. 41, pp. 69-77, 1998/01/01 1998.
- [145] E. Liu and S. D. Kouame, "An XPS Study on the Composition of Zinc Dialkyl Dithiophosphate Tribofilms and Their Effect on Camshaft Lobe Wear," *Tribology Transactions*, vol. 57, pp. 18-27, 2014/01/02 2013.
- [146] F. G. Rounds, "Additive Interactions and Their Effect on the Performance of a Zinc Dialkyl Dithiophosphate," *A S L E Transactions*, vol. 21, pp. 91-101, 1978/01/01 1978.

- [147] S. Plaza, "The Effect of Other Lubricating Oil Additives on the Adsorption of Zinc Diisobutylidithiophosphate on Fe and  $\gamma$  - Fe<sub>2</sub>O<sub>3</sub> Powders," *ASLE Transactions*, vol. 30, pp. 241-247, 1987/01/01 1987.
- [148] P. Kapsa, J. Martin, C. Blanc, and J. Georges, "Antiwear mechanism of ZDDP in the presence of calcium sulfonate detergent," *Journal of Tribology*, vol. 103, pp. 486-494, 1981.
- [149] M. Kasrai, M. S. Fuller, G. M. Bancroft, and P. R. Ryason, "X-Ray Absorption Study of the Effect of Calcium Sulfonate on Antiwear Film Formation Generated From Neutral and Basic ZDDPs: Part 1—Phosphorus Species," *Tribology Transactions*, vol. 46, pp. 534-542, 2003/01/01 2003.
- [150] N. E. Gallopoulos and C. K. Murphy, "Interactions Between a Zinc Dialkylphosphorodithioate and Lubricating Oil Dispersants," *ASLE Transactions*, vol. 14, pp. 1-7, 1971/01/01 1971.
- [151] S. Davis, "Croda Lubricity Additives and Friction Modifier " vol. 1, pp. 1-54, 2009.
- [152] K. Topolovec-Miklozic, F. Lockwood, and H. Spikes, "Behaviour of boundary lubricating additives on DLC coatings," *Wear*, vol. 265, pp. 1893-1901, 2008.
- [153] T. Shinyoshi, Y. Fuwa, and Y. Ozaki, "Wear analysis of DLC coating in oil containing Mo-DTC," SAE Technical Paper 0148-7191, 2007.
- [154] S. Kosarieh, A. Morina, E. Lainé, J. Flemming, and A. Neville, "The effect of MoDTC-type friction modifier on the wear performance of a hydrogenated DLC coating," *Wear*, 2013.
- [155] B. Vengudusamy, J. H. Green, G. D. Lamb, and H. A. Spikes, "Behaviour of MoDTC in DLC/DLC and DLC/steel contacts," *Tribology International*, vol. 54, pp. 68-76, 2012.
- [156] B. De Barros, C. Matta, T. Le-Mogne, J. Michel Martin, T. Sagawa, S. Okuda, *et al.*, "Improved mixed and boundary lubrication with glycerol-diamond technology," *Tribology-Materials, Surfaces & Interfaces*, vol. 1, pp. 28-32, 2007.
- [157] W. Habchi, C. Matta, L. Joly-Pottuz, M. I. De Barros, J. M. Martin, and P. Vergne, "Full film, boundary lubrication and tribochemistry in steel circular contacts lubricated with glycerol," *Tribology Letters*, vol. 42, pp. 351-358, 2011.
- [158] C. Matta, M. De Barros Bouchet, T. Le-Mogne, B. Vachet, J. Martin, and T. Sagawa, "Tribochemistry of tetrahedral hydrogen-free amorphous carbon coatings in the presence of OH-containing lubricants," *Lubrication Science*, vol. 20, pp. 137-149, 2008.
- [159] Anonymous, "Conventional Microscopes," [http://www.eng.utah.edu/~lzanq/images/Lecture\\_3\\_conventional-Microscope.pdf](http://www.eng.utah.edu/~lzanq/images/Lecture_3_conventional-Microscope.pdf).
- [160] C. B. C. David B. Williams, "Transmission Electron Microscopy, Spectroscopy IV," *Book*, pp. 555 - 600, 1966.
- [161] T. Shinyoshi, Y. Fuwa, and Y. Ozaki, "Wear Analysis of DLC Coating in Oil Containing Mo-DTC," 2007.

- [162] S. Equey, S. Roos, U. Mueller, R. Hauert, N. D. Spencer, and R. Crockett, "Tribofilm formation from ZnDTP on diamond-like carbon," *Wear*, vol. 264, pp. 316-321, 2008.
- [163] C. Grossiord, J. Martin, T. Le Mogne, and T. Palermo, "UHV friction of tribofilms derived from metal dithiophosphates," *Tribology letters*, vol. 6, pp. 171-179, 1999.
- [164] M. I. De Barros, J. Bouchet, I. Raoult, T. Le Mogne, J. M. Martin, M. Kasrai, *et al.*, "Friction reduction by metal sulfides in boundary lubrication studied by XPS and XANES analyses," *Wear*, vol. 254, pp. 863-870, 2003.
- [165] R. Unnikrishnan, M. C. Jain, A. K. Harinarayan, and A. K. Mehta, "Additive-additive interaction: An XPS study of the effect of ZDDP on the AW/EP characteristic of molybdenum based additives," *Wear*, vol. 252, pp. 240-249, 2002.
- [166] E. C. Onyiriuka, "Zinc phosphate glass surfaces studied by XPS," *Journal of Non-Crystalline Solids*, vol. 163, pp. 268-273, 1993.
- [167] M. C. Tobin. (1971). *Laser Raman Spectroscopy*. 35.
- [168] D. Uy, S. J. Simko, A. E. O'Neill, R. K. Jensen, A. K. Gangopadhyay, and R. O. Carter, "Raman Characterization of Anti-Wear Films Formed from Fresh and Aged Engine Oils," 2006.
- [169] G. Adamopoulos, K. Gilkes, J. Robertson, N. Conway, B. Kleinsorge, A. Buckley, *et al.*, "Ultraviolet Raman characterisation of diamond-like carbon films," *Diamond and Related Materials*, vol. 8, pp. 541-544, 1999.
- [170] "International Standard Organisation " in *Metallic Materials - Instrumented indentation test for hardness and material parameters - Part 1.*, ed, 2002, pp. 1 - 32.
- [171] W. C. Oliver and G. M. Pharr, "Improved technique for determining hardness and elastic modulus using load and displacement sensing indentation experiments," *Journal of Materials Research*, vol. 7, pp. 1564-1583, 1992.
- [172] *Micro Star Technologies; Nano-indenters*. Available: [www.microstartech.com](http://www.microstartech.com)
- [173] J. Durham and A. Kidson, "The effects of low sulfated ash, phosphorus and sulfur oils on camshaft/tappet tribocouples with various diamond-like-carbon coated tappets in motored and fired engines," *Lubrication Science*, 2014.
- [174] M. Bromark, M. Larsson, P. Hedenqvist, M. Olsson, and S. Hogmark, "Influence of substrate surface topography on the critical normal force in scratch adhesion testing of TiN-coated steels," *Surface and Coatings Technology*, vol. 52, pp. 195-203, 1992.
- [175] J. Jiang and R. D. Arnell, "The effect of substrate surface roughness on the wear of DLC coatings," *Wear*, vol. 239, pp. 1-9, 2000.
- [176] K. Oguri and T. Arai, "Low friction coatings of diamond-like carbon with silicon prepared by plasma-assisted chemical vapor deposition," *Journal of Materials Research*, vol. 5, pp. 2567-2571, 1990.
- [177] J. Meneve, E. Dekempeneer, W. Wegener, and J. Smeets, "Low friction and wear resistant aC: H/a-Si 1- x C x: H multilayer coatings," *Surface and Coatings Technology*, vol. 86, pp. 617-621, 1996.

- [178] N. Wada, P. J. Gaczi, and S. A. Solin, "'Diamond-like" 3-fold coordinated amorphous carbon," *Journal of Non-Crystalline Solids*, vol. 35, pp. 543-548, 1980/01/01 1980.
- [179] B. Vengudusamy, R. A. Mufti, G. D. Lamb, J. H. Green, and H. A. Spikes, "Friction properties of DLC/DLC contacts in base oil," *Tribology International*, vol. 44, pp. 922-932, 2011.
- [180] H. A. Rothbart, "Cam Design Handbook," *Book*, vol. 1, 2004.
- [181] A. Lonsdale, "Dynamic rotary torque measurement using surface acoustic waves," *Sensors-the Journal of Applied Sensing Technology*, vol. 18, pp. 51-55, 2001.
- [182] R. A. Mufti and M. Priest, "Experimental and theoretical study of instantaneous engine valve train friction," *Transactions of the ASME. Journal of Tribology*, vol. 125, pp. 628-37, 07/ 2003.
- [183] A. S. C. P. 7.x, "Industrial drives - ABB," vol. 1, pp. 1-174, 2012.
- [184] K. W. page, "Load Washers  
for Forces of 7,5 ... 1 200 kN," vol. 1, pp. 1-9, 2015.
- [185] J. M. Pieprzak, P. A. Willermet, and D. P. Dailey, "Experimental Evaluation of Tappet/Bore and Cam/Tappet Friction for a Direct Acting Bucket Tappet Valvetrain," 1990.
- [186] P. A. Willermet, J. M. Pieprzak, and D. P. Dailey, "Tappet Rotation and Friction Reduction in a Center Pivot Rocker Arm Contact," *Journal of Tribology*, vol. 112, pp. 655-661, 1990.
- [187] R. Muller, "The effect of Lubrication on Cam and Tappet Performance, Motor Tech " *MIRA Translation, No 27/66*, vol. 27, pp. 58-61, 1966.
- [188] A. Comfort, "An Introduction to Heavy-Duty Diesel Engine Frictional Losses And Lubricant Properties Affecting Fuel Economy - Part I," 2003.
- [189] A. Dyson and H. Naylor, "Application of the Flash Temperature Concept to Cam and Tappet Wear Problems," *Proceedings of the Institution of Mechanical Engineers: Automobile Division*, vol. 14, pp. 255-280, January 1, 1960 1960.
- [190] M. Masuda, M. Ujino, K. Shimoda, K. Nishida, I. Marumoto, and Y. Moriyama, "Development of Titanium Nitride Coated Shim for a Direct Acting OHC Engine," 1997.
- [191] S. G. Ahn, H. O. Ban, B. L. Jo, S. C. Kim, and S. C. Jung, "Development of Supercarburized Tappet Shim to Improve Fuel Economy," 2000.
- [192] T. Kanzaki, N. Hara, A. Mori, and K. Ohtsubo, "Advantage of Lightweight Valve Train Component on Engines," 1998.
- [193] A. Ito, L. Yang, and H. Negishi, "A Study on Cam Wear Mechanism with a Newly Developed Friction Measurement Apparatus," 1998.
- [194] T. Haque, A. Morina, and A. Neville, "Tribological performance evaluation of a hydrogenated diamond-like carbon coating in sliding/rolling contact—effect of lubricant additives," *Proceedings of the Institution of Mechanical Engineers, Part J: Journal of Engineering Tribology*, vol. 225, pp. 393-405, 2011.

- [195] J. M. Martin, C. Grossiord, T. Le Mogne, S. Bec, and A. Tonck, "The two-layer structure of ZnDTP tribofilms: Part I: AES, XPS and XANES analyses," *Tribology International*, vol. 34, pp. 523-530, 2001.
- [196] S.-H. Choa, K. C. Ludema, G. E. Potter, B. M. DeKoven, T. A. Morgan, and K. K. Kar, "A model for the boundary film formation and tribological behavior of a phosphazene lubricant on steel," *Tribology Transactions*, vol. 38, pp. 757-768, 1995.
- [197] A. Kodai, T. Mori, and T. Inukai, "APPLYING HARD THIN COATINGS TO TAPPETS TO REDUCE FRICTION," 2001.
- [198] M. Ofune, P. Banks, A. Morina, and A. Neville, "Development of valve train rig for assessment of cam/follower tribochemistry," *Tribology International*, 2015.
- [199] H. Fujita and H. A. Spikes, "Study of Zinc Dialkyldithiophosphate Antiwear Film Formation and Removal Processes, Part II: Kinetic Model," *Tribology Transactions*, vol. 48, pp. 567-575, 2005/10/01 2005.
- [200] S. Bec, A. Tonck, J. M. Georges, R. C. Coy, J. C. Bell, and G. W. Roper, "Relationship between mechanical properties and structures of zinc dithiophosphate anti-wear films," *Proceedings of the Royal Society of London. Series A: Mathematical, Physical and Engineering Sciences*, vol. 455, pp. 4181-4203, December 8, 1999 1999.
- [201] P. N. de Aza, C. Santos, A. Pazo, S. de Aza, R. Cuscó, and L. Artús, "Vibrational Properties of Calcium Phosphate Compounds. 1. Raman Spectrum of  $\beta$ -Tricalcium Phosphate," *Chemistry of Materials*, vol. 9, pp. 912-915, 1997/04/01 1997.
- [202] M. Crobu, A. Rossi, F. Mangolini, and N. D. Spencer, "Chain-length-identification strategy in zinc polyphosphate glasses by means of XPS and ToF-SIMS," *Analytical and bioanalytical chemistry*, vol. 403, pp. 1415-1432, 2012.
- [203] P. A. Bennett, "A Surface Effect Associated with the Use of Oils Containing Zinc Dialkyl Dithiophosphate," *A S L E Transactions*, vol. 2, pp. 78-90, 1959/01/01 1959.
- [204] K. Varlot, M. Kasrai, J. Martin, B. Vacher, G. Bancroft, E. Yamaguchi, *et al.*, "Antiwear film formation of neutral and basic ZDDP: influence of the reaction temperature and of the concentration," *Tribology Letters*, vol. 8, pp. 9-16, 2000.
- [205] R. C. Rosenberg, "General friction considerations for engine design," SAE Technical Paper 0148-7191, 1982.
- [206] A. Schamel, M. Grischke, and R. Bethke, "Amorphous carbon coatings for low friction and wear in bucket tappet valvetrains," SAE Technical Paper 0148-7191, 1997.
- [207] A. Gangopadhyay, P. Willermet, M. Tamor, and W. Vassell, "Amorphous hydrogenated carbon films for tribological applications I. Development of moisture insensitive films having reduced compressive stress," *Tribology International*, vol. 30, pp. 9-18, 1997.
- [208] C. Donnet, "Recent progress on the tribology of doped diamond-like and carbon alloy coatings: a review," *Surface and Coatings Technology*, vol. 100, pp. 180-186, 1998.
- [209] D. Lee, S. Fayeulle, K. Walter, and M. Nastasi, "Internal stress reduction in diamond like carbon thin films by ion irradiation," *Nuclear Instruments and Methods in Physics Research Section B: Beam Interactions with Materials and Atoms*, vol. 148, pp. 216-220, 1999.

- [210] B. Lung, M.-J. Chiang, and M.-H. Hon, "Effect of gradient a-SiC x interlayer on adhesion of DLC films," *Materials chemistry and physics*, vol. 72, pp. 163-166, 2001.
- [211] M. Ban and T. Hasegawa, "Internal stress reduction by incorporation of silicon in diamond-like carbon films," *Surface and Coatings Technology*, vol. 162, pp. 1-5, 2003.
- [212] U. Müller and R. Hauert, "The coefficient of static friction of silicon containing diamond-like carbon films," *Surface and Coatings Technology*, vol. 177, pp. 552-557, 2004.
- [213] M.-G. Kim, K.-R. Lee, and K. Y. Eun, "Tribological behavior of silicon-incorporated diamond-like carbon films," *Surface and Coatings Technology*, vol. 112, pp. 204-209, 1999.
- [214] M. De Feo, M. D. B. Bouchet, C. Minfray, T. Le Mogne, F. Meunier, L. Yang, *et al.*, "MoDTC lubrication of DLC-involving contacts. Impact of MoDTC degradation," *Wear*, vol. 348, pp. 116-125, 2016.
- [215] I. Nedelcu, E. Piras, A. Rossi, and H. Pasaribu, "XPS analysis on the influence of water on the evolution of zinc dialkyldithiophosphate-derived reaction layer in lubricated rolling contacts," *Surface and Interface Analysis*, vol. 44, pp. 1219-1224, 2012.
- [216] J. Erjavec and R. Thompson, *Automotive technology: a systems approach*: Cengage Learning, 2014.
- [217] T. Gilles, *Automotive Engines: Diagnosis, Repair, Rebuilding*: Cengage Learning, 2014.
- [218] S. Okuda, T. Dewa, and T. Sagawa, "Development of 5W-30 GF-4 Fuel-saving Engine Oil for DLC-coated Valve Lifters," 2007.
- [219] M. Gautam, K. Chitoor, M. Durbha, and J. C. Summers, "Effect of diesel soot contaminated oil on engine wear—investigation of novel oil formulations," *Tribology International*, vol. 32, pp. 687-699, 1999.
- [220] S. George, S. Balla, and M. Gautam, "Effect of diesel soot contaminated oil on engine wear," *Wear*, vol. 262, pp. 1113-1122, 2007.
- [221] A. Gauthier and T. Delvigne, "Soot Induced Cam Wear in Diesel Engines: An Investigation Using Thin Layer Activation," 2000.
- [222] E. de Almeida Leme, A. R. Wagner, A. Gutierrez, G. Santos, and H. G. da Silva, "Friction Torque Measurement and Analysis of Influence Factors on Engine Valvetrain," 2014.
- [223] S.-Y. Hwang, K.-T. Kang, B.-S. Lim, and Y.-S. Lim, "Noise Reduction and Sound Quality Improvement of Valve Train in V6 Gasoline Engine," 2005.
- [224] M. Hanaoka and S. Fukumura, "A Study of Valve Train Noises and a Method of Cam Design to Reduce the Noises," 1973.
- [225] B. K. Geist, W. Resh, S. Fisher, I. McLean, and M. Hannon, "Assessing the Propensity for Valve Train Tick Noise," *SAE Int. J. Engines*, vol. 6, pp. 637-646, 2013.
- [226] E. Kamiyama and S. Yasuhara, "Improvement of DOHC Valve Train Noise by Analysis of Valve and Tappet Movement," 1991.

- [227] J. A. Mc Geehan and P. R. Ryason, "Preventing Catastrophic Camshaft Lobe Failures in Low Emission Diesel Engines," 2000.
- [228] T. Hioki, Y. Itoh, A. Itoh, S. Hibi, and J. Kawamoto, "Tribology of carbonaceous films formed by ion-beam-assisted deposition of organic material," *Surface and Coatings Technology*, vol. 46, pp. 233-243, 1991.
- [229] M. De Feo, C. Minfray, M. D. B. Bouchet, B. Thiebaut, and J. Martin, "MoDTC friction modifier additive degradation: Correlation between tribological performance and chemical changes," *RSC Advances*, vol. 5, pp. 93786-93796, 2015.
- [230] M. A. Nicholls, T. Do, P. R. Norton, G. M. Bancroft, M. Kasrai, T. W. Capehart, *et al.*, "Chemical and mechanical properties of ZDDP antiwear films on steel and thermal spray coatings studied by XANES spectroscopy and nanoindentation techniques," *Tribology Letters*, vol. 15, pp. 241-248, 2003.
- [231] K. Torii, H. Chida, K. Otsubo, and Y. Tsusaka, "Anti-Wear Properties of Engine Oils-Effects of Oil Additives on Valve Train Wear," 1977.
- [232] D. Sun and R. Rosenberg, "An experimental study of automotive cam-lifter interface friction," *ASLE transactions*, vol. 30, pp. 167-176, 1987.
- [233] C. Bona and F. Ghilardi, "Influence of Tappet Rotation on Cam and Tappet Surface Deterioration," *Proceedings of the Institution of Mechanical Engineers: Automobile Division*, vol. 180, pp. 269-278, 1965.
- [234] R. A. Mufti, R. Zahid, F. Qureshi, J. Aslam, N. Afzal, and M. U. Bhutta, "Measuring the tribological performance of all the tappets in a production engine using magnetometer sensors and the effect of lubricant rheology," *Lubrication Science*, vol. 27, pp. 251-263, 2015.
- [235] E. W. Schneider and D. H. Blossfeld, "Real-Time Measurement of Camshaft Wear in an Automotive Engine - a Radiometric Method," 1990.
- [236] H. Gao, J. McQueen, E. Black, A. Gangopadhyay, and R. Jensen, "Reduced phosphorus concentration effects on tribological performance of passenger car engine oils," *Tribology Transactions*, vol. 47, pp. 200-207, 2004.
- [237] J. Hu and C. Wei, "Research on the Friction Behaviors of Two Rough Surfaces Covered with Boundary Film," *Tribology Letters*, vol. 53, pp. 487-496, 2014.
- [238] J. Hol, V. Meinders, M. de Rooij, and A. van den Boogaard, "Multi-scale friction modeling for sheet metal forming: the boundary lubrication regime," *Tribology international*, vol. 81, pp. 112-128, 2015.
- [239] S. Andersson, A. Söderberg, and S. Björklund, "Friction models for sliding dry, boundary and mixed lubricated contacts," *Tribology international*, vol. 40, pp. 580-587, 2007.
- [240] A. Akchurin, R. Bosman, P. M. Lugt, and M. van Drogen, "On a Model for the Prediction of the Friction Coefficient in Mixed Lubrication Based on a Load-Sharing Concept with Measured Surface Roughness," *Tribology Letters*, vol. 59, pp. 1-11, 2015.
- [241] R. Bosman and D. J. Schipper, "Running-in of systems protected by additive-rich oils," *Tribology letters*, vol. 41, pp. 263-282, 2011.

- [242] A. Ghanbarzadeh, M. Wilson, A. Morina, D. Dowson, and A. Neville, "Development of a new mechano-chemical model in boundary lubrication," *Tribology International*, vol. 93, pp. 573-582, 2016.